



The  
University  
Of  
Sheffield.

# Proteomic analysis of acclimation in the *Arabidopsis thaliana* thylakoid membrane

Sarah Elizabeth Flannery

Faculty of Science

Department of Molecular Biology and Biotechnology

A thesis submitted for the degree of Doctor of Philosophy

March 2021

## Abstract

Photosynthetic acclimation is the ability of photosynthetic organisms to respond to light irradiance by adjusting the composition of the thylakoid membrane to maintain photosynthetic efficiency. The work described in this thesis utilises mass spectrometry-based proteomics to quantify the changes in thylakoid protein abundance that occur during acclimation in *Arabidopsis thaliana*. A novel strategy for label-free quantitative thylakoid proteomics was developed and combined with electron microscopy, structured illumination microscopy, and various biochemical and spectroscopic analyses to further our understanding of thylakoid proteome remodelling in response to environmental conditions. First, the thylakoid proteomes of *Arabidopsis* plants grown under low, moderate and high light intensity were compared. *Arabidopsis* grown outdoors in naturally fluctuating light conditions were then investigated to identify mechanisms particularly important for photosynthesis in the field. Finally, the phosphorylation mutants *stm7* and *tap38*, the former previously reported as defective in long term acclimation, grown under different light irradiances were subjected to proteomic analysis, as well as the proton gradient regulation mutant *pgr5*. The results of this thesis revealed changes in protein abundance associated with light harvesting, electron transfer, thylakoid architecture and photoprotection. STN7 is not essential for acclimation but the effects of perturbed LHCII (de)phosphorylation on grana size and light harvesting are compensated for by alterations to photosystem stoichiometry. While phosphorylation regulates dynamic thylakoid stacking, proteomic analysis revealed changes in CURT1 and RIQ1/2 protein abundance associated with long term alterations in grana size. Low light plants maintain fast relaxation of quenching whereas plants acclimated to high light intensity increase their capacity for linear electron transfer and rapid induction of quenching. Constant light acclimated plants favour PGR5/PGRL1-mediated cyclic electron transfer while those in a natural environment focus on increasing NDH. While individual changes in thylakoid protein abundance have been studied extensively in the past, this data, which includes many regulatory proteins not previously quantified, provides a view of thylakoid proteome remodelling in unprecedented detail.

## Acknowledgements

First, I would like to thank my supervisor, Matt, for the opportunity to undertake this PhD. His ongoing support and enthusiasm, as well as the fun and friendly culture of the lab group, has kept me motivated throughout the project. I would also like to thank my second supervisor, Mark, and the rest of the Dickman group for welcoming me into their lab meetings and, of course, pub trips.

I would like to thank all past and present members of the E6 office for being a great bunch of people and for consistently improving my day with your silliness, and to give another thanks to everyone else in the wider Hunter/Johnson lab for the hilarious pub trips, games nights and prosecco-fuelled office celebrations. Particularly, thank you to Will Wood for helping me get started at the beginning of my PhD. I would also like to thank both Will and Tommy Emrich-Mills for their contributions to this work through SIM, as well as Dr Chris Hill at the Electron Microscopy facility for the EM images of chloroplasts. For her contributions to the field Arabidopsis project of Chapter 5 and for being a fantastic summer student, I would like to thank Federica Pastorelli. To Mo and Liz, thank you for keeping the Hunter/Johnson lab running like a well-oiled machine.

Next, I would like to say a huge thank you to Phil Jackson. None of the work in this thesis would have happened without the time and effort he has invested in my mass spectrometry training, which ignited my enthusiasm for the technique and led to me carrying out my PIPS in a mass spec facility. I also learned about various other tangentially related topics like brewing, grammar pedantry, being a DJ in the 80s, and how operating a mass spectrometer is similar to flying a plane. Another big thank you is to Holger, Alex and Joao at the LMS Biological Mass Spectrometry Facility for teaching me so much and for helping me to really make the most of my time in London.

Finally, I would like to thank my friends and family for supporting me over the course of my PhD and throughout my time in Sheffield. Thank you to all past and present members of 'The House' at Heavygate and St Barnabas for all the good times, especially to Dave, who has been a constant source of sanity and stability for the past eight years. A last thank you goes to my mum and dad for their love and support. While they may not manage to read much of this thesis, I know they are very proud of me and that is more than enough.

## Declaration

I, the author, confirm that the Thesis is my own work. I am aware of the University's Guidance on the Use of Unfair Means ([www.sheffield.ac.uk/ssid/unfair-means](http://www.sheffield.ac.uk/ssid/unfair-means)). This work has not been previously been presented for an award at this, or any other, university.

The work described in this Thesis contributed to the following research publication:

Flannery, S.E., Hepworth, C., Wood, W.H.J., Pastorelli, F., Neil Hunter, C., Dickman, M.J., Jackson, P.J., and Johnson, M.P. (2021). Developmental acclimation of the thylakoid proteome to light intensity in *Arabidopsis*. *Plant J.* *105*, 223–244.

# Contents

Abstract.....	i
Acknowledgements.....	ii
Declaration.....	iii
Figures.....	viii
Tables.....	xi
Abbreviations.....	xii
1 Introduction.....	1
1.1 Photosynthesis in higher plants.....	1
1.2 Structure and function of the key photosynthetic complexes.....	6
1.2.1 The photosystems and their light-harvesting antennas.....	6
1.2.2 Cytochrome <i>b<sub>6</sub>f</i> .....	9
1.2.3 ATP synthase.....	11
1.2.4 NDH.....	11
1.3 Thylakoid architecture.....	14
1.4 Adaptation of photosynthesis to the light environment.....	16
1.4.1 PSII damage and repair.....	17
1.4.2 Short term responses to light intensity.....	17
1.4.3 The link between short and long term responses.....	22
1.4.4 Long term acclimation to light intensity.....	23
1.5 <i>Arabidopsis thaliana</i> as a photosynthetic model organism.....	26
1.6 Proteomics as a tool for studying photosynthesis.....	27
1.7 Principles of mass spectrometry-based proteomics.....	31
1.8 Aims.....	33
2 Experimental procedures.....	34
2.1 Growth of <i>Arabidopsis thaliana</i> .....	34
2.1.1 Conditions for growth of <i>Arabidopsis</i> .....	34
2.2 Materials, buffers and reagents.....	35
2.3 Preparation of thylakoid membranes.....	36

2.4	Spectroscopic analysis of pigments .....	36
2.4.1	Chlorophyll analysis .....	36
2.4.2	Low temperature fluorescence spectroscopy .....	37
2.5	Protein assay .....	37
2.6	BN-PAGE .....	37
2.7	SDS-PAGE and immunoblotting.....	38
2.8	Imaging of chloroplasts.....	38
2.8.1	Electron microscopy of leaf thin sections .....	38
2.8.2	Structured illumination microscopy .....	39
2.9	Mass spectrometry .....	39
2.9.1	Protein digestion in 60% methanol .....	39
2.9.2	In-gel protein digestion .....	40
2.9.3	In-solution protein digestion .....	40
2.9.4	Protein digestion in sodium laurate.....	40
2.9.5	Peptide desalting .....	41
2.9.6	Hypercarb fractionation of peptides.....	41
2.9.7	Analysis of peptides by mass spectrometry .....	41
2.9.8	Identification of proteins from mass spectrometry data.....	42
2.9.9	Mass spectrometry-based protein quantification .....	42
3	Developing a method for proteomic analysis of the Arabidopsis thylakoid membrane .....	44
3.1	Introduction.....	44
3.2	Selection of a digestion method for thylakoid protein mass spectrometry .....	45
3.3	Label-free relative quantification of the thylakoid proteome.....	51
3.4	Discussion.....	54
4	Acclimation of the photosynthetic machinery to light environment in Arabidopsis .....	57
4.1	Introduction.....	57
4.2	Growth of <i>Arabidopsis thaliana</i> and characterisation of the light-acclimated thylakoid membrane.....	58
4.3	Proteomic analysis of key photosynthetic complexes and their antenna .....	61

4.4	Thylakoid architecture changes in light acclimation .....	66
4.5	Electron transfer and photoprotection .....	68
4.6	Repair of photosystem II in the light-acclimated thylakoid membrane .....	73
4.7	Discussion .....	76
5	Proteomic analysis of the thylakoid membrane in Arabidopsis in the laboratory and in the field	80
5.1	Introduction .....	80
5.2	Field-grown Arabidopsis experienced dramatically different light and temperature conditions to those grown in the laboratory .....	81
5.3	Morphological changes in field-grown Arabidopsis are accompanied by biochemical and spectroscopic differences .....	83
5.4	Proteomic analysis of Arabidopsis grown in a natural light environment reveals changes in key photosynthetic complexes and their antenna .....	86
5.5	Thylakoid architecture is altered in a natural light environment .....	90
5.6	The thylakoid proteome of field grown plants implies a greater capacity for linear electron transfer, cyclic electron transfer and photoprotection .....	93
5.7	Upregulation of PSII repair machinery in the field .....	96
5.8	Proteins specific for acclimation to a fluctuating natural light environment .....	98
5.9	Discussion .....	99
6	Thylakoid proteome analysis of photosynthetic mutants: LHCII phosphorylation and proton gradient regulation .....	102
6.1	Introduction .....	102
6.2	Growth and acclimation of <i>stn7</i> and <i>tap38</i> to varying light intensity .....	104
6.3	Phosphorylation mutants <i>stn7</i> and <i>tap38</i> are capable of long term acclimation to light intensity	106
6.4	Long term changes in thylakoid architecture in <i>stn7</i> and <i>tap38</i> .....	109
6.5	Electron carrier protein abundance is affected in <i>stn7</i> and <i>tap38</i> .....	112
6.6	Candidate proteins for an STN7-mediated signalling pathway .....	115
6.7	The <i>pgr5</i> mutant is comparable to wild type in supercomplex formation and grana diameter	116
6.8	Widespread downregulation of thylakoid protein abundance in <i>pgr5</i> .....	118
6.9	Downregulation of PSII repair machinery in <i>pgr5</i> .....	121

6.10 Discussion.....	123
7 Final summary .....	125
Bibliography .....	132
Appendices.....	158

## Figures

Figure 1: Electron transfer through the thylakoid membrane. ....	4
Figure 2: Structural organisation of the photosystems and their antenna .....	8
Figure 3: Structural arrangement of the chloroplast ATP synthase. ....	11
Figure 4: Electron micrographs of Arabidopsis chloroplasts.....	15
Figure 5: Emission spectrum of fluorescent lighting used for Arabidopsis growth.....	35
Figure 6. Assessment of digestion methods by SDS-PAGE.....	46
Figure 7: Analysis of strategies to increase thylakoid proteome coverage .....	48
Figure 8: Method selection for preparation of thylakoid membranes for MS analysis by digestion ....	50
Figure 9: Processing of MS data from light-acclimated thylakoids.....	53
Figure 10: Growth of light-acclimated Arabidopsis plants.....	59
Figure 11: Characterisation of acclimated thylakoid membranes.....	61
Figure 12: Acclimation involves changes in the relative abundance of key photosynthetic complexes. .....	64
Figure 13: Acclimation involves changes in the relative abundance of antenna proteins .....	65
Figure 14: Thylakoid membrane stacking changes associated with acclimation are paralleled by changes in the relative abundance of CURT1A, B and RIQ1, 2 proteins.....	67
Figure 15: Acclimation to high light causes upregulation of proteins involved in LET and CET .....	69
Figure 16: The relative abundance of proteins involved in light harvesting regulation changes in acclimation.....	71
Figure 17: Acclimation to high light leads increased abundance of the PSII repair cycle machinery..	75
Figure 18: A comparison of high light versus low light acclimation in the thylakoid membrane proteome. ....	77
Figure 19: Arabidopsis plants grown outdoors are exposed to highly variable light and temperature conditions and exhibit very different morphologies to controlled environment plants .....	82
Figure 20: Lab and field thylakoid membranes have different spectroscopic properties and reduced formation of supercomplexes.....	85

Figure 21: Adaptation to a natural environment involves changes in the relative abundance of key photosynthetic complexes.....	87
Figure 22: Thylakoids from field Arabidopsis have altered levels of minor antenna subunits.....	89
Figure 23: Thylakoid architecture changes in Field thylakoids are associated with increases in CURT1 and RIQ proteins but not STN7 or TAP38..	92
Figure 24: Acclimation to a natural environment causes upregulation of proteins involved in LET and CET .....	94
Figure 25: Arabidopsis in a natural environment have increases in the relative abundance of proteins involved in light harvesting regulation .....	96
Figure 26: Upregulation of the PSII repair machinery in a natural environment .....	97
Figure 27: A comparison of natural versus controlled environment adaptation in the thylakoid membrane proteome.....	99
Figure 28: Phosphorylation mutant Arabidopsis plants acclimated to low, moderate and high light intensity.....	104
Figure 29: Clear native PAGE analysis of phosphorylation mutants .....	106
Figure 30: Principle component analysis of MS data to compare phosphorylation mutants .....	107
Figure 31: Abundance of STN7 and TAP38 in phosphorylation mutants .....	108
Figure 32: Acclimation-related changes in the abundance of key photosynthetic complexes in phosphorylation mutants.....	109
Figure 33: Long-term changes in thylakoid architecture are affected by LHCII phosphorylation .....	110
Figure 34: Abundance of proteins involved in thylakoid architecture in phosphorylation mutants ...	112
Figure 35: Abundance of electron transfer proteins in phosphorylation mutants .....	114
Figure 36: Abundance of potential phosphorylation targets of STN7 .....	115
Figure 37: The <i>pgr5</i> mutant has similar supercomplex formation and thylakoid architecture to wild type .....	117
Figure 38: Downregulation of key complexes in <i>pgr5</i> . .....	118
Figure 39: A comparison of the thylakoid proteome in <i>pgr5</i> to <i>gl-1</i> .....	120

Figure 40: Depletion of PSII repair machinery in *pgr5* ..... 122

## Tables

Table 1: Subunits of photosystem II .....	7
Table 2: Subunits of the PSI reaction centre.....	9
Table 3: Subunits of cytochrome <i>b<sub>6</sub>f</i> .....	10
Table 4: Subcomplexes of the NDH complex and their subunits. ....	13
Table 5: <i>Arabidopsis thaliana</i> strains .....	34
Table 6: Buffers and solutions .....	35
Table 7: Software and database versions .....	42
Table 8: Stoichiometry of key photosynthetic complexes and antenna .....	63
Table 9: Stoichiometry electron transfer proteins .....	70
Table 10: Stoichiometry of regulatory and photoprotective proteins .....	73
Table 11: Chlorophyll <i>a/b</i> ratios of phosphorylation mutants following light acclimation .....	105
Table 12: Relative abundance of thylakoid-associated proteins in acclimation .....	158
Table 13: Relative abundance of thylakoid-associated proteins in the Field versus the Lab.....	174
Table 14: Relative abundance of thylakoid-associated proteins in light-acclimated phosphorylation mutants.....	188
Table 15: Relative abundance of thylakoid-associated proteins in <i>pgr5</i> .....	205

## Abbreviations

ACN	acetonitrile
ANOVA	analysis of variance
ATP	adenosine triphosphate
CBB cycle	Calvin-Benson-Bassham cycle
CET	cyclic electron transfer
Chl	chlorophyll
<i>Cytb<sub>6</sub>f</i>	cytochrome <i>b<sub>6</sub>f</i>
Fd	ferredoxin
FNR	ferredoxin-NADP <sup>+</sup> reductase
FQR	ferredoxin-plastoquinone oxidoreductase
FRET	Förster resonance energy transfer
G3P	glyceraldehyde-3-phosphate
HL	high light
LET	linear electron transfer
LL	low light
MAP	Mehler-ascorbate peroxidase pathway
MDH	malate dehydrogenase
ML	moderate light
MS	mass spectrometry
MS/MS	tandem mass spectrometry
NADP <sup>+</sup>	nicotinamide adenine dinucleotide phosphate
NADPH	reduced nicotinamide adenine dinucleotide phosphate
nanoLC	nano liquid chromatography
OEC	oxygen evolving complex
PCA	principle component analysis
PGA	glycerate-3-phosphate
PQ/PQH <sub>2</sub>	plastoquinone/plastoquinol
PSI	photosystem I
PSII	photosystem II
PTOX	plastid terminal oxidase
RuBP	ribulose-1,5-bisphosphate
TCEP	tris(carboxyethyl)phosphine-HCl
ΔpH	proton gradient

# 1 Introduction

## 1.1 Photosynthesis in higher plants

Photosynthesis evolved 3.5 billion years ago and now sustains nearly all life on Earth. In its earliest form, bacteria gained the ability to construct an assembly of light-absorbing pigments and other cofactors for oxidation/reduction on a protein scaffold in a lipid bilayer: a reaction centre. Protons transferred across a membrane, powered by reaction centres, created a chemiosmotic gradient, which could be used to generate adenosine triphosphate (ATP), used in biosynthesis. Evolution of increasingly complex photosynthetic systems gave rise to their divergence into two main reaction centre types: those that use iron-sulphur clusters, similar to photosystem I (PSI), and those that transfer electrons through pheophytin and quinone molecules, similar to photosystem II (PSII) of plants. These are termed type I and type II reaction centres, respectively. Cyanobacteria contain both reaction centre types, along with an enzyme capable of harvesting protons and electrons from the splitting of a water molecule using a manganese cluster. This enzyme is known as the oxygen evolving complex (OEC) because of the oxygen released as part of the water-splitting reaction. The evolution of oxygenic photosynthesis resulted in a dramatic change in the Earth's atmosphere and eventually led to the appearance of the first eukaryotic organisms. An endosymbiotic event, 600-2000 million years ago (McFadden and Van Dooren, 2004), whereby a cyanobacterium was taken up by a eukaryotic cell led to the evolution of the chloroplast, the site of oxygenic photosynthesis in algae and higher plants. While the chloroplast retains its own small circular genome, endosymbiotic gene transfer over time means that the majority of chloroplast proteins are now encoded by the nucleus.

Integral to human life, plant photosynthesis provides us with all of our food and much of our fuel, making it a vital area of research within the context of a changing environment, an increasing world population, and the consequent strain on agriculture. Photosynthesis in the plant chloroplast involves the capture of light energy from the sun to produce ATP and reduced nicotinamide adenine dinucleotide phosphate (NADPH) in order to convert atmospheric CO<sub>2</sub> into complex organic compounds. The structure of the chloroplast consists of a double envelope surrounding another continuous enclosed membrane structure known as the thylakoid membrane in an aqueous environment called the stroma. The stroma contains the enzymes that carry out the 'dark reactions' of the Calvin-Benson-Bassham cycle (CBB cycle) for CO<sub>2</sub> fixation whereas the thylakoid membrane is the site of the 'light reactions'. It is important to note that both the light and the dark reactions – also known as the 'light-independent' reactions – occur during daylight hours. In higher plants, chloroplasts are mostly located in specialised mesophyll cells in the leaves – organs specialised for photosynthesis by their large surface area for light absorption and efficient gas exchange through pores known as stomata (Smith et al., 1997). Some plant species use specialised chloroplasts in separate tissues to physically segregate the light and dark reactions and reduce the inhibitory effect of oxygen on CO<sub>2</sub> fixation. Ribulose-1,5-bisphosphate

carboxylase/oxygenase, or Rubisco, is the enzyme responsible for CO<sub>2</sub> fixation, the first step of the dark reactions where atmospheric CO<sub>2</sub> is used to carboxylate ribulose-1,5-bisphosphate (RuBP) and produce two molecules of glycerate-3-phosphate (PGA). Using NADPH as a reductant, the PGA is then converted to glyceraldehyde-3-phosphate (G3P), which is used for both glucose synthesis and the regeneration of RuBP (Stirbet et al., 2019).

The light reactions of photosynthesis function to generate ATP and NADPH, which feed into the dark reactions to fix atmospheric CO<sub>2</sub>. To power the light reactions, solar energy is absorbed by pigments such as chlorophyll and carotenoids held on a protein scaffold embedded in the thylakoid membrane. Pigments with different absorbance spectra are arranged in different environments to broaden the absorbance cross-section and maximise the number of photons absorbed. Chlorophylls are the main pigments involved in chloroplast light absorption and photochemistry and feature a phytol tail and a tetrapyrrole ring chelated with a magnesium ligand. The two types of chlorophyll in higher plants are chlorophyll *a* and *b*, which absorb light energy from the violet and red, and the blue and orange regions of the visible light spectrum, respectively. While only chlorophyll *a* is involved in the chemistry of the photosynthetic reaction centres, chlorophyll *b* is found mostly in the light-harvesting antenna complexes. Antenna complexes collect light energy, which is transferred between pigment molecules by Förster resonance energy transfer (FRET) (transfer of excitation energy from one electron to another) or Dexter energy transfer (exchange of electrons with different excitation energies) and funnelled into the reaction centres of either photosystem I (PSI) or photosystem II (PSII). Here, a special pair of chlorophyll molecules becomes excited resulting in electron transfer and charge separation. These are P700 (in PSI) and P680 (in PSII), named for the wavelength of their absorption peak. The differences in the absorption spectra of the two photosystems broaden the spectrum of light available for use in photosynthesis. However, when there is preferential excitation from variations in the spectral quality of absorbed light, these differences make the system susceptible to imbalances in the relative amounts of ATP and NADPH produced (Johnson, 2016).

PSII regenerates its special pair chlorophylls using electrons released from splitting a water molecule, a process that also releases two protons into the thylakoid lumen. PSII then reduces a plastoquinone (PQ) molecule from the 'PQ pool' within the thylakoid membrane. The reduced PQ (plastoquinol/PQH<sub>2</sub>) diffuses back out into the PQ pool, where it can be taken up by the cytochrome *b<sub>6</sub>f* complex (*cyt<sub>b6</sub>f*) and oxidised. Using these electrons from PQ, *cyt<sub>b6</sub>f* then reduces the small soluble protein plastocyanin (PC) in the thylakoid lumen while transferring two more protons from the stroma to the lumen. Absorption of light energy by PSI results in excitation of the P700 special pair, electron transfer and charge separation. Reduced plastocyanin supplies electrons to regenerate P700<sup>+</sup> and PSI uses the energy-boosted electrons to reduce the stromal iron-sulphur protein ferredoxin (Fd). This protein works with ferredoxin-NADP<sup>+</sup> reductase (FNR), to produce NADPH. As the lateral transfer of electrons through the thylakoid membrane is coupled to uptake of protons from the stroma and release

of protons into the thylakoid lumen, a transmembrane proton gradient ( $\Delta\text{pH}$ ) accumulates, which powers the synthesis of ATP by ATP synthase. Chloroplastic ATP synthase produces one molecule of ATP for every 4.67 protons that pass through it (Hahn et al., 2018; Petersen et al., 2012). Since the photolysis of one water molecule results in the transfer of 6 protons into the thylakoid lumen, the process has a net output of 1.28 ATP and one NADPH. This route of electron transfer is termed linear electron transfer (LET) or the 'Z scheme' and is shown on the top panel of Figure 1.

The CBB cycle uses 1.5 ATP for every NADPH. Therefore, if linear electron transfer were the only way to generate substrates for the CBB cycle, there would be a shortfall in the amount of ATP produced. Instead, there is an additional, alternative route termed cyclic electron transfer (CET), which involves only PSI, where electrons from Fd are returned to the PQ pool by a ferredoxin-plastoquinone oxidoreductase (FQR) instead of continuing on to the CBB cycle. This process allows additional proton motive force generation and ATP synthesis without any net NADPH production (Johnson, 2007). CET may be triggered when there is not enough  $\text{NADP}^+$  available to accept electrons, or when the cell has a particularly high demand for ATP. Since the relative demand for ATP and NADPH is affected by a range of environmental and developmental factors, flexibility in the balance of LET and CET is critical for maintaining photosynthetic efficiency. ATP demand is elevated during high levels of biosynthesis, such as in young leaves, and in photorespiration, where Rubisco oxygenates, rather than carboxylates, RuBP. Instead of one of the two PGA molecules, phosphoglycolate, which cannot be productively utilised by the CBB cycle, is produced and the extensive process of converting it back to PGA requires ATP. Conversely, nitrogen assimilation decreases ATP/NADPH demand, thus requiring less CET. Another function of CET may be to decrease lumenal pH for the activation of photoprotective quenching mechanisms and photosynthetic control (Nawrocki et al., 2019).

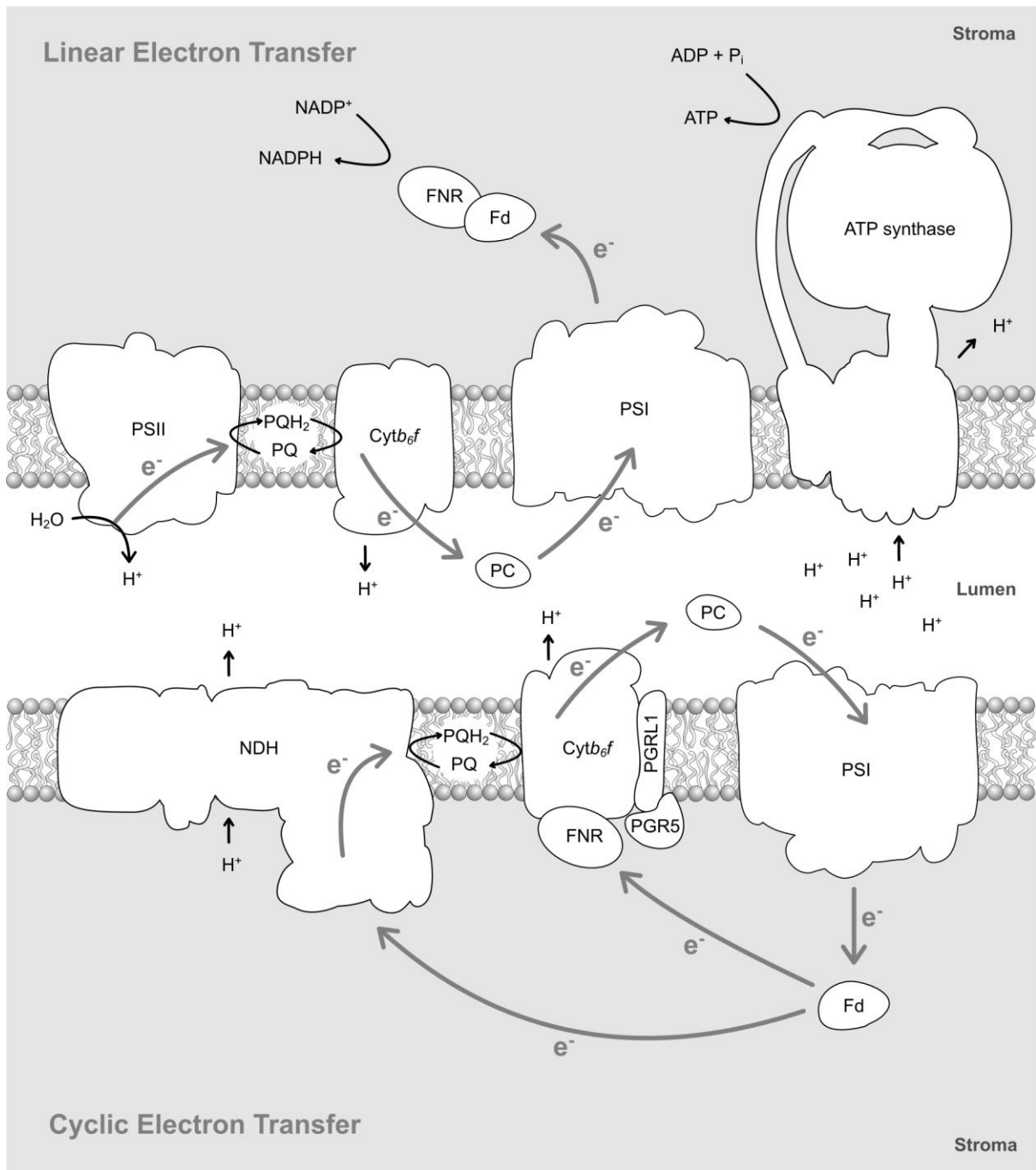


Figure 1: Electron transfer through the thylakoid membrane.

Two routes of CET are thought to exist, and are shown on the bottom panel of Figure 1: The NDH-dependent pathway and the PGR5/PGRL1-dependent pathway. The NADH dehydrogenase-like complex (NDH), now increasingly referred to as ‘Photosynthetic Complex I’, is a large but low-abundance multi-subunit protein complex, which shares at least 11 subunits with the mitochondrial and bacterial respiratory Complex I and is thought to be a direct FQR (Nawrocki et al., 2019). It forms a supercomplex with PSI via LHCA5 and LHCA6 of the PSI antenna (Peng et al., 2009). The structure and function of the NDH complex is discussed further in Section 1.2.4. As shown in Figure 1, PSI

receives electrons from *cytb<sub>6</sub>f* via plastocyanin (PC) and reduces Fd, but these electrons are then returned to the PQ pool via NDH, coupled to the transfer of protons into the thylakoid lumen.

The second route, involving PGR5/PGRL1, is suggested to play an important role in protection of PSI under high or fluctuating light. Figure 1 shows the transfer of electrons from the reduced Fd generated by PSI to *cytb<sub>6</sub>f* via FNR and PGR5, which is tethered to the thylakoid membrane on the stromal side by PGLR1 (Nawrocki et al., 2019). As well as forming a complex with PGR5, PGRL1 has been shown to interact with FNR, Fd, *cytb<sub>6</sub>f*, and PSI (DalCorso et al., 2008). Despite evidence of the ability of the PGRL1/PGR5 complex to accept electrons from Fd and reduce PQ (Hertle et al., 2013), there remains discussion about the function of these proteins, whether they are direct FQR's, mostly act in a regulatory role, and about the presence of an additional FQR (Nawrocki et al., 2019; Suorsa, 2015). However, it was recently demonstrated that PGR5 is necessary for the switching of *cytb<sub>6</sub>f* between the LET Q-cycle (Section 1.2.2) and a modified Q-cycle for CET (Buchert et al., 2020).

Aside from LET and CET, other more minor electron transfer routes exist. In higher plants and algae, one of these pathways is chlororespiration. In this process, NDH reduces PQ, which is then oxidised by the plastid terminal oxidase (PTOX) and the electrons used to produce water (Kanervo et al., 2005). The Mehler-ascorbate peroxidase pathway (MAP), or water-water cycle, involves the reduction of O<sub>2</sub> to make water. Various functions are proposed for the MAP pathway, including ROS scavenging and as an electron sink. Two water molecules are split by the PSII OEC, releasing O<sub>2</sub>, which is then reduced by PSI in the Mehler reaction. Superoxide dismutase uses the resulting ROS to make H<sub>2</sub>O<sub>2</sub>, which is in turn reduced and converted to back to water by ascorbate peroxidase using electrons from ascorbate. The MAP pathway also contributes to ΔpH and, therefore, ATP synthesis (Kanervo et al., 2005; Miyake, 2010).

High levels of flux through the electron transfer chain can cause a build-up of excess reducing equivalent such as NADPH, resulting in ROS production, known to cause oxidative damage to the photosynthetic machinery and trigger regulatory networks (Foyer, 2018). Because, unlike NADP<sup>+</sup>, NADPH cannot be transferred across membranes to meet demands elsewhere in the cell, a mechanism known as the 'malate valve' is necessary to maintain redox homeostasis in the chloroplast. Under redox stress, reduced Fd from the electron transport chain can reduce thioredoxin in a system referred to as the ferredoxin-thioredoxin system, which reduces disulphide bonds within a number of enzymes to regulate their activity. One of these enzymes is malate dehydrogenase (MDH), which is activated upon disulphide bond reduction and catalyses the reversible NADPH-dependent conversion of oxaloacetate to malate, releasing NADP<sup>+</sup>. Malate may then leave the chloroplast via dicarboxylate translocators and be taken up elsewhere where reducing equivalent is needed, such as the mitochondria, and be dehydrogenated by MDH to produce NADPH or NADH (Selinski and Scheibe, 2019; Zhao et al., 2020b).

## 1.2 Structure and function of the key photosynthetic complexes

### 1.2.1 The photosystems and their light-harvesting antennas

Photosystem II, the first complex of the LET chain, reduces plastoquinone (PQ) to plastoquinol (PQH<sub>2</sub>) and replenishes the lost electrons by splitting a water molecule (Kern and Renger, 2007). The reaction centre of the complex consists of a heterodimer of the proteins D1 and D2, which hold the P680 special pair chlorophylls, one of which becomes the highly oxidising P680<sup>+</sup> chlorophyll capable of splitting water. Two other core proteins, CP43 and CP47, bind the OEC, which is stabilised by an additional protein, PSBO. The OEC, coordinated in the luminal side of the thylakoid membrane by residue side chains of CP43 and D1, is a cubane cluster of manganese ions, a calcium ion, and oxygen atoms with the formula Mn<sub>4</sub>O<sub>5</sub>Ca. The cluster binds and splits two water molecules, extracting two oxygen atoms to be released as O<sub>2</sub>, 4 protons for release into the thylakoid lumen to generate a proton gradient, and 4 electrons which are transferred sequentially to a tyrosine residue of D1 (Tyr-Z). Oxidation of the D1 P680 chlorophyll by an absorbed photon is reversed by the electron from this tyrosine residue. Electrons from P680 transfer to pheophytin then to a plastoquinone in D2 (Q<sub>A</sub>) then to a second plastoquinone in D1 (Q<sub>B</sub>). This Q<sub>B</sub> plastoquinol leaves the reaction centre and diffuses into the lipid bilayer. The subunits of the PSII reaction centre are shown in Table 1.

Table 1: Subunits of photosystem II

Subunit	Alternative names
PSBA	D1
PSBB	CP47
PSBC	CP43
PSBD	D2
PSBE	Cytochrome b559 subunit $\alpha$
PSBF	Cytochrome b559 subunit $\beta$
PSBH	
PSBI	
PSBJ	
PSBK	
PSBL	
PSBM	
PSBO1	Oxygen-evolving enhancer protein 1-1
PSBO2	Oxygen-evolving enhancer protein 1-2
PSBP1	Oxygen-evolving enhancer protein 2-1
PSBP2	Oxygen-evolving enhancer protein 2-2
PSBQ1	Oxygen-evolving enhancer protein 3-1
PSBQ2	Oxygen-evolving enhancer protein 3-2
PSBR	
PSBS	
PSBT	

Bound to the PSII reaction centre are additional chlorophyll-containing proteins – the light-harvesting antenna complexes (Figure 2). These exist as the monomeric antenna proteins LHCB4/CP29, LHCB5/CP26, and LHCB6/CP24, and LHCII trimers consisting of LHCB1, LHCB2 and LHCB3 in different combinations. The reaction centre subunits D1 and D2 are linked to the monomeric antenna via CP47 and CP43, and a number of low molecular weight subunits span the membrane and stabilise the core. Monomeric antenna proteins link the PSII core to the peripheral LHCII trimers, controlling the formation of supercomplexes and directing excitation energy into the reaction centre. PSII is mostly present in the thylakoid membrane as a dimer, in supercomplexes containing variable numbers of LHCII trimers. These trimers are named according to the strength of their interaction with the PSII core (C): strongly bound (S), moderately bound (M), and loosely bound (L) trimers. Single particle cryo-electron microscopy (cryo-EM) has revealed the structure of the C<sub>2</sub>S<sub>2</sub>M<sub>2</sub> supercomplex from plant thylakoids (van Bezouwen et al., 2017; Su et al., 2017). However, while PSII supercomplexes are also thought to

exist in the forms  $C_2S_2$ ,  $C_2S_2M$ ,  $C_2S_2M_2L$ , and  $C_2S_2M_2L_2$  (Sheng et al., 2019), the most abundant in physiologically relevant conditions varies according to species. Early work in barley plants grown in greenhouse conditions identified LHCII as the most abundant protein in the thylakoid membrane, constituting around 30% of all protein (Peter and Thornber, 1991), though this value likely varies substantially in response to environmental conditions. The composition of the LHCII trimers, whether homotrimeric or heterotrimeric, determines their position in the supercomplex and functional role. LHCBI, of which there are five isoforms LHCBI.1-1.5 in Arabidopsis, is the most abundant component and is able to form homotrimers. Between 20 and 30% of LHCII trimers contain two LHCBI and one LHCBI2 (Vener, 2007), which is the main target of phosphorylation by the kinase STN7 (Leoni et al., 2013). LHCBI2 is present as three nearly identical isoforms in Arabidopsis: LHCBI2.1, 2.2 and 2.4. The third component of LHCII trimers, LHCBI3, forms heterotrimers with LHCBI1 and is only present in the M trimers (Damkjær et al., 2009). Complexes lacking M trimers, i.e. the  $C_2S_2$  complex, lack both LHCBI3 and the monomeric antenna LHCBI6, which acts as a linker to the PSII core (Pagliano et al., 2014). The S trimer, on the other hand, is linked to the core by LHCBI5.

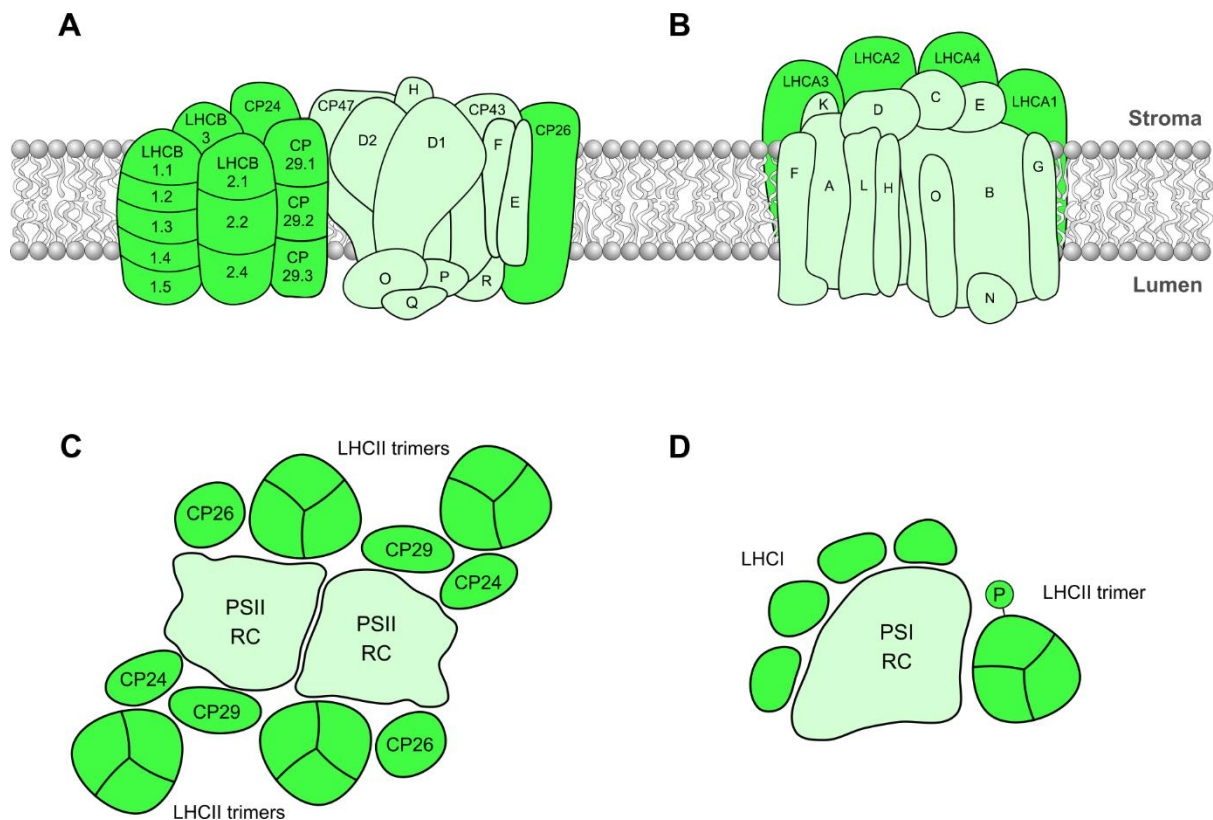


Figure 2: Structural organisation of the photosystems and their antenna. Schematic diagrams to represent A, the positions of PSII reaction centre proteins and its antenna subunits, B, the positions of PSI reaction centre subunits and its antenna, C, the arrangement of the PSII  $C_2S_2M_2$  supercomplex, and D, the arrangement of the PSI-LHCI-LHCII supercomplex. Antenna proteins are shown in bright green, whereas reaction centres are light green.

The second photosystem of the LET chain and the only photosystem involved in CET is PSI, the reaction centre of which consists of 14 subunits shown in Table 2. The two main subunits of the PSI

reaction centre are PSAA and PSAB, which hold the P700 special chlorophyll pair. When the P700 special chlorophyll pair absorbs light energy, an electron is promoted to a higher energy level and transfers to a modified chlorophyll *a* molecule termed  $A_0$  and is replaced by an electron from plastocyanin, which binds at the PSAF subunit. The high-energy electron from P700 passes from  $A_0$  to the phylloquinone  $A_1$ , then through a series of iron-sulphur centres coordinated by the subunits PSAB and PSAC. These electrons are then used for the reduction of Fd on the stromal side of the membrane, at the PSAE subunit (Erik et al., 2007). Fd interacts with FNR and its electrons are directed to either NADPH synthesis or CET to increase ATP synthesis. The reaction centre of PSI is flanked by a row of at least 4 monomeric antenna proteins: LHCA1, LHCA2, LHCA3 and LHCA4 (Figure 2). In Arabidopsis there are two more isoforms, LHCA5 and LHCA6, which are proposed to bind NDH (Peng et al., 2009). The PSAH and PSAL subunits are capable of binding a LHCII trimer (Erik et al., 2007) via its LHCB2 subunit, when phosphorylated, to direct more energy to PSI in a process known as state transitions (Section 0).

Table 2: Subunits of the PSI reaction centre.

Subunit	Alternative names
PSAA	PSI P700 chlorophyll <i>a</i> protein A1
PSAB	PSI P700 chlorophyll <i>a</i> protein A2
PSAC	PSI iron-sulphur center
PSAD1	
PSAD2	
PSAE1	
PSAE2	
PSAF	
PSAG	
PSAH1	
PSAH2	
PSAI	
PSAJ	
PSAK	
PSAL	
PSAN	
PSAO	

### 1.2.2 Cytochrome *b<sub>6</sub>f*

The second protein complex and rate-limiting step of the LET chain is *cytb<sub>6</sub>f*, which links PSII to PSI by accepting electrons from PQH<sub>2</sub> and transferring electrons to plastocyanin in the lumen. *Cytb<sub>6</sub>f* also

functions to transfer protons into the thylakoid lumen and contributes to the formation of  $\Delta pH$  for ATP synthesis. The four main subunits (Table 3) of *cytb<sub>6</sub>f* are cytochrome *f* (PETA), cytochrome *b<sub>6</sub>* (PETB), the Rieske iron-sulphur protein (PETC), and subunit IV (PETD). Four smaller subunits (PETG, PETL, PETM and PETN) surround the periphery of the complex, which is found as a dimer. The complex contains various cofactors including a 2Fe-2S cluster (known as the Rieske iron-sulphur cluster), four haems, of which two are b-type and two are c-type, as well as chlorophyll *a* and  $\beta$ -carotene. Recently, the cryo-EM structure of the spinach *cytb<sub>6</sub>f* complex revealed a role for the chlorophyll *a* molecule as a ‘gating’ mechanism for PQH<sub>2</sub> access to its binding site, dependent on the redox state of the PQ pool (Malone et al., 2019).

Table 3: Subunits of cytochrome *b<sub>6</sub>f*

Subunit	Alternative names
PETA	Cytochrome <i>f</i>
PETB	Cytochrome <i>b<sub>6</sub></i>
PETC	Iron-sulphur subunit
PETD	Subunit IV
PETG	
PETL	
PETM	
PETN	

The process by which *cytb<sub>6</sub>f* catalyses the oxidation of PQH<sub>2</sub> and the reduction of PQ is termed the quinol cycle (Q-cycle). When a PQH<sub>2</sub> molecule binds and is oxidised, at a location known as the Q<sub>p</sub> site on the luminal side of the complex, two protons are released into the thylakoid lumen and the two electrons bifurcate into separate redox potential pathways. One is the high potential pathway leading to plastocyanin via the Rieske iron-sulphur cluster, while the other, the low potential pathway, leads to a bound PQ molecule at the Q<sub>n</sub> site on the stromal side via the b-type haems. A second PQH<sub>2</sub> is oxidised and used, along with two protons from the stroma, to regenerate the bound PQ molecule at the Q<sub>n</sub> site to PQH<sub>2</sub> via the low potential pathway. In this way, *cytb<sub>6</sub>f* doubles the number of protons transferred into the thylakoid lumen for each PQH<sub>2</sub> that is oxidised. PQH<sub>2</sub> oxidation at the Q<sub>p</sub> site is the rate-limiting step of the LET chain, rather than the reduction of PQ and diffusion of PQH<sub>2</sub> to *cytb<sub>6</sub>f* (Tikhonov, 2014). When *cytb<sub>6</sub>f* senses reduction of the PQ pool through PQH<sub>2</sub> binding at the Q<sub>p</sub> site, it signals to activate the LHCII kinase STN7 through binding at the Rieske subunit, making this complex important as a redox-sensing hub in addition to its role in electron transfer (Shapiguzov et al., 2016; Vener et al., 1997).

### 1.2.3 ATP synthase

ATP synthase utilises the  $\Delta\text{pH}$  generated by the light reactions of photosynthesis. Protons flowing across the thylakoid membrane into the stroma power a rotational motor mechanism for ATP production. Cryo-EM was used recently to determine the structure of chloroplast ATP synthase from spinach at a resolution of 2.9 to 3.4 Å (Hahn et al., 2018). In total, the enzyme is made up of 26 subunits, divided between two regions; the arrangement of which is shown in Figure 3. The hydrophilic head region ( $\text{cF}_1$ ), which catalyses the phosphorylation of ADP to ATP, contains three  $\alpha$  and three  $\beta$  subunits alternating in a ring around a  $\gamma$  and an  $\epsilon$  subunit making up the central stalk of the hydrophobic motor region ( $\text{cF}_0$ ). The peripheral stalk of  $\text{cF}_0$ , made up of the  $b$ ,  $b'$  and  $\delta$  subunits, connects to the proton-translocating, membrane-embedded  $c$ -ring. The  $c$ -ring of chloroplast ATP synthase contains 14 monomers, compared to the yeast mitochondrial ATP synthase with 10  $c$  subunits. The size of the  $c$ -ring in plant mitochondrial ATP synthase is currently unknown (Zancani et al., 2020). Chloroplast ATP synthase has features specific to photosynthesis that are not present in respiratory forms. To prevent ATPase activity – the reverse reaction of ATP synthase where ATP hydrolysis powers pumping of protons into the thylakoid lumen - in the dark when photosynthesis is not occurring, chloroplast ATP synthase is inhibited by a redox switch. In the dark, when conditions in the chloroplast are more oxidising, a redox loop located in the  $\gamma$  subunit forms a disulphide bond and interacts with a  $\beta$  subunit to block rotation.

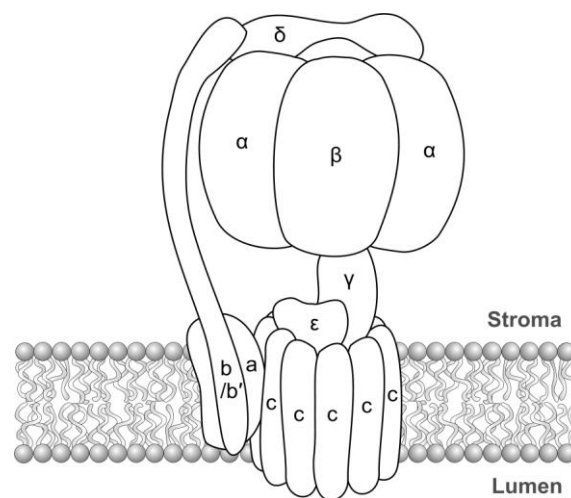


Figure 3: Structural arrangement of the chloroplast ATP synthase.

### 1.2.4 NDH

In Arabidopsis, NDH is a very large but low-abundance complex comprises five subcomplexes. While NDH was first named for its supposed NADPH dehydrogenase activity, the complex is now increasingly referred to as ‘photosynthetic complex I’ as it is highly homologous to the respiratory complex I but, unlike the mitochondrial complex, NDH does not actually appear to function as such.

Rather, it is now thought to catalyse the Fd-dependent reduction of PQ (Munekage et al., 2004; Shikanai, 2016). Through this activity, NDH mediates CET to augment ATP production by diverting electrons from PSI into the PQ pool. The NDH complex is more efficient for enhancing ATP synthesis than other routes of CET, transferring eight protons into the thylakoid lumen for every PQ molecule it reduces. Interestingly, mutants lacking NDH components, at least in C3 plants, do not have dramatic photosynthetic or growth phenotypes so the biological significance and redundancy of this complex is uncertain. Possibly, under some conditions where there is a surplus of ATP, NDH may function in reverse to generate more reduced Fd, powered by  $\Delta\text{pH}$  (Strand et al., 2019). Another proposed role is that the complex functions in chlororespiration alongside PTOX, similarly to complex I in the respiratory chain. NDH forms supercomplexes with PSI, whereby up to 6 PSI monomers may associate with one NDH complex to improve the localised efficiency of NDH-dependent CET (Yadav et al., 2017). The minor PSI antenna proteins LHCA5 and LHCA6, present at substoichiometric amounts relative to PSI (Ganeteg et al., 2004), are required for the formation of these supercomplexes, which are proposed to link PSI and NDH to one another (Peng et al., 2009).

Table 4: Subcomplexes of the NDH complex and their subunits.

Subcomplex	Subunit
M	NDHA
	NDHB
	NDHC
	NDHD
	NDHE
	NDHF
	NDHG
A	NDHH
	NDHI
	NDHJ
	NDHK
	NDHL
	NDHM
	NDHN
NDHO	
B	PNSB1
	PNSB2
	PNSB3
	PNSB4
	PNSB5
L	PNSL1/PPL2
	PNSL2/PQL
	PNSL3/PQL
	PNSL4/FKB16-2
	PNSL5/CYP20-2
EDB	NDHS
	NDHV
	NDHT/CRRJ
	NDHU/CRRL

NDH shares evolutionary origins with NDH-1 in cyanobacteria. However, NDH features additional subdomains absent in cyanobacteria and is encoded from a mixture of nuclear and plastid genes. The five subdomains of NDH in chloroplasts are subcomplex A and the membrane subcomplex (subcomplex M), both of which are also found in cyanobacteria, subcomplex B, the luminal subcomplex (subcomplex L), and the electron donor binding subcomplex (EDB subcomplex). The individual subunits and their corresponding subcomplexes are shown in Table 4. Subcomplex A corresponds to the Q module in respiratory complex I and functions to reduce PQ. It is not required for interaction of NDH with PSI. Subcomplex A forms a Fd binding site along with the EDB subcomplex,

which also contains J proteins (NDHT and NDHU), a type of molecular chaperone. The function of subcomplex B is currently unclear, but it is required for stability of the complex. Subcomplex B contains an Fe-S cluster but is unlikely to be involved in electron transfer between Fd and PQ because it is missing in the cyanobacterial equivalent complex NDH-1. Subcomplex M is comparable to the P module in complex I, functioning in proton translocation into the thylakoid lumen. Subcomplex L in the thylakoid lumen is required for stability of the complex. It contains proteins homologous to those of the OEC of PSII, PSBP and PSBQ, as well as proteins with peptidyl-prolyl cis-trans isomerase activity, thought to be involved in protein folding (Shikanai, 2016).

### 1.3 Thylakoid architecture

The thylakoid membrane of higher plants is one of the most complicated membrane superstructures known. It has a heterogeneous and dynamic three dimensional structure, which is divided into densely packed cylinders of stacked membranes, called the grana, and connecting sections of membrane called the stroma lamellae. PSI and ATP synthase are found only in the stroma lamellae whereas PSII is located mostly in the grana stacks (Andersson and Anderson, 1980). Another region, known as the grana margins, is thought to contain a mixture of the two photosystems and may have roles in PSII repair, although its existence as a distinct domain remains contentious. The two photosystems are physically separated primarily to prevent energy spillover from PSII into PSI, which acts as an energy sink, and to separate linear and cyclic electron transfer. CET takes place in the stroma lamellae only (Albertsson, 2001). Segregation and balance of activity from the two photosystems is important for maximum efficiency of electron transfer, while tight stacking of thylakoid membranes allows more chlorophyll-containing proteins to be packed into a given volume of chloroplast. An electron micrograph of an *Arabidopsis* chloroplast is shown in Figure 4. While negative stain EM of leaf thin sections can be used to observe and analyse thylakoid membrane structure within a chloroplast, cryo-electron tomography has revealed a number of additional features of its three dimensional structure (Austin and Staehelin, 2011; Daum et al., 2010; Kowalewska et al., 2016). Firstly, the darker colour of the stroma indicates a higher protein density than in the luminal space. The grana form cylinders, around which the stroma lamellae protrude and wrap helically. Between the grana and stroma lamellae are the grana margin connecting regions, which are staggered between grana membrane layers. ATP synthase is located only in the stroma lamellae regions and the flat regions of stroma-exposed end membranes at the top and bottom of the grana. While *cyt<sub>b</sub><sub>6</sub>f* dimers are distributed throughout both the grana and stroma lamellae, in the grana they have been found to be located in close proximity to PSII to increase the efficiency of PQ transfer between the complexes (Johnson et al., 2014). The physical basis for membrane stacking in the grana comes from multiple factors and protein-protein interactions. Granal LHCII trimers interact with one another between membrane layers (Day et al., 1984) through non-specific but complementary positively and negatively charged areas on the stromal side. Another important factor to consider regarding thylakoid structure is its lipid composition. Lipids make up around 20% of the dry mass of

chloroplasts and are integral to protein complex formation. Around 50% of the lipid in the thylakoid membrane is monogalactosyldiacylglycerol, followed by digalactosyldiacylglycerol at around 30% (Garab et al., 2000), and the galactolipid composition of the thylakoid membrane contributes significantly to its complex structure (Kowalewska et al., 2019).

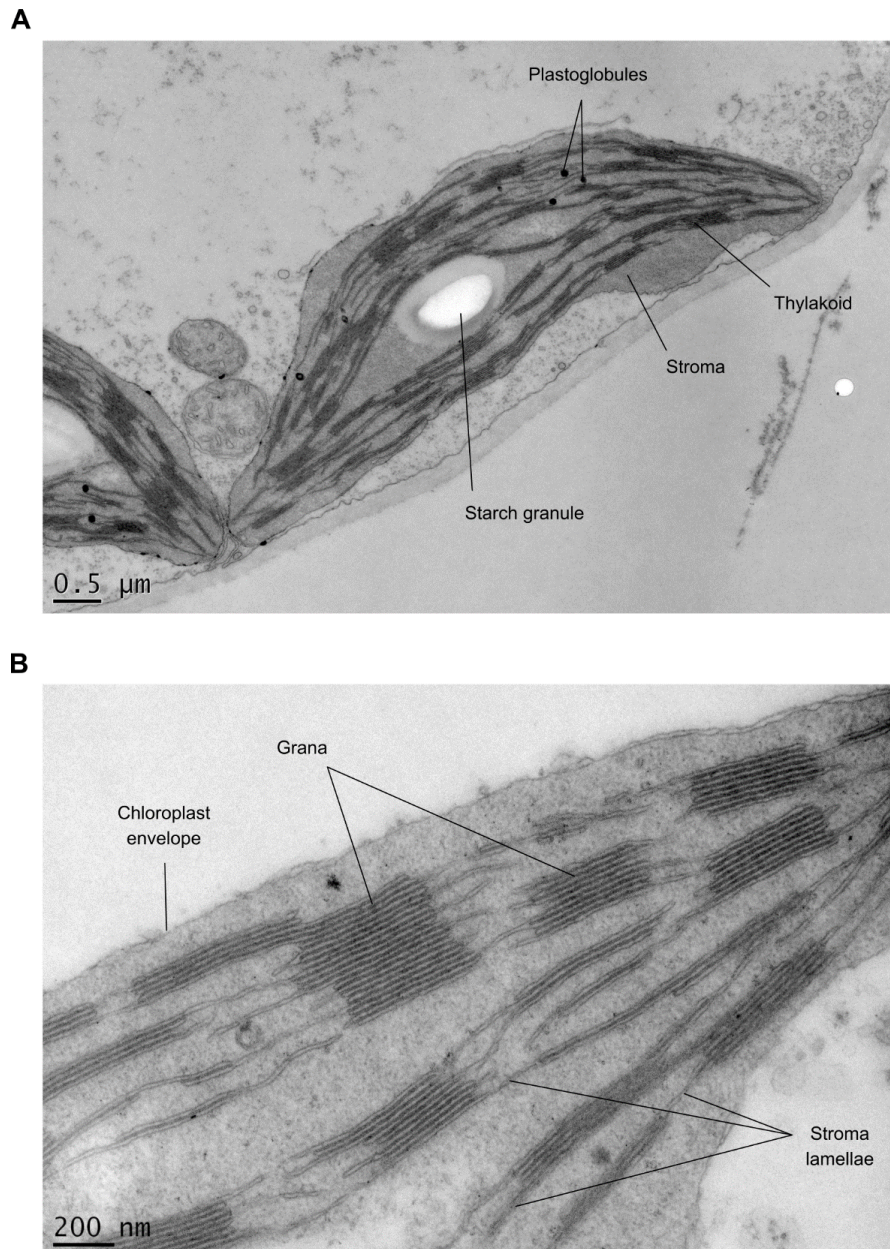


Figure 4: Electron micrographs of *Arabidopsis* chloroplasts at **A**, 2900× and **B**, 9300× magnification.

A less well-studied feature of the thylakoid membrane, highlighted in Figure 4A, is the plastoglobule. Initially viewed as passive storage spaces for thylakoid lipids and carotenoids, proteomic analysis has revealed plastoglobules as crucial participants in chloroplast metabolism, redox regulation, and remodelling of the photosynthetic machinery to adapt to environmental stresses (Nacir and Bréhélin, 2013). Plastoglobules are contiguous with the thylakoid membrane, formed from the outer leaflet of the

thylakoid membrane both constitutively at lower levels and at higher levels as a stress response and during chloroplast senescence, comprising a membrane microdomain for the recruitment and concentration of metabolic enzymes and products (Lundquist et al., 2013). They contain various lipids including phylloquinone (also found in PSI), PQ, triacylglycerol,  $\alpha$ -tocopherol, and the enzymes for their synthesis such as VTE1 for tocopherol synthesis and phytyl esterases. NDC1 is capable of reducing PQ, while the ABC1 kinase PGR6 phosphorylates and possibly regulates the activity of VTE1 (Martinis et al., 2014). None of the proteins in the plastoglobule are membrane proteins, structurally, and some may associate with the hydrophilic heads of lipids on the outside of the globule. For example, plastoglobules contain structural proteins called fibrillins, many of which contain lipocalin domains, suggesting additional or alternative roles in metabolite transport. A proteomic analysis by Lundquist et al., 2012, assigned 30 proteins to the plastoglobule proteome, with seven fibrillins and six ABC1 kinases making up over 70% of the total protein. Plastoglobules may also play a role in the regulation of starch synthesis, since the starch synthase SS4 associates with plastoglobular fibrillins (Gamez-Arjona et al., 2014).

#### 1.4 Adaptation of photosynthesis to the light environment

Plants have evolved to survive and flourish in a wide range of light environments from arid sun-soaked deserts to the deep shade of the rainforest floor. Even within particular environmental niches, the intensity and spectral quality of irradiance can fluctuate dramatically according to the season, time of day, meteorological conditions and because of dynamic shading within plant canopies. Changing light intensity affects the balance between solar energy absorption and its utilisation in photosynthesis, potentially leading to metabolic imbalances that trigger photooxidative stress and/or slower growth and development (Foyer and Noctor, 2005; Li et al., 2009). In low light, the rate of photosynthesis is limited primarily by the efficiency of light capture by antenna complexes and delivery of energy to the reaction centres. In high light, the rate of photosynthesis is limited by factors within both the light and dark reactions. The slow rate of carboxylation by Rubisco limits sink capacity in the stroma, while high light intensity reaching the thylakoid membrane, as well as the difference in the rate of energy capture and transfer compared to the relatively slower rate of electron transport, causes saturation and damage to reaction centres (Mann, 1999; Ruban, 2009). Therefore, being mostly immobile, land plants must react to changing light levels to maximise their photosynthetic efficiency. Plants have evolved a complex network of short and long-term responses to optimise photosynthesis to the prevailing light environment allowing them to control the amount of light absorbed as well as those that help them to manage that energy. The short-term responses take place on a timescale of seconds to minutes and involve regulatory mechanisms that alter the structure and function of existing proteins (Ruban, 2016; Theis and Schroda, 2016; Tikkanen and Aro, 2014; Yamori and Shikanai, 2016). In contrast, long-term responses involve both *de novo* synthesis and specific degradation of proteins that lead to changes in leaf morphology, number of chloroplasts per cell, organisation of the chloroplast thylakoid membranes, their protein

composition and that of the surrounding stroma that contains the enzymes of the CBB cycle (Adams et al., 2007; Anderson et al., 1988; Boardman, 1977; Schöttler and Tóth, 2014; Walters, 2005). The long-term response to growth light irradiance of an individual plant is termed ‘acclimation’ and is controlled by multiple regulatory mechanisms to produce distinct reactions to low light and high light (Bailey et al., 2001; Kouřil et al., 2013).

#### 1.4.1 PSII damage and repair

The reaction centre of PSII is highly susceptible to damage from excess light, termed photoinhibition. Excess excitation arising from high irradiance leads to production of more electrons than the photosynthetic machinery has the capacity to utilise. Reactive oxygen species are generated, aided by triplet chlorophyll and lipid peroxidation, and can damage protein structure and electron transport components. Visible light can also damage the  $Mn_4Ca$  cluster, which can then lead to further damage through the formation of the  $P680^+$  and  $Tyr-Z^+$  oxidising radicals (Johnson, 2007). Most damage to PSII occurs at the D1 reaction centre subunit, at a level directly proportional to light intensity. In barley plants grown at  $500 \mu\text{mol m}^{-2} \text{s}^{-2}$ , D1 has a half-life of 2.4 h (Nelson et al., 2014). In order to repair this component, the whole of the PSII complex – containing 28 subunits – must be disassembled. Before the complex is disassembled, damaged PSII must be moved from the grana to the stroma lamellae, where many components of the repair machinery are enriched. Phosphorylation of D1, D2, CP43 and PSBH by kinases including STN8 and, to a lesser extent, STN7 facilitates monomerisation of PSII and movement out of the grana into the non-appressed stroma lamellae regions. Once mobilised, PSII is dephosphorylated by PBCP and other phosphatases. The damaged D1 protein is degraded by the FTSH and DEG proteases then a new D1 is inserted into the complex. PSII is reassembled and migrates back to the grana where it dimerises and forms active PSII-LHCII supercomplexes. Whilst the PSII repair machinery is subject to complex regulation in response to high light, the damage and repair process occurs continually in all light conditions (Järvi et al., 2015; Nath et al., 2013). It was previously assumed that photoinhibition by PSII damage was a fault of the system, which was compensated for by the extensive repair machinery. However, a recently proposed theory is that there is a physiological purpose for PSII damage and repair, in that it reduces damage to PSI, which lacks the extensive repair machinery of PSII and takes much longer to replace (Järvi et al., 2015).

#### 1.4.2 Short term responses to light intensity

To deal with faster fluctuations in light intensity such as changing cloud cover and the movement of leaves in the wind, plants have short-term responses, occurring on a timescale of seconds to minutes, that are readily reversible. These responses occur on various levels, from leaf movement to physically reach or avoid light, opening and closing of stomata to control gas exchange, Rubisco activation in control of  $\text{CO}_2$  fixation, down to the regulation of light harvesting and electron transfer in the thylakoid membrane. The aim of short-term high light responses in the thylakoid membrane is generally photoprotection through downregulation of light harvesting and electron transfer (Gjindali et al., 2021),

whereas the long-term aim is to restore homeostasis by adjusting the sink capacity of the system to better utilise the increased light level. The aim of short-term low light responses is generally to manage and divert absorbed light energy to balance the ATP and NADPH output to maintain efficient CO<sub>2</sub> fixation. Although proteins involved in these processes are generally regulated by post-translational modifications such as protonation or phosphorylation, rather than by alterations in transcription or translation, the capacity for these responses may be affected by long-term acclimation.

Short-term mechanisms are activated not by the intensity of light that the leaf is exposed to but by mismatches in the electron transfer rate and sink capacity of the photosynthetic machinery. When there is an increase in electron flux that exceeds the sink capacity for those electrons, the system must decrease electron transfer to avoid damage. Likewise, when electron flux is lower than is optimal for the system, energy absorption and transfer is maximised. Therefore, the activation of short-term mechanisms depends on the position of the photosynthetic 'steady state' arising from long-term acclimation to the light environment. Plants adapted to different light environments will initiate short-term responses at different light intensities from one another.

#### *1.4.2.1 Non-photochemical quenching*

Photoinhibition is the loss of PSII electron transfer activity through photooxidative damage to the reaction centre induced by light. To avoid photoinhibition, plants possess several mechanisms of photoprotective energy dissipation. The dissipation of excess excitation energy as heat can be measured as the non-photochemical quenching (NPQ) of chlorophyll *a* fluorescence (Schreiber, 1986). Several different components of NPQ exist that can be distinguished on the basis of their temporal evolution. The major component is energy (i.e.  $\Delta\text{pH}$ )-dependent quenching (qE), which forms and relaxes on a timescale of seconds to minutes. qE is triggered by a decrease in the luminal pH resulting in the protonation of the violaxanthin de-epoxidase enzyme (VDE) and the PSBS protein. VDE converts LHCII-bound violaxanthin to zeaxanthin and this together with the protonation induced monomerisation of PSBS allosterically promotes a conformational change in LHCII, from a light harvesting mode to a dissipative mode, leading to its reversible aggregation (Johnson et al., 2011; Murchie and Ruban, 2020). Part of the NPQ induced during the excess light period is maintained for several hours afterwards due to the slow reconversion of zeaxanthin back to violaxanthin by the enzyme zeaxanthin epoxidase and is known as qZ. Depending on the efficiency of qE induction, some photoinhibition of PSII may still occur leading to another persistent form of NPQ known as qI, which involves damage to the RC and requires PSII repair (Matsubara and Chow, 2004). A third form of sustained quenching known as qH, recently discovered, involves the luminal located lipocalin protein (LCNP) (Malnoë et al., 2018). Reversal of qH occurs through the action of the SOQ1 and ROQH1 proteins, though the exact mechanisms involved remain to be elucidated (Amstutz et al., 2020; Brooks et al., 2013).

#### 1.4.2.2 *Photosynthetic control*

While considered less susceptible to photooxidative damage than the reaction centre of PSII, damage to and inactivation of PSI is costly. Unlike PSII, PSI does not have the extensive machinery for disassembly, storage of non-damaged peripheral subunits, and reassembly, so the entire complex must be replaced. The main source of damage to the PSI reaction centre is electron transfer to the acceptor side, where over-reduction of the electron transfer chain causes oxidative damage to Fe-S clusters on the stromal side of PSI. Therefore, photoprotection of PSI is linked to the downregulation of LET, which is in turn controlled by PSII activity. For this reason, photoprotection of PSI is connected to that of PSII. Mechanisms that control energy transfer to and activity of PSII, such as NPQ and state transitions, indirectly protect PSI. However, the primary photoprotective mechanism of PSI is ‘photosynthetic control’ (Rumberg et al., 1968; West and Wiskich, 1968). Photosynthetic control is the regulation of electron transfer through the thylakoid membrane to account for changing demands and capacity for ATP production, while also protecting PSI by limiting the build-up of electrons on the acceptor side (Suorsa et al., 2013).

When plants are exposed to high light irradiance, the increased  $\Delta\text{pH}$  slows the turnover of the *cytb<sub>6</sub>/f* complex via protonation of the His-ligands of the 2Fe-2S cluster of PETC, which normally acts as H-bond acceptor during PQH<sub>2</sub> oxidation (Jahns et al., 2002; Malone et al., 2021; Suorsa et al., 2013). By regulating the rate of electron delivery to plastocyanin, photosynthetic control promotes the oxidation of P700, the PSI special pair. P700<sup>+</sup> is then available for photoprotective charge recombination if the downstream electron acceptors are saturated. The importance of photosynthetic control to plant fitness is illustrated by the phenotype of the *Arabidopsis pgr5* mutant, which lacks the proton gradient regulation protein PGR5. The absence of PGR5 leads to diminished  $\Delta\text{pH}$  and over-reduction and photo-damage to PSI, particularly in fluctuating light (Suorsa et al., 2012). As with NPQ, photosynthetic control is critical in a fluctuating light environment and warrants significant consideration as a target for engineering crops to improve yields (Chaux et al., 2015; Tikkanen et al., 2014).

#### 1.4.2.3 *State transitions*

‘State transitions’ are a short or medium term response to changing light conditions, either in the intensity or spectral quality of the light environment or to the metabolic state of the leaf. The spectrum of light reaching a particular chloroplast may be affected by the diurnal cycle or filtration through other leaves, creating unbalanced excitation of PSI and PSII, which absorb slightly different wavelengths of light. In addition, the variable demand for ATP compared to NADPH may require fine adjustment of the CET/LET ratio and thus relative activities of PSI compared to PSII. In both cases, state transitions serve to optimise the excitation balance between PSI and PSII through control of their relative antenna sizes (Ruban and Johnson, 2009). In state transitions, a subset of LHCII trimers are thought to be fulfil this role as the ‘mobile’ antenna (Galka et al., 2012).

Dissociation of LHCII from PSI is triggered by phosphorylation by the kinase STN7, which is essential for state transitions (Bellafiore et al., 2005). STN7 acts as a redox sensor and is activated upon binding of plastoquinol to *cytb<sub>6</sub>f*. Far red light, which preferentially excites PSI, or darkness causes the PQ pool to become more oxidised. The oxidised PQ pool does not activate STN7, so LHCII is maintained in a dephosphorylated state by the constitutively active phosphatase TAP38 and associates with PSII; this is 'state 1'. Low light irradiance or red light, which preferentially excites PSII, causes the PQ pool to become more reduced and activates STN7. Phosphorylated LHCII associates with PSI; this is 'state 2'. While both LHCB1 and LHCB2 are phosphorylation targets of STN7, LHCB2 is phosphorylated faster and is essential for state transitions (Leoni et al., 2013; Pietrzykowska et al., 2014). Sequence differences around the phosphorylation sites of LHCB1 and LHCB2, located at the N terminus, regulate the rate of phosphorylation (Liu et al., 2016). The third trimer component, LHCB3, is not directly involved in state transitions as it lacks the necessary phosphorylation site but may function to slow down or regulate the process (Damkjær et al., 2009). Phosphorylated LHCII associates with PSI via the PSAH, PSAL and PSAO subunits. However, in the grana margins additional LHCII trimers may associate with PSI in an interaction mediated by LHCA proteins (Benson et al., 2015; Crepin and Caffarri, 2015; Erik et al., 2007; Galka et al., 2012; Pan et al., 2018).

Recently it was discovered that, in addition to phosphorylation, lysine acetylation is critical for state transitions (Koskela et al., 2018, 2020). Arabidopsis mutants lacking the chloroplast lysine acetyltransferase NSI are unable to perform state transitions and cannot form LHCII-PSI complexes, despite LHCII phosphorylation remaining at wild type levels, suggesting an important role for lysine acetylation in the regulation of light harvesting. It is proposed either that acetylated lysine residues on LHCII and PSAH are necessary for the interaction of phosphorylated LHCII with PSI, or that acetylated lysine residues on PSBP and LHCII are necessary for dissociation of L trimers from PSII. Lysine acetylation has been found as a post-translational modification of Arabidopsis proteins in a wide range of different biological processes, including many in photosynthesis (Wu et al., 2011).

Earlier studies of mutants lacking STN7 indicated that state transitions are of limited importance in a natural light environment, since the particular fluctuating light regimes used produced plants that are only very slightly developmentally and photosynthetically impaired (Bellafiore et al., 2005; Frenkel et al., 2007). Later work, however, showed that a broad spectrum of *stn7* phenotypes could be produced depending on growth conditions and that LHCII phosphorylation was indeed crucial under fluctuating light (Grieco et al., 2012; Tikkanen et al., 2010). Mutant Arabidopsis lacking STN7 shows slower growth only under fluctuating light, whereas under constant light intensity, it is able to counter the loss of LHCII phosphorylation and hence the association of LHCII with PSI by increasing the number of PSI reaction centres. In *stn7* grown in fluctuating light, the lack of antenna for PSI causes a steady-state imbalance in photosystem activity that led to damage to PSI.

#### 1.4.2.4 Dynamic thylakoid stacking

In *Arabidopsis* plants grown at a moderate light intensity, grana size changes rapidly in response to changes in light intensity and spectral quality in an STN7/TAP38-dependent way via control of LHCII phosphorylation (Hepworth et al., 2021; Kyle et al., 1983; Pietrzykowska et al., 2014; Wood et al., 2018, 2019). Under low light conditions when LHCII phosphorylation by STN7 is at a maximum, grana have fewer membrane layers and narrower diameters, whereas there are more membrane layers per granum and wider diameters when LHCII is dephosphorylated by TAP38 in both high light and darkness upon inactivation of STN7. These changes occur on a timescale of around 10 min (Wood et al., 2019). The mechanism of short term granal unstacking may involve repulsion between layers and fission of connecting regions between layers, followed by rotation and further separation, resulting in the generation of multiple smaller grana from one large granum (Chuartzman et al., 2008). Since dynamic thylakoid stacking is governed by LHCII phosphorylation level, it was originally proposed to facilitate the exchange of LHCII between PSII in the grana and PSI in the stromal lamellae (Kyle et al., 1983). However, dynamic thylakoid stacking has been shown to occur in the absence of phospho-LHCII binding to PSI (Wood et al., 2019). Recent work has showed that state transitions and dynamic thylakoid stacking work synergistically to optimise the LET/CET balance under variable light conditions (Hepworth et al., 2021; Wood et al., 2018). Under low light, LHCII phosphorylation promotes the interaction of LHCII with PSI and thus enhances CET, while simultaneously the smaller grana that ensue enhance the oxidation of PQH<sub>2</sub> by shortening the diffusion distance between PSII and stromal *cytb<sub>6</sub>f*, thereby promoting LET. In contrast, upon high light exposure when LHCII is dephosphorylated and returns to PSII, the resulting larger grana increase the diffusion distances for PQH<sub>2</sub> and plastocyanin to travel to reach stromal *cytb<sub>6</sub>f* and PSI. This is suggested to simultaneously promote redox poisoning of the CET pathway in high light by preventing rapid reduction of the stromal PQ pool by PSII and help to maintain PSI in an oxidised state for photoprotection by decreasing its equilibrium constant with plastocyanin (Hepworth et al., 2021; Wood et al., 2018).

PSII phosphorylation, governed by STN8 kinase and PBCP phosphatase, has also been shown to modulate grana size in response to light intensity (Herbstova et al., 2012; Puthiyaveetil et al., 2014). Under photoinhibitory conditions PSII phosphorylation increases, initiating repair of PSII while simultaneously provoking a reduction in grana size that increases contact between the grana and stroma lamellae to facilitate faster diffusion of damaged PSII complexes out of the grana for repair (Goral et al., 2010). In the absence of the PSII kinase STN8, constitutively larger grana are observed (Fristedt et al., 2009a).

A recently discovered factor in thylakoid stacking is the CURT1 family of proteins, located at the grana margins, which oligomerise to induce membrane curvature. Chloroplasts lacking these proteins form very large, elongated grana with no margins, while overexpressors feature enhanced stacking (Armbruster et al., 2013; Wood et al., 2019). Dynamic thylakoid stacking in fluctuating light may be

regulated by phosphorylation and acetylation of CURT1 proteins (Trotta et al., 2019). Two other contributors to thylakoid stacking are the reduced induction of non-photochemical quenching (RIQ) proteins, RIQ1 and RIQ2, the absence of which enhances grana stacking. In chloroplasts lacking both CURT1A and either RIQ1 or RIQ2, grana were elongated as in the *curt1a* mutant but contained more membrane layers (Yokoyama et al., 2016).

While less extensively studied as a contributor to thylakoid architecture, the plastoglobules also appear to play a significant role in remodelling of the thylakoid membrane under high light. A complex formed by the plastoglobule kinases PGR6 and ABC1K3 functions in lipid metabolism, stress responses and thylakoid remodelling in response to high light intensity. The chloroplasts of mutants lacking these proteins produced hyperstacked grana under high light irradiance, accompanied by dramatic losses in PSII, NDH and the calcium sensor phosphoprotein, CAS (Lundquist et al., 2013). The antioxidant compound  $\alpha$ -tocopherol, synthesised in the plastoglobules by VTE1, is also induced in high light (Piller et al., 2014). The plastoglobule-associated fibrillins are required for proper acclimation to high light and cold stress. Under stress, the absence of these proteins causes growth retardation, deficiencies in anthocyanin accumulation and altered thylakoid architecture with fewer plastoglobules and swollen thylakoids. Jasmonic acid plays a role in long-term acclimation and its biosynthesis is associated with accumulation of plastoglobules and fibrillin proteins therein (Youssef et al., 2010).

#### 1.4.3 The link between short and long term responses

Arabidopsis mutants lacking STN7 are deficient in both state transitions and long term acclimation (Bonardi et al., 2005). While the two processes are linked, state transitions themselves are not essential for long term acclimation. Instead, STN7 appears to activate a signalling pathway leading to acclimation-related changes in the thylakoid proteome (Pesaresi et al., 2009a). STN7 kinase activity is triggered by the redox state of the PQ pool. It then phosphorylates both LHCI, inducing short term responses including state transitions, and another unknown protein, which leads to long term acclimation responses. One candidate for this unknown substrate of STN7 is TSP9. TSP9 is an intrinsically disordered peripheral thylakoid membrane protein on the stromal side with no known homologues outside of plant species. Light irradiance induces phosphorylation in a stepwise fashion at three threonine residues and subsequent release of TSP9 from the thylakoid membrane, a feature that implies a role in signalling and regulation of gene expression during acclimation to light intensity (Carlberg et al., 2003). Transcriptomic data of mutant Arabidopsis lacking TSP9 supports the suggestion of a role for TSP9 in the high light acclimation response, and the mutants are also defective in state transitions (Fristedt et al., 2009b). Pesaresi et al. (2009) sought to further investigate the role of TSP9 in acclimation and state transitions. In their study, acclimation was to either PSI light or PSII light rather than high or low irradiance and the extent of acclimation was recorded as chlorophyll *a/b* to indicate the proportion of Chl *b* in LHCI. The mutant lacking TSP9 behaved similarly to wild type in terms of chlorophyll *a/b* ratios, suggesting that the signalling pathway for long term acclimation does

not involve TSP9. However, if there are separate mechanisms for acclimation to high light and low light (Bailey et al., 2001), or different pathways exist for responding to light with different spectral qualities rather than intensity, a regulatory role for TSP9 cannot be completely ruled out. Another candidate for STN7-induced signalling in acclimation is the chloroplast sensor kinase (CSK) (Puthiyaveetil et al., 2008), however its specific role is as yet unclear.

#### 1.4.4 Long term acclimation to light intensity

Long-term acclimation can be categorised as either dynamic or developmental. Dynamic acclimation is the process by which fully mature leaves undergo *de novo* synthesis and degradation of specific proteins, leading to changes in the organisation of the chloroplast thylakoid membranes, their protein composition, and that of the surrounding stroma containing the enzymes of the CBB cycle (Athanasίου et al., 2010; Suorsa et al., 2012; Walters and Horton, 1994; Yin and Johnson, 2000). Developmental acclimation, which is the focus of the work in this thesis, is the alteration of leaf development and morphology in addition to these changes in chloroplast composition (Anderson, 1986; Anderson et al., 1988; Bailey et al., 2001, 2004; Boardman, 1977; Schöttler and Tóth, 2014; Vialet-Chabrand et al., 2017; Walters, 2005). The ability to acclimate to light intensity varies not only between species (Murchie and Horton, 1997), but also between different accessions within single species (Athanasίου et al., 2010). The signalling pathways that trigger acclimation are not yet fully understood. However, significant roles have been described for the redox state of the electron carrier PQ (Huner et al., 1996; Pfannschmidt et al., 1999; Rosso et al., 2009), the activity of the LHCII kinase STN7 (Pesaresi et al., 2009a), and the glucose-6-phosphate/phosphate translocator GPT2 (Athanasίου et al., 2010). Recent findings demonstrate that acclimation is vital to plant fitness in terms of seed production in fluctuating light environments (Athanasίου et al., 2010; Townsend et al., 2018).

When plants are exposed to high or low light in the long term, they alter their proteome through transcriptional, translational and post-translational regulation of gene expression on a timescale of minutes to hours. Changes may be observed on the level of growth and development speed, leaf morphology, pigment content, number of chloroplasts per cell, and thylakoid superstructure. Long term acclimation to different growth light intensities has been studied at the level of chloroplast organisation and composition in a wide range of different plant species (Bailey et al., 2001; Ballottari et al., 2007; Chow and Anderson, 1987; Chow and Hope, 1987; Chow et al., 1988; Miller et al., 2017; Petersen et al., 2011; Schumann et al., 2017). The process of acclimation is controlled by multiple regulatory mechanisms, as demonstrated by the separate responses seen in chloroplast composition to high and low light (Bailey et al., 2001; Kouřil et al., 2013). Two key features of the acclimation response are adjustment of photosystem antenna size and alteration of the PSI to PSII ratio. In low light, plants increase the amount of thylakoid membrane stacking and the ratio of light harvesting LHCII and PSI to PSII. Low light acclimated plants may run their metabolism at a lower overall energy cost (Boardman, 1977), growing slower and taking longer to reach maturity, to balance levels of respiration with limited

carbon fixation. High light, on the other hand, leads to decreased stacking, reduction in the LHCII/PSII and PSI/PSII ratios and increased levels of ATP synthase, *cytb<sub>6</sub>f* and Rubisco relative to total chlorophyll (Bailey et al., 2001; Ballottari et al., 2007; Chow and Anderson, 1987; Chow and Hope, 1987; Chow et al., 1988; Miller et al., 2017; Petersen et al., 2011; Schumann et al., 2017). Consequently, while high light grown plants have a higher overall capacity for LET and CO<sub>2</sub> assimilation coupled with an increased resistance to photoinhibition, adaptations to low light intensity allow the plant to utilise low irradiance more effectively (Anderson et al., 1988; Boardman, 1977; Gray et al., 1996). Acclimation to light intensity is thought to be primarily triggered by changes in the redox state of the PQ pool (Huner et al., 1996; Pesaresi et al., 2009a; Pfannschmidt et al., 1999; Rosso et al., 2009). The redox-triggered signalling pathway leading to long term acclimation branches into separate pathways for regulation of chloroplast and nuclear gene expression, where chloroplast gene regulation is controlled on the transcript level while nuclear gene regulation control happens on multiple levels (Pesaresi et al., 2009a).

It has been widely demonstrated that the abundance of PSI increases relative to PSII under low light (Anderson et al., 1988; Fan et al., 2007; Melis, 1991). Under low light conditions, when the proton motive force is lower, basal leakage of protons across the membrane has a more significant effect on net proton movement (Berry and Rumberg, 1996). The increase in PSI may compensate for this by increasing CET to maintain the correct ratio of ATP to NADPH production. The NDH complex and its associated route of CET is proposed to have an important role under low growth light, as rice mutants lacking this complex in the thylakoid membrane have impaired growth under low light but not high light (Yamori et al., 2015). Another possible reason for changes in PSI abundance may be that filtering of light through canopy leaves may affect the spectral quality of light reaching plants grown in the shade, since the two photosystems have different absorption spectra. However, a recent acclimation study of pea plants using quantitative proteomics showed no change in the PSII/PSI ratio (Albanese et al., 2018), although this experiment may not accurately reflect their behaviour in a natural environment since artificial low and high lighting will be spectrally similar.

Previous acclimation studies have highlighted how, in low light, plants generally expand their light harvesting antenna system relative to the PSII reaction centre, but have a generally lower maximum LET capacity (Adams et al., 2007; Bailey et al., 2001; Ballottari et al., 2007; Chow and Anderson, 1987; Chow and Hope, 1987; Chow et al., 1988; Miller et al., 2017; Petersen et al., 2011; Schumann et al., 2017). The antenna size of PSI and PSII behave differently in response to light acclimation. Whilst the expression of some LHCII peptides increases under low light, the amounts of the LHCI antenna proteins relative to the core PSI proteins appear to remain the same. PSI light harvesting efficiency may be regulated only by the ratio of PSI to PSII, which increases under low light, and by association or dissociation of mobile LHCII trimers during state transitions (Ballottari et al., 2007).

Despite lower relative abundance of PSII under low light, there is generally a large increase in expression of LHCII trimer subunits LHCB1 and LHCB2 as well as smaller increases in the core PSII antenna peptides LHCB5 and LHCB6. The number of ‘L’ and ‘M’ trimers changes to a different extent during low and high light acclimation, suggesting that specific regulatory mechanisms must exist for both ‘bound’ and ‘mobile’ LHCII (Kouřil et al., 2013). Changes in expression in response to high or low light can be seen in specific components of the PSI and PSII core antenna, including isoforms which may have important protective or regulatory roles (Bailey et al., 2001). Previous work has determined that PSII efficiency declines as its antenna cross section increases, since the additional peripheral L-type LHCII trimers are less efficiently coupled to the reaction centre (Ware et al., 2015; Wientjes et al., 2013a). However, the loss in efficiency is offset by the overall increase in absorption cross-section such that the number of pigment molecules per reaction centre times the quantum yield is higher (Wientjes et al., 2013a). The grana of low light acclimated plants may have large areas containing LHCII but no PSII and generally, plant species adapted to low light environments have chloroplasts containing fewer grana with more membrane layers (Anderson et al., 2012).

High light acclimation requires an increase in capacity for LET, so electron carriers and photosynthetic machinery must be adjusted together to maintain efficiency. *Cytb<sub>6</sub>f* and FNR, complexes that both have a substantial impact on LET flux (Hajirezaei et al., 2002; Kirchhoff et al., 2000), are likely upregulated in plants adapted to high light intensity. Indeed, overexpression and increased abundance of *cytb<sub>6</sub>f* in the thylakoid membrane increases electron transfer rate and results in a greater capacity for CO<sub>2</sub> assimilation, increased biomass and seed yield (Ermakova et al., 2019; Simkin et al., 2017), making this complex a target for genetic manipulation of agriculturally-relevant plant species. Plastocyanin is another component reported to undergo significant regulation in response to changing light intensity. Expression of this electron carrier has been shown to increase under high light intensity, possibly to prevent photosynthetic rate being limited by electron transfer to and from *cytb<sub>6</sub>f* (Burkey, 1993). However, *Arabidopsis* mutants with a 90% reduction in plastocyanin levels displayed no LET-related phenotype but were more susceptible to copper (Cu) stress, suggesting another role for plastocyanin in Cu storage (Pesaresi et al., 2009b). High light intensity increases susceptibility to photoinhibition, so high light acclimation requires readjustment of protein stoichiometries of the short-term photoprotective mechanisms, including state transitions and NPQ. Another photoprotective strategy affected by high light acclimation is chlororespiration, which aims to protect reaction centres by minimising production of ROS (Kanervo et al., 2005). It involves NDH and the PTOX, which can oxidise plastoquinol to prevent over-reduction of the PQ pool and has been found to increase in abundance under high light irradiance (Carol et al., 1999; Kanervo et al., 2005; Miyake, 2010). Despite an enhanced electron transfer and photoprotective capacity in high light acclimated plants, increased PSII activity raises the risk of reaction centre damage resulting in a high rate of turnover for this complex. Therefore, high light acclimation likely also involves upregulation of the extensive PSII repair machinery.

Much work has been carried out to investigate protein expression changes during acclimation in the thylakoid membrane. However, many of the techniques commonly used for protein detection and quantification are inaccurate, time-consuming and require specific, well-characterised target proteins, or are limited to proteins containing light-absorbing cofactors, as is the case with absorbance-based spectrophotometric assays. Important regulatory proteins may be present at relatively low levels, making changes in expression hard to detect. Immunoblotting is commonly used to detect proteins and, whilst being qualitatively informative, is subject to several limitations (Ghosh et al., 2014). Firstly, it is generally restricted to a single target protein for which a commercially-available antibody has been produced or requires the protein to be isolated and purified for production of specific serum in-house. Additionally, immunoblotting is only accurate for relative quantification over a very narrow range specific to a single target protein and antibody, and absolute quantification can only be carried out using purified target protein at a known amount as a standard. Cross-reactivity, low sensitivity, and poor reproducibility also affect the reliability of quantification. In recent years, there have been significant developments in high-resolution mass spectrometry and processing of proteomic datasets (Van Oudenhove and Devreese, 2013). Mass spectrometry can be used to analyse highly complex protein mixtures and enables the identification and quantification of potentially thousands of proteins from a single sample, making this technique an attractive alternative to single-protein quantitative techniques. We know that the thylakoid membrane undergoes significant remodelling in response to environmental conditions with many interlinked regulatory processes. Therefore, mass spectrometry-based quantification is a highly valuable tool for the study of photosynthetic acclimation.

### 1.5 *Arabidopsis thaliana* as a photosynthetic model organism

*Arabidopsis thaliana* is a small flowering plant, which became the first plant species to be used as a model organism. It grows in a wide range of climates throughout the world as several ecotypes, originating in Europe, Africa and Asia. The species was first described in 1577 by Johannes Thal, after whom it was eventually named, and was adopted as a model system in the mid-20<sup>th</sup> century with the first International Arabidopsis Symposium taking place in 1965 (Somerville and Koornneef, 2002). A number of features of Arabidopsis physiology make it ideal for its role as a model organism. One of these is the small size of the plant and its ability to grow at high density in the restricted space of a laboratory or growth chamber. Arabidopsis seeds, which may be harvested in the thousands from a single self-pollinating plant, are simple to sow and take around 6 weeks to reach maturity and go to seed. Leaves grow outwards in a rosette, from the centre of which the flowering stem emerges. Arabidopsis has a relatively small and simple genome compared to other plants, in that it is diploid and has a length of around 140 Mb across five chromosomes. Genetic transformation of Arabidopsis is a relatively simple procedure compared to other multicellular organisms. The process involves dipping the flowers into a suspension of *Agrobacterium tumefaciens* and collection of resulting transgenic seeds. Widespread use in plant research lead to Arabidopsis being the first plant species to have its genome

fully sequenced, a project that was started in 1990 and completed in 2000. A subsequent project, known as ‘The 2010 Project’ aimed to find the function of every gene in the Arabidopsis genome (Chory et al., 2000). Now, Arabidopsis data of various types - including genetic, proteomic, transcriptomic data – is compiled in The Arabidopsis Information Resource (TAIR) database (Swarbreck et al., 2008). Seed stock centres such as the Nottingham Arabidopsis Stock Centre store supply a variety of strains in addition to well-characterised knockout mutants for most of the genome. While not agriculturally or economically important, the establishment of Arabidopsis as a model plant and its associated resources has contributed greatly to plant biology.

Understanding of photosynthesis progressed dramatically throughout the 20<sup>th</sup> century. In 1943, photosynthetic yield measurements at different wavelengths of light revealed the first evidence for two distinct photosystems. The use of radioactive tracers allowed the discovery of the CBB cycle in 1957, then in 1960 came the first proposals of the ‘Z scheme’ of the light reactions (Tanaka and Makino, 2009). However, research into photosynthesis and other areas of plant science have historically been isolated from one another because the links between photosynthesis and the other biological processes of plants had not yet been established. While in the past photosynthesis research has mostly focused on technologies measuring factors such as chlorophyll fluorescence and gas exchange, it now utilises these alongside the wide range of molecular biology and genetic strategies used in broader plant science. Similarly, while the plants used for early photosynthesis research were generally chosen for practical availability and the ease at which chloroplasts and thylakoid membranes could be isolated – such as spinach and pea – or to compare plant species found naturally in different climates and environmental niches, the move to Arabidopsis provided many more opportunities. The existing Arabidopsis research community made available a wealth of developmental and genetic information, in addition to well-established protocols such that mutants could be generated to further our understanding of photosynthetic processes. Aside from Arabidopsis, *Setaria viridis* is now used as a model of C4 photosynthesis (Brutnell et al., 2010) while other simpler models of oxygenic photosynthesis include the green alga *Chlamydomonas reinhardtii* and cyanobacteria such as *Synechocystis*. These species may be used for fundamental research into principles of photosynthesis or with the intention of growing these organisms for biofuels, production of useful chemicals/materials, or carbon fixation to combat global warming. Research into plant photosynthesis on the other hand, as with Arabidopsis, is generally for the long-term aim of improving the efficiency of photosynthesis and increasing crop yields. The vast array of techniques in modern photosynthesis research spanning physics, chemistry, molecular biology and bioinformatics have made these goals realistic. Proteomic mass spectrometry, the main technique used for the work in this thesis, is one of these relatively recent additions to the field.

## 1.6 Proteomics as a tool for studying photosynthesis

Proteomics is the study of all of the proteins in a biological system. When studying global protein abundance and regulation in chloroplasts, proteomics has advantages over other –omics methods such

as genomics and transcriptomics. This is because the chloroplast proteome is transcribed from a mixture of nuclear- and chloroplast-encoded genes (Martin et al., 1998). Environmental changes, such as the intensity or spectral quality of light, may be detected in the chloroplast then this information must be sent to the nucleus to regulate transcription of photosynthetic components, which are then transported back to the chloroplast and imported. Therefore, quantification of photosynthetically relevant mRNA transcripts could be misleading and may not accurately reflect stoichiometry changes in the thylakoid membrane. Proteomic mass spectrometry (detailed in Section 1.7), on the other hand, informs about the ‘end product’ of transcriptional and translational regulation rather than the process, and is more appropriate when investigating photosynthetic function. However, one caveat is the regulation of the proteome by post-translational modification, either transient or permanent, such that quantity of a protein will not directly reflect the amount of activity from that protein. While some *in vivo* modifications, such as protonation, will not be detectable by mass spectrometry, others such as phosphorylation and acetylation have the potential to be quantified and provide more detail about the regulatory state of a protein than just its quantity. While mass spectrometry-based proteomics was applied to the analysis of the thylakoid membrane fairly extensively in the 2000s, more recent studies of this type are relatively limited despite significant advances in instrumentation and data processing.

The aim of some of the first proteomic analyses of chloroplasts was simply to identify as many chloroplast-specific proteins as possible, assign proteins to their specific sub-organellar location, and infer functions and processes of those locations based on the types of proteins found within them. One of these first studies was of the *Arabidopsis* thylakoid lumen, where protein separation on 2-D electrophoretic gels and MS identification of spots identified a novel plastocyanin and an ascorbate peroxidase (Kieselbach et al., 2000). Two more analyses of the thylakoid lumen by a similar strategy determined more functions of luminal proteins and assigned 81 proteins to the luminal proteome (Peltier et al., 2002; Schubert et al., 2002). MS identification of separated thylakoid proteins highlighted the thylakoid membrane as a site of protein synthesis and assembly, with many new protein functions identified in translation and protein folding as well as proteolysis. Many known low-abundance and very hydrophobic proteins were also identified and the data were compiled to produce a resource named the Plastid Proteome Database (PPDB) and annotated (Friso et al., 2004). A different strategy was employed by Peltier et al. (2004) to analyse the thylakoid proteome, where the membranes were thoroughly purified and proteins were either fractionated and digested with trypsin or separated by SDS-PAGE and digested in-gel. Tryptic peptides were analysed by nanoLC-MS/MS, as is most commonly done in more recent proteomic analyses, and proteins were identified using the PPDB. Of the 242 proteins identified, at least 40% (around 97) were predicted to be integral membrane proteins and the fractionation method allowed detection of additional lower abundance proteins, such as those involved in tetrapyrrole synthesis and protein translocation. In another study, proteomics of the whole chloroplast proteome with a similar MS method revealed more detail about the functions of stromal and envelope

proteins (Kleffmann et al., 2004). Other early uses of thylakoid protein MS included the identification of phosphosites on a number of key photosynthetic proteins including those from PSII, LHCII, and PSI by trypsin treatment of thylakoid membranes to release surface peptides (Hansson and Vener, 2003; Vener et al., 2001).

Progressing from initial descriptions of the thylakoid proteome, later analyses aimed to detect or quantify global changes in protein abundance occurring in response to developmental or environmental factors, or to reveal more structural detail about photosynthetic proteins. Giacomelli et al. (2006) compared the high light acclimation response of the *Arabidopsis thaliana* wild type thylakoid proteome to that of an ascorbate-deficient mutant. This study involved a time course experiment where the plants were acclimated to  $1000 \mu\text{mol}\cdot\text{m}^{-2}\cdot\text{s}^{-1}$  for 5 days. Protein samples from the plants were separated by 2-D electrophoresis and the spots that changed in intensity were identified by MS. In this case, quantification of changes in protein abundance was performed by analysis of gel spot intensity rather than by MS. Only 45 proteins were shown to change in abundance due to either high light, genotype, or both. The response of the thylakoid membrane to iron deficiency has been analysed by this gel spot quantification and identification strategy (Andaluz et al., 2006), but also by a combination of 2-D electrophoresis with in-gel digestion and intact protein LC-MS from sucrose density gradient bands, with relative quantification performed using extracted ion chromatograms (Timperio et al., 2007). LC-MS analysis of intact thylakoid proteins for quantification, with additional tryptic digestion to validate protein identities, was used again to study iron deficiency (Laganowsky et al., 2009) and to investigate specific features of LHCII isoform constituents, revealing oxidation and N-terminal acetylation as common modifications of these proteins (Galetskiy et al., 2008).

With improvements in instrumentation, such as high-resolution Fourier transform-based mass analysers, came more attempts to quantify the thylakoid proteome and map proteins to more specific structures and complexes. Zybailov et al. (2008) performed in-gel digestion and label free quantification of the chloroplast proteome in the form of spectral counting, resulting in the identification of 1325 chloroplast proteins with measured abundances spanning four orders of magnitude, and the abundance data were deposited in the PPDB. Later, another chloroplast proteome database, AT\_CHLORO, was produced by Ferro et al. (2010) containing information about the properties of 1323 proteins and their localisation within the chloroplast, determined by spectral counting. Further studies aimed to find proteins localised within the plastoglobules (Lundquist et al., 2012), and within the grana, the grana margins and the stroma lamellae (Tomizioli et al., 2014; Yin et al., 2015). MS has also been combined with structural analysis to determine the contents of isolated complexes from pea thylakoids to assess the compositional differences between the PSII supercomplexes,  $\text{C}_2\text{S}_2\text{M}_2$  and  $\text{C}_2\text{S}_2$  (Pagliano et al., 2014).

Relative and absolute quantification of the thylakoid proteome in recent work has been performed through a range of strategies and there is no definite consensus on the correct or optimum method. The thylakoid membrane is a particularly challenging system to work with through mass spectrometry-based proteomics because of the physicochemical properties of integral membrane proteins as well as the abundance distribution of its proteome; thylakoids are dominated by the light harvesting apparatus and core photosynthetic machinery, obscuring many of the less abundant regulatory proteins (Whitelegge, 2003). Earlier strategies, such as 2-D electrophoresis and relative quantification of gel spots between conditions followed by in-gel digestion and MS identification, are still used, as in an analysis by Wang et al., (2016b) of thylakoids at different developmental stages. Isobaric labelling is also used, as in a relative quantification of chloroplast proteins from dark-treated *Arabidopsis* against a control by TMT labelling (Wang et al., 2016a). However, label-free proteomics was recently used for absolute quantification of proteins of the thylakoid membrane to determine stoichiometries of complexes and subunits to one another by McKenzie et al., 2020. Thylakoids were isolated from *Arabidopsis* plants grown at a single moderate light intensity and the proteins subjected to in-solution digestion. Label-free protein quantification indicated that for every PSII core complex there were 0.58 PSI cores, 0.35 *cytb<sub>cf</sub>* complexes, 0.7 ATP synthases, while NDH was much less abundant at 0.013 per PSII. Total LHCI was not calculated, but the analysis determined LHCB1.5 to be the most abundant trimer component compared to the other two identified, LHCB1.4 and LHCB3. The label-free absolute quantification method used for this work accounts for differences in protein size. However, it does not account for the tendency of hydrophobic membrane proteins such as those of thylakoids to resist tryptic digestion, so either relative quantification between conditions or the use of known isobaric protein standards may be regarded as more accurate and precise.

Albanese et al. (2018) carried out the first study using label-free relatively quantitative MS to quantify the changes in the thylakoid membrane proteome that occur during long term acclimation. The plant investigated was pea, a non-model organism for which there was no full genome sequence known and therefore, no proteome database available. Protein sequences were determined from transcriptomic data, increasing the number of proteins that could be identified and quantified. Contrary to previous studies, no difference in the PSII/PSI ratio was found between thylakoid membranes from plants acclimated to low, moderate and high light intensity. Compared to plants grown under high light, low light thylakoids contained around half as much of each of LHCB1, 2 and 3, but the LHCI components identified were constant between conditions. Proteins increasing in abundance with growth light intensity included plastoglobular and ribosomal proteins and those of the *cytb<sub>cf</sub>* complex, NDH and ATP synthase. Many proteins with roles in electron transfer increased with light intensity, such as FNR and PGR5, whereas plastocyanin was constant in all conditions. While these abundance changes are informative about long-term acclimation of the thylakoid membrane of pea, a number of proteins were absent from the analysis

and the data may not translate directly to Arabidopsis, which is more widely used for photosynthesis research.

## 1.7 Principles of mass spectrometry-based proteomics

In mass spectrometry, molecules are ionised then sorted according to their mass to charge ratio ( $m/z$ ) to give a mass spectrum. The technique can be used for biological applications such as analysis of proteins and metabolites. Proteomic mass spectrometry is the analysis of the 'proteome', or total set of proteins in a biological system, by detecting constituent peptides from a sample. Proteins are first prepared from a biological sample then chemically modified by reduction and alkylation of cysteine residues to prevent the formation of unwanted covalent bonds between proteins. The modified proteins are then digested by an enzyme, usually trypsin, to give a mixture of peptide fragments (Dittrich et al., 2015). Trypsin is a serine protease that cleaves peptide bonds on the C-terminal side of lysine or arginine residues with high specificity to give suitably sized peptide fragments for analysis by mass spectrometry. During mass spectrometric analysis, peptide fragments are usually separated by nano liquid chromatography (nanoLC) before being ionised and detected in a peptide ion (MS1) scan. The most intense peptide ions in the MS1 scan are selected and fragmented to produce a product ion (MS2) spectrum. Information from the two spectra combined to determine the amino acid sequences of the peptides, which are then searched against the organism's proteome database to determine which proteins were present in the original sample.

Proteomic mass spectrometry can be used for a wide range of tasks. Primarily, these tasks include: identification of new proteins and generation of proteomic databases; mapping the localisation of proteins within a cell or organelle; investigation of post-translational modifications to study regulatory mechanisms; calculation of changes in relative amounts of proteins in response to different environmental conditions or drugs, and; determination of absolute amounts of a protein or proteins in a proteome as they are in a natural biological context (Aebersold and Mann, 2003).

Relative quantification of a peptide requires two or more conditions and can give information in terms of 'fold' changes in amounts of protein. This can be useful for looking at the effect of an environmental condition or treatment with a drug on protein expression and regulation. Relative quantification can be simpler, does not require known targets or a specific hypothesis, and can be used to investigate more proteins at once. This is known as 'bottom-up' or 'shotgun' proteomics. However, relative quantification gives results without units and does not give information about the absolute amounts of each protein, i.e. the number of protein molecules per cell (Drissi et al., 2013).

While relative quantification compares the abundance of one protein in different samples, absolute quantification compares the abundance of different proteins in the same sample. It can also be used to calculate the absolute molar amount of a protein. Differences in detectability and ionisation efficiency of distinct peptides mean that their peak intensity does not indicate how much of a given peptide is

present. However, when the intensity of a peptide is compared to that of an identical but isotopically labelled peptide with a known mass-shift, the difference in intensity between the two peptides will accurately reflect the difference in their amounts. Stable isotope labelling by amino acids in cell culture (SILAC) exploits this for accurate relative quantification. It involves the growth of two populations of organisms in otherwise identical conditions, where one is grown on stable isotope-labelled substrate. Peptide samples from the two populations are analysed together to determine their relative amounts for proteomic analysis (Drissi et al., 2013). Alternatively, a known quantity of that peptide may be used to determine the relationship between peak intensity and the amount of peptide. Therefore, absolute quantification can be achieved using identical but isotopically-labelled peptides at known amounts. A QconCAT (Swainston et al., 2011) is a recombinant artificial protein made up of concatenated target peptides for quantification. It is produced in *E. coli* or yeast grown in stable isotope-labelled media and purified, then a known amount is added to the protein mixture for digestion and use in mass spectrometry analysis. The QconCAT method is time-consuming and requires specific target proteins. Other methods for quantification include peptide labelling methods such as isobaric tag for relative and absolute quantification (iTRAQ). In this strategy, protein samples are labelled with different reagents, then the labelled samples are pooled together. All of these tags give peptides the same additional mass and therefore the peptides are indistinguishable in the MS1 scan. Upon fragmentation, the differentially-labelled product ions have distinguishable mass to charge ratios, so relative amounts of the peptides can be calculated (Wiese et al., 2007).

More recently, absolute quantification of proteins has been more frequently performed in the absence of mass labelling strategies. In label-free quantitative proteomics, absolute quantification of proteins is based either on MS1 peptide intensities or on the number of MS2 spectra associated with a particular peptide, termed spectral counting. There exists a number of methods for MS1 intensity-based absolute quantification, which have been extensively compared for accuracy and precision (Fabre et al., 2014; Välikangas et al., 2018; Zhang et al., 2015; Zhao et al., 2020a), available in a range of both commercial and freely-available software. Some quantification strategies aim to relate total protein intensity (the sum of all peptide intensities for that protein) to molar amounts by dividing protein intensity by a value representing that protein's size, such as its molecular weight. One of these methods is intensity-based absolute quantification (iBAQ), whereby protein intensity is divided by the number of peptides that would theoretically be released upon digestion of that protein (Schwanhäusser et al., 2011). Other strategies normalise peptide or protein intensities across multiple MS experiments to adjust protein intensities such that they can act as proxies for molar quantities. One of these methods is MaxLFQ (Cox et al., 2014), implemented in the freely-available software MaxQuant (Cox and Mann, 2008), which normalises protein intensity using peptide intensity ratios between experiments under the assumption of an unchanging 'background' proteome. While there have been significant advances in label-free absolute quantification, relative quantification is generally considered more robust and precise.

## 1.8 Aims

There has yet been no quantitative or semi-quantitative analysis of the proteome of the *Arabidopsis thaliana* thylakoid membrane under high and low light conditions. Rather than investigating changes in protein expression, most existing proteomic studies on the plant thylakoid membrane have focused on increasing the number of membrane protein identifications or determining the localisation of proteins within the chloroplast or within the thylakoid membrane (Tomizioli et al., 2014). Quantitative analysis of plant proteomes through SILAC is challenging because of the need for isotope-labelled media, and a QconCAT-based approach requires specific target proteins. Advances in the sensitivity and accuracy of modern mass spectrometers (Scheltema et al., 2014) mean that labelling methods such as iTRAQ are no longer essential for relative quantification. A label-free global analysis of the thylakoid membrane proteome under different light environments will allow semi-quantitative comparative analysis of light acclimation. This approach has the potential to identify important low-abundance regulatory proteins that were not previously known to have roles in acclimation. The work presented in this thesis aims, firstly, to develop a reliable method for relative quantification of the proteins of the thylakoid membrane using label-free quantitative mass spectrometry-based proteomics. The method is then applied to *Arabidopsis* plants grown in a controlled environment to investigate remodelling of the thylakoid proteome in response to different light intensities and is combined with structural and biochemical analyses to relate these changes to biological processes. However, since plants grown in a natural light and temperature environment are exposed to very different conditions to those in a controlled environment, it is important to view any observations and conclusions about light acclimation in the context of a natural environment. Therefore, a comparison of the thylakoid proteome from *Arabidopsis* grown in a natural environment to that from a controlled environment is performed using the same method. Finally, to take the investigation further than a descriptive account of acclimative changes, the strategy is applied to photosynthetic mutants to investigate how the thylakoid proteome is remodelled to account for missing proteins or processes and to assess the relationship between phenotype and proteome in these mutants. The final results chapter first describes a large comparative proteomic analysis to determine the roles of the proteins STN7 and TAP38 in long term light acclimation. This is followed by an analysis of the *pgr5* *Arabidopsis* mutant in order to speculate on what changes in the thylakoid proteome may contribute to the lethality of this mutation in a natural or fluctuating light environment.

## 2 Experimental procedures

### 2.1 Growth of *Arabidopsis thaliana*

Table 5: *Arabidopsis thaliana* strains

Strain	Description
col-0	Columbia ecotype
<i>stn7</i>	T-DNA insertion in intron (SALK 073254)
<i>tap38</i>	T-DNA insertion in 5' UTR (SALK 025713)
<i>gl-1</i>	Spontaneous mutant defective in trichome development
<i>pgr5</i>	Point mutation in <i>gl-1</i> background (Munekage et al., 2002; Shikanai et al., 1999)

#### 2.1.1 Conditions for growth of *Arabidopsis*

*Arabidopsis thaliana* seeds were sown on M3 compost and stored at 4°C for 48 h before germination by transferring to a Conviron plant growth room with day/night temperatures of 21°C/18°C. Seedlings were transplanted to individual pots containing a mixture of M3 compost, perlite, and vermiculite at a ratio of 4:1:1, respectively. Between 10 and 15 plants per condition were grown under fluorescent bulbs (emission spectrum in Figure 5) at 150  $\mu\text{mol photons m}^{-2} \text{ s}^{-1}$  with either a 12 h photoperiod (Chapters 3, 4, and 5) or an 8 h photoperiod (Chapter 6). Light intensity was measured as photosynthetically active radiation (PAR) on a LI-190 light meter. After 2 weeks, or until rosettes reached a diameter of around 3 cm, plants were transferred to their respective environmental conditions to be compared, either in a controlled environment growth chamber or to an outdoor growth facility (Arthur Willis Environment Facility, University of Sheffield) where the pots were positioned above ground on tables and watered regularly to avoid drought stress. Plants were acclimated for different lengths of time prior to harvesting to account for variable maturation rate depending on day length and light intensity (Cho et al., 2017). Local weather data for the acclimation period of outdoor-grown plants was provided by the Weston Park Weather Station, Sheffield, which recorded minimum and maximum temperatures of each day along with sunshine hours. Sunshine hours were defined as the number of hours per day at which the light intensity exceeded 120  $\text{W/m}^2$ . The approximate conversion of  $\text{W/m}^2$  to  $\mu\text{mol photons m}^{-2} \text{ s}^{-1}$  was performed as follows:  $1 \text{ W/m}^2 = 4.57 \mu\text{mol photons m}^{-2} \text{ s}^{-1}$  (Thimijan and Heins, 1983).

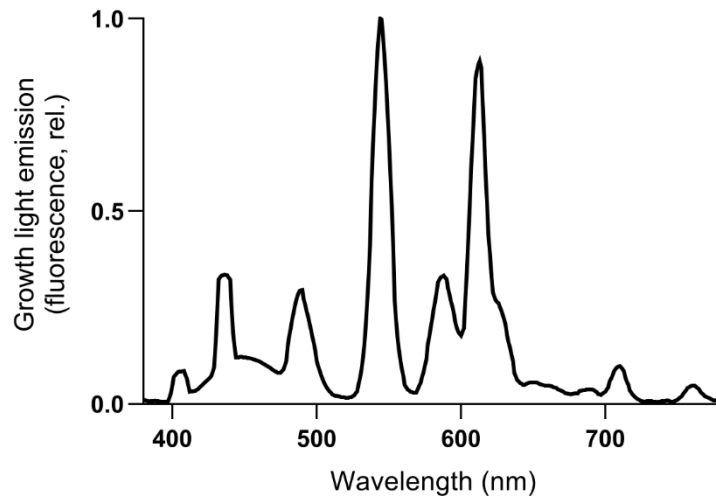


Figure 5: Emission spectrum of fluorescent lighting used for Arabidopsis growth.

## 2.2 Materials, buffers and reagents

Unless otherwise stated, reagents and chemicals from Fisher Scientific UK Ltd (Loughborough, UK) or Sigma-Aldrich Company Ltd. (Dorset, UK). Solutions were made up in Milli-Q® Integral ultrapure water produced by a Milli-Q® Integral Water Purification System (Millipore (UK) Ltd., Watford, UK) with a purity of 18.2 mΩ cm at 25°C, unless otherwise stated (as in Section 2.9).

Table 6: Buffers and solutions

Experiment	Solution	Reagent concentration
Thylakoid membrane preparation, structured illumination microscopy, low temperature fluorescence spectroscopy	Preparation medium	50 mM sodium phosphate buffer pH 7.4 5 mM MgCl <sub>2</sub> 300 mM sucrose 10 mM NaF
	Break medium	5 mM MgCl <sub>2</sub> 10 mM Tricine pH 7.4 10 mM NaF
	Double osmotic medium	5 mM MgCl <sub>2</sub> 10 mM Tricine pH 7.4 400 mM sucrose 10 mM NaF
	Thylakoid storage buffer	10 mM sodium phosphate buffer pH 7.4 5 mM MgCl <sub>2</sub> 5 mM NaCl

		200 mM sucrose 10 mM NaF
Immunoblotting	Transfer buffer	10 mM NaCO <sub>3</sub> 3 mM Na <sub>2</sub> CO <sub>3</sub> 10% (v/v) methanol
	Tris buffered saline (TBS)	50 mM Tris HCl pH 7.6 150 mM NaCl
	Blocking buffer	0.2% (w/v) TWEEN 20 50 mM Tris HCl pH 7.6 150 mM NaCl 5% (w/v) milk powder
	Antibody buffer	0.05% (w/v) TWEEN 20 50 mM Tris HCl pH 7.6 150 mM NaCl
Mass spectrometry	Loading solvent	0.5% (v/v) trifluoroacetic acid 3% (v/v) acetonitrile (ACN)

## 2.3 Preparation of thylakoid membranes

Arabidopsis thylakoid membranes were prepared according to Albertsson et al., 1994, with the addition of 10 mM NaF to all buffers (Table 6). Leaves were blended in cold preparation medium in a waring blender. The leaf homogenate was filtered through two layers of muslin followed by another two layers of muslin with absorbent cotton wool in between. Chloroplasts were pelleted by centrifugation of the cell lysate for 15 min at 3750 rpm on a Thermo Scientific Sorvall ST 16R centrifuge at 4°C. To lyse chloroplast envelopes, the pellet was resuspended in break medium and incubated on ice for 1 min. An equal volume of double osmotic medium was added before centrifugation for 10 min at 3750 rpm at 4°C. Pelleted membranes were resuspended and washed in thylakoid storage buffer before a final 10 min centrifugation step. The pelleted thylakoid membranes were then resuspended in approximately 1 mL of thylakoid buffer. Thylakoid membranes were stored in aliquots at -80°C after flash freezing, with the addition of ethylene glycol at 5% sample volume.

## 2.4 Spectroscopic analysis of pigments

### 2.4.1 Chlorophyll analysis

Absorption spectra were taken on an Agilent Technologies Cary 60 UV-VIS spectrophotometer. For analysis of chlorophyll content, 4 µL of thylakoids were vortexed with 2 mL of 80% (v/v) acetone then the mixture was centrifuged at 13000 × *g* for 2 min. The absorption of the supernatant at 750, 663 and 645 nm was used to calculate the chlorophyll concentration and chlorophyll *a* to *b* ratios of the thylakoid

samples according to Porra et al. (1989). The equations for calculation of concentrations and ratios are shown below.

$$\text{Chl } a = 0.01225(A^{663}-A^{750}) - 0.00255(A^{645}-A^{750})$$

$$\text{Chl } b = 0.02031(A^{645}-A^{750}) - 0.00491(A^{663}-A^{750})$$

$$\text{Chls } a + b = 0.01776(A^{645}-A^{750}) + 0.00734(A^{663}-A^{750})$$

#### 2.4.2 Low temperature fluorescence spectroscopy

Thylakoids were diluted in thylakoid storage buffer to  $A^{680} = 0.1$  and transferred to a 1 cm polymethyl methacrylate cuvette. The fluorescence of samples plunged into liquid nitrogen was measured using a FluoroLog FL3-22 spectrofluorimeter (Jobin Yvon). Emission spectra from excitation at 435 nm were normalised to the peak at 684 nm emission. PSII excitation spectra (emission at 695 nm) were normalised to the peak at 675 nm excitation. PSI excitation spectra (emission at 735 nm) were normalised either to 705 nm excitation or to the maximum value between 550 and 720 nm.

#### 2.5 Protein assay

For calculation of protein concentration in thylakoid membranes, sodium laurate (SL) was added to a concentration of 1% (w/v). The sample was subject to two rounds of sonication for 10 min followed by shaking at 1500 rpm for 5 min at 20°C, then starch granules were removed by centrifugation at  $10,000 \times g$  for 2 min. The Bio-Rad DC protein assay was used to determine protein concentration of the solubilised thylakoids with absorbance read at 750 nm. Sample concentration was calculated using a standard curve of bovine serum albumin (BSA) standards at 0.2, 0.5, 0.8, 1.2 and 1.5 mg/mL in 1% (w/v) SL. Ratios of protein:Chl were produced by calculating the protein concentration of thylakoids solubilised at a known Chl concentration (0.1 mg/mL).

#### 2.6 BN-PAGE

Stromal lamellae were solubilised at 0.5 mg/mL Chl in 2% (w/v) digitonin, 50 mM Bis Tris pH 7.2, 10 mM NaF, 10% (v/v) glycerol, for 1 h on ice. Grana membranes were solubilised in 0.5% (w/v) *n*-hexadecyl  $\beta$ -D-maltoside, 0.2% (w/v) *n*-dodecyl  $\alpha$ -D-maltoside, 50 mM Bis-Tris pH 7.2, 10 mM NaF, 10% (v/v) glycerol, for 1 h on ice. For comparison of lab and field grown plants, the granal fractions were instead solubilised in 1% (w/v) *n*-dodecyl  $\alpha$ -D-maltoside, 50 mM Bis-Tris pH 7.2, 10 mM NaF, 10% (v/v) glycerol. Complexes solubilised from the stromal lamellae were separated by centrifugation at  $15,000 \times g$  at 4°C, with the supernatant collected. Granal complexes were solubilised from the pellet and separated by centrifugation at  $15,000 \times g$  at 4°C. The two supernatants were centrifuged at  $15,000 \times g$  at 4°C for a second time, and the supernatants collected. Solubilised complexes were mixed with 100 mM Bis Tris pH 7.2, 30% (w/v) sucrose, 50 mg/mL Coomassie Blue G250, 0.5 M aminocaproic acid at a ratio of 9:1, respectively, and centrifuged for 2 min at  $13,000 \times g$  at room temperature and the supernatant was loaded on Invitrogen Bis-Tris NativePAGE 3 to 12% precast gels. Complexes were

separated by electrophoresis at 160 V for 120 min at 4°C in Invitrogen NativePAGE running buffer, with the addition of 2 mL of cathode buffer to the inner chamber. Gels were stained with Coomassie Brilliant Blue G250 for protein visualisation.

## 2.7 SDS-PAGE and immunoblotting

Thylakoid membranes were solubilised in NuPAGE lithium dodecyl sulphate sample buffer for 1 h at ambient temperature then centrifuged at  $10,000 \times g$ . The supernatant was then separated by SDS-PAGE on Invitrogen 12% Bis-Tris NuPage precast gels (Thermo Fisher Scientific) in MES running buffer (Life technologies) for 80 min at 150 V. Precision Plus unstained protein marker was used for molecular weight indication and thylakoid sample loading was normalised to equal amounts of chlorophyll. Gels were stained with Coomassie Brilliant Blue G250 for protein visualisation. For SDS-PAGE gels intended for use in immunoblotting, Precision Plus pre-stained protein marker was used and the gel was not Coomassie Blue stained.

Immunoblots were carried out with primary antibodies raised against PSBD, PSBA, PETA, and ATPH (Agrisera). A poly(vinylidene difluoride) membrane (PVDF, Novex) was activated by soaking in MeOH for 1 min. The membrane was washed in transfer buffer, along with the gel, two sheets of filter paper and sponges, then assembled in a transfer tank. Transfer was carried out at 4°C in transfer buffer either overnight at 35 mM or for 1 h at 350 mM. At room temperature with mixing, the membrane was subject to three 5 min washes in TBS then incubated with blocking buffer for 1 h. Blocking buffer was removed before addition of antibody buffer containing primary antibody serum at the dilution recommended by the manufacturer. After 4 h, the primary antibody buffer was removed and the membrane was subject to three 5 min washes in antibody buffer. Secondary antibody (horseradish peroxidase-conjugated anti-rabbit, Sigma-Aldrich) was diluted 1:10,000 in antibody buffer and incubated with the membrane for 1 h. The secondary antibody buffer was discarded and the membrane washed in antibody buffer three times for 5 min. The membrane was allowed to dry slightly before application of 1 mL of WESTAR SUN chemiluminescence substrate (Cyanagen) and imaging using an Amersham Imager 600 (GE Healthcare).

## 2.8 Imaging of chloroplasts

### 2.8.1 Electron microscopy of leaf thin sections

Leaf discs of 1 cm diameter were taken at the point of harvest from positions in the centre of exposed leaves. Leaf thin sections were prepared and imaged by Dr Chris Hill (Electron Microscopy Facility, University of Sheffield) as in Wood et al. (2018). The leaf discs were first infiltrated with 3% glutaraldehyde/0.1 M sodium cacodylate overnight then washed and fixed with 2% osmium tetroxide. The samples were washed briefly with water then dehydrated with serial ethanol treatments. Epoxypropane was used to clear the samples before infiltration with a mixture of araldite resin and epoxypropane at a 1:1 ratio. This mixture was replaced twice over 8 h before curing at 60°C for 48-72

h. A Leica UC 6 ultramicrotome was used to cut ultrathin sections to around 85 nm, which were mounted onto copper grids and stained with aqueous uranyl acetate for 30 min, followed by Reynold's lead citrate for 5 min. Leaf thin sections were imaged at an accelerating voltage of 80Kv with a FEI Tecnai Transmission Electron Microscope, with micrographs recorded using a Gatan Orius 1000 digital camera and Digital Micrograph software.

### 2.8.2 Structured illumination microscopy

Samples were prepared, imaged and analysed according to Wood et al., 2019. Leaf discs of 1 cm diameter were ground using a (pre-cooled) pestle and mortar in 1 mL cold preparation medium. Chloroplasts in leaf homogenate were imaged on a DeltaVision OMX V4 microscope (GE Healthcare) with a Blaze-3D SIM module and a 603 1.42 oil planapochromat lens. Chlorophyll was excited with a 642 nm wavelength laser and emission collected through a bandpass filter of 683/40 nm. The structured illumination pattern was projected onto the sample at 3 angles in a series of 5 phases (15 images per axial slice). Image reconstruction was performed with Soft-WoRxOMX 6.0 software (GE Healthcare). The SIMcheck ImageJ plugin was used to threshold and 16-bit convert the reconstructed images before grana FWHM measurements in the same software.

## 2.9 Mass spectrometry

All solutions were made in LC grade water (Sigma-Aldrich).

The mass spectrometer (Q Exactive HF, Thermo Scientific) was regularly calibrated and quality control assessments were carried out with HeLa cell tryptic digest standards before and after every experiment. Blank injections of loading solvent were spaced at least every 5 sample injections with an identical nanoLC gradient but full MS scan mode was set to centroid rather than profile. Where data was to be used for protein quantification, running order of samples was randomised to reduce the impact of batch effects.

Protein identifications were assigned as being associated with the thylakoid membrane, lumen or plastoglobules using a combination of SUBA4 (Hooper et al., 2017), GO annotations, and manual annotation based on literature and online resources such as UniProtKB.

### 2.9.1 Protein digestion in 60% methanol

Thylakoid membranes containing 10 µg of Chl (approximately 50 µg protein) were diluted to 10 µL in HPLC-grade water. Proteins were reduced by addition of 1.5 µL 100 mM tris(2-carboxyethyl)phosphine-HCl (TCEP) and 5 µL MeOH and incubation at 37°C for 30 min. Protein alkylation was performed with the addition of 1.5 µL 200 mM iodoacetamide in 100 mM triethylammonium bicarbonate (TEAB) pH 8.5 and incubation in the dark at ambient temperature for 30 min. Samples were adjusted to 50 µL volume before addition of 2 µg trypsin (Promega) for

proteolytic digestion overnight at 37°C. Peptide samples were dried by vacuum centrifugation, then resuspended in loading solvent (Table 6) by sonication and desalted (see Section 2.9.5).

### 2.9.2 In-gel protein digestion

Thylakoid membranes containing 5 µg Chl were separated by SDS-PAGE as described earlier (see Section 2.7) with the modification that thylakoids were heated to 95°C with 10 µL SDS loading dye for 3 min. After staining with Coomassie Blue, the gel lane was excised and divided into sections. Each section was cut into 1 mm cubes and subject to in-gel reduction, S-alkylation and tryptic digestion as described by Pandey et al. (2000). The peptide extracts were dried by vacuum centrifugation and stored at -20°C.

### 2.9.3 In-solution protein digestion

Thylakoid membranes containing 10 µg Chl (approximately 50 µg of protein) were diluted to 20 µL in LC-MS grade water. The protein samples were precipitated and cleaned up using the GE Healthcare 2D Cleanup Kit according to the manufacturer's instructions. The resulting protein pellets were solubilised in 10 µL 8 M urea, 100 mM Tris-HCl pH 8.5. For the reduction reaction, 1 µL 50 mM tris(carboxyethyl)phosphine-HCl (TCEP) was added and incubated at 37 °C for 30 min. The samples were allowed to cool to room temperature then the proteins were alkylated by addition of 1 µL 100 mM iodoacetamide in 100 mM Tris-HCl pH 8.5 and incubation at room temperature in the dark for 30 min. Proteolytic digestion was started by addition of 2 µg of pre-mixed trypsin/endoproteinase Lys-C (eLys-C, Promega) and incubation at 37°C for 2 h. The sample was then diluted with 75 µL 50 mM Tris-HCl pH 8.5, 10 mM CaCl<sub>2</sub> and incubated at 37°C overnight. Finally, 5 µL 10% trifluoroacetic acid was added to the samples then the peptides were dried by vacuum centrifugation and stored at -20°C.

### 2.9.4 Protein digestion in sodium laurate

Thylakoid membranes were solubilised in 1% (w/v) sodium laurate (SL) by two rounds of sonication for 10 min followed by 1 min shaking as described previously (Lin et al., 2013). Starch granules were then removed by centrifugation at 10,000  $\times$  g for 2 min. Aliquots of the supernatant containing 50 µg protein (Bio-Rad DC assay) were adjusted to 15 µL with 1% (w/v) SL, 100 mM triethylammonium bicarbonate (TEAB) pH 8.5 then reduced by the addition of 1.5 µL 100 mM TCEP and incubation at 37°C for 30 min. Proteins were S-alkylated by the addition of 1.5 µL of 200 mM iodoacetamide in 100 mM TEAB pH 8.5 and incubation at ambient temperature in the dark for 30 min. Samples were adjusted to 50 µL with 1% (w/v) SL, 100 mM TEAB pH 8.5 and proteolytic digestion was carried out after the addition of 2 µg pre-mixed trypsin/eLys-C (Promega) and incubation for 3 h at 37°C. Extraction of SL was performed as previously described (Lin et al., 2013) by adding an equal volume of ethyl acetate and acidification with 10 µL 10% (v/v) trifluoroacetic acid (TFA). The samples were vortexed for 1 min then centrifuged at 15,700  $\times$  g for 5 min to accelerate phase separation. The peptide-containing lower phase was isolated, dried by vacuum centrifugation and dissolved in 50 µL 0.5% (v/v) TFA, 3%

(v/v) ACN before desalting with C18 spin columns (Thermo Scientific) as described in Section 2.9.5. The peptides were again dried by vacuum centrifugation and stored at -20 °C.

### 2.9.5 Peptide desalting

Vacuum dried digested peptides were dissolved in loading solvent by sonication then desalted using reversed-phase chromatography C18 spin columns (Thermo Scientific) with 30 µg capacity. Centrifugation steps were carried out at 500 rpm in a microcentrifuge. The spin columns were first activated by two 200 µL washes with 50% (v/v) MeOH before two equilibration washes with loading solvent. The sample was applied to a spin column and the flow-through was collected for a second pass through the column. Another two washes with loading solvent were performed before elution of the peptides in 70% (v/v) ACN followed by vacuum centrifugation.

### 2.9.6 Hypercarb fractionation of peptides

Desalted peptides were first dissolved in loading solvent by sonication. Centrifugation steps were carried out at 1000 rpm in a microcentrifuge. Hypercarb spin columns (Thermo Scientific) were activated by two 200 µL washes with 70% (v/v) MeOH then equilibrated with two 200 µL washes with loading solvent. The sample was applied to a spin column and the flow-through was collected for a second pass through the column. A further two washes were carried out with 200 µL loading solvent. Peptides were eluted sequentially with 50 µL 0.1% (v/v) TFA containing 10, 20, 30, 40, 50 and 70% (v/v) ACN and the fractions collected separately. The fractions eluted at 10% and 70% (v/v) ACN were pooled then all fractions were dried by vacuum centrifugation.

### 2.9.7 Analysis of peptides by mass spectrometry

For analysis by nano-flow liquid chromatography coupled to mass spectrometry (nanoLC-MS/MS), the peptides were dissolved in loading solvent by 5 min sonication and 5 min mixing at 1500 rpm at room temperature. Samples were centrifuged at 10,000  $x$   $g$  for 5 min to remove any precipitate before 400 ng peptides from each of three replicate digests were analysed in triplicate in randomised order. Peptides were resolved on an EASY-Spray PepMap RSLC C<sub>18</sub> column (Thermo Scientific, 50 cm  $x$  75 µm ID, 2 µm, 40 °C) with the following gradient profile delivered at 300 nL/min by a Dionex RSLCnano chromatography system (Thermo Scientific): 97% solvent A (0.1% (v/v) formic acid in water) to 10% solvent B (0.08% (v/v) formic acid in 80% (v/v) ACN) over 5 min, then 10% to 50% solvent B over 3 h. For prefractionated samples, solvent B was instead delivered from 10% to 50% over 75 min. The mass spectrometer was a Q Exactive HF hybrid quadrupole-Orbitrap system (Thermo Scientific) programmed for data dependent acquisition with profile full MS scans at 120,000 resolution and a maximum of 10 centroid product ion scans at 30,000 resolution per cycle. For analysis of in-gel digests the MS was programmed to exclude the trypsin autoproteolytic peptide sequences VATVSLPR and LSSPATLNSR.

### 2.9.8 Identification of proteins from mass spectrometry data

MS data files were searched using either MaxQuant (Cox and Mann, 2008) or Mascot Daemon (Perkins et al., 1999) against the most recent *Arabidopsis thaliana* UniProtKB reference proteome database ([www.uniprot.org/proteomes/UP000006548](http://www.uniprot.org/proteomes/UP000006548)). MS raw files were converted to mgf files using MSConvert prior to processing in Mascot, the method for such was as follows: enzyme = trypsin; max missed cleavages = 2; peptide charge = 2+ and 3+; peptide tolerance = 0.01; variable modifications = M oxidation; fixed modifications = C carbamidomethyl. For label-free quantification, MS raw files were processed by MaxQuant with the intensity-based absolute quantification (iBAQ) (Cox and Mann, 2008; Schwanhäusser et al., 2011) option selected. MaxLFQ (Cox et al., 2014) was enabled with the minimum peptide ratio set to 2. Search parameters were: carbamidomethyl-Cys (fixed modification), Met oxidation, protein N-terminal acetylation, Lys acetylation and Gln to pyro-Glu conversion (variable modifications) with a maximum of two missed cleavages. The enzyme was set to Trypsin/P.

Table 7: Software and database versions

Database/software	Date downloaded/version
uniprot-proteome_UP000006548.fasta	24/10/2016
	10/12/2018
	17/12/2019
	11/03/2020
MaxQuant	v1.6.3.4
	v1.6.10.43
	v1.6.11.0
Perseus	v1.6.0.7
	v1.6.2.3
	v1.6.10.50
Mascot Daemon	v2.5.1.0

### 2.9.9 Mass spectrometry-based protein quantification

Quantification results in the form of iBAQ (Cox and Mann, 2008; Schwanhäusser et al., 2011) intensities, as generated by MaxQuant (Cox and Mann, 2008) for the identified proteins, were processed and statistically analysed using Perseus (Tyanova et al., 2016). To compensate for variation due to sample loading and MS spectral acquisition timing, iBAQ intensities for the target proteins were normalised to the intra-analysis sum of iBAQ intensities of key photosynthetic complexes PSII (PSBA, PSBB, PSBC, PSBD, PSBE, PSBF, PSBH, PSBO1, PSBO2, PSBP1, PSBP2, PSBQ1, PSBQ2, PSBR), PSI (PSAA, PSAB, PSAC, PSAD, PSAE1, PSAE2, PSAF, PSAG, PSAH, PSAK, PSAL, PSAN, PSAO), *Cytb<sub>cf</sub>* (PETA, PETB, PETC, PETD), and ATP synthase (ATPA, ATPB, ATPC, ATPD, ATPE,

ATPF, ATPH, ATPI). In Perseus, filtering was performed to remove identifications arising from the contaminants database, reverse sequences, and proteins only identified by a modification site. MS data from repeat injections was averaged (mean) with missing values excluded. Statistical analyses to identify significant changes in protein abundance by ANOVA (analysis of variance) and/or t-test were performed in Perseus (Tyanova et al., 2016) with additional truncation by permutation-based FDR (false discovery rate) of 5% based on a null distribution generated by 250 randomisations, with significance reported as  $q$  value ( $q < 0.05$ ). Where more than two conditions were compared, significant proteins were determined by one-way ANOVA prior to identification of significant pairs of conditions. The significance of changes in protein expression between plant growth conditions was determined using Welch's t-test. Protein intensities were displayed graphically as a percentage of the mean value of the control condition. Ratios of protein abundance between conditions were calculated using the median value from triplicate analyses and assigned colours for summary diagrams using Microsoft Excel. Calculation of protein stoichiometries was performed using MaxLFQ-normalised datasets by dividing protein LFQ intensity of one protein with that of another. Ratio calculations involving multi-subunit complexes were performed using a stoichiometry-adjusted mean of the LFQ intensities of all subunits quantified in 3 replicates.

## 3 Developing a method for proteomic analysis of the Arabidopsis thylakoid membrane

### 3.1 Introduction

Until recently, there was no published relative quantification of the plant thylakoid proteome by mass spectrometry. Much of the early proteomic analysis of thylakoid membranes was performed using 1D or 2D gel electrophoresis followed by in-gel digestion of specific spots or bands for the purpose of identification or mapping to a particular subcellular location rather than quantification (Friso et al., 2004; Kieselbach et al., 2000; Peltier et al., 2002, 2006; Schubert et al., 2002; Timperio et al., 2004). More recently, thylakoid sub-compartments were isolated by Tomizioli et al., 2014 and the protein concentrated in an SDS-PAGE gel between the stacking and separating region of the gel, before excision of the band and in-gel digestion. Gomez et al. (2002) used an alternative method for identification of thylakoid proteins, where they performed LC-MS to separate and analyse the intact mass of PSII-enriched thylakoid membrane proteins with the aim of assigning proteins to the grana. Relative quantification of proteins in acclimation or other conditions has also been performed by first measuring intensity of spots on 2D gels then identifying spots with differential regulation by LC-MS (Andaluz et al., 2006; Giacomelli et al., 2006; Timperio et al., 2007). Many laboratory methods used for proteomic analysis of thylakoid membrane proteins in the past focused on fractionation to increase coverage (Peltier et al., 2004) but have been superseded by improvements in high resolution MS. These advances were accompanied by developments in and increased availability of bioinformatics tools for processing of MS data. Quantitative proteomics without the need for metabolic labelling or isobaric mass tags is now commonplace in biomedical fields such as cancer biomarker discovery. However, studies involving relative quantification of proteomes within a sub-organellar fraction such as the thylakoid membrane are lacking. For this reason, it was not possible to rely on existing protocols and some consideration was required for the choice of method for sample preparation, data processing, normalisation and quantification.

A recent MS study provided the first relative quantification of the thylakoid proteome in pea grown under low, moderate and high light intensity, at 30, 150 and 800  $\mu\text{mol photons m}^{-2} \text{ s}^{-1}$ , respectively (Albanese et al., 2018). This study used an in-solution digestion method employing both eLys-C and trypsin in urea. The MS data used for quantification of proteins was acquired using a time-of-flight (TOF) MS in a data independent acquisition (DIA) mode, rather than the Orbitrap in data dependent acquisition (DDA) mode used in this work. Another caveat of their work was the absence of a pre-existing proteome database for *Pisum sativum*. Although this issue was overcome by the use of protein sequences deduced from transcriptomic data, there was poorer coverage of the proteome with only 194 proteins quantified, not all of which were thylakoid-associated.

Overall, very little work has been carried out with the aim of using MS-based proteomics to quantify abundance changes in the thylakoid proteome and much of the existing literature came prior to significant technological enhancements. This gap presented the opportunity for development and optimisation of each stage of the analysis rather than repetition of previous methods and has resulted in a straightforward and reliable procedure, which is readily applicable to other photosynthetic membranes.

### 3.2 Selection of a digestion method for thylakoid protein mass spectrometry

*Arabidopsis thaliana* was chosen for proteomic analysis of the thylakoid membrane because, as a model organism, it is of wide interest to the plant biology community with a vast array of mutants available for follow-up studies. Most importantly, *Arabidopsis* has a fully-sequenced genome and accompanying proteome databases that are well-annotated and updated with functional data. While proteomic analysis of *Arabidopsis* is well established in areas of plant biology other than photosynthesis, there are limited numbers of studies specifically investigating the thylakoid membrane. Rather than proceeding with a whole-cell approach, preparation of protein samples for MS analysis was carried out on isolated thylakoid membranes in order to maximise in-depth coverage of the thylakoid proteome. A particular emphasis of this study was to identify and provide relative quantification of those more low-abundance, hydrophobic or low molecular weight protein components of the thylakoid that were absent from previous studies. Thylakoid membranes were isolated from *Arabidopsis* leaf tissue by mechanical cell lysis followed by a series of centrifugation steps. Following homogenisation of leaf tissue, insoluble, structural leaf material was filtered out and the cell lysate was centrifuged to pellet chloroplasts. The chloroplasts were then lysed by osmotic shock and the thylakoid membranes, along with starch granules that pellet alongside them, were centrifuged and washed in a gentle purification procedure. A known inhibitor of thylakoid membrane phosphatases, sodium fluoride (NaF), was used throughout to freeze the phosphorylation state and hence maintain phosphorylation-dependent interactions within photosynthetic supercomplexes. Additionally, magnesium chloride ( $MgCl_2$ ) was used throughout the procedure to maintain stacking interactions between membrane layers in the grana. Whilst the maintenance of native interactions is not relevant to protein digestion for MS, this meant that the isolated thylakoid membranes were suitable for various spectroscopic analyses in addition to proteomics.

The hydrophobic nature of membranes means that analysis of their proteomes can be challenging (Alfonso-garrido et al., 2015), so a number of preparation strategies were trialled and assessed for their efficacy when applied to thylakoids. The thylakoid proteins needed to be extracted from the membrane and unfolded sufficiently to allow proteolytic cleavage without simultaneously denaturing or inactivating the protease. One strategy tested utilises the ability of trypsin to digest proteins in the presence of up to 65% methanol (MeOH) (Simon et al., 2001). Digestion of protein samples in 60% MeOH has been found to increase the number of membrane proteins identified in MS experiments compared to when solubilised in 1% sodium dodecyl sulphate (SDS) (Zhang et al., 2007) making this

a popular strategy for increasing coverage of membrane proteomes (Moore et al., 2016). However, when this method was applied to Arabidopsis thylakoid membranes, a total of only 185 proteins were identified (Figure 6A). To determine whether this very low number of protein identifications was a result of incomplete protein digestion, a time course analysis was carried out with fractions taken at 1 h, 3 h and 20 h following addition of trypsin and analysed by SDS-PAGE (Figure 6A). At each time point, even after 20 h incubation, bands were visible at ~60 kDa and ~25 kDa with additional Coomassie Blue staining in the higher molecular weight region of the gel. This confirms that solubilisation of thylakoid membranes in 60% MeOH does not allow complete tryptic digestion of thylakoid membrane protein.

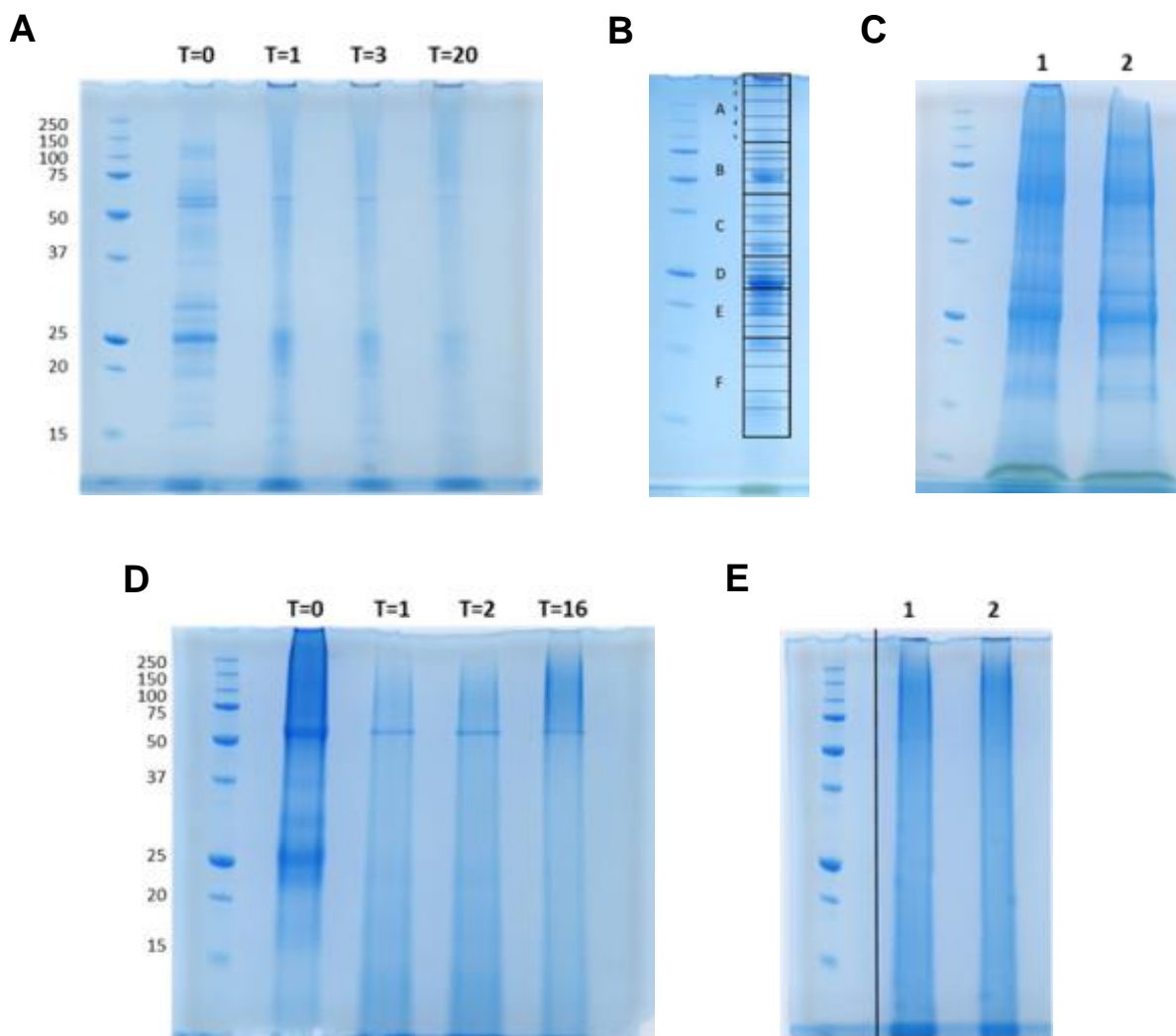


**Figure 6.** Assessment of digestion methods by SDS-PAGE. **A**, Thylakoid membranes before ( $T=0$ ) and after solubilisation in 60% methanol and incubation with trypsin at 37°C before quenching at 1 h ( $T=1$ ), 3 h ( $T=3$ ) and 20 h ( $T=20$ ). **B**, Gel slices excised and subject to separate in-gel digestion with post-digestion pooling group indicated (A-F). **C**, Thylakoid membranes solubilised in 1% SL before (1) and after (2) removal of starch granules by centrifugation. **D**, Thylakoid membranes solubilised in 1% SL before ( $T=0$ ) and after incubation with trypsin at 37°C before quenching at 1 h ( $T=1$ ), 2 h ( $T=2$ ) and 16 h ( $T=16$ ). **E**, Overnight-digested peptides before (1) and after (2) extraction of SL in ethyl acetate.

An important aspect of MS-based proteomics is sample fractionation to increase sensitivity and proteome coverage. In addition to the chromatographic separation of peptides coupled to the mass spectrometer, additional, prefractionation can be carried out at various stages of sample preparation, before or after protein digestion. A well-established and widely-used method of prefractionation is SDS-PAGE followed by in-gel digestion (Aebersold and Mann, 2003). The SDS-PAGE gel, either one or two-dimensional, containing the denatured protein of interest is cut into 1 mm cubes and subject to reduction, alkylation and digestion. Following digestion, peptides can diffuse out of the gel pieces ready for desalting and MS analysis. In-gel digestion was applied to Arabidopsis thylakoid membranes separated in one dimensional SDS-PAGE and divided into sections as shown in Figure 6B. Each of the 30 gel strips was subject to in-gel digestion independently then the eluted peptides were pooled into 6 fractions (A-F) to be analysed independently by nanoLC-MS/MS. This resulted in the identification of 681 proteins, much higher than by digestion in MeOH. However, despite the apparent increase in identifications, coverage of specifically thylakoid-associated proteins was poor, with several proteins of interest missing from the dataset. One issue with in-gel digestion is contamination by exogenous proteins as a result of the considerable amount sample handling involved with processing the gel. Indeed, when looking at the MS data for this experiment, common contaminants – such as keratin – contributed 29% of the total protein intensity.

A third digestion method trialled was in-solution digestion with eLys-C and trypsin in 8 M urea. For the protein sample to be solubilised in 8 M urea, it must first be precipitated in acetone and cleaned up to remove other membrane components such as lipids and pigments. The cleaned and precipitated protein pellet was resuspended in 8 M urea and subject to reduction and alkylation before the addition of the two-enzyme mixture. The enzyme eLysC is active in 8 M urea and cleaves after lysine residues so it can cleave the unfolded protein into large but more accessible peptides. The mixture was then diluted to bring the urea concentration down to 2 M urea and allow trypsin to refold and complete the digestion. However, one issue arising from this method was poor solubility of the precipitated protein pellet in 8 M urea following the clean-up step. Despite this difficulty, the initial in-solution digestion experiment resulted in the identification of 422 proteins (Figure 6A).

Strategies to increase detection of lower-abundance proteins and improve proteome coverage focus on simplifying the mixture of peptides to be analysed. Prefractionation of the digested peptide mixture before analysis by LC-MS can facilitate detection and identification of peptides previously obscured by more intense peptide ions eluting at the same time. Fractionation of tryptic peptides generated from in-solution digestion, as described above, was performed using columns containing a porous graphitic carbon stationary phase (Hypercarb), where the peptides were bound then eluted sequentially with increasing concentrations of ACN. The retention mechanisms of this material differ to those of the reversed phase chromatography system used to separate peptides prior to elution onto the MS. To determine whether these mechanistic differences were reflected in the separation of peptides, fractions

eluted from the Hypercarb columns were analysed separately by LC-MS and a selection of peptides was used to generate an orthogonality plot (Figure 7A). When retention time was plotted against Hypercarb elution fraction, it was observed that there was only weak correlation, and particularly peptides from the 40% and 50% ACN fraction were retained on the LC for variable lengths of time. This suggests that Hypercarb fractionation may be an effective way to increase identifications. However, prefractionation in this way did not translate into increased numbers of protein identifications (Figure 7B).

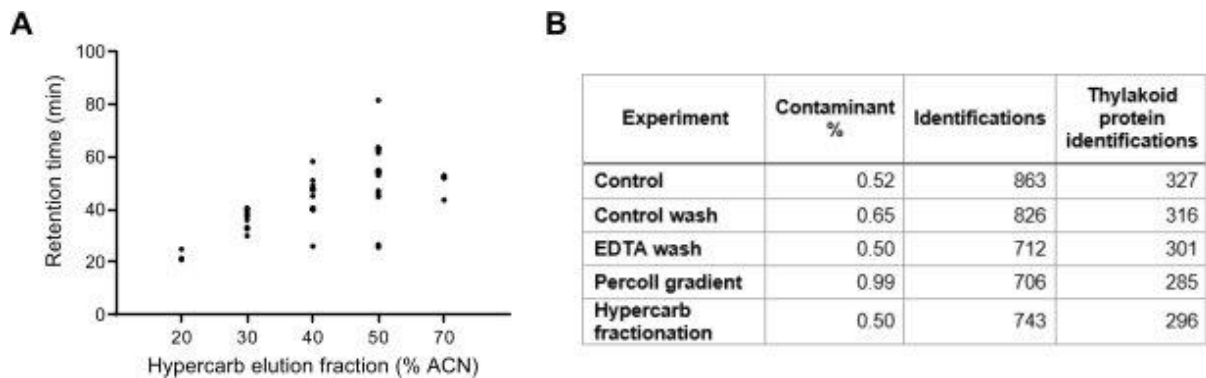


Figure 7: Analysis of strategies to increase thylakoid proteome coverage. **A**, Orthogonality plot of peptide ion ( $n = 50$ ) nanoLC retention time against acetonitrile (ACN) concentration required for elution from Hypercarb spin columns. **B**, Table to show the number of proteins identified (Identifications), the number of thylakoid proteins identified (Thylakoid protein identifications), and the percentage of total MS intensity arising from known contaminant proteins (Contaminant %) for thylakoid membranes digested in-solution. Samples compared were thylakoid membranes without extra clean up steps or prefractionation (Control), with an additional wash in thylakoid storage buffer (Control wash), an additional wash with thylakoid storage buffer supplemented with 2 mM EDTA (EDTA wash), further purified on a Percoll gradient, and digested peptides fractionated by sequential elution from Hypercarb spin columns at increasing concentrations of ACN.

When prefractionation proved ineffective at increasing identifications, the focus was turned instead to the purity of the thylakoid membrane sample prior to digestion. If the sample could be simplified by reducing contamination of the thylakoids by other cellular components then, in theory, more low-abundance proteins would be raised above the detection threshold. To increase purity, thylakoid membranes were either given an additional wash with storage buffer (control wash) or washed with storage buffer supplemented with EDTA to disrupt metal ion-mediated interactions. Thylakoids were also further purified on a Percoll gradient to separate the membranes from other cellular components pelleting alongside them during preparation. The further-purified thylakoid membranes were digested in-solution as described earlier and analysed by MS to assess whether additional steps affected the number of proteins identified and, more importantly, coverage of the thylakoid proteome. Surprisingly, there was no increase in the number of identifications resulting from additional purification steps (Figure 7B). In fact, they resulted in fewer thylakoid protein identifications, possibly due to the loss of loosely associated peripheral membrane proteins and more transient interactions. Notably, many luminal proteins such as plastocyanin were absent from the EDTA-washed dataset. This could suggest

that washing with EDTA damages the thylakoid membrane such that soluble proteins in the lumen are able to leak out. More stringent purification strategies and prefractionation do not appear to compensate for poor digestion efficiency or poor suitability of a digestion technique for this type of sample.

When commonly used protein digestion methods proved suboptimal for analysis of the thylakoid membrane proteome, a less well-established method was tested. The detergent sodium laurate (SL) was proposed by Lin et al. (2013) as an effective reagent for extraction, solubilisation, and digestion of membrane proteins by trypsin. This study demonstrated that digestion in SL was superior with respect to the number of membrane proteins identifications obtained relative to Rapigest and sodium dodecylcholate, two detergents commonly used in tryptic digestion. These findings suggest that digestion in SL may be an appropriate method for thylakoid protein analysis, so a number of experiments were performed to assess its efficacy.

Firstly, detergent solubilisation of thylakoids presented an opportunity to separate protein from starch granules. To determine whether SL could be used for this purpose without losing thylakoid proteins, solubilised protein was analysed by SDS-PAGE before and after removal of starch by centrifugation (Figure 6C). The similar profile of bands from the starch-containing and starch-free samples indicated that there was not a substantial loss of protein resulting from centrifugation. To test the method for efficiency of digestion when applied to thylakoid proteins, a time course experiment was performed with aliquots quenched at 1 h, 2 h and 16 h after the addition of trypsin/endo-LysC mix and analysed by SDS-PAGE (Figure 6D). Aside from one band at ~60 kDa which resisted digestion even after 16 h, digestion of thylakoid protein appeared complete after 2 h. At 16 h some aggregation of digested peptides was observed in the higher molecular weight region of the gel. Another reported advantage is the ease with which the detergent may be extracted from the peptide sample following digestion. Briefly, an equal volume of ethyl acetate is added following acidification by TFA, and the peptide-containing, detergent-free aqueous phase is collected. To determine whether there was a significant loss of peptides into the organic phase following detergent extraction, thylakoid proteins were digested in 1% SL overnight and another SDS-PAGE analysis was performed with digested peptides before and after detergent removal (Figure 6E). The profile of Coomassie Blue staining in the two lanes was very similar, suggesting that the ethyl acetate-based extraction of SL does not dramatically affect the composition of the peptide sample. Interestingly, no band was visible at ~60 kDa indicating more complete digestion.

Once each step of this method had been validated, digestion in SL was used to prepare thylakoids for proteomic analysis. Since longer incubation times caused peptide aggregation, thylakoid proteins were digested for just 3 h in 1% SL and the cleaned-up peptides were analysed by LC-MS. This resulted in the identification of 900 proteins (Figure 8A), including 370 thylakoid-associated proteins. Because of the simplicity, speed, and high proteome coverage of this method, digestion in SL was selected as the

protocol for thylakoid proteome analysis and quantification for the proteomics experiments described in this thesis (Figure 8B).

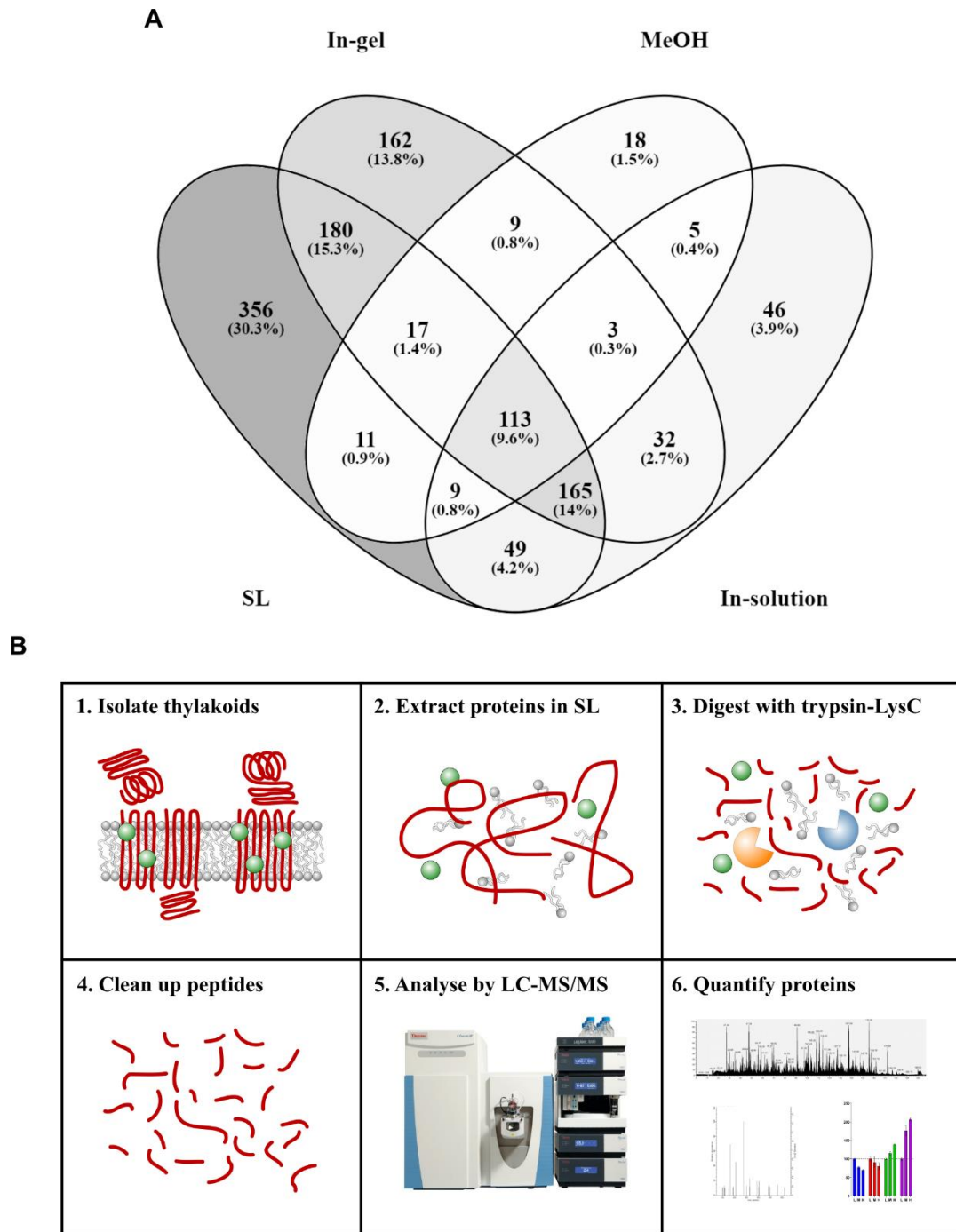


Figure 8: Method selection for preparation of thylakoid membranes for MS analysis by digestion. **A**, Venn diagram showing proteins identified from MS analysis following processing of thylakoid membrane proteins by in-gel digestion (In-gel), digestion in 60% methanol (MeOH), digestion in 1% sodium laurate (SL), and digestion in solution in urea (In-solution). MS files were processed in Mascot Daemon. **B**, Schematic diagram outlining the method for proteomic analysis of thylakoid membranes in SL.

### 3.3 Label-free relative quantification of the thylakoid proteome

Once chosen, the SL-based digestion method and MS analysis was applied to thylakoid membrane from *Arabidopsis* plants acclimated to low, moderate and high light intensity. The results of this experiment are discussed in Chapter 4. In order to use this MS data to quantify the differences in thylakoid protein abundance between samples, an appropriate normalisation and quantification strategy must be applied.

The processing of raw MS files to sequence peptides, search the *Arabidopsis* proteome database and quantify identified proteins was performed in the software MaxQuant. This software features MaxLFQ, a widely-used inbuilt algorithm which normalises between MS experiments accounting for differences in the amount of sample injected and random variations in spectral acquisition patterns. MaxLFQ also functions to quantify proteins and may be used as a proxy for molar amounts (Cox et al., 2014; McKenzie et al., 2020; Zhao et al., 2020a). MaxLFQ bases protein quantification on an unchanging ‘background’ proteome, aiming to minimise the differences within this protein subset using ratios of peptide intensity values in different experiments. This algorithm, and indeed most proteomics platforms, were generally designed for whole-cell or whole-tissue analysis where the aim is to identify proteins which are significantly up- or downregulated but where most proteins will be relatively unchanging. For example, a disease biomarker may be detected from a sample at a level many orders of magnitude above its normal abundance while thousands of other proteins are unchanging. In contrast, this study of the thylakoid proteome involves a very different sample type, a subcellular fraction, and the aim of the experiment is instead to quantify a large number of relatively small changes (likely within the same order of magnitude) which together result in remodelling of the entire system. Since there is no set of ‘housekeeping’ proteins within the thylakoid membrane known to remain at a constant level under the environmental conditions tested, this lack of a ‘background’ proteome may prohibit accurate quantification by MaxLFQ and distort the data. Therefore, factors such as the sample type, data distribution and specific experimental aims must be considered when selecting an appropriate strategy for normalisation and quantification of proteomic datasets.

Mass spectra were searched through the UniProtKB *Arabidopsis thaliana* proteome database in MaxQuant (Cox and Mann, 2008) to map peptide sequences to proteins. Peptides with molecular mass alterations arising from the posttranslational modification by Lysine acetylation were included in the search because this modification is widespread in *Arabidopsis* (Wu et al., 2011) and is found as a feature of light harvesting proteins (Michel et al., 1991) in addition to N-terminal acetylation (Galetskiy et al., 2008). The MaxLFQ algorithm was enabled, as was intensity-based absolute quantification (iBAQ) (Schwanhäusser et al., 2011). The iBAQ method compensates for either molecular mass or the number of detectable peptides generated by proteolysis and is unaffected by variable sample complexity. It does not normalise between MS experiments, but adjusts raw intensities by dividing by the number of theoretical tryptic peptides released upon digestion of that protein. Therefore, iBAQ data is suitable for

and requires normalisation to either an internal standard present at constant levels – a ‘housekeeping’ protein or set of proteins – or to total protein.

To determine which relative quantification method is most appropriate, it is important to assess the distribution of the raw MS intensity data within each experiment and the differences between sample types. The first noticeable difference between MS data from different plant growth light intensities was the overall number of proteins identified. Indeed, there were significant differences in the number of non-zero values between sample types, with the number of identifications increasing with light intensity (Figure 9A). To investigate these differences further, the median raw intensity of each protein was taken from each light intensity and used to plot histograms of LL (Figure 9B), ML (Figure 9C) and HL (Figure 9D). The data does not show a normal distribution in any light intensity, rather one that is right-skewed and possibly multi-modal. Protein identifications that were determined to be thylakoid-associated by SUBA4, GO annotation and manual curation (see Section 2.9) appeared to have a similar intensity distribution in different light intensities. However, in LL compared to HL, there were more thylakoid proteins in the lower and upper ranges of protein intensity. Non-thylakoid proteins made up a substantial portion of total protein identifications in each light condition, although their place in the overall distribution of intensities differed according to light condition. In LL (Figure 9B), non-thylakoid proteins were shifted further towards the lower-intensity region than in HL (Figure 9D), suggesting that the LL thylakoids contained a lesser degree of contamination from other cellular components. A scatter plot of protein raw intensities in HL vs LL (Figure 9E) also showed differences in the distribution of thylakoid and non-thylakoid proteins. To confirm whether these differences reflected inconsistencies in the ‘purity’ of the isolated thylakoids, the proportion of thylakoid protein intensity relative to total intensity was calculated (Figure 9F). For LL data, thylakoid proteins contributed around 98% of the total raw intensity whereas in HL this figure was about 10% lower. This discrepancy was also seen in data processed by both MaxLFQ and iBAQ, although in the latter the difference was narrowed slightly. The total intensity of each MS experiment with and without MaxLFQ normalisation is shown in Figure 9G. While MaxLFQ appears to normalise data well between MS experiments from the same light condition, it puts the total intensity in HL to half that of LL.

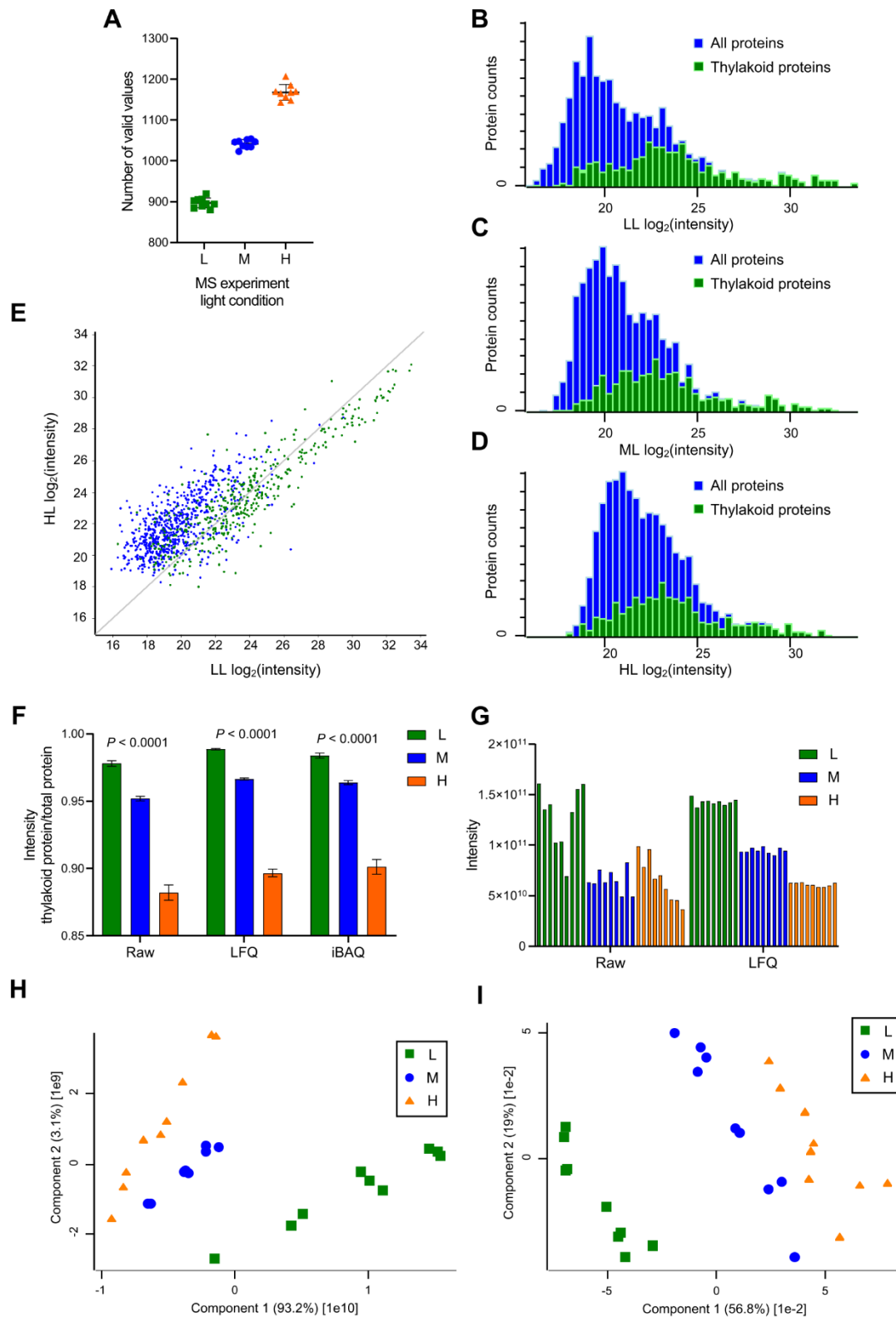


Figure 9: Processing of MS data from light-acclimated thylakoids. **A**, The number of proteins identified in each MS experiment, grouped by acclimation growth light. **B**, **C**, **D**, Histograms to show the intensity distribution of protein identifications from median values from low (**B**), moderate (**C**) and high (**D**) light conditions. Distribution of thylakoid proteins within all identifications is highlighted in green. **E**, Median intensity values of proteins in high light (HL) versus those in low light (LL). Thylakoid proteins are green, while non-thylakoid proteins are blue. The grey line indicates  $LL \log_2(\text{intensity}) = HL \log_2(\text{intensity})$ . **F**, Intensity of all thylakoid proteins divided by total intensity for raw MS data (Raw), MaxLFQ-normalised

data (LFQ), and iBAQ, grouped by plant growth light condition. Significance (*P*) was determined by one-way ANOVA, *n* = 9. **G**, Total intensity of MS experiments without normalisation (Raw) and with MaxLFQ normalisation (LFQ). **H**, Raw data from MS experiments, filtered to remove non-thylakoid proteins, subject to principle PCA as implemented in Perseus. **I**, iBAQ data normalised to the intra-analysis sum of key photosynthetic component PSII, PSI, Cytb<sub>6</sub>f and ATP synthase from MS experiments, filtered to remove non-thylakoid proteins, subject to PCA as implemented in Perseus.

Together, this data suggests that MaxLFQ is not a suitable method for normalisation and relative quantification of MS data from thylakoid membranes from different light conditions. However, this method may be appropriate for normalisation between data from a single light condition or between datasets which do not differ substantially in purity. The differences in purity also preclude normalisation to total protein intensity as this would bias all thylakoid protein intensity values towards LL. The differences in the distribution of thylakoid protein intensities also discourage normalisation to total thylakoid protein, which could see changes in highly abundant proteins such as the light harvesting antenna having undue influence on the rest of the data. Instead, a strategy was chosen where normalisation is based on the four main complexes of the linear electron transfer chain: PSII, Cytb<sub>6</sub>f, PSI and ATP synthase. The sum of the iBAQ values for the constituent proteins of these complexes was summed and used for normalisation of the whole dataset. A principle component analysis (PCA) of thylakoid protein intensities from raw data (Figure 9H) and normalised iBAQ data (Figure 9I) showed an improvement in grouping of light intensities in two dimensions. This normalisation and quantification method was chosen as the standard for relative quantification of thylakoid proteins in this thesis.

### 3.4 Discussion

Efficient digestion of membrane proteomes is not as straightforward as that of soluble protein fractions due to their hydrophobicity, poor solubility, and lower frequency of trypsin cleavage sites compared to cytosolic proteins. There may also be too frequent cleavage sites for chymotrypsin, specific for aromatic residues, within transmembrane helices such that digestion yields peptides too small for identification (Alfonso-garrido et al., 2015; Fischer and Poetsch, 2006). For these reasons, isolated *Arabidopsis thaliana* thylakoids were subject to a range of methods to select a strategy that achieved the most efficient digestion and the best proteome coverage. Despite the reported suitability for membrane proteins, tryptic digestion in 60% MeOH proved ineffective for solubilisation and digestion of thylakoid proteins and it was demonstrated that some proteins remained intact, even after overnight digestion. In-gel digestion gave good coverage of the thylakoid proteome but the lengthy sample handling involved introduced a substantial amount of keratin contamination and made the technique less favourable for multiple samples and replicate digestions. In-solution digestion in urea gave reasonably good proteome coverage, although some difficulty was encountered prior to digestion when the precipitated thylakoid protein solubilised poorly in 8 M urea. This poor solubilisation following precipitation is likely to reduce the digestion efficiency and MS detection of hydrophobic proteins, which are more prone to

aggregation when removed from a lipid bilayer. Despite this issue, in-solution digested peptides were subject to prefractionation in an attempt to increase detection of low-abundance proteins. Thylakoids were also subject to more stringent purification prior to digestion. When neither of these strategies proved effective for increasing sensitivity, an alternative and less well-established digestion method was explored. Digestion of thylakoid membranes in SL detergent (Lin et al., 2013) proved superior to other methods in both simplicity and in the number of proteins identified.

Once MS data was obtained from digestion of light-acclimated thylakoids in SL, database searching and protein quantification was carried out in MaxQuant (Cox and Mann, 2008). For quantitative MS, particularly in label-free methods, protein intensity values are not inherently quantitative and require strategies to account for random variations in digestion efficiency and spectral acquisition. Raw intensity values are often highly variable, sometimes across more than one order of magnitude, for subunits which are highly likely based on structural determination to be present at or near equimolar amounts within the same complex. The explanation for this lies in the tendency for larger proteins to produce more peptides upon digestion, so a very abundant but low molecular weight protein could give rise to the same MS intensity as a very large but low-abundance protein. Similarly, very hydrophobic proteins of high abundance can be underrepresented due to their failure to release the number of MS-compatible peptides which would be expected for its size. The MaxLFQ algorithm aims to normalise between MS experiments and operates under the assumption that the samples are of a similar complexity and feature an unchanging background proteome, from which dramatically up- or down-regulated proteins can be identified (Cox et al., 2014). An assessment of the data distribution in thylakoids isolated from different light environments was performed to determine whether the in-built MaxLFQ algorithm was appropriate for normalisation and quantification of the proteins in this sample type. The differences in the protein profiles of the samples such as complexity, distribution and purity of the isolated thylakoid membranes suggested that MaxLFQ would skew the data and would not be useful for relative quantification between light environments. However, MaxLFQ may be appropriate when applied to a single light intensity for estimation of absolute stoichiometries. This approach was used by McKenzie et al. (2020) for the calculation of relative abundance of the photosynthetic machinery in *Arabidopsis thaliana* grown at a single moderate light condition. However, because of the poor accessibility of trypsin cleavage sites in membrane proteins, intensity values of membrane proteins may not be truly representative of molar amounts. Therefore, label-free proteomics is more reliable when used for relative quantification between biological conditions and absolute stoichiometries calculated this way should be treated with caution.

Relative quantification between light conditions was carried out using protein iBAQ values. Because iBAQ accounts for how differences in the molecular weight of proteins affect the number of peptides released and, therefore, the MS intensity, iBAQ values for proteins of the same complex can be summed to give a value for the abundance of that complex. Therefore, iBAQ enabled normalisation to the intra-

analysis sum of key photosynthetic complexes PSII, PSI, ATP synthase and *cytb<sub>6</sub>f*, which together contributed around 50% of the total iBAQ intensity. This method of normalisation is not affected by differences in sample complexity and avoids reliance on a single ‘housekeeping’ protein. Relative quantification of thylakoid proteins by this SL digestion, mass /MS and iBAQ normalisation shows thylakoid proteome remodelling in an unprecedented level of detail and can be combined with other biochemical techniques to gain a more complete understanding of how these changes relate to biological functions.

## 4 Acclimation of the photosynthetic machinery to light environment in *Arabidopsis*

The work described in this chapter contributed to the following research publication:

Flannery, S.E., Hepworth, C., Wood, W.H.J., Pastorelli, F., Neil Hunter, C., Dickman, M.J., Jackson, P.J., and Johnson, M.P. (2021). Developmental acclimation of the thylakoid proteome to light intensity in *Arabidopsis*. *Plant J.* *105*, 223–244.

### 4.1 Introduction

As sessile organisms, plants are subject to differences in light intensity in the long term depending on their growth environment. The intensity of sunlight reaching the leaves will differ depending on the season, climate, and shading by other plants or structures, and has a profound effect on photosynthesis. To grow successfully, plants must tailor the composition of the thylakoid membrane in a process known as acclimation to optimally utilise available light energy, maintain photosynthetic efficiency, and minimise damage to photosynthetic reaction centres. Long-term acclimation may be categorised as either ‘dynamic’ or ‘developmental’. Dynamic acclimation takes place in fully mature leaves and involves *de novo* synthesis and degradation of specific proteins, leading to changes in the organisation of the chloroplast thylakoid membranes, their protein composition and that of the surrounding stroma that contains the enzymes of the CO<sub>2</sub>-fixing CBB cycle (Athanasίου et al., 2010; Suorsa et al., 2012; Walters and Horton, 1994; Yin and Johnson, 2000). Developmental acclimation, which is the focus of this work, is the alteration of leaf development and morphology in addition to the changes in chloroplast composition (Anderson, 1986; Anderson et al., 1988; Bailey et al., 2001, 2004; Boardman, 1977; Schöttler and Tóth, 2014; Vialet-Chabrand et al., 2017; Walters, 2005). Vital to plant fitness, it is unclear whether acclimation is fully optimised in many species, presenting an opportunity for future manipulation in agriculturally relevant species.

Long-term acclimation to the light environment has been studied extensively in the past but much of this work was done prior to the discovery of the vast array of regulatory proteins that support the light reactions. There is little information on how the relative abundance of these regulatory proteins is affected by light intensity. Whilst valuable, previous studies tended to use techniques that quantify just a single protein at once, such as immunoblotting, or focus on parts of the photosynthetic apparatus that contain light harvesting pigments and can be quantified spectroscopically. Mass spectrometry (MS)-based proteomics, on the other hand, allows relative quantification of the entire proteome and does not rely on the subset of thylakoid proteins that absorb visible light. By determining how the thylakoid proteome is remodelled in response to a long term change in light intensity, a more complete understanding can be gained of how the photosynthetic machinery operates and how different regulatory and photoprotective mechanisms are integrated. Unlike in many other techniques, small

differences in the amino acid sequences of minor isoforms of very similar proteins, such as antenna proteins, can be distinguished in a MS analysis, allowing these isoforms to be independently quantified and providing clues to their different functions. The data can be combined with other spectroscopic, structural and functional analyses to determine how changes in abundance relate to changes in function. Mass spectrometry also has the potential to identify proteins previously not known to have roles in long-term acclimation without generation of mutants and reveal possible targets for genetic manipulation. Because photosynthetic acclimation is an area of research with implications for agricultural crop yields, a better understanding could eventually facilitate the design of strains more suited to particular climates.

Here, a novel protein extraction and digestion method (discussed in Chapter 3) was used to prepare thylakoid membranes for label-free proteomic analysis by nano liquid chromatography mass spectrometry (LC-MS). A total of 402 thylakoid-associated proteins were relatively quantified between low (LL), moderate (ML) and high growth light intensity (HL) to investigate the effect on the key photosynthetic complexes, light-harvesting antenna proteins, electron transfer routes, structural components and many regulatory proteins not previously quantified. The proteomic analysis was combined with various other techniques such as blue-native polyacrylamide gel electrophoresis (BN-PAGE), electron microscopy (EM) and structured illumination microscopy (SIM).

#### 4.2 Growth of *Arabidopsis thaliana* and characterisation of the light-acclimated thylakoid membrane

*Arabidopsis* plants were grown for 2 weeks at a moderate light intensity ( $150 \mu\text{mol photons m}^{-2} \text{s}^{-1}$ , ML), typical of that used by a large number of research groups, to a rosette diameter of around 3 cm. Following this 2-week period, plants were either maintained for a further 3 weeks at ML or alternatively transferred to low light ( $25 \mu\text{mol photons m}^{-2} \text{s}^{-1}$ , LL) or high light ( $800 \mu\text{mol photons m}^{-2} \text{s}^{-1}$ , HL) (Figure 10). All mature leaf material was formed under acclimation light, producing developmental rather than dynamic acclimation, and the amount of time the plants were exposed to acclimation light conditions was adjusted to account for faster maturation under higher light intensity, with plants exposed to LL for 5 weeks, plants exposed to HL for just 2 weeks. All plants were harvested prior to flowering to minimise the effects of senescence on thylakoid composition. The different growth light intensities had a profound effect on leaf morphology with LL plants displaying elongated petioles, while HL plants showed truncated petioles and wrinkled leaves compared to ML plants, as observed previously (Schumann et al., 2017). Outwardly, the HL plants displayed no obvious signs of light stress such as accumulation of anthocyanins. Corresponding gas exchange and chlorophyll fluorescence data reported elsewhere (Flannery et al., 2021) demonstrated acclimation-related differences in photosynthetic function between plants grown at the three light intensities, with higher growth light being associated with greater maximum capacity for  $\text{CO}_2$  assimilation and PSII electron transfer rates.

For experiments requiring isolated thylakoids, leaf material from 15 plants was combined and used to produce a pooled sample from which technical replicates could be generated.

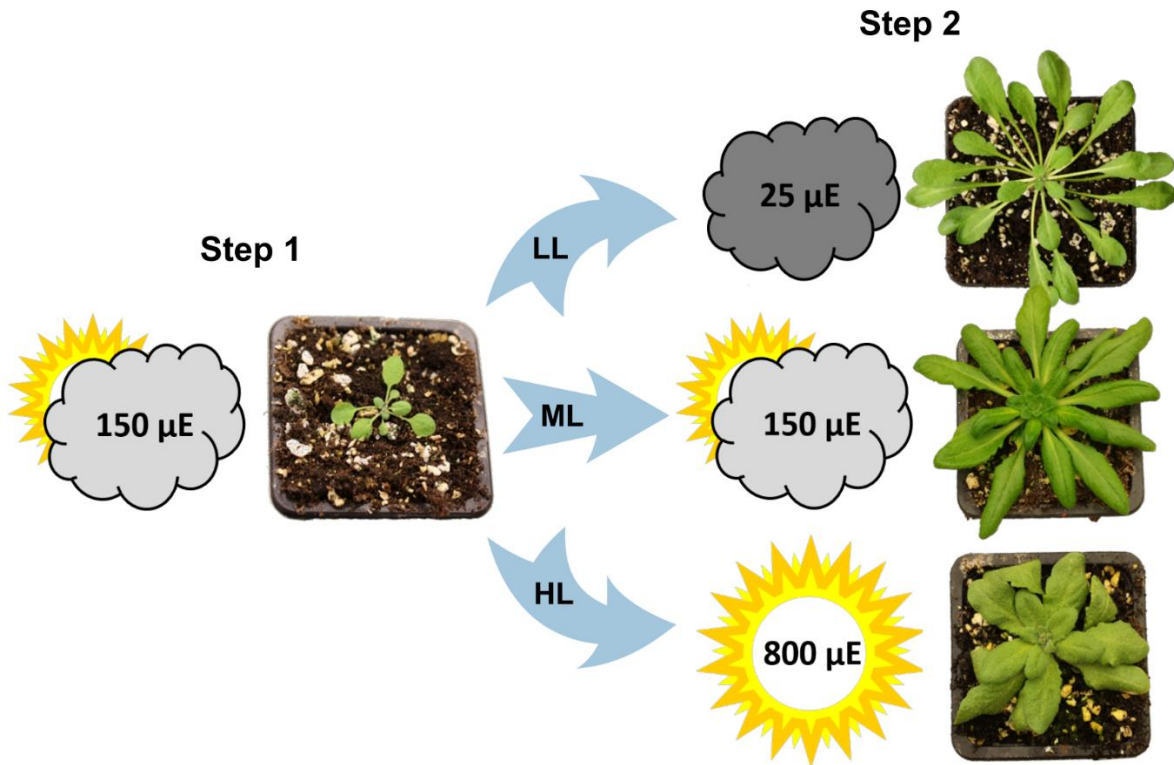


Figure 10: Growth of light-acclimated Arabidopsis plants. Seedlings were grown at ML ( $150 \mu\text{E}$ ) until they reached a diameter of around 3 cm (Step 1) then transferred to LL ( $25 \mu\text{E}$ ), ML ( $150 \mu\text{E}$ ) or HL ( $800 \mu\text{E}$ ) and harvested on the day of photographing (Step 2). Here,  $\mu\text{E} = \mu\text{mol photons m}^{-2} \text{s}^{-1}$ .

Ratios of chlorophyll *a* to chlorophyll *b* in the thylakoids were calculated as an indicator of acclimation to the light environment (Dale and Causton, 1992) since PSII, PSI and LHCII differ in their chlorophyll composition. The chlorophyll *a/b* ratio of the thylakoids increased slightly with growth light intensity, as did the protein to chlorophyll ratios (Figure 11A). Relative to PSII and its core antenna, LHCII contains a higher ratio of chlorophyll *b* whereas PSI contains more chlorophyll *a*, so it is still possible for the stoichiometry of the three complexes to change without a net change in the *a/b* ratio. However, the relative increase in chlorophyll *a* observed would imply a decrease in antenna size under higher light. Protein to chlorophyll ratios in isolated thylakoids, on the other hand, were used to indicate how much of the thylakoid proteome is dedicated to light harvesting and photochemistry and suggest that in LL a greater proportion of total protein is for the purpose of light absorption.

To confirm that changes in thylakoid protein abundance have arisen from growing the plants under the chosen acclimation conditions, immunoblotting was performed for components of some of the key complexes. In Figure 11B, immunoblots against the D2 (PSII), PSAA (PSI), PETA (*cytb<sub>f</sub>*) and ATPH (ATP synthase) proteins from an SDS-PAGE of total thylakoid proteins loaded on an equal chlorophyll basis are shown. Consistent with previous reports, the PSI level was somewhat constant, while PSII,

*cytb<sub>6</sub>f* and ATP synthase levels increased with growth light intensity relative to total chlorophyll (Anderson et al., 1988). The expected acclimation-related changes were also clearly observed in the blue native polyacrylamide gel electrophoresis (BN-PAGE) analysis at the whole complex level in Figure 11C. Here, thylakoid membranes were solubilised at equal chlorophyll concentration from LL, ML and HL plants stepwise, first with digitonin to remove the unstacked PSI-enriched stromal lamellae domain of the thylakoids, then the stacked PSII-enriched grana were solubilised with a mixture of *n*-hexadecyl  $\beta$ -D-maltoside and *n*-dodecyl  $\alpha$ -D-maltoside (Wood et al., 2018). Native gels can show qualitative changes in supercomplex formation as well as changes in the amounts of particular complexes. The ATP synthase complex, recovered in the stromal lamellae fraction, increased with growth light intensity as did that of *cytb<sub>6</sub>f*. Changes in the amounts of LHCII were also clearly seen in the BN-PAGE with fewer free L-type trimers observed with increasing growth light intensity in both grana and stromal lamellae. Changes in the amounts of the PSII-LHCII supercomplexes and their sizes were also observed with growth light intensity consistent with previous results (Albanese et al., 2016; Ballottari et al., 2007; Kouřil et al., 2013). Within the grana fraction there are larger C<sub>2</sub>S<sub>2</sub>M<sub>2</sub> type PSII-LHCII supercomplexes, composed of a dimeric PSII RC linked to two copies each of the minor monomeric antenna complexes CP29 (LHCB4), CP26 (LHCB5) and CP24 (LHCB6), and to four LHCII trimers, two of which are strongly attached ‘S’-trimers composed of a mixture LHCB1 and LHCB2 (Caffarri et al., 2009). The level of these supercomplexes decreased with increasing growth irradiance. Levels of the smaller C<sub>2</sub>S<sub>2</sub>M-type supercomplex (lacking one CP24 and one M-trimer) and C<sub>2</sub>S<sub>2</sub>-type supercomplex (lacking both CP24 and both M-trimers) were more constant. Additionally, the fraction of C<sub>2</sub>S<sub>2</sub>M<sub>2</sub> and C<sub>2</sub>S<sub>2</sub>M supercomplexes recovered from the stromal lamellae actually increased in ML and HL compared to LL, suggesting that some redistribution of components between domains occurs with acclimation, or that they are more easily liberated from the grana by digitonin solubilisation. In the stromal lamellae, the amount of PSI-LHCII supercomplexes declined with increasing growth light intensity. While qualitatively informative, this BN-PAGE analysis may not be truly representative of the absolute amounts of these complexes since normalisation is done on a chlorophyll, not protein, basis and properties of the membranes such as protein interactions, density and lipid profile may affect the solubility of complexes.

Native thylakoid membranes were used for low temperature (77K) fluorescence experiments to further assess antenna size and relative abundance of complexes. At room temperature, emission from PSI is very weak and is not comparable with that of PSII, whereas a distinct and strong PSI emission band can be detected at 77K. Light absorption from both photosystems peaks with excitation at a wavelength of 435 nm, which is used to compare their (and their linked antenna’s) absorption cross sections by measuring their emission spectra. The larger ratio of the PSI to PSII emission bands observed in the 77K emission spectrum (Figure 11D) is consistent with the increased antenna cross-section of PSI in LL seen in BN-PAGE. To measure excitation spectra from PSII and PSI, emission is recorded from 695

nm and 735 nm, respectively, and normalised to the Soret region so that the relative spectral contribution of chlorophyll *b* may be used to infer changes in antenna size. The 77K PSII and PSI excitation spectra (Figure 11E, F) also showed that the antenna cross-section of each photosystem decreased with increasing growth irradiance.

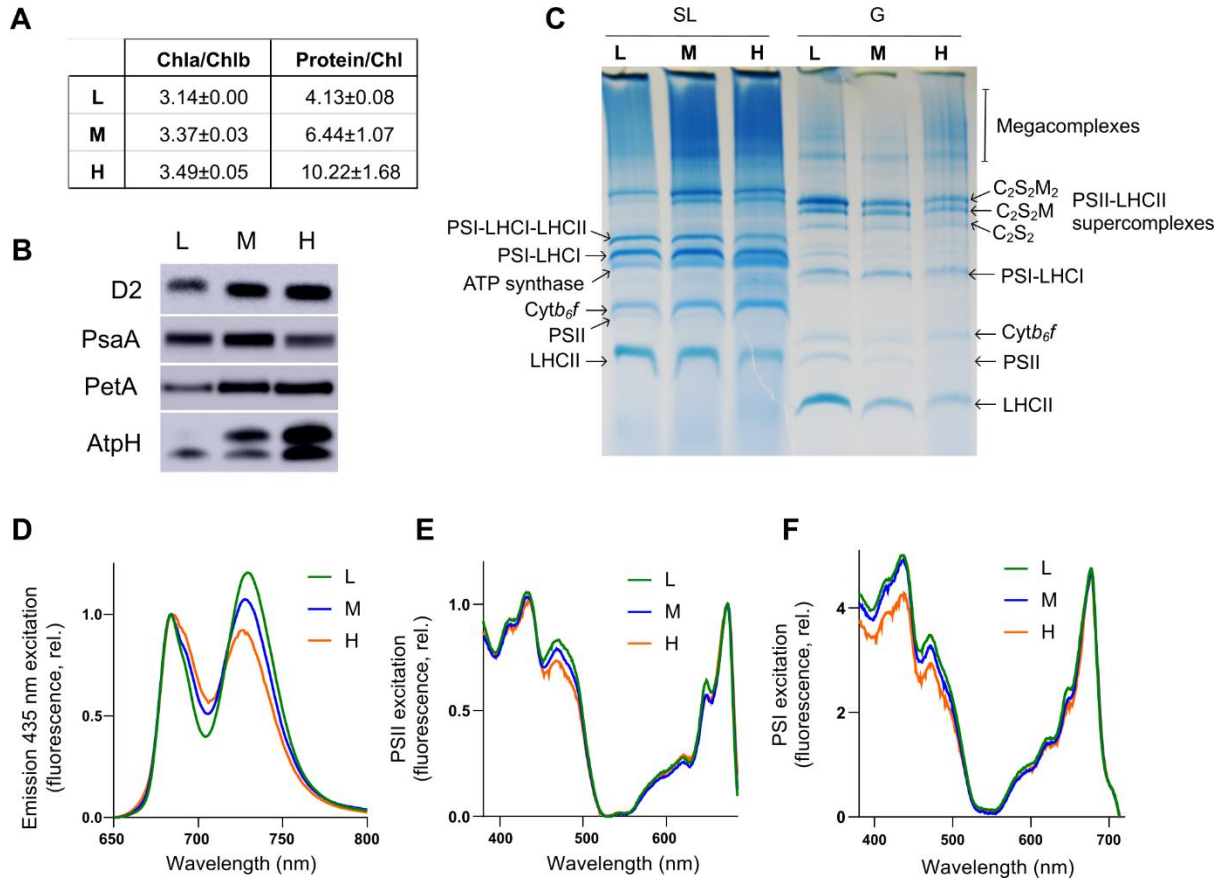


Figure 11: Characterisation of acclimated thylakoid membranes. **A**, Ratio of chlorophyll *a* to chlorophyll *b* and of protein to chlorophyll in isolated thylakoid membranes from low (L), moderate (M) and high (H) light intensity. **B**, Immunoblots of LL, ML and HL thylakoids, with loading normalised to chlorophyll, to qualitatively assess the abundance of PSII (D2), PSI (PsaA), Cytb<sub>6</sub>f (PetA) and ATP synthase (AtpH). **C**, BN-PAGE of solubilised stromal lamellae (SL) and granal (G) thylakoid fractions. **D**, 77 K fluorescence emission spectra of LL (green), ML (blue) and HL (orange) thylakoids using 435 nm excitation. **E**, 77 K fluorescence excitation spectra of PSII (695 nm) from LL (green), ML (blue) and HL (orange) thylakoids. **F**, 77 K fluorescence excitation spectra of PSI (735 nm) from LL (green), ML (blue) and HL (orange) thylakoids.

### 4.3 Proteomic analysis of key photosynthetic complexes and their antenna

Three sets of thylakoid proteins from the LL, ML and HL plants were prepared for proteomic analysis by solubilisation in 1% SL and proteolytic digestion with a combination of eLysC and trypsin. The resulting peptide fragments were desalted and analysed by nanoLC-MS/MS with data dependent acquisition in triplicate. Mass spectra were searched against the UniProtKB Arabidopsis proteome database to identify and quantify a total of 1,082 proteins present across all light conditions, of which 402 were positively identified as being thylakoid-associated. The stoichiometry of the major photosynthetic complexes (Table 8) was compared between each light condition using the MaxLFQ

label free protein quantification option (Cox et al., 2014) within MaxQuant (Cox and Mann, 2008) to generate normalised intensity values for the individual subunits. The stoichiometry-adjusted mean MaxLFQ intensity value of the component subunits of each photosynthetic complex was used as the abundance score for that complex, the same approach as described by McKenzie et al. (2020). Table 8 shows that the PSII:PSI ratio changed from 2.2 under LL to 2.4 under ML and 3.2 under HL. Similarly, and consistent with the BN-PAGE and immunoblots discussed above, the stoichiometry of *cytb<sub>6</sub>f* and ATP synthase also increased relative to PSI. The *cytb<sub>6</sub>f*:PSI ratio increased from 0.34 in LL to 0.66 in HL, while ATP synthase:PSI increased from 0.47 in LL to 0.71 in HL. These values for *cytb<sub>6</sub>f* and ATP synthase were broadly consistent with those previously reported for Arabidopsis (e.g. McKenzie et al., 2020; Pribil et al., 2014). PSII:PSI ratios for Arabidopsis were more variable depending on the method used, with electron paramagnetic resonance (EPR) based quantification giving a PSII:PSI of ~0.89 for ML (Suorsa et al., 2015), while absorption spectroscopy gave a ratio of ~1.5 (Chow et al., 2012; Wientjes et al., 2013; McKenzie et al., 2020). The stoichiometries reported here and by McKenzie et al. (2020), ranging from 2.2 to 3.2, are considerably higher. One explanation for this difference is that MS detects not only functional PSII as in absorption spectroscopy and EPR but also non-functional PSII being assembled/disassembled during the PSII repair cycle. The stoichiometries calculated here for LHCII were 1.9 trimers per PSII in LL, 1.66 in ML and 1.44 in HL, unexpectedly low given the high abundance of PSII-LHCII supercomplexes and free LHCII trimers observed by BN-PAGE (Figure 11C). Indeed a previous study using SDS-PAGE showed that in LL in Arabidopsis the number of LHCII trimers per PSII was 3.1 in LL, 2.4 in ML and 1.7 in HL (Wientjes et al., 2013a). When the same method is applied to the data published recently by McKenzie et al (2020), the calculated stoichiometry in their study is just 1.15 LHCII trimers per PSII core. The potential limitations of absolute label-free quantification of protein stoichiometries when applied to membrane protein samples are discussed in Chapter 3.

Table 8: Stoichiometry of key photosynthetic complexes and antenna

LL	PSII	PSI	Cytb <sub>6</sub> f	ATPase	NDH	LHCII trimers	LHCI
PSII	1	2.22±0.02	6.51±0.26	4.86±0.20	324.4±13.2	0.53±0.02	0.65±0.0.03
PSI	0.45±0.03	1	2.93±0.17	2.18±0.13	145.9±8.7	0.24±0.01	0.29±0.02
Cytb <sub>6</sub> f	0.154±0.003	0.34±0.01	1	0.75±0.02	49.9±1.2	0.081±0.002	0.100±0.002
ATPase	0.206±0.001	0.458±0.001	1.340±0.003	1	66.8±0.2	0.1082±0.0003	0.1341±0.0003
NDH	0.0031±0.0001	0.0069±0.0001	0.0201±0.0003	0.0150±0.0002	1	0.00162±0.00002	0.00201±0.00003
LHCII trimers	1.90±0.13	4.23±0.29	12.4±0.85	9.24±0.63	617.6±42.3	1	1.24±0.09
LHCI	1.54±0.06	3.42±0.13	10.0±0.4	7.46±0.28	498.4±18.6	0.81±0.03	1
ML	PSII	PSI	Cytb <sub>6</sub> f	ATPase	NDH	LHCII trimers	LHCI
PSII	1	2.49±0.07	5.86±0.18	7.65±0.31	161.5±4.9	0.60±0.02	0.76±0.02
PSI	0.40±0.02	1	2.35±0.15	1.06±0.07	64.9±4.0	0.24±0.01	0.31±0.02
Cytb <sub>6</sub> f	0.17±0.01	0.43±0.02	1	1.20±0.03	27.6±1.4	0.10±0.01	0.13±0.01
ATPase	0.131±0.003	0.94±0.02	0.83±0.02	1	41.5±0.8	0.209±0.004	0.232±0.004
NDH	0.0062±0.0001	0.0154±0.0004	0.0363±0.0008	0.0241±0.0004	1	0.0037±0.0001	0.0047±0.0001
LHCII trimers	1.66±0.16	4.15±0.39	9.75±0.92	16.0±1.1	268.9±25.4	1	1.27±0.12
LHCI	1.31±0.01	3.27±0.03	7.69±0.08	4.32±0.04	212.1±2.2	0.79±0.01	1
HL	PSII	PSI	Cytb <sub>6</sub> f	ATPase	NDH	LHCII trimers	LHCI
PSII	1	3.20±0.06	4.89±0.09	4.53±0.09	141.4±2.7	0.69±0.01	0.79±0.02
PSI	0.312±0.007	1	1.53±0.03	1.41±0.03	44.2±1.0	0.217±0.005	0.25±0.01
Cytb <sub>6</sub> f	0.205±0.006	0.66±0.02	1	0.93±0.03	28.9±0.8	0.142±0.004	0.162±0.004
ATPase	0.221±0.004	0.71±0.01	1.08±0.02	1	31.3±0.6	0.153±0.003	0.174±0.003
NDH	0.0071±0.0001	0.0226±0.0004	0.035±0.001	0.032±0.001	1	0.0049±0.0001	0.0056±0.0001
LHCII trimers	1.44±0.10	4.61±0.32	7.04±0.48	6.52±0.45	203.7±14.0	1	1.14±0.08
LHCI	1.27±0.04	4.06±0.13	6.19±0.20	5.73±0.18	179.2±5.7	0.88±0.03	1

In order to utilise peptide ion intensities as a proxy for protein molar amounts, processing methods that compensate for either molecular mass or the number of detectable peptides generated by proteolysis such as ‘intensity-based absolute quantification’ or iBAQ (Schwanhäusser et al., 2011) are required (Fabre et al., 2014). Using this approach, each dataset was first normalised to the intra-analysis sum of the total subunit iBAQ values from PSI, PSII, ATP synthase and *cytb<sub>6</sub>f*. Using Perseus software (Tyanova et al., 2016), normalised iBAQ values for the three technical repeats were averaged and protein abundances affected by light intensity at  $q < 0.05$  were identified by a modified one-way ANOVA (Section 2.9.9). Significant proteins were subjected to a modified Welch’s t-test (Section 2.9.9,  $q < 0.05$ ) to identify pairs of significant differences for relative quantification of proteins between light conditions. For relative quantification of multi-subunit protein complexes, the sum of iBAQ intensities from all identified subunits of that complex was used. The normalised iBAQ values of the major photosynthetic complexes are presented in Figure 12 and displayed relative to ML at 100% for

clarity. When normalised to protein iBAQ the level of PSII is only very slightly different between LL, ML and HL in contrast to the data in Figure 11B and C, which are normalised on a chlorophyll basis. Similarly, while on a chlorophyll basis PSI is largely unchanging, on an iBAQ basis it increases by ~30% in LL and decreases by ~15% in HL. LHCII increases in LL by ~10% and decreases by ~15% in HL, *cytb6f* decreases by 15% in LL and increases by 20% in HL and ATP synthase decreases by 45% in LL and increases by ~20% in HL. Using the MS data in the form of normalised iBAQ values is arguably more relevant to determining how the relative protein composition of the thylakoid changes between light conditions since the chlorophyll/protein ratio clearly declines with light intensity (Figure 11A), thus chlorophyll-based normalisation is skewed by this.

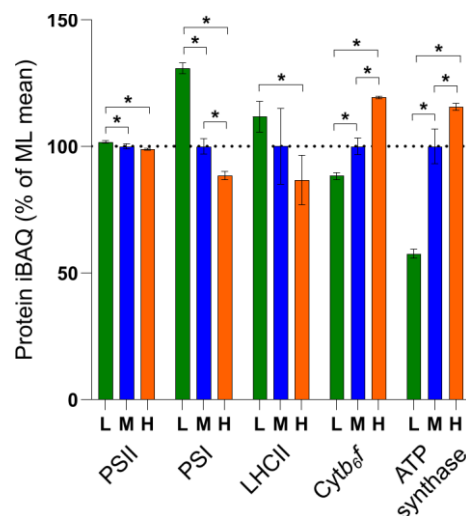


Figure 12: Acclimation involves changes in the relative abundance of key photosynthetic complexes. MS analysis showing the relative abundance in low (L), moderate (M), and high (H) light-acclimated thylakoids of key photosynthetic complexes PSII, PSI, LHCII, *cytb6f* and ATP synthase, expressed as a percentage of the mean at ML. The bars represent the average of three independent peptide preparations ( $n = 3$ ), derived from a pooled thylakoid sample from 15 plants, which were subject to MS analysis in triplicate in a randomised order and the values averaged. Error bars indicate mean  $\pm$  SD. Significant differences between light conditions were determined by a modified Welch's *t*-test (Section 2.9.9,  $*q < 0.05$ ).

The change in the relative abundance of the major trimer LHCII subunits LHCB1, 2, 3 and minor monomeric antenna subunits 4, 5, and 6 is presented in Figure 13A. Of the five LHCB1 isoforms (LHCB1.1-1.5) in the Arabidopsis genome (Pietrzykowska et al., 2014), LHCB1.1, 1.2 and 1.3 did not produce unique tryptic peptides to allow them to be individually distinguished so the relative abundance in Figure 13A is representative of their collective level, which decreased ~25% in HL but was unchanged in LL compared to ML. LHCB1.4 did release unique peptides and so could be separately quantified, increasing by ~10% in LL relative to ML and HL, whereas LHCB1.5 was not identified in the MS analysis. The sequence similarities of the LHCB2.1, 2.2 and 2.4 isoforms prevent differentiation but collectively they increased by 10% in LL and decreased by 20% in HL. LHCB3, the less abundant LHCII trimer constituent found solely in the M-type trimer, remained constant in each light condition. Similarly, the levels of the minor monomeric antenna complex LHCB6 that is most closely associated

with the M-trimer were also relatively constant across the three light intensities. These results contrast with studies on Arabidopsis (Ballottari et al., 2007; Kouřil et al., 2013) which showed LHCB3 and 6 both decrease under high growth light (Bailey et al., 2001; Ballottari et al., 2007), but consistent with another study which showed it was relatively unchanged (Bailey et al., 2001). The levels of LHCB5 increased markedly in LL, a result previously seen in Arabidopsis (Bailey et al., 2001). The content of LHCB4.1 and 4.2 showed a 15% and 5% decrease in HL respectively, and both a 15% increase in LL. In contrast, the minor LHCB4.3 isoform increased dramatically (+255%) in HL consistent with observations of Miller et al. (2017) and Albanese et al. (2018) and decreased by 95% in LL.

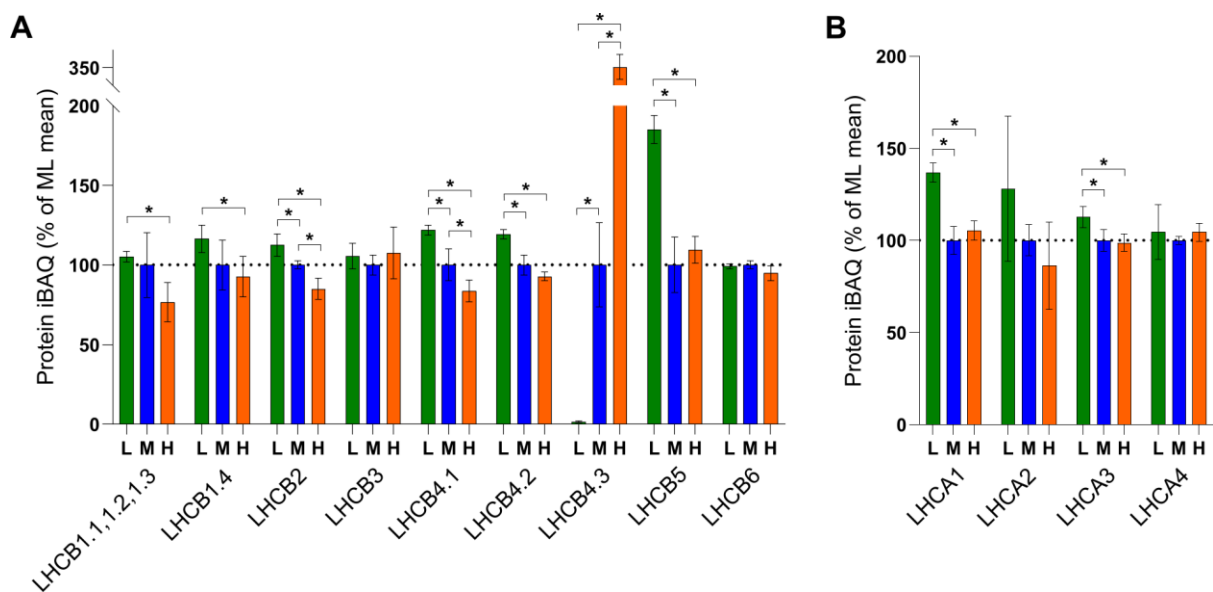


Figure 13: Acclimation involves changes in the relative abundance of antenna proteins. **A**, MS analysis showing the relative abundance of LHCII subunits. **B**, MS analysis showing the abundance of LHCI. Sampling details are as stated in Figure 12.

The change in the relative abundance of the LHCI subunits LHCA1, 2, 3 and 4 is presented in Figure 13B. The high resolution PSI complexes from maize (Pan et al., 2018) and pea (Mazor et al., 2015; Qin et al., 2015) show a stoichiometry of 1:1:1:1 for PSI relative to LHCA1, 2, 3 and 4. Unlike PSII, where changes in antenna size have been consistently observed, the LHCI antenna size of PSI has been reported to be unaffected by changes in light intensity in some studies (Albanese et al., 2018; Ballottari et al., 2007), but altered in another (Bailey et al., 2001). Indeed, a recent study showed that PSI in Arabidopsis can bind additional copies of LHCA1 and 4 (Crepin et al., 2020) suggesting the antenna size can undergo acclimation. When normalised to protein iBAQ, there is a 40% and 10% increase in LHCA1 and 3, respectively, in LL compared to ML but no significant change in HL. However, since PSI itself increases in LL by around 30% these changes in LHCA proteins may not actually reflect changes in antenna size for each PSI core. Since LHCA4 remains constant despite these changes in PSI abundance this may suggest that there are more LHCA proteins associated with PSI in HL relative to LL. The stoichiometries calculated for LHCI/PSI varied between 3.27 and 4.06, which are broadly consistent with those expected from the high resolution structures (Mazor et al., 2015) (Table 8). In this

MS analysis the minor LHCA5 and 6 proteins, which are involved in binding the NDH complex to PSI (Peng et al., 2009; Yadav et al., 2017), were not detected.

#### 4.4 Thylakoid architecture changes in light acclimation

Using thin section electron microscopy (EM) increased grana thylakoid stacking (membrane layers per granum) was observed in plants grown in LL compared to ML, while HL plants showed a significant decrease (Figure 14A, B), consistent with observations in a number of different plant species (Bailey et al., 2001; Ballottari et al., 2007; Chow and Anderson, 1987; Chow and Hope, 1987; Chow et al., 1988; Miller et al., 2017; Petersen et al., 2011; Schumann et al., 2017). More recently, changes in grana stacking have been found to be accompanied by changes in grana diameter (Pietrzykowska et al., 2014; Wood et al., 2018, 2019). Consistent with these changes, analysis of chloroplast ultrastructure by structured illumination microscopy (SIM) revealed that increased grana stacking in LL leaves was paralleled by an increase in the grana diameter (measured as the full width half maximum of the chlorophyll fluorescence signal from each granum) (Figure 14C, D). Similarly, decreased grana stacking in HL leaves was accompanied by a reduction in grana diameter. Previously, changes in the degree of grana stacking have largely been attributed to alterations in the content of LHCII proteins, since cationic interactions between their stromal faces are known to mediate this phenomenon (Day et al., 1984). However, more recently the thylakoid curvature protein family (CURT1) was shown to exert a major influence on thylakoid structure with the *curt1abcd* mutant showing grossly enlarged pseudo-grana up to 1.3  $\mu\text{m}$  in diameter, compared to 0.4-0.5  $\mu\text{m}$  for the wild-type, despite similar levels of LHCII (Armbruster et al., 2013). In contrast, Arabidopsis plants overexpressing CURT1A showed smaller grana than the wild-type with a diameter of just 0.3  $\mu\text{m}$  (Armbruster et al., 2013). This MS analysis allowed, for the first time, quantification of how the levels of these key proteins changed upon light acclimation (Figure 14E). The relative abundance of CURT1A and B increased by 30% and 40% respectively in HL compared to ML, while in LL both decreased by  $\sim$ 10%. There were small increases of  $\sim$ 10% in the level of CURT1C in both LL and HL relative to ML and CURT1D was not detected. The reduced induction of quenching (RIQ) proteins RIQ1 and 2 have been shown to negatively regulate grana size (Yokoyama et al., 2016). Consistent with this earlier finding, the relative abundance of RIQ1 and 2 increased by 75% and 50% respectively in HL compared to ML, while RIQ2 decreased by  $\sim$ 20% in LL. There is evidence that phosphorylation of PSII and LHCII also strongly influences grana stacking, with mutants lacking the PSII (STN8) and LHCII (STN7) kinases showing larger grana, while those lacking the LHCII (TAP38) phosphatase show smaller grana (Armbruster et al., 2013; Fristedt et al., 2009a). The iBAQ analysis also revealed that the relative abundances of STN7 and STN8 were similar in ML and LL but both increased slightly in HL acclimated plants. In contrast, the relative abundance of TAP38 decreased to a similar extent in both LL and HL plants compared to ML. The stoichiometry data indicated that the ratio of STN7 to TAP38 increased with light intensity, ranging from half as much TAP38 as STN7 in LL to only one TAP38 to every 6 STN7 in HL (Table 10). The

calcium sensor kinase protein, CAS, which also plays a role in regulating photo-acclimation in high light by promoting dephosphorylation of LHCII (Cutolo et al., 2019), also increased in abundance in HL by ~70% and decreased in LL by ~30%.

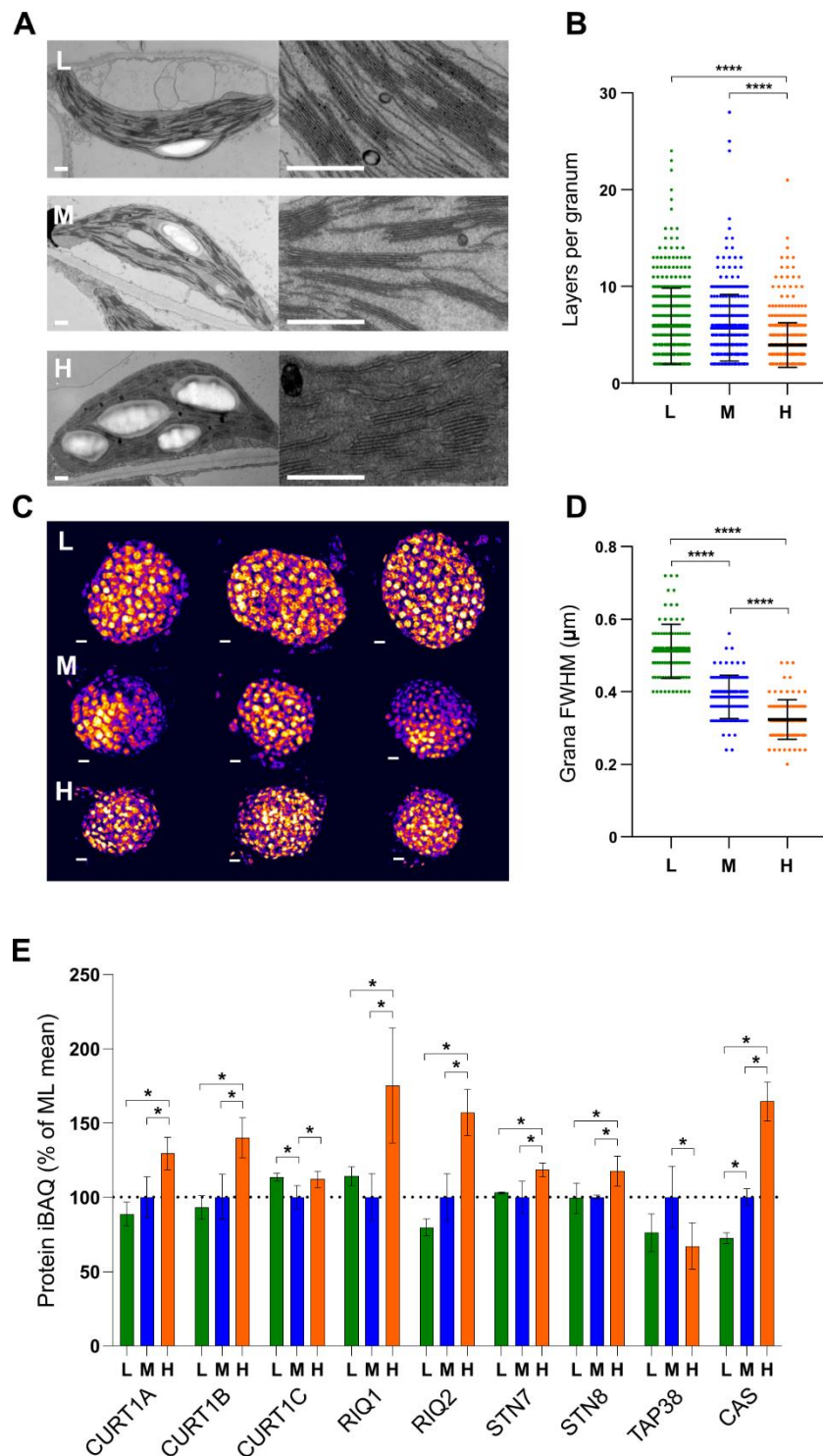


Figure 14: Thylakoid membrane stacking changes associated with acclimation are paralleled by changes in the relative abundance of CURT1A, B and RIQ1, 2 proteins. **A**, Thin-section electron micrographs of chloroplasts in plants acclimated to LL (top row, L), ML (middle row, M), and HL (bottom row, H) (scale bar: 0.5  $\mu$ m). **B**, Number of membrane layers per granum stack calculated from electron microscopy images of chloroplasts in LL (n = 379 granum stacks), ML (n = 354), and HL (n =

507) leaves (One-way ANOVA with Tukey's multiple comparisons. \*\*\*\* $P < 0.0001$ ). Error bars indicate mean  $\pm$  SD. **C**, 3D-SIM images (shown as Max Projections on the z-axis with tricubic sharp interpolation) of chloroplasts in plants acclimated to LL (top row, L), ML (middle row, M), and HL (bottom row, H). **D**, Full width at half-maximum (FWHM) fluorescence intensity of the fluorescent spots (grana) in three-dimensional SIM images of chloroplasts in LL ( $n = 97$ ), ML ( $n = 100$ ), and HL ( $n = 100$ ) leaves (One-way ANOVA with Tukey's multiple comparisons. \*\*\*\* $P < 0.0001$ ). Error bars indicate mean  $\pm$  SD. **E**, MS analysis showing the relative abundance of proteins involved in modulation of thylakoid membrane architecture, expressed as a percentage of the mean at ML. Sampling details are as stated in Figure 12.

#### 4.5 Electron transfer and photoprotection in light acclimation

The MS analysis showed that increasing light intensity was associated with significant increases in the abundance of many proteins involved in LET or its regulation. One of these proteins was *cytb<sub>6</sub>f* (Figure 12), which has been shown in previous studies to have a LET flux control coefficient of 0.8 (Kirchhoff et al., 2000) under high light conditions, meaning that it has a large effect on electron transfer rates through the whole chain. Another protein which may affect LET flux is PGR6, a protein kinase associated with the plastoglobules which functions to regulate the number of PQ molecules in the photoactive pool of the thylakoid membrane rather than stored in the plastoglobules. Mutants lacking PGR6 are unable to adapt to high light irradiance (Pralon et al., 2019). Indeed, the MS analysis shows a dramatic increase in PGR6 with light intensity, doubling from LL to ML and ML to HL. Another limiting step for LET under high irradiance is the step involving transfer of electrons from Fd to NADP<sup>+</sup> via FNR at the PSI acceptor side. Indeed, antisense inhibition of FNR in tobacco strongly reduced LET (Hajirezaei et al., 2002). This provides the rationale for the 50-60% increases in the abundance of FNR1 and 2 with high growth light intensity (Figure 15A); the stoichiometry relative to PSI rises from 0.15 in LL to 0.34 in HL for FNR1 and 0.18 in LL to 0.6 in HL for FNR2 (Table 9), values slightly lower than those reported by McKenzie et al. (2020). FNR can exist in two states, either soluble in the stroma or bound to the thylakoid membrane via the TIC62 (Benz et al., 2009) or TROL (Jurić et al., 2009) tethering proteins. The *trol* mutant showed strong perturbation in LET under HL conditions (Benz et al., 2009), whereas the *tic62* mutant showed no obvious electron transfer related phenotype (Jurić et al., 2009). Nevertheless, it was TIC62 that showed the largest change in relative abundance; a ~50% increase was observed in HL, whereas there was no significant effect of light intensity on levels of the TROL protein (Figure 15A). The effect of these changes on the TROL and TIC62/FNR stoichiometries can be seen in Table 9; while TROL/FNR declines the TIC62/FNR ratio is steady. Interestingly, the relative abundance of the PSI electron donor plastocyanin (PC) was significantly higher (+160%) in LL than in ML and HL plants (Figure 15A) but there was still a 40% increase in HL relative to LL. The explanation for increased plastocyanin in LL plants may relate to their increased grana size. A disadvantage of larger grana diameter is the slowing of LET, resulting from increased diffusion distance for the mobile electron carriers PQ and plastocyanin (Kirchhoff, 2014; Wood et al., 2018); the increase in plastocyanin in LL may be necessary to mitigate this effect.

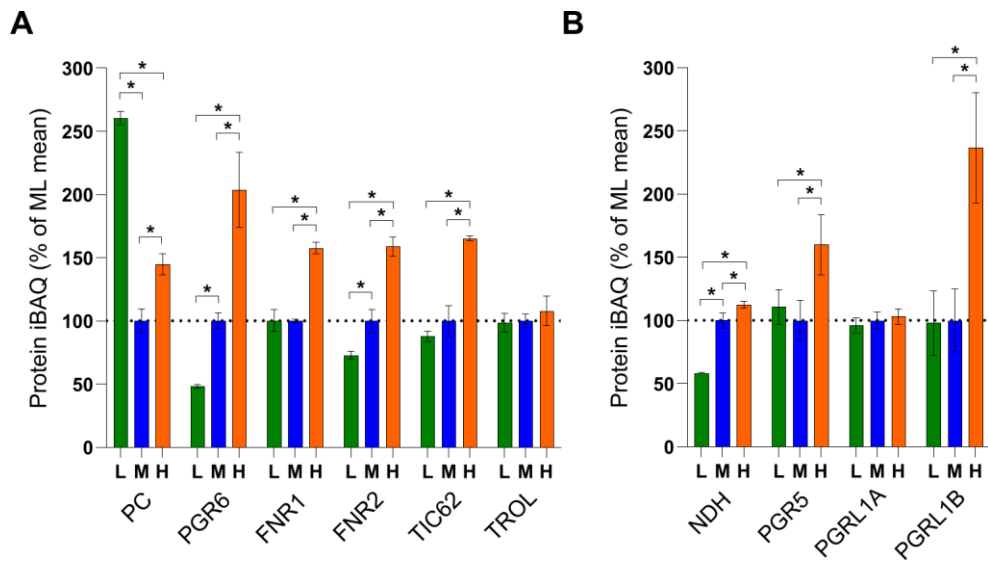


Figure 15: Acclimation to high light causes upregulation of proteins involved in LET and CET. **A**, MS analysis showing the relative abundance of LET related proteins, expressed as a percentage of the mean at ML. **B**, MS analysis showing the relative abundance of CET related proteins, expressed as a percentage of the mean at ML. Sampling details are as stated in Figure 12.

Table 9: Stoichiometry electron transfer proteins

LL	PSI	Cytb <sub>6</sub> f	FNR1	FNR2	TIC62	TROL	PGR5	PGRL1
PSI	1	2.93±0.17	6.86±0.41	5.42±0.32	11.7±0.7	10.4±0.6	43.2±2.6	12.6±0.8
Cytb <sub>6</sub> f	0.34±0.01	1	2.34±0.06	1.85±0.05	3.99±0.10	3.55±0.09	14.8±0.36	4.31±0.11
FNR1	0.15±0.01	0.43±0.04	1	0.79±0.08	1.70±0.17	1.51±0.15	6.30±0.64	1.84±0.19
FNR2	0.18±0.01	0.54±0.03	1.27±0.07	1	2.15±0.11	1.92±0.10	8.00±0.42	2.33±0.12
TIC62	0.086±0.006	0.251±0.019	0.59±0.04	0.46±0.03	1	0.89±0.07	3.70±0.27	1.08±0.08
TROL	0.096±0.011	0.28±0.03	0.66±0.07	0.52±0.06	1.12±0.13	1	4.16±0.46	1.21±0.14
PGR5	0.023±0.001	0.068±0.004	0.16±0.01	0.13±0.01	0.27±0.02	0.24±0.02	1	0.29±0.02
PGRL1	0.079±0.006	0.23±0.02	0.54±0.04	0.43±0.03	0.92±0.06	0.82±0.06	3.42±0.24	1
ML	PSI	Cytb <sub>6</sub> f	FNR1	FNR2	TIC62	TROL	PGR5	PGRL1
PSI	1	2.35±0.15	6.55±0.41	3.59±0.22	10.7±0.67	9.89±0.61	63.4±3.9	10.6±0.7
Cytb <sub>6</sub> f	0.43±0.02	1	2.78±0.14	1.52±0.08	4.57±0.24	4.21±0.22	27.0±1.4	4.52±0.23
FNR1	0.153±0.004	0.36±0.01	1	0.55±0.02	1.64±0.05	1.51±0.05	9.69±0.30	1.62±0.05
FNR2	0.28±0.02	0.66±0.06	1.83±0.15	1	3.00±0.25	2.76±0.23	17.7±1.5	2.96±0.25
TIC62	0.09±0.01	0.22±0.02	0.61±0.06	0.33±0.03	1	0.92±0.10	5.90±0.62	0.99±0.10
TROL	0.101±0.004	0.24±0.01	0.66±0.02	0.36±0.01	1.09±0.04	1	6.41±0.23	1.07±0.04
PGR5	0.016±0.001	0.037±0.002	0.10±0.01	0.057±0.004	0.17±0.01	0.16±0.01	1	0.17±0.01
PGRL1	0.094±0.004	0.22±0.01	0.62±0.02	0.34±0.01	1.01±0.04	0.93±0.04	5.96±0.23	1
HL	PSI	Cytb <sub>6</sub> f	FNR1	FNR2	TIC62	TROL	PGR5	PGRL1
PSI	1	1.48±0.03	2.73±0.06	1.72±0.04	4.27±0.09	8.02±0.18	28.7±0.6	7.68±0.17
Cytb <sub>6</sub> f	0.67±0.02	1	1.79±0.05	1.13±0.03	2.80±0.08	5.25±0.14	18.8±0.5	5.03±0.14
FNR1	0.34±0.03	0.50±0.04	1	0.58±0.05	1.43±0.13	2.69±0.24	9.62±0.85	2.57±0.23
FNR2	0.60±0.01	0.87±0.02	1.60±0.04	1	2.51±0.06	4.71±0.10	16.9±0.4	4.51±0.10
TIC62	0.22±0.01	0.33±0.02	0.60±0.04	0.38±0.02	1	1.77±0.11	6.33±0.38	1.69±0.10
TROL	0.15±0.02	0.21±0.02	0.39±0.04	0.25±0.03	0.61±0.07	1	4.11±0.45	1.10±0.12
PGR5	0.032±0.003	0.047±0.004	0.087±0.007	0.055±0.005	0.14±0.01	0.26±0.02	1	0.24±0.02
PGRL1	0.12±0.01	0.18±0.01	0.33±0.02	0.21±0.01	0.52±0.03	0.98±0.06	3.50±0.21	1

While LET produces ATP and NADPH, which is mostly consumed by the CBB cycle in the stroma for CO<sub>2</sub> fixation, CET produces only ATP and as such may play a key role in balancing the ATP/NADPH budget in the chloroplast under different light conditions (Kramer and Evans, 2011). Since CET increases proton flux into the lumen it may also be important for the down-regulation of PSII and PSI activity by NPQ and photosynthetic control, respectively (Ruban, 2016; Theis and Schroda, 2016; Yamori and Shikanai, 2016). Two pathways of CET, which involve the recycling of electrons from Fd at the PSI acceptor side to the PQ pool, are thought to exist. The first involves the NADPH dehydrogenase-like complex (NDH) a multi-subunit proton-pumping Fd-PQ oxidoreductase (FQR),

while the second involves proton gradient regulation complex proteins PGR5 and PGRL1, which may act directly as an FQR or regulate putative CET activity of a Fd-FNR-cyt<sub>b6/f</sub> complex (Joliot and Johnson, 2011; Yamori and Shikanai, 2016). The MS analysis showed contrasting light acclimation responses for these CET proteins (Figure 15B). The relative abundance of NDH complex decreased by ~50% in LL and increased by ~10% in HL relative to ML (Figure 15B). The NDH complex is a much less abundant component of the thylakoid membrane and it is not obvious in the BN-PAGE gel (Figure 11C). Indeed, the stoichiometry data shows it is present at just 2.2% of the level of PSI in HL and only 0.6% in LL (Table 8). In contrast, the relative abundance of the PGR5 protein of the second CET pathway was similar in LL and ML but increased by ~50% HL (Figure 15B). Despite their high sequence similarity, PGRL1A and PGRL1B showed contrasting behaviour. The relative abundance of PGRL1B increased by 150% in HL whereas PGRL1A showed no significant increase, suggesting their expression may be differentially regulated. Neither protein decreased in LL relative to ML, suggesting that upregulation is triggered by high light irradiance. Unfortunately, in the MaxLFQ analysis used for calculation of stoichiometries, the sequence similarity of PGRL1A and B prevented individual quantification. The stoichiometries confirmed earlier reports that PGRL1 (A + B) is significantly more abundant relative to PSI than the NDH complex with ratios of 0.079 in LL increasing to 0.12 in HL similar to the values reported by McKenzie et al. (2020) for ML plants, which is consistent with the notion that the PGR5-PGRL1 dependent CET pathway is dominant in Arabidopsis (Strand et al., 2017) (Table 8). As found previously PGR5 was substoichiometric relative to PGRL1, with a ratio of 0.02 per PSI in LL and 0.032 in HL (Table 9).

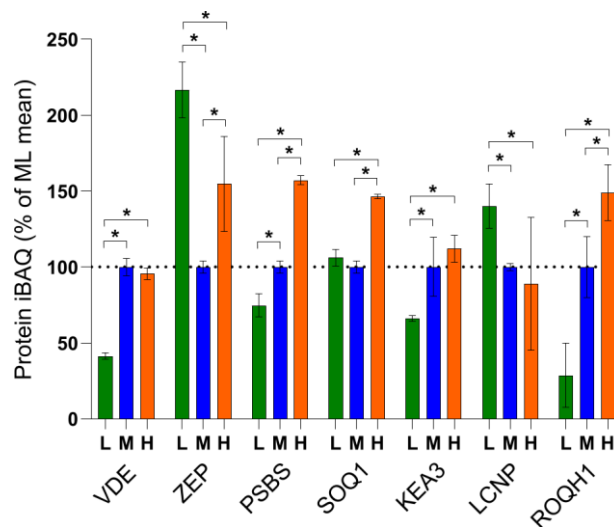


Figure 16: The relative abundance of proteins involved in light harvesting regulation changes in acclimation. MS analysis showing the relative abundance of NPQ related proteins, expressed as a percentage of the mean at ML. Sampling details are as stated in Figure 12.

As light intensity rises, the increased electron transfer activity results in an increased transfer of protons from the stroma to the lumen. The influx of protons via coupled LET and CET activity is balanced by

proton efflux via the ATP synthase and  $H^+/K^+$  anti-porter KEA3 (Armbruster et al., 2014). Where proton influx exceeds efflux, the increasing  $\Delta pH$  triggers the activation of photoprotective energy dissipation in the PSII antenna system to reduce the excitation pressure on PSII reaction centres. The dissipation of excess excitation energy as heat can be measured by NPQ of chlorophyll fluorescence and is triggered by the protonation of both violaxanthin de-epoxidase (VDE), which converts LHCII bound violaxanthin to zeaxanthin, and the PSBS protein (Ruban, 2016). Together PSBS and zeaxanthin induce conformational changes in LHCII that result in the formation of dissipative chlorophyll-carotenoid or chlorophyll-chlorophyll interactions, protecting PSII from photooxidative damage (Li et al., 2009; Ruban, 2016). Using stoichiometry data, it was calculated that in ML there is one PSBS protein for every 5 LHCII trimers and this ratio is doubled in HL (Table 10). The MS analysis also showed that abundance of PSBS increased markedly with light intensity (Figure 16), whereas VDE was constant between ML and HL but decreased in LL. The abundance of zeaxanthin epoxidase (ZEP), which catalyses the reversion of zeaxanthin to violaxanthin, increased in both LL and HL (Figure 16). Together these results suggest an increased capacity for NPQ in HL plants. In contrast with ZEP, the  $K^+/H^+$  antiporter protein KEA3, which modulates the relaxation of  $\Delta pH$  upon high to low light transitions by releasing protons into the stroma (Armbruster et al., 2014), was downregulated in LL (Figure 16) but remained constant in ML and HL. The LCNP protein, which is involved in promoting the sustained slowly-relaxing component of NPQ termed qH (Malnoë et al., 2018), showed the highest abundance in LL while SOQ1 and ROQH1, which suppress qH, were most abundant in HL. Therefore, the HL grown plants appear to reduce their capacity for the slow-relaxing qH form of NPQ, while increasing their capacity for the fast-relaxing qE form compared to LL.

Table 10: Stoichiometry of regulatory and photoprotective proteins

LL	LHCII	STN7	STN8	TAP38	PSBS	SOQ1	CAS	
LHCII		1	403.7±27.6	265.8±18.2	750.9±51.4	7.164876317	150.2208744	25.21801261
STN7	0.0025±0.0001		1	0.66±0.03	1.86±0.09	0.018±0.001	0.37±0.02	0.062±0.003
STN8	0.0038±0.0002	1.52±0.09		1	2.82±0.16	0.027±0.002	0.57±0.03	0.095±0.005
TAP38	0.0013±0.0001	0.54±0.05	0.35±0.04		1	0.0095±0.0010	0.20±0.02	0.034±0.003
PSBS	0.14±0.01	56.3±4.2	37.1±2.8	104.8±7.8		1	21.0±1.6	3.52±0.26
SOQ1	0.0067±0.0007	2.69±0.28	1.77±0.19	5.00±0.53	0.048±0.005		1	0.17±0.02
CAS	0.040±0.002	16.0±0.7	10.5±0.4	29.8±1.25	0.28±0.01	5.96±0.25		1
ML	LHCII	STN7	STN8	TAP38	PSBS	SOQ1	CAS	
LHCII		1	249.8±23.6	595.7±56.4	908.2±85.9	4.58±0.43	164.6±15.6	15.5±1.5
STN7	0.0040±0.0003		1	2.39±0.17	3.64±0.26	0.018±0.001	0.66±0.05	0.062±0.004
STN8	0.0017±0.0002	0.42±0.04		1	1.52±0.15	0.0077±0.0007	0.28±0.03	0.026±0.003
TAP38*	0.0011	0.28	0.66		1	0.005	0.18	0.017
PSBS	0.22±0.02	54.5±3.8	130.1±9.0	198.3±13.7		1	35.9±2.5	3.39±0.23
SOQ1	0.0061±0.0005	1.52±0.12	3.62±0.28	5.52±0.42	0.028±0.002		1	0.094±0.007
CAS	0.064±0.006	16.1±1.4	38.4±3.3	58.5±5.1	0.29±0.03	10.6±0.9		1
HL	LHCII	STN7	STN8	TAP38	PSBS	SOQ1	CAS	
LHCII		1	173.6±11.9	397.7±27.4	1035.3±71.2	2.55±0.18	91.3±6.3	8.34±0.57
STN7	0.0055±0.0003		1	2.15±0.34	5.59±0.34	0.014±0.001	0.49±0.03	0.045±0.003
STN8	0.0025±0.0001	0.43±0.02		1	2.54±0.12	0.0063±0.0003	0.22±0.01	0.020±0.001
TAP38*	0.00099	0.17	0.38		1	0.0025	0.088	0.0081
PSBS	0.400±0.003	67.6±0.4	155.0±1.02	403.4±2.7		1	35.6±0.2	3.25±0.02
SOQ1	0.0112±0.0004	1.90±0.06	4.35±0.15	11.3±0.4	0.028±0.001		1	0.091±0.003
CAS	0.13±0.01	21.2±1.2	48.6±2.8	126.6±7.4	0.31±0.02	11.2±0.7		1

#### 4.6 Repair of photosystem II in the light-acclimated thylakoid membrane

In high light, PSII is prone to photooxidative damage, particularly to the reaction centre D1 subunit (reviewed in Theis and Schroda, 2016). Photodamaged PSII is repaired via a complex repair cycle involving the migration of PSII from the grana to stromal lamellae, partial disassembly of the PSII core and associated OEC, proteolytic excision of D1, *de novo* synthesis of D1, its reinsertion into the PSII complex, and the subsequent reassembly of the dimeric PSII before it is returned to the grana (Aro et al., 1993). This MS analysis was used to determine the effect of growth light intensity on the relative abundance of proteins involved in the repair cycle (Figure 17A, B). Phosphorylation of the PSII core proteins D1, D2, PSBH and CP43 by STN8 is thought to promote the migration of photodamaged PSII to the stromal lamellae for repair (Tikkanen et al., 2008) and its relative abundance was increased in HL plants (Figure 14). However, prior to repair PSII must be dephosphorylated by PBCP and possibly TL18.3; the former was not detected in this study but relative abundance of the latter underwent small

changes in abundance, increasing by 25% in LL and 10% in HL relative to ML (Figure 17A). This process may be instead enhanced via decreases in the level of the immunophilin CYP38, which negatively regulates PSII core phosphatase activity (Vener et al., 1999), and indeed its relative abundance significantly decreased in HL compared to LL (Figure 17B). The abundance of HHL1 and LQY1, which mediate the release of CP43 from photodamaged PSII prior to D1 proteolysis (Jin et al., 2014), behaved differently; the former was significantly increased in ML and HL compared to LL, while the relative abundance of the latter was increased in both LL and HL compared to ML (Figure 17A). Consistent with a greater role for the repair cycle, the relative abundance of the DEGP1 protease was markedly increased in ML and HL (Figure 17A). The behaviour of the FTSH zinc metalloproteinase subunits was more complex; FTSH2 and FTSH5 increased as expected in ML and HL, but there was no observed change in FTSH1 (Figure 17A). FTSH8 showed the same behaviour as LQY1 increasing under both LL and HL compared to ML. The content of the membrane insertase ALB3 (Schneider et al., 2014) significantly decreased in ML and HL compared to LL, while VIPP1 which is involved in the formation of lipidic microdomains to assist insertase activity increased with growth light intensity (Liu et al., 2005) (Figure 17B). The MPH1 protein has been implicated in the protection of PSII from photodamage rather than in PSII repair (Theis and Schroda, 2016) and accordingly its relative abundance increased in ML and HL. The LPA1 and MET1 proteins, which function as chaperones in PSII assembly (Theis and Schroda, 2016), also showed significant increases with growth light intensity. The luminal protein PPL1, which has an as-yet undefined role in the PSII repair cycle decreased in HL and ML relative to LL (Figure 17B), despite the fact that Arabidopsis mutants lacking this protein show slower PSII recovery following excess illumination (Ishihara et al., 2007). Proteins involved in the reassembly of the Mn cluster, such as PSB27, were lowest in ML, while there was no significant change in FKBP20-2, which is involved in reassembly of PSII supercomplexes (Theis and Schroda, 2016). The collective changes of the PSII repair cycle machinery proteins in HL relative to LL are illustrated by the schematic diagram in Figure 17C.

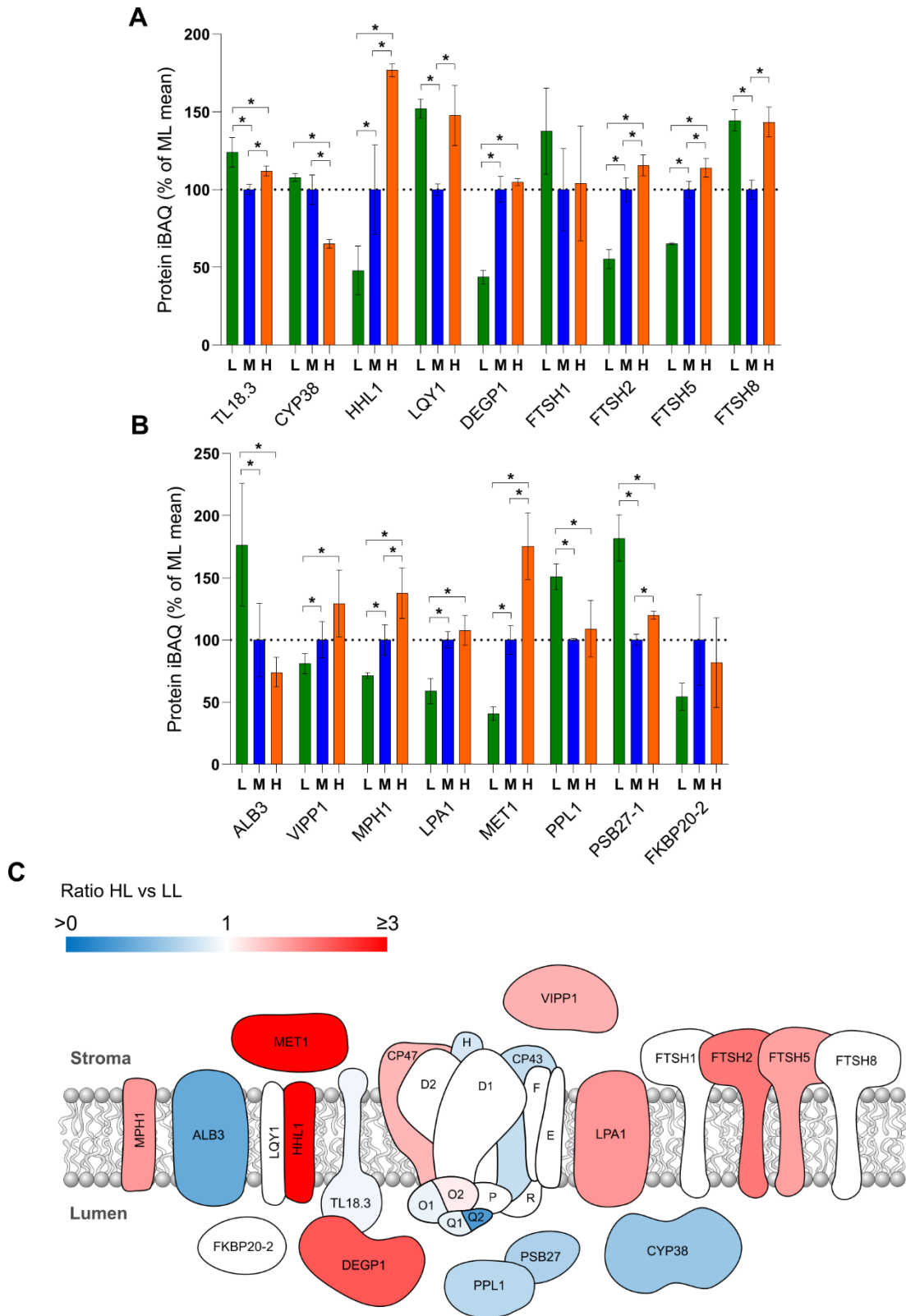


Figure 17: Acclimation to high light leads increased abundance of the PSII repair cycle machinery. **A**, **B**, MS analysis showing the relative abundance of proteins involved in PSII repair, expressed as a percentage of the mean at ML. Sampling details are as stated in Figure 12. **C**, Diagram indicating the abundance of PSII repair proteins in HL versus LL. Blue proteins are more abundant in LL, whereas red/pink proteins are more abundant in HL. For quantified proteins where no significant difference was detected, they are displayed in white.

## 4.7 Discussion

In this study, quantitative mass spectrometry was combined with biochemical and structural analyses to provide novel insights into the mechanisms of light acclimation in the model organism *Arabidopsis*. The MS analysis reveals how the relative abundance of over 400 thylakoid-associated proteins, including a range of recently discovered regulatory and structural proteins, change in response to altered growth irradiance. These findings, summarised in Figure 18, show familiar patterns long associated with photosynthetic acclimation, such as the decrease of LHCII and the increase in *cytb<sub>6</sub>f* and ATPase levels (Anderson, 1986; Anderson et al., 1988; Schöttler and Tóth, 2014; Walters, 2005) with growth irradiance, as well as previously unreported changes in key regulatory proteins such as PGR6, PGR5, PGRL1, CURT1, RIQ and STN7/8. A relatively quantitative approach was used, normalising each dataset to the intra-analysis sum of iBAQ intensities for the combination of PSI, PSII, *cytb<sub>6</sub>f* and ATP synthase, which represent 50-60% of total protein iBAQ. The data presented here thus offer an interesting counterpoint to previous acclimation studies where, generally, protein abundance is normalised on a chlorophyll basis. Arguably, since the protein/chlorophyll ratio changes considerably, normalisation to these core photosynthetic complexes provides a more straightforward and meaningful view of differences in the thylakoid proteome.

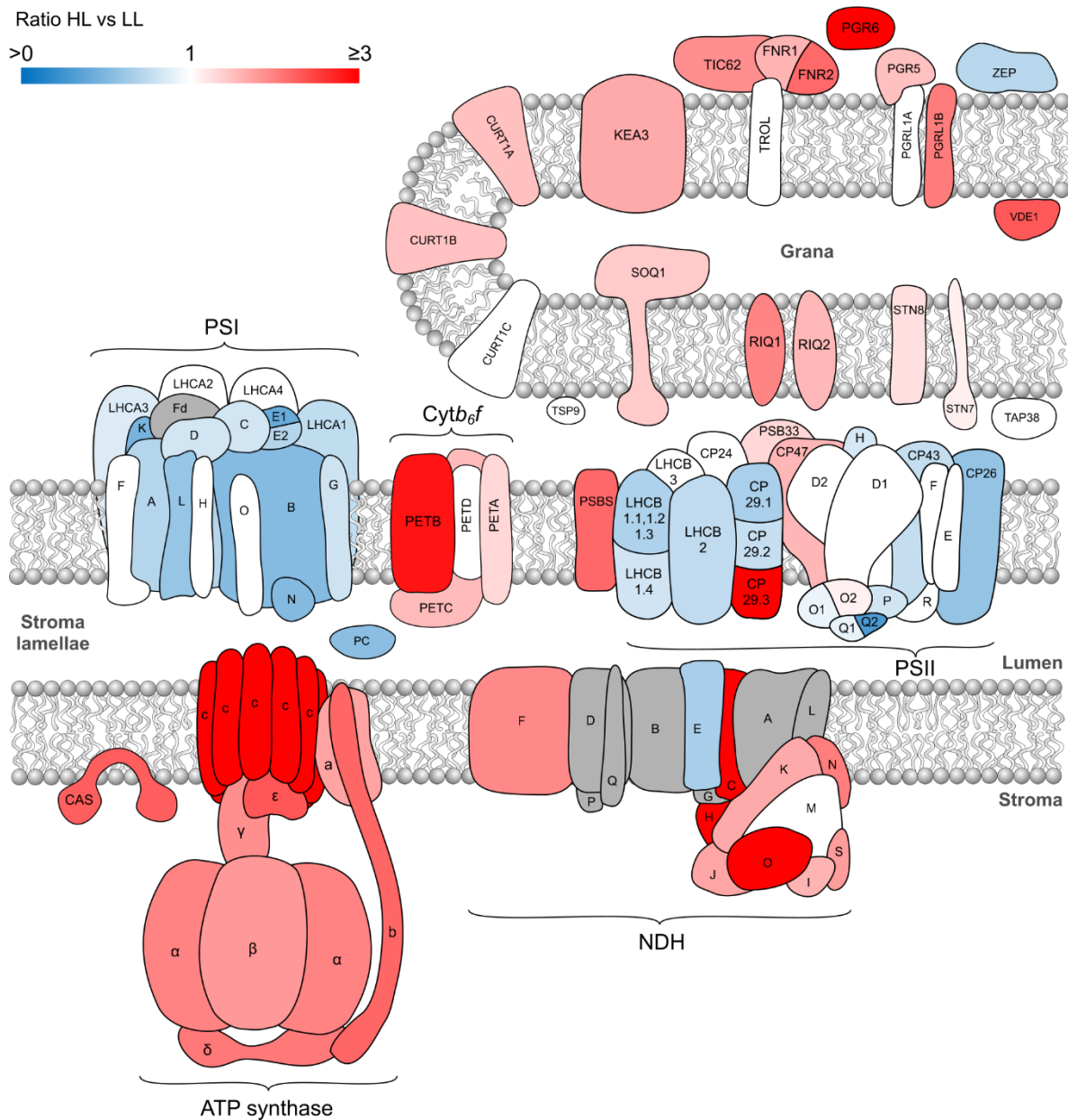


Figure 18: A comparison of high light versus low light acclimation in the thylakoid membrane proteome. Schematic diagram indicating the relative abundance of thylakoid proteins in HL versus LL. Blue proteins are more abundant in LL, whereas red/pink proteins are more abundant in HL. Where no significant difference was detected for a quantified protein it is displayed in white. Proteins not identified by MS analysis are shown in grey.

A key issue with mass spectrometry data is that of normalisation to compensate for random variations in sample loading and spectral acquisition patterns. One widely-used normalisation strategy, MaxLFQ, was recently applied in the MS study of McKenzie et al. (2020) to calculate the stoichiometries of the major photosynthetic complexes in ML grown *Arabidopsis* plants. For comparison, that same approach was applied to this data to assess stoichiometries of thylakoid proteins in light acclimation. Some of the stoichiometries produced are very similar to those in McKenzie et al. (2020), such as a PSII/PSI ratio of ~2 in ML and a *cytb<sub>6</sub>/f*/PSI ratio of 0.5 in ML. However, the stoichiometries generated for LHCII trimers/PSII were significantly lower than expected: 1.7 LHCII trimers per PSII in ML, compared to

values between 3 and 5 in the literature (Kouřil et al., 2013; Wientjes et al., 2013a). This supports the notion that MaxLFQ-generated stoichiometries should be treated with caution, and that the method is unsuited to absolute protein quantification when applied to a membrane proteome such as this one. Relative quantification using iBAQ, on the other hand, is appropriate and reliable for the investigation of changes in the thylakoid proteome and will be applied throughout the rest of this thesis.

Previous acclimation studies have highlighted how, in low light, plants generally expand their light harvesting antenna system relative to the PSII reaction centre, but have a generally lower maximum LET capacity (Adams et al., 2007; Bailey et al., 2001; Ballottari et al., 2007; Chow and Anderson, 1987; Chow and Hope, 1987; Chow et al., 1988; Miller et al., 2017; Petersen et al., 2011; Schumann et al., 2017). Consistent with these findings, this MS analysis of the light harvesting proteins in *Arabidopsis* showed an increased relative abundance of the major trimeric LHCII complex components LHCB1 and 2 in LL compared to HL (Figure 13A), consistent with the Chl *a/b* ratios and biochemical analysis (Figure 11). The increased LHCII content in LL plants is also associated with wider diameter thylakoid grana with an increased number of membrane layers per stack (Figure 14). The relative decrease in CURT1A, B and RIQ2 proteins in LL also likely contributes to this increase given their known effect on grana size (Armbruster et al., 2013). Another change observed in LL plants is an increase in the PSI/PSII ratio in LL (Figure 12), in contrast to that seen in pea (Albanese et al., 2018) but in line with previous work in *Arabidopsis* (Bailey et al., 2001). A reason for light limitation in a natural environment may be filtering by the leaves of other plants, altering the spectral quality of the light environment such that it contains a greater proportion of far-red wavelengths. Since PSII is more efficient at absorbing red and blue light, the increased PSI content, as well as an increased PSI antenna size by augmentation with LHCII (Figure 11), could reflect an attempt to balance the relative excitation level of the photosystems to optimise LET when light is limiting. Previously it has been suggested that in LL, when ATP when proton deposition by LET into the lumen is low or when there is an ATP shortfall arising from lower respiratory activity, LL acclimated plants increase their PSI levels in order to enhance CET and maintain  $\Delta pH$  at a level sufficient for generation of ATP (Bailey et al., 2001). However, the abundance of NDH decreases significantly in LL, contrary to the suggestion that this complex plays a crucial role in LL (Yamori et al., 2015), and there is no change in the abundance of the other CET proteins PGR5, PGRL1A or PGRL1B.

In HL, the preference for the PGR5/PGRL1B pathway, which shows a lower  $e^-/H^+$  coupling ratio of 2 compared to 4 for the NDH pathway (Strand et al., 2017), may reflect a priority of CET in HL to alleviate inhibition of electron acceptance in PSI, rather than to augment the ATP/NADPH ratio. However, in each case it is noteworthy that the stoichiometries calculated for these proteins relative to PSI are very low with NDH only present at 2.2% the level of PSI, even in HL, and PGRL1 at 10% (Table 8). In HL, the excitation levels of the reaction centres can exceed the capacity of downstream electron sinks, potentially leading to the generation of ROS that damage the photosynthetic machinery.

One of the primary photoprotective mechanisms is NPQ, which functions to protect PSII from photooxidative damage. The increased relative abundance of VDE, which accelerates zeaxanthin synthesis, and PSBS, both of which have been shown to adjust the  $\Delta\text{pH}$  sensitivity of NPQ (Ruban, 2016), indicate a greater capacity for NPQ in HL plants. Finally, HL plants appear to greatly increase their capacity for PSII repair, with several proteins known to be involved in the repair cycle found to be upregulated in these plants (Figure 17). The replacement of LHCB4.1 and LHCB4.2 with the third isoform, LHCB4.3, which lacks a stromal-side 'anchor' present in the isoforms, may facilitate faster PSII supercomplex disassembly before PSII repair.

To bring the current understanding of photosynthetic acclimation closer to agricultural applications, work must be done to assess how its mechanisms differ in natural environments where light, temperature and water availability can be much more variable than the growth room conditions used here (Schumann et al., 2017). Previous studies have indicated that plants adopt some of the features of both low and high light plants in such environments (Schumann et al., 2017; Violet-Chabrand et al., 2017), so an analysis of the thylakoid proteome of *Arabidopsis* grown in natural light would help to contextualise these acclimation-related changes.

## 5 Proteomic analysis of the thylakoid membrane in *Arabidopsis* in the laboratory and in the field

### 5.1 Introduction

Most of the current understanding of photosynthesis and acclimation is based on studies of the model organism *Arabidopsis thaliana* under controlled laboratory conditions. However, *Arabidopsis* plants grown in their natural environment show a very different phenotype to plants grown under controlled conditions, differing substantially in thylakoid membrane protein composition and pigment content as well as leaf morphology (Mishra et al., 2012). Various fitness-related traits, such as seed size and germination rate, vary greatly in the field (Malmberg et al., 2005), while many mutant phenotypes in *Arabidopsis* cannot be observed under low-stress controlled environmental conditions (Frenkel et al., 2008). The use of a constant light intensity, temperature and humidity in the laboratory growth chamber improves reproducibility of results but hinders our understanding of acclimation in the plant's natural environment. Stress responses in the thylakoid membrane have been studied extensively but independently, limiting understanding of how different protective mechanisms are integrated together. Plants grown in the field – such as crops – are continually exposed to multiple stresses from day/night cycles, moving cloud cover, shading by leaves, and weather. All of these factors can affect the rate of damage to photosynthetic machinery, the rate of electron transport, and demand for water, leading to decreased photosynthetic efficiency and lower crop yields (Poorter et al., 2016).

Despite the discrepancies between photosynthesis in a controlled environment and in the field, only a few studies have directly compared plants from the two environments. Using *Arabidopsis* mutants, Külheim et al. (2002) found that NPQ is beneficial for plant fitness in a natural environment with fluctuating light intensity rather than high light per se; it does not give a significant advantage to plants grown in a controlled environment. Norén et al. (2003) identified that the ELIP proteins are specifically upregulated in pea plants grown outdoors. When grown in the field, mutants deficient in enzymes of tocopherol synthesis were found by Semchuk et al. (2009) to experience increased oxidative stress and have reduced chlorophyll accumulation. Similarly to the work described in this thesis, Mishra et al. (2012) compared phenotypes of light-acclimated wild type lab-grown *Arabidopsis* to that of those grown in the field. Plants were grown under controlled moderate light, then either transferred to low, moderate or high light intensity, or moved outdoors. Leaf measurements, pigment analysis, immunoblot- and spectroscopy-based protein quantification, and photosynthetic parameter measurements showed that the field plants were generally more distinct than any of the controlled environment plants were from one another. Wituszyńska et al. (2013) also germinated *Arabidopsis* seeds in a controlled environment then transferred half of the seedlings to the field. This study measured various photosynthetic parameters such as NPQ and CO<sub>2</sub> assimilation, and combined this information with pigment analysis and transcriptomics. A study by Schumann et al. (2017) analysed photosynthesis

in low, moderate, high and natural light-grown *Arabidopsis* by measuring CO<sub>2</sub> assimilation, grana size, and relative abundance of some key proteins, among other parameters. They revealed, in the outdoor plants, dynamic and flexible adaptations to fluctuating light and a high capacity for energy dissipation. *Arabidopsis* mutants grown in both controlled and field conditions have been used further to study photoprotection in natural light, such as those lacking the PSII repair protein MPH2 (Liu and Last, 2017). Kono et al. (2017) used NDH-deficient mutants grown in the lab and the field to study the effect of far-red light – as present in sunlight – on PSI photoinhibition in fluctuating light. While Wituszyńska et al. (2013) had proposed that the higher and more variable light irradiances were the main cause of differences observed between indoor and outdoor plants, a one-year field study of *Arabidopsis* plants from seeds sown in the field found that temperature was as influential as light intensity on plant fitness and pigment content (Pescheck and Bilger, 2019). Recently, mass spectrometry-based proteomics was used to analyse acclimation to fluctuating controlled light in *Arabidopsis* leaves (Niedermaier et al., 2020). However, no proteomic analysis has yet been performed to study the thylakoid membrane of plants grown under field conditions.

Here, mass spectrometry was used to perform a quantitative proteomic comparison of the thylakoid membranes of outdoor and laboratory-grown *Arabidopsis thaliana* plants to further our understanding of acclimation and photoprotection in the thylakoid membrane. Such an analysis highlights those proteins and regulatory mechanisms that are particularly important in developmental adaptation of *Arabidopsis* to natural light conditions, providing context for the work on constant light acclimation described in Chapter 4.

## 5.2 Field-grown *Arabidopsis* experienced dramatically different light and temperature conditions to those grown in the laboratory

*Arabidopsis* seedlings were grown for 2 weeks in a controlled environment at a moderate light intensity (150  $\mu\text{mol photons m}^{-2} \text{s}^{-1}$ ) under fluorescent artificial lighting (Figure 19A). Plants were subject to 12 h of light per day with a daytime temperature of 21°C and a night time temperature of 18°C (Figure 19B, C). Following this 2-week period, plants were either maintained for a further 3 weeks in the growth chamber (lab, or ‘L’ plants) or moved outdoors (Arthur Willis Environment Centre, University of Sheffield). The outdoor, or field (F) plants, were positioned such that there was minimal shading of sunlight from buildings or other structures so that the intensity of sunlight reaching the plants would be more representative of the weather conditions and of the gradual increases and decreases in light intensity of the day/night cycle. The emission spectra of the fluorescent lights in the growth chamber and of sunlight are shown in Figure 19A. The spectrum of sunlight was broader and more consistent across a wide range of wavelengths than that of the fluorescent lamps. In particular, sunlight showed a much greater relative emission at the longer wavelengths, around the far-red region, which preferentially excites PSI (Johnson and Wientjes, 2020). Both lab and field grown plants were watered

regularly to avoid drought stress, and precautions were taken to reduce predation of the field plants, without the use of pesticides.

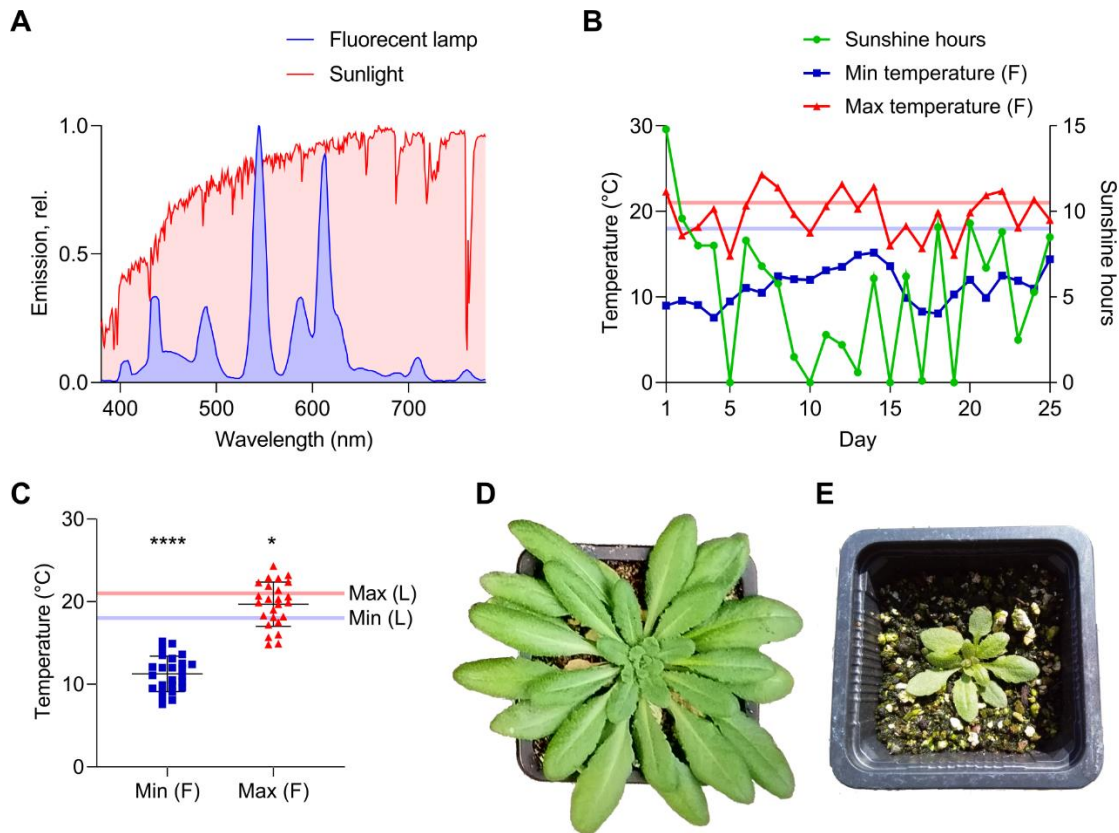


*Figure 19: Arabidopsis plants grown outdoors are exposed to highly variable light and temperature conditions and exhibit very different morphologies to controlled environment plants. A, Graph to compare the spectral composition of light from the sun and from fluorescent lamps. B, Weather data (provided by Western Park weather station, Sheffield, UK) in the form of daily maximum temperature, minimum temperature and hours of sunshine for the 25-day period from 21<sup>st</sup> May to the 14<sup>th</sup> June 2018. Sunshine hours were defined as the number of hours during that day in which the light intensity exceeded 120 W/m<sup>2</sup>. The pale red and blue lines indicated the daytime and nighttime temperatures, respectively, of the growth chamber for comparison. C, Minimum and maximum daily temperatures experienced by Field (F) Arabidopsis compared to Lab (L) Arabidopsis (pale blue and red lines). Asterisks indicate significance from two-tailed one-sample t-tests comparing minimum Field temperature to minimum Lab temperature (\*\*\*\*P < 0.0001) and maximum Field temperature to maximum Lab temperature (\*P < 0.05). D, Representative images of Lab Arabidopsis plants and Field (E) plants.*

The field plants were grown outdoors for a 25-day period from the 21<sup>st</sup> May to the 14<sup>th</sup> June 2018 before harvesting. Weather data for this period, provided by the Weston Park Weather Station, Museums Sheffield, is shown in Figure 19B. The data recorded by the weather station consists of daily minimum temperature, maximum temperature, and sunshine hours, defined as the number of hours per day in which the light intensity exceeded 120 W/m<sup>2</sup>. With the conversion of 1 W/m<sup>2</sup> = 4.57 μmol photons m<sup>-2</sup> s<sup>-1</sup> (Thimijan and Heins, 1983), this means that ‘sunlight hours’ were those that exceeded approximately 548 μmol photons m<sup>-2</sup> s<sup>-1</sup>. While this comparison is only a rough estimate because of the differences in

the spectra of the light sources, the intensity during ‘sunlight hours’ is much higher than in the growth chamber. If so, the field plants were exposed to a light intensity exceeding that of the growth chamber on all but 4 of the days, and on one day were exposed to 14.8 h of sunshine. This means that, overall, the field plants experienced a great deal more light than those grown in the lab. The outdoor temperature was also extremely variable compared to the controlled environment (Figure 19B, C). While the temperature of the growth chamber only varied by 3°C, on the hottest day outdoors there was a difference of 13.8°C between the minimum and maximum temperature. On average, both the maximum and the minimum temperatures outdoors were significantly lower than those of the growth chamber (Figure 19C). High light intensity combined with low temperature is particularly stressful for photosynthetic processes, more so than one or the other. High light intensity causes a build-up of excitation energy, while low temperature reduces the rate of electron transfer reactions, reducing the capacity of the photosynthetic machinery to utilise this energy and increasing the risk of photooxidative damage to the reaction centres. Low temperature also slows down the reactions of the CBB cycle, reducing the electron sink capacity of the system such that NADP<sup>+</sup> is regenerate less efficiently. In a one-year study of *Arabidopsis* grown in the field, Pescheck and Bilger (2019) found that temperature had a comparable effect on various developmental parameters to light intensity.

*Arabidopsis* plants showed dramatic morphological differences when grown in a controlled environment (Figure 19D) compared to those grown in the field (Figure 19E) as previously reported (Mishra et al., 2012; Schumann et al., 2017). The leaves of the field plants were smaller, fewer, and less curled compared to the lab plants. Previously, *Arabidopsis* grown under natural light were shown to have significantly thicker leaves than those grown under moderate constant light, but very similar morphology to those grown under high intensity constant light (Schumann et al., 2017). One caveat of these observations is the difference in day length, which has a greater impact on leaf size than the growth light intensity (Mishra et al., 2012). The growth chamber was set to a 12 h day, whereas daylight can last 16-17 h in the location and time of year in which the Field plants were grown. The field plants showed little indication of anthocyanin accumulation in the form of purple pigmentation, suggesting they had acclimated to their environment and were not significantly stressed (Kovinich et al., 2014). The lab-grown plants had a much larger rosette diameter with much more vegetative growth and, like the field plants, did not show signs of anthocyanin accumulation or stress.

### 5.3 Morphological changes in field-grown *Arabidopsis* are accompanied by biochemical and spectroscopic differences

Thylakoid membranes were isolated from Lab and Field *Arabidopsis* from leaf tissue pooled from at least 15 plants per condition. Despite clear phenotypic differences, calculated ratios of chlorophyll *a* to *b* (Figure 20A) were very similar between plants from the different environments. However, this similarity not necessarily indicate a similar antenna size, since Chl *a/b* ratios are affected by both

antenna size and by the ratio of PSI/PSII. Other analyses have found an increase in the relative amount of chlorophyll *a* in natural light compared to a controlled environment with a moderate light intensity (Mishra et al., 2012; Schumann et al., 2017). Although the Lab plants were grown under very similar conditions to those used for the moderate light (ML) acclimated plants in Chapter 4, the Chl *a/b* ratio of isolated thylakoids was lower in this analysis (3.13) than for the ML thylakoids (3.37). The ratio of protein to chlorophyll of the Field and Lab thylakoids was determined and was found to be higher in the Field plants. Analysis of the thylakoid membranes by BN-PAGE revealed greater differences (Figure 20B). Digitonin solubilisation of the stromal lamellae fraction demonstrated that the PSI-LHCI-LHCII supercomplex was absent in the field thylakoids, a result that contrasts with the findings of Wientjes et al. (2013b), where the amount of the supercomplex was comparable to that of the lab-grown plants. The abundance of the *Cytb<sub>6</sub>f* complex appeared to increase in abundance in the Field plants. Unlike in the comparison of controlled environment thylakoids described in Chapter 4, the granal fraction from Field thylakoids was very poorly solubilised in the mixture of *n*-hexadecyl  $\beta$ -D-maltoside and *n*-dodecyl  $\alpha$ -D-maltoside (Wood et al., 2018) and very few complexes were visible. Because of this, the granal fraction was instead solubilised in a higher concentration (1%, rather than 0.2%) of only *n*-dodecyl  $\alpha$ -D-maltoside, which was more successful in liberation of complexes from the membranes. Different detergents produce different micelle sizes, which affects migration of complexes in native PAGE. The observed differences in solubility of complexes from Lab and Field thylakoids could indicate altered lipid-protein and lipid-lipid interactions. A reduction in the number of 'free' or L-type LHCII trimers was observed in the Field plants, in addition to all observable PSII-LHCII supercomplexes. However, since the apparent abundance of the C<sub>2</sub>S<sub>2</sub> supercomplex decreases to a similar extent as the larger PSII supercomplexes, this may reflect differences in membrane solubility or redistribution of complexes between domains rather than absolute abundance. These differences in membrane solubility may reflect changes in the lipid profile in addition to those of the proteome. Both glycolipid and phospholipid content has been shown to differ depending on the light environment, at different constant light regimes and in natural light (Schumann et al., 2017). Cold stress has also been shown to reduce the amounts of some galactolipids (Liu et al., 2018).

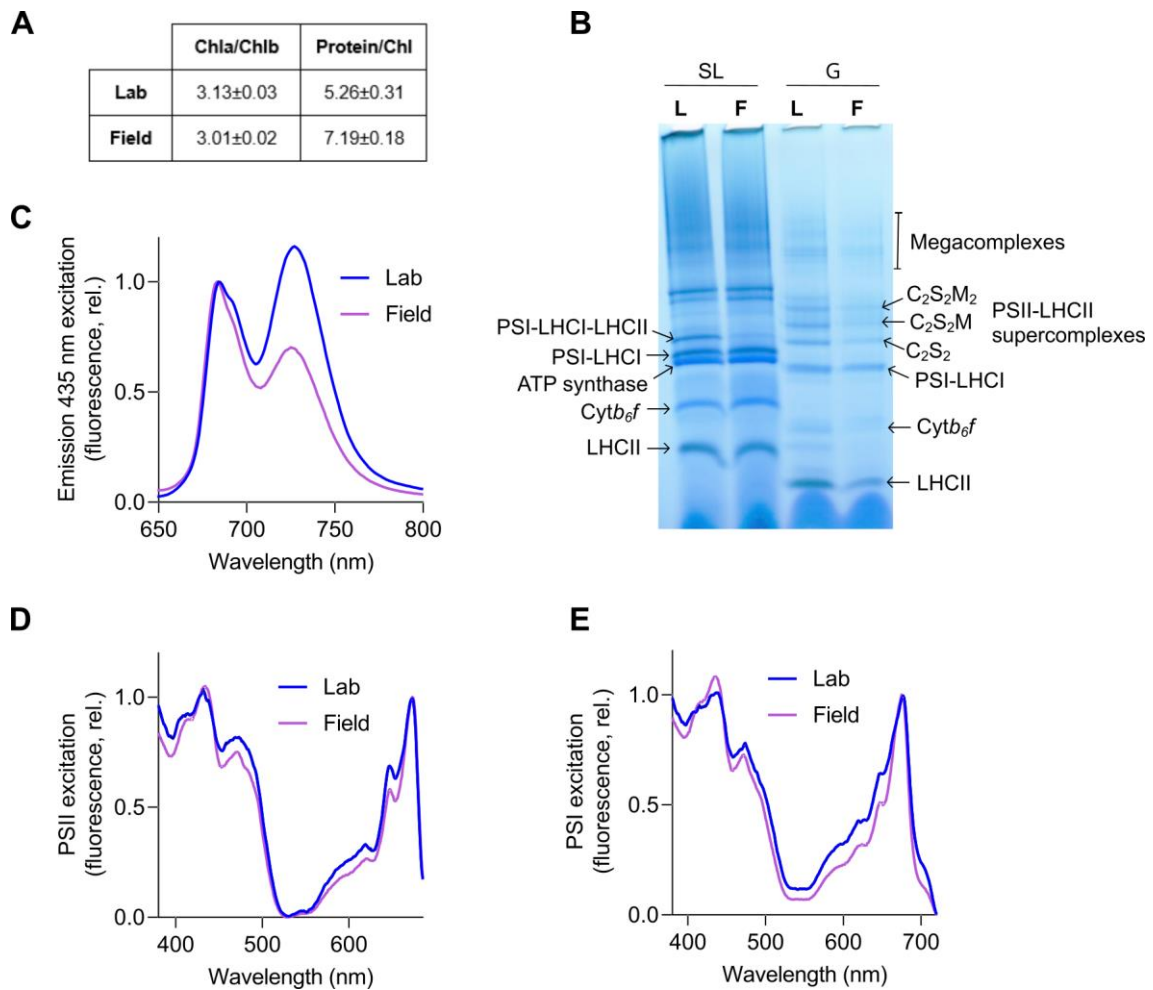


Figure 20: Lab and field thylakoid membranes have different spectroscopic properties and reduced formation of supercomplexes. **A**, Ratio of chlorophyll a to chlorophyll b and of protein to chlorophyll in isolated thylakoid membranes from Lab and Field Arabidopsis. **B**, BN-PAGE of solubilised stromal lamellae (SL) and granal (G) thylakoid fractions from Lab (L) and Field (F) plants. **C**, 77 K fluorescence emission spectra of Lab (blue) and Field (purple) thylakoids using 435 nm excitation. **D**, 77 K fluorescence excitation spectra of PSII (695 nm) from Lab (blue) and Field (purple) thylakoids. **E**, 77 K fluorescence excitation spectra of PSI (735 nm) from Lab (blue) and Field (purple) thylakoids.

Clear differences between the Lab and Field plants were observed when their native thylakoid membranes were analysed by 77K fluorescence. Upon excitation at 435 nm (Figure 20C), Field thylakoids showed a dramatic reduction in the relative emission from PSI, consistent with its reduced antenna size seen in the BN-PAGE (Figure 20B). While there was slightly more emission from the PSI band in the Lab thylakoids, this band was substantially lower than that of PSII in the Field thylakoids. The antenna size of PSII also was also reduced in the Field thylakoids, as observed in the PSII excitation spectrum (Figure 20D), but perhaps to a lesser extent to that of PSI (Figure 20E). The PSI (735 nm) excitation spectrum of the Field thylakoids shows reduced relative fluorescence at 710 nm and 650 nm, suggesting fewer LHCI and LHCII proteins, respectively. Together, these results shown in Figure 20 demonstrate that, similarly to high light acclimation in a controlled environment (Chapter 4), the higher light intensity experienced by the Field plants (Figure 19C) caused them to reduce their capacity for

light absorption by both photosystems. The difference in the spectral quality of light from the sun, rather than fluorescent bulbs (Figure 19A), also had profound effects on the relative emission from the two photosystems. The increased amount of far-red light in sunlight, which preferentially excites PSI (Johnson and Wientjes, 2020), resulted in a significant reduction of the PSI antenna.

#### 5.4 Proteomic analysis of *Arabidopsis* grown in a natural light environment reveals changes in key photosynthetic complexes and their antenna

Thylakoid membranes from Lab and Field *Arabidopsis* were prepared for proteomic analysis in triplicate by solubilisation in 1% SL and digestion by trypsin/eLysC. Desalted peptides were analysed by nanoLC-MS/MS in triplicate with data dependent acquisition. MS data were searched against the UniProtKB proteome database to identify and quantify a total of 2,926 proteins across both conditions, of which 460 were identified as being thylakoid-associated. As discussed in Chapter 4, relative quantification based on normalisation to equal amounts of chlorophyll may not give a realistic picture of changes in protein abundance when the ratio of protein to chlorophyll changes significantly. Indeed, as in plants acclimated to high light intensity in a controlled environment, Field thylakoids have an increased amount of protein relative to chlorophyll. Relative quantification of proteins from MS data was performed using iBAQ values (Cox and Mann, 2008; Schwanhäusser et al., 2011) normalised to the intra-analysis sum of proteins from the key photosynthetic complexes PSII, PSI, *cytb<sub>6</sub>f* and ATP synthase. Using Perseus software (Tyanova et al., 2016), normalised iBAQ values for the three technical repeats were averaged and protein abundances with significant differences between Lab and Field conditions at  $q < 0.05$  were identified by a modified Welch's t-test (Section 2.9.9). For relative quantification of multi-subunit protein complexes, the sum of iBAQ intensities from all identified subunits of that complex was used. The normalised iBAQ values of the major photosynthetic complexes are presented in Figure 21 and displayed with the mean Lab value set to 100% for clarity. Consistent with data from plants acclimated to constant light intensity described in Chapter 4 and with a previous study of natural light *Arabidopsis* by Schumann et al., 2017, PSII remained at a constant level relative to the other key photosynthetic complexes. Field plants had 25% less PSI compared to those grown in the lab, similarly to results reported previously (Schumann et al., 2017). Given the massive reduction in 77K relative emission of PSI (Figure 20C), this would seem quite a small change. However, with the absence of the PSI-LHCI-LHCII supercomplex seen in the BN-PAGE (Figure 20B), the accompanying loss of energetically connected LHCII trimers may contribute to the magnitude of this difference. Previously, downregulation of antenna proteins has been observed in *Arabidopsis* grown outdoors (Wituszyńska et al., 2013). Consistent with this, and with the reduction in antenna size observed in the 77K excitation spectra, MS analysis revealed a dramatic decrease in the number of LHCII trimers in Field thylakoids (Figure 21). This 30% decrease was significantly larger than that observed in the HL thylakoids in Chapter 4, which was only around 15%. This dramatic reduction in antenna size of Field thylakoids appears to be contradicted by the ratio of Chl *a* to *b*, which did not change substantially

(Figure 20). However, the reduction in the relative amount of Chl *b* in the antenna may be mitigated by the decrease in PSI, enriched in Chl *a*. The MS data shows that *cytb<sub>6</sub>f* increases by 50% in Field thylakoids – a much more dramatic increase than the 20% increase seen in HL plants (Figure 12) and contrary to the 16% reduction described previously by Schumann et al. (2017). Since the amount of *cytb<sub>6</sub>f* has a significant effect on photosynthetic rate, i.e. it is a rate-limiting step (Kirchhoff et al., 2000), this enhanced response may be a result of overall colder temperatures in the field (Figure 19C). The change in the amount of ATP synthase (+40%) is also greater than that of constant HL plants.

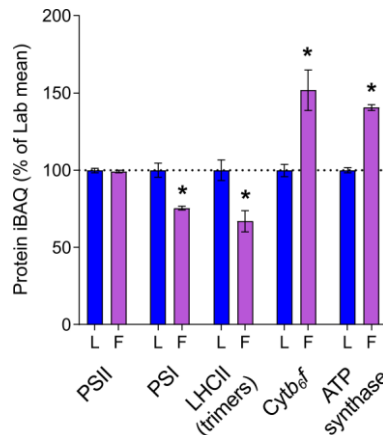


Figure 21: Adaptation to a natural environment involves changes in the relative abundance of key photosynthetic complexes. MS analysis showing the relative abundance in Lab (L) and Field (F) thylakoids of key photosynthetic complexes PSII, PSI, LHCII, *Cytb<sub>6</sub>f* and ATP synthase, expressed as a percentage of the mean in the Lab. The bars represent the average of three independent peptide preparations ( $n = 3$ ), derived from a pooled thylakoid sample, which were subject to MS analysis in triplicate in a randomised order and the values averaged. Error bars indicate mean  $\pm$  SD. Significant differences between conditions were determined by a modified Welch's *t*-test (Section 2.9.9, \* $q < 0.05$ ).

The MS analysis indicated varying behaviours of different LHCII constituent isoforms, shown in Figure 22A, in both trimeric and monomeric antenna proteins in the field. In this analysis, additional peptides were identified which allowed more isoforms of LHCB1 to be differentiated and quantified individually than in the experiment described in Chapter 4. Of the five LHCB1 isoforms in the Arabidopsis genome (Pietrzykowska et al., 2014), LHCB1.1 and 1.2 could not be distinguished from one another because they have identical amino acid sequences but LHCB1.3, LHCB1.4 and LHCB1.5 were quantified separately. While the total number of LHCII trimers decreased by 30% and there were substantial reductions in the amounts of LHCB1.1,1.2 (40%), LHCB1.4 (80%) and LHCB2 (25%), the LHCB1.3 isoform actually increased by 20%. This could imply a role for this less-abundant isoform in adaptation to fluctuating light or temperature. LHCB1.3 differs from LHCB1.1 and 1.2 by one residue near the N-terminus, where an asparagine is replaced by a lysine, creating an additional trypsin cleavage site and producing one peptide unique to LHCB1.3. This lysine may have a biological function and may be subject to posttranslational modification by acetylation, a common means of regulation of thylakoid membrane proteins (Wu et al., 2011). Lysine acetylation by the acetyltransferase NSI is essential for state transitions, and mutants lacking this protein had reduced acetylation in other isoforms of LHCB1

(Koskela et al., 2018). However, the position of another lysine, 3 residues earlier in LHCB1.3, prevents the detection of the tryptic peptide containing this residue so the acetylation state cannot be determined. Similarly to results reported previously comparing field and lab plants (Mishra et al., 2012) and to its behaviour under constant light acclimation described in Chapter 4, LHCB3, which is only present in M trimers (Caffarri et al., 2009), remained at a fairly constant level. This could suggest that the reduction in the amount of LHCII arises mostly from fewer L trimers. However, LHCB6 (CP24), which links M trimers to the PSII core via LHCB3, showed a small decrease of around 10% in Field plants, while LHCB5 (CP26) remained constant. Isoforms of another monomeric antenna protein associated with PSII, LHCB4 (CP29), also underwent some stoichiometric changes as a result of outdoor acclimation. For this protein, a 20% reduction in the LHCB4.2 isoform was countered by increases in LHCB4.1 (10%), and LHCB4.3 (400%). The latter is missing the stromal C-terminal domain, which interacts with both M-trimers and LHCB6 (Pagliano et al., 2014) and mediates the interaction of PSII supercomplexes between granal membrane layers (Su et al., 2017). The 5-fold increase seen in the amount of LHCB4.3 in Field thylakoids may play a photoprotective role, by decreasing the affinity of PSII supercomplexes for M-trimers or by disrupting interactions of PSII supercomplexes between membrane layers (Albanese et al., 2019), possibly to ease the disassembly of PSII during repair. The 10% increase in LHCB4.1 in the field compares to the response of this isoform to low light acclimation described in Chapter 4.

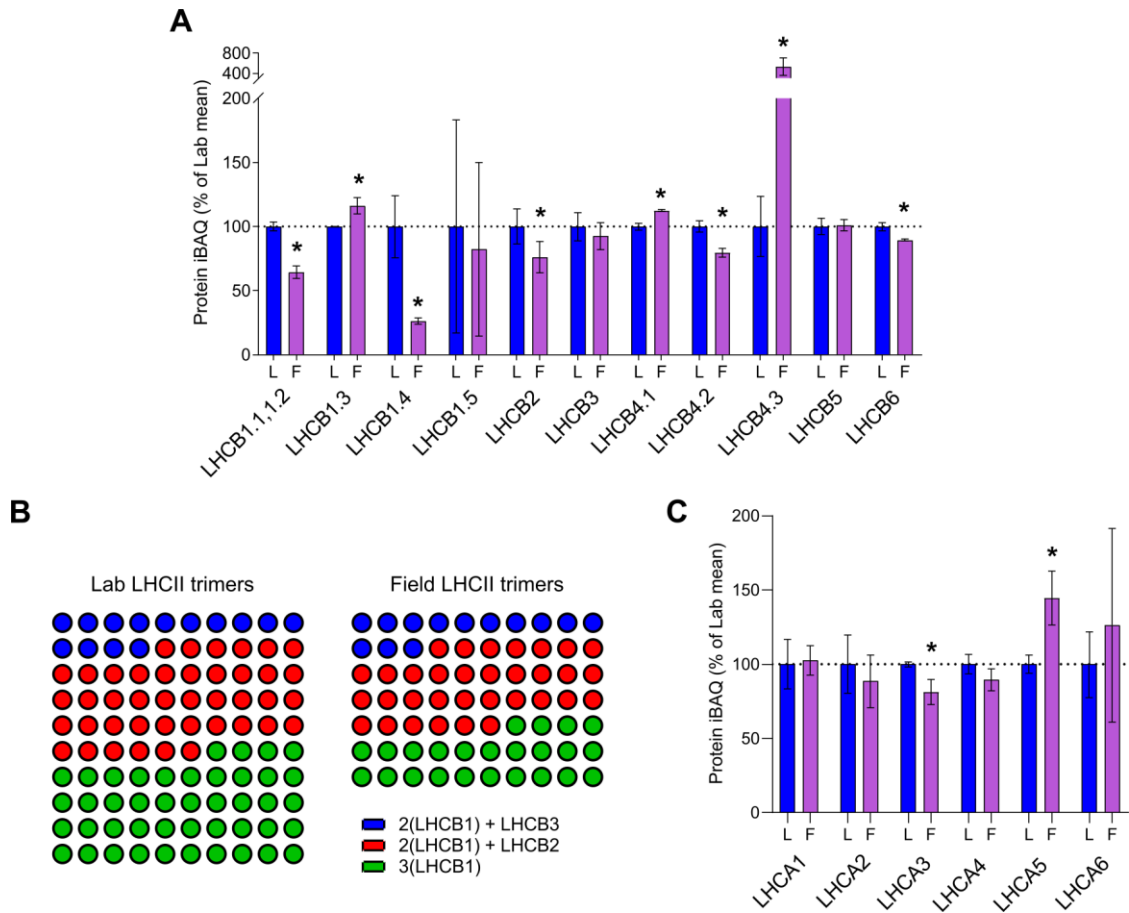


Figure 22: Thylakoids from field Arabidopsis have altered levels of minor antenna subunits. **A**, MS analysis showing the relative abundance of LHCII subunits. **B**, Diagram representing relative number of LHCII trimers as dots in Lab and Field thylakoids and the distribution of trimer types. The number of trimers in Lab thylakoids is set to 100, and the trimers are categorised into trimers containing LHCB3 (blue dots), containing LHCB2 (red dots), or only LHCB1 (green). MS data for all LHCB1 isoforms (LHCB1.1, 1.2, 1.3, 1.4, 1.5) was summed. **C**, MS analysis showing the abundance of LHCI. MS data sampling details are as stated in Figure 21.

A simplified visualisation of differences in the composition of the LHCII trimers calculated from the MS data is shown in Figure 22B. Each dot represents one trimer, with the total number of dots representing the difference in the number of trimers between Lab and Field thylakoids: for every 100 trimers in Lab thylakoids there are 70 trimers in Field thylakoids. An assumption was made that there are three possible combinations of LHCB1/2/3, such that the trimers may be composed of 2(LHCB1) + LHCB3 (blue dots, mostly M-trimers), 2(LHCB1) + LHCB2 (red dots, mostly trimers capable of performing state transitions), and trimers containing only LHCB1 (green dots). This diagram shows that the Field thylakoids have very similar numbers of M-trimers and a modest reduction in the number of trimers containing LHCB2, but that the main difference between the two samples is the number of trimers containing only LHCB1. The LHCB1 isoform contributes more significantly than the other isoforms to large grana stacks (Pietrzykowska et al., 2014), which may be less desirable for the Field plants in their high-light low-temperature environment. Compared to the LHCB1-only trimers, those containing LHCB2 may have a greater importance in variable light and temperature conditions because

of their involvement in regulation of light harvesting and photoprotection in the form of the enhancement of release of 'extra' trimers upon phosphorylation (Pietrzykowska et al., 2014).

The MS analysis identified and quantified all six LHCI proteins present in Arabidopsis (Figure 22C). Despite a reduction in the number of PSI core complexes, there was no significant change in LHCA1, LHCA2 and LHCA4. This result compares to that reported by Mishra et al. (2012), where most of the LHCA proteins stay constant, but the relative abundance of PSI is not calculated. Only one LHCI isoform, LHCA3, decreased in abundance in the field plants in line with PSI by 20%. LHCA5, one of the two LHCA proteins known to mediate interactions with the NDH complex (Peng et al., 2009; Yadav et al., 2017), showed a 40% increase in the field plants, implying a greater role for CET in the natural environment. However, this contradicts the data by Mishra et al. (2012) where LHCA5 was depleted in field plants.

### 5.5 Thylakoid architecture is altered in a natural light environment

Differences in thylakoid membrane stacking between Lab and Field plants were analysed using thin section electron microscopy (Figure 23A) to determine the number of membrane layers per granum (Figure 23B). Qualitatively, the chloroplasts of lab plants appeared more densely packed with thylakoid membranes than those of the Field plants, in which large expanses of stroma free of membranes were observed. Granal stacking was significantly ( $P < 0.0001$ ) reduced in the Field chloroplasts with dramatically fewer membrane layers per granum. This difference was also observed by Pribil et al. (2018), where growth under natural light conditions caused a 2 to 5-fold reduction in grana height, and may be a result of the reduction in the number of LHCB1-only trimers (Figure 22B) since LHCB1 contributes more significantly to stacking (Pietrzykowska et al., 2014). The number of membrane layers in Field chloroplasts was also less variable than those grown in the Lab, with no visible grana having more than 8 layers. Interestingly, when structured illumination microscopy (Figure 23C) was used to compare grana diameter between the two conditions (as a measurement of grana full width half maximum of the chlorophyll fluorescence signal from each granum), it was observed that the decrease in membrane layers in the Field chloroplasts was accompanied by a slight increase ( $P < 0.01$ ) in grana diameter (Figure 23D). Since the Field plants were exposed to colder temperatures (Figure 19C), this factor may have affected thylakoid ultrastructure in addition to the light environment. Cold stress has been reported to increase chloroplast size, a measurement not taken in this experiment but one that appears to apply qualitatively. However, cold stress also increases membrane layers per granum (Liu et al., 2018); the opposite is observed in this case.

Changes in the extent of grana stacking can be attributed to LHCI interactions between layers (Day et al., 1984), phosphorylation/dephosphorylation by STN7 and TAP38 (Fristedt et al., 2009a; Wood et al., 2019), and bending of the thylakoid membrane by CURT1 oligomers (Armbruster et al., 2013). The latter process, involving the CURT1 family of proteins (CURT1A/B/C/D), likely plays an important

role in dynamic thylakoid stacking in natural environments, as evidenced by Pribil et al. (2018). They found that when grown outdoors, mutants lacking all four CURT1 proteins were significantly impaired in a number of photosynthetic parameter measurements but those overexpressing CURT1A were comparable to wild type. They suggest that the amount of CURT1 does not change in response to short term changes in light intensity; rather, its regulation occurs at the posttranslational level. This MS analysis showed that Field plants had around 60% more CURT1A compared to those grown in the Lab. Similarly, Pribil et al., 2018 observed a 2-fold increase in the abundance of CURT1A in field-grown plants compared to those grown in a controlled environment. They found that the amount of CURT1B increased 4-fold, contrary to this proteomic analysis, which saw a smaller response in this protein of just 25%. No significant difference was found between Lab and Field thylakoids for the proteins CURT1C and CURT1D. Mutants lacking CURT1A and RIQ1/2 show opposite phenotypes with respect to the number of stacks per granum (Armbruster et al., 2013; Yokoyama et al., 2016). According to the MS analysis, both RIQ1 and RIQ2, the absence of which results in an increased number of membrane layers per granum (Yokoyama et al., 2016), increased by around 60% in Field thylakoids in line with CURT1A and with the changes observed during acclimation to HL (Chapter 4).

Phosphorylation of LHCII and PSII by STN7 and STN8, respectively, decreases grana stacking by through repulsion on the stromal side of the membrane while dephosphorylation by TAP38 increases stacking (Fristedt et al., 2009a). Interestingly, the MS analysis shows contrasting behaviour of STN7 and STN8 (Figure 23E). STN8, which phosphorylates PSII to initiate its repair cycle (Järvi et al., 2015; Nath et al., 2013) was 60% more abundant in the Field thylakoids, whereas STN7 and its paired phosphatase, TAP38, both decreased by around 40%. The reduction in these enzymes involved in phosphorylation of LHCII, as well as the decrease in the amount of LHCB2 (Figure 22A), supports the loss of the PSI-LHCI-LHCII supercomplex observed in the BN-PAGE gel (Figure 20B) and suggests a reduced role for state transitions in the natural environment. However, while Mishra et al. (2012) also reported reduced LHCB2, they found the field plants were capable of performing state transitions at a similar level to indoor plants. Long term changes in stacking or capacity for dynamic remodelling may relate to faster turnover of PSII. The lower levels of STN7 seen in the Field plants must not relate solely to the higher light intensity experienced because the opposite effect is seen under controlled light acclimation to high light (Figure 14). CAS, a regulatory calcium sensor which promotes dephosphorylation of LHCII (Cutolo et al., 2019), is raised by 25% in Field thylakoids. This is a smaller increase than that observed in controlled high light (70%, Figure 14) which may reflect a reduced need for LHCII dephosphorylation since there is less STN7.

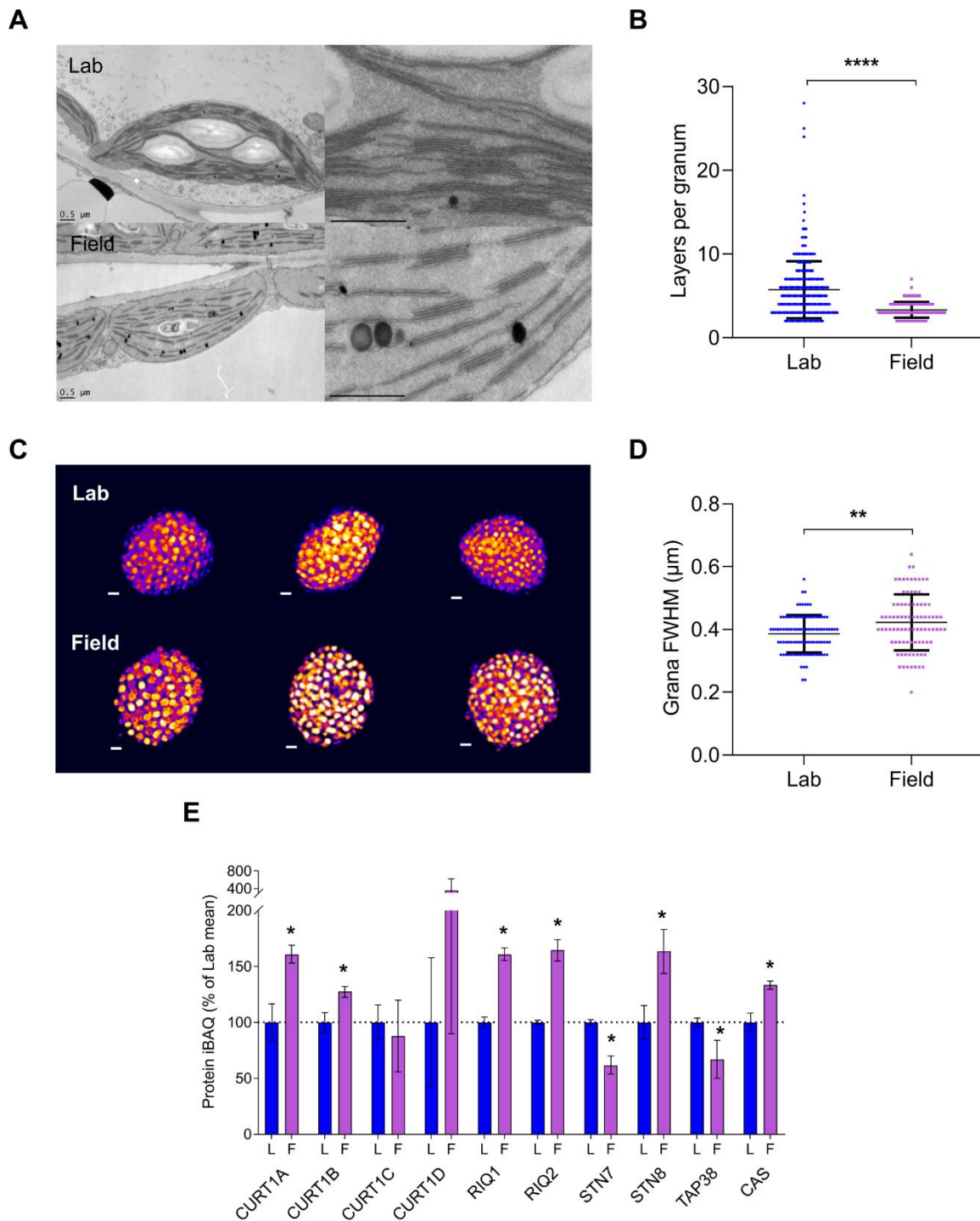


**Figure 23: Thylakoid architecture changes in Field thylakoids are associated with increases in CURT1 and RIQ proteins but not STN7 or TAP38. A, Thin-section electron micrographs of chloroplasts in plants from a controlled environment (Lab, top row) and outdoors (Field, bottom row) (scale bar: 0.5  $\mu\text{m}$ ). B, Number of membrane layers per grana stack calculated from electron microscopy images of chloroplasts in Lab ( $n = 354$  grana stacks) and Field ( $n = 317$ ) leaves (Welch's  $t$ -test. \*\*\*\* $P < 0.0001$ ). Error bars indicate mean  $\pm$  SD. C, 3D-SIM images (shown as Max Projections on the  $z$ -axis with tricubic sharp interpolation) of chloroplasts from Lab (top row) and Field (bottom row) plants. D, Full width at half-maximum (FWHM) fluorescence intensity of the fluorescent spots (grana) in three-dimensional SIM images of chloroplasts from Lab ( $n = 100$ ) and Field ( $n = 88$ ) plants (Welch's  $t$ -test. \*\* $P < 0.01$ ). Error bars indicate mean  $\pm$  SD. E, MS analysis showing the relative**

*abundance of proteins involved in modulation of thylakoid membrane architecture, expressed as a percentage of the mean in Lab thylakoids. Sampling details are as stated in Figure 21.*

## 5.6 The thylakoid proteome of field grown plants implies a greater capacity for linear electron transfer, cyclic electron transfer and photoprotection

The MS analysis showed differences in the relative amounts of proteins involved in LET arising from growth in a natural light environment, which were not equivalent to the differences seen in constant light acclimation. As shown in Figure 21, Field thylakoids had 50% more *cytb<sub>6</sub>f* than those from plants in a controlled environment, a larger increase than that seen from constant high light, whereas FNR1 and FNR2 increased to a lesser extent (25% and 20%, respectively) than in controlled high light. This could suggest that LET in the Field plants is constrained more by transfer of electrons through the chain than by the sink capacity. The FNR tethering proteins TIC62 and TROL were both upregulated similarly to one another by 40-50% in the Field thylakoids, in contrast with the results described in Chapter 4, where TROL was present at a constant level in every light condition. This discrepancy indicates a role for TROL in fluctuating light specifically. PGR6, the plastoglobule-associated regulator of the photoactive PQ pool (Pralon et al., 2019) whose relative abundance increases with growth light intensity, increased dramatically (+250%) in Field thylakoids. In constant HL plants (Chapter 4), PGR6 increases to a much lesser extent (+100%). Acclimation to cold can be triggered by redox sensing of PSII and the PQ pool and increases cold-adapted plants' resistance to photoinhibition by increasing the amount of PQ relative to PSII (Gray et al., 1996; Huner et al., 1996). Therefore, this difference in the magnitude of the response of PGR6 is likely a result of the lower temperatures experienced by the Field plants. Interestingly, plastocyanin (PC), the electron donor for PSI, was unchanging between Lab and Field thylakoids. However, since PSI decreases in abundance in the Field thylakoids, this constant level of plastocyanin overall may represent an increase relative to PSI. While the behaviour of these LET proteins in Field thylakoids does not directly compare to high light acclimation, this MS data contradicts the idea proposed previously that the electron transport machinery of natural light acclimated plants is most similar to that of constant low light acclimated plants (Schumann et al., 2017).

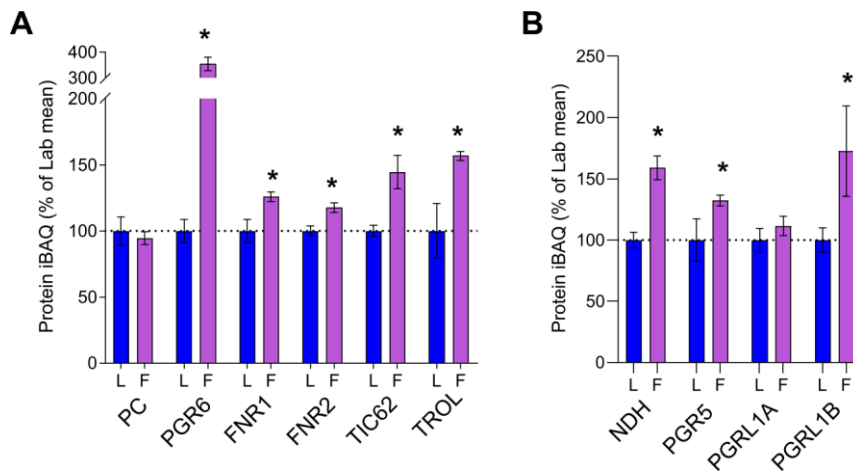


Figure 24: Acclimation to a natural environment causes upregulation of proteins involved in LET and CET. **A**, MS analysis showing the relative abundance of LET related proteins, expressed as a percentage of the mean Lab thylakoids. **B**, MS analysis showing the relative abundance of CET related proteins, expressed as a percentage of the mean in Lab thylakoids. Sampling details are as stated in Figure 21.

The MS analysis shows an increase in the relative abundance of proteins involved in cyclic electron transfer in Field thylakoids (Figure 24B). In particular, there is a significant upregulation of NDH (60%) and the LHCA5 subunit of LHCI (Figure 22C), which links NDH to PSI (Peng et al., 2009; Yadav et al., 2017). NDH is necessary for rapid induction of P700 oxidation – a mechanism for reducing ROS formation – under light fluctuating at a high frequency (Shimakawa and Miyake, 2018). PGR5 and PGRL1B increase in abundance by 30% and 70%, respectively – a smaller difference than that seen in plants acclimated to constant high light (Figure 15B). This is surprising, given that the *pgr5* mutation is lethal under fluctuating light (Tikkanen et al., 2010), suggesting a greater importance in fluctuating light. The behaviour of PGRL1A, a phosphorylation target of STN8 (Reiland et al., 2011), differed to that of PGRL1B, the former remaining constant in all light environments analysed. Despite previous reports that the two proteins are functionally redundant (DalCorso et al., 2008) but as seen in previous work where PGRL1B changed differently to PGRL1A (Jin et al., 2017), the two proteins appear to be differentially regulated, suggesting they may fulfil different roles in regulation of CET. Shown to form a stable complex with both PGRL1A and B (Endow and Inoue, 2013), the chloroplast processing peptidase PLSP1 increases in abundance 2-fold in the Field (Figure 27). Together, the MS data from constant light acclimation (Chapter 4) and natural light adaptation suggest a greater role for NDH-dependent cyclic electron transfer in the natural environment than cyclic electron transfer via PGR5. Indeed, under both artificial and natural fluctuating light, mutants deficient in NDH-mediated CET are more susceptible to PSI photoinhibition than those deficient in PGR5-mediated CET (Kono et al., 2017).

Since energy-dependent NPQ (qE) is probably more important for fluctuations in light intensity than for high light specifically (Külheim et al., 2002), MS analysis was used to determine the relative amounts of proteins involved in the short term regulation of light harvesting in Arabidopsis from the

Lab and the Field (Figure 25). In a sudden transition to high light, where increased proton pumping by PSII and *cyt<sub>b</sub><sub>6</sub>f* exceeds the immediate capacity for ATP generation by ATP synthase, protons build up and cause a pH decrease in the thylakoid lumen. The pH change results in protonation of VDE and consequent conversion of LHCII-associated violaxanthin to zeaxanthin via the antheraxanthin intermediate. Zeaxanthin promotes aggregation of LHCII trimers and dissipation of energy as heat through chlorophyll-chlorophyll and carotenoid-chlorophyll interactions (Li et al., 2009; Ruban, 2016). The MS analysis shows Field plants have a higher level of both VDE and ZEP, the latter of which converts zeaxanthin back to violaxanthin in the transition to the light harvesting state. VDE increases to a greater extent (60%) than ZEP (30%), with both proteins responding differently to fluctuating light than to acclimation to constant light intensities as described in Chapter 4. Constant high light acclimation did not affect the abundance of VDE, whereas ZEP increased by around 50% (Figure 16), suggesting VDE is more important for fluctuating light than for constant high light irradiance where long term acclimation has reduced the need for rapid initiation of quenching. High light induced low luminal pH also triggers protonation of luminal glutamate residues of PSBS, triggering monomerisation of this protein and reorganisation of the PSII antenna network into a dissipative state (Bergantino et al., 2003; Correa-Galvis et al., 2016; Sacharz et al., 2017). According to the MS analysis, PSBS increases 2-fold in the field – a greater increase than the 1.34-fold increase previously reported (Schumann et al., 2017). The difference in the relative abundances of the proteins VDE, ZEP and PSBS agrees with the observation of Mishra et al., 2012, that field-grown plants have a much greater capacity for NPQ. After quenching of excess light, the K<sup>+</sup>/H<sup>+</sup> antiporter KEA3 responds to sudden reductions in light intensity by releasing protons into the stroma, speeding up the return of LHCII to its light harvesting state in fluctuating light (Armbruster et al., 2014). Indeed, this protein showed an approximate increase of 45% in Field plants. The change measured in the amount of KEA3 in a natural light environment, but not upon acclimation to constant high light (Figure 16), supports the importance of its role in a natural environment.

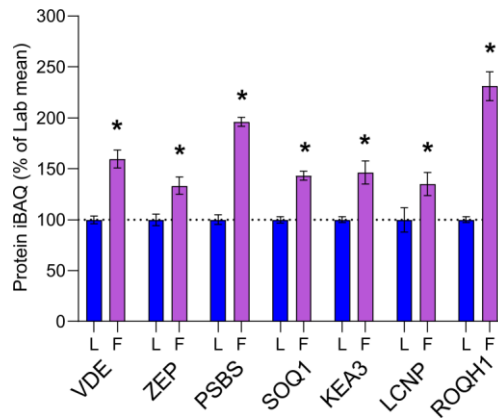


Figure 25: Arabidopsis in a natural environment have increases in the relative abundance of proteins involved in light harvesting regulation. MS analysis showing the relative abundance of NPQ related proteins, expressed as a percentage of the mean in the Lab. Sampling details are as stated in Figure 21.

While much work has been done to study quenching involving PSBS and zeaxanthin, less is known about the sustained slowly relaxing form of NPQ (qH) which involves SOQ1, ROQH1 and LCNP. SOQ1 and ROQH1 both function to suppress qH. The mutant lacking SOQ1 (suppressor of quenching 1) was found to suppress the NPQ phenotype of mutants lacking PSBS (Brooks et al., 2013), increasing this form of NPQ despite the absence of qE. When this mutant was combined with the mutation to inactivate ROQH1 (Amstutz et al., 2020) Arabidopsis growth under low light intensity was severely limited due to constitutive high levels of qH. The chloroplastic lipocalin LCNP, on the other hand, promotes this sustained form of quenching (Malnoë et al., 2018). Therefore, it is interesting that Field thylakoids contain elevated levels of all of these proteins (Figure 25), a result which differs from that seen in constant light acclimation described in Chapter 4. Constant low light acclimated plants appear to increase their capacity for qH, observed as the upregulation of LCNP, whereas high light acclimated plants suppress it by increasing their levels of SOQ1 and ROQH1 (Figure 16). In the natural environment, the expression patterns of proteins involved in regulation of light harvesting and quenching do not compare directly to those described in Chapter 4 of either low light or high light. Instead, these proteins show a mixture of behaviours from both.

### 5.7 Upregulation of PSII repair machinery in the field

The relative amounts of proteins of the PSII repair machinery in Field versus Lab thylakoids calculated from MS data is shown in Figure 26. As would be expected for a natural environment with significant stress from high, variable light irradiance and cold temperatures, the majority of the proteins involved in PSII repair are upregulated in the Field. However, there are some exceptions. One is MPH2 (maintenance of PSII under high light 2), a luminal protein required for normal growth under natural fluctuating light and temperature conditions (Liu and Last, 2017). It was observed to interact with PSII core subunits in a way that suggests a role in the disassembly of PSII upon initiation of repair. MPH1 was proposed by Liu and Last (2017) to fill a regulatory role for PSII repair in long term acclimation to

fluctuating light rather than just maintenance of PSII under high light. Therefore, it is surprising that in the MS analysis no significant difference in the amount of MPH2 was observed between Lab and Field thylakoids. Another protein present at constant levels was the immunophilin CYP38. Since this protein negatively regulates phosphatase activity on the PSII core (Vener et al., 1999), increased abundance of this protein under stress might negatively impact PSII repair. In this analysis, the detection of multiple isoforms of proteins with different behaviour is notable. One possible model of PSII repair (Weisz et al., 2019) involves the storage of PSII subunits CP47, CP43, PSBH, several lower molecular weight subunits and the assembly factor PSB27 in a stable complex lacking a reaction centre to avoid harmful photochemical reactions during the repair cycle. The identification of two isoforms of PSB27, only one of which is upregulated in Field thylakoids, implies varied roles or regulation of this factor. Additional proteins behaving unexpectedly in Field thylakoids are the one-helix proteins OHP1 and OHP2. They are thought to interact with HCF244, another factor involved in PSII biogenesis, and parts of the PSII reaction centre to form a complex that aids in the cotranslational assembly of new D1 (Hey and Grimm, 2018; Li et al., 2019). Therefore, it is surprising that one of these proteins, OHP2, is less abundant in the Field thylakoids since OHP2 has previously been shown to increase its expression in response to high light intensity (Andersson et al., 2003) and the Field Arabidopsis were grown in a higher light environment than the Lab plants. OHP2 has been shown to associate with PSI (Andersson et al., 2003), the decrease of which in Field thylakoids could explain the reduced need for OHP2. However, analysis of mutant Arabidopsis lacking OHP1 also suggested roles for this protein in assembly of both PSII and PSI (Myouga et al., 2018) so this explanation seems inadequate.

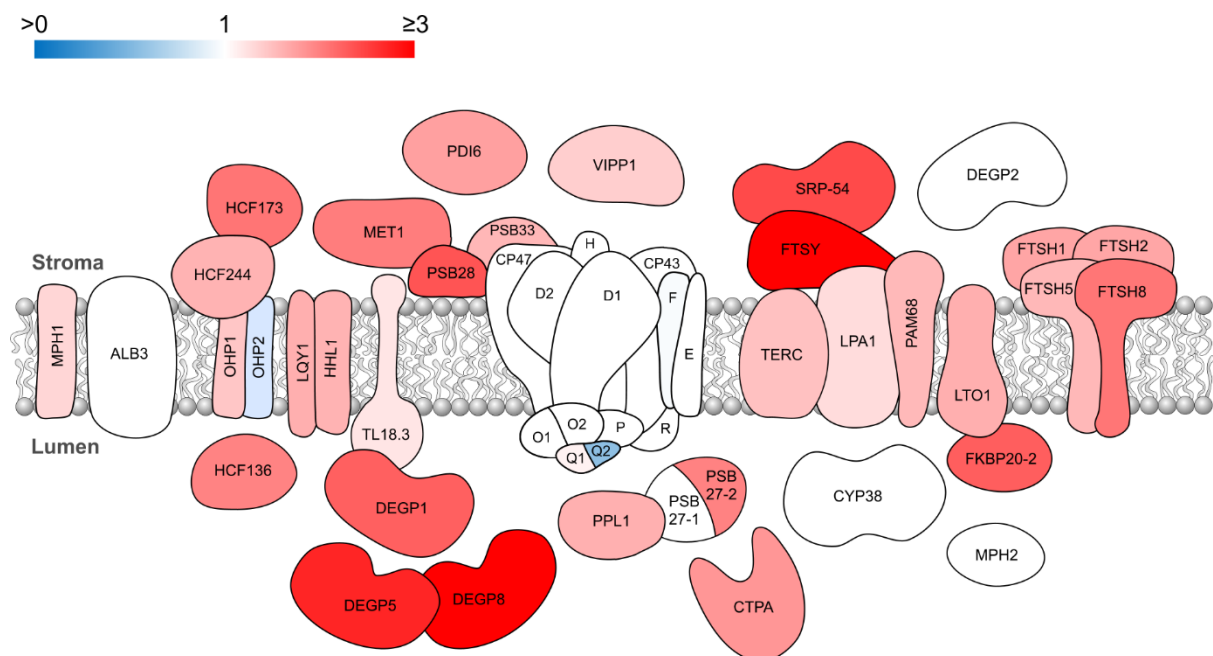


Figure 26: Upregulation of the PSII repair machinery in a natural environment. Schematic diagram indicating the relative abundance of PSII repair proteins in Field versus Lab thylakoids. Blue proteins are more abundant in the Lab, whereas

*red/pink proteins are more abundant in the Field. Where no significant difference was detected for a quantified protein, it is displayed in white.*

## 5.8 Proteins specific for acclimation to a fluctuating natural light environment

Previously it has been shown that the early light induced proteins (ELIPs) are significantly upregulated in or only detectable from plants grown in a natural light environment (Mishra et al., 2012; Norén et al., 2003). The expression of ELIPs is also upregulated as a response to low temperature (Norén et al., 2003). The MS analysis confirmed this with the identification of both ELIP1 and ELIP2 in Field thylakoids only (Figure 27). Constant high light and low temperature causes accumulation of ELIP1 and 2 in wild type but does not cause a dramatic phenotype in mutants lacking these proteins (Rossini et al., 2006). Although the precise biological function or mechanism of these proteins is not currently known, ELIPs may function to prevent photooxidative damage in high light stress through sequestration of free chlorophyll molecules or stabilisation of complexes during turnover of chlorophyll-containing proteins (Hutin et al., 2003).

One notable protein that increased in abundance in Field thylakoids but in response to constant light acclimation was TSP9, which showed a 2-fold increase in the natural environment. TSP9 is found mostly in the grana and associates with LHCII but also with peripheral subunits of both PSII and PSI (Hansson et al., 2007). It is a phosphorylation target of STN7 and its absence affects both state transitions and NPQ, and it has been suggested that TSP9 aids in the dissociation of antenna proteins from the PSII core under fluctuating light irradiance (Fristedt et al., 2008, 2009b). Therefore, more TSP9 in Field plants may have contributed to reduced supercomplex formation seen by BN-PAGE (Figure 20B). Another protein significant for fluctuating light intensity is the FLAP1 (fluctuating light acclimation protein 1) protein. FLAP1 is located in both the thylakoid membrane and the chloroplast envelope and has a role in the regulation of NPQ. Mutants lacking this protein have higher levels of NPQ and a pale green phenotype, resulting from lower leaf chlorophyll content, under fluctuating light (Sato et al., 2017). FLAP1 has been proposed to regulate NPQ through energy dependent quenching (qE) involving PSBS and zeaxanthin (Trinh et al., 2019). Consistent with other NPQ-related proteins, MS analysis showed it increased by around 50% in Field plants (Figure 27).



fluorescence spectroscopy, BN-PAGE and microscopy to analyse how changes in protein abundance relate to structural and functional differences necessary for growth under increased environmental stress.

The reason for maintenance and recording of controlled environmental conditions in plant science is the extreme variability of the natural environment and its effects on reproducibility of results. Therefore, an obvious caveat of this experiment is that it can never be reproduced exactly. The recording of weather data is important to contextualise any observations made but also comes with caveats, in that the light intensity data recorded here is not directly comparable to that of the growth chamber in its format and because of the differences in the spectral cross section of fluorescent lighting and sunlight (Figure 19A). However, if the ultimate aim of photosynthetic research is to improve photosynthesis and yield in crops, generally grown in fields and subject to the variations and stresses of the natural environment, then it is vitally important to place our current understanding of photosynthetic mechanisms in the context of the field. Comparisons of plants grown in the lab and in the field can reveal which photosynthetic processes are of greatest importance for crops and direct further research towards these. Although *Arabidopsis* is not an agriculturally relevant species, the time and location used for the outdoor growth of the plants in this experiment were chosen so as to closely replicate a field; the plants were watered regularly to mimic irrigation, grown during summer, and with minimal shading from buildings or canopy. Additional experiments of this kind with *Arabidopsis* grown at different times of year, under canopy, or with a species currently used in agriculture would surely give greater and more useful insights into photosynthesis in a natural environment. Another angle would be to assess the effect of the spectral quality of growth light in an otherwise controlled environment on the thylakoid proteome. A comparative gene expression analysis of *Arabidopsis* plants grown under different artificial light environments (Seiler et al., 2017), including fluorescent bulbs and LEDs of various intensities and spectral qualities, demonstrated that spectral composition affected RNA levels for proteins involved in a wide range of different processes. However, the observed gene expression changes were only loosely correlated with phenotype, suggesting the need for a proteomic analysis.

The application of the MS method developed in Chapter 3 and used in Chapter 4, whereby protein iBAQ (Schwanhäusser et al., 2011) is normalised to the intra-analysis sum of the key photosynthetic complexes (PSII, *cytb<sub>6</sub>f*, PSI and ATP synthase), to a further analysis has provided further assurance of its validity. Again, while the current understanding of thylakoid proteome remodelling in response to environmental conditions is that PSII is subject to differential regulation and that PSI remains constant (Anderson et al., 1988), this MS analysis suggests the opposite. Therefore, it appears that normalisation to chlorophyll content, as is frequently used in photosynthesis research, may be outdated and misleading when calculating changes in relative amounts of proteins. The general impression of the Field thylakoid proteome is one of increased complexity with a greater capacity for NPQ, cyclic electron transfer and PSII repair, a lower requirement for PSI and the light harvesting antenna, and possibly a reduced

capacity for state transitions. It may be that the relatively high contribution of far red light to the spectrum of sunlight means that while less PSI is needed, a greater proportion of the existing PSI is associated with NDH and participating in CET to meet the high ATP demands of rapid protein and pigment turnover arising from increased environmental stress. Schumann et al. (2017) proposed that the electron transport machinery of natural light acclimated plants is most similar to that of constant low light acclimated plants, while proteins involved in photoprotective mechanisms are present at comparable levels to in constant high light. The MS analysis described here contradicts this idea of Field plants having a mixture of low and high light responses, pointing towards a more extreme version of the constant high light response, in general. However, their study involves several photosynthetic parameter measurements providing more detail on how the changes in the stoichiometry of thylakoid proteins relate to functional differences. To combine thylakoid proteome analysis of Field plants with direct measurements of CET, CO<sub>2</sub> assimilation, photoprotective quenching and other parameters would help to validate these ideas. Overall, the data described here demonstrates that regulation and remodelling of the thylakoid proteome is highly intricate and flexible. Therefore, in order to gain further insights into photosynthetic mechanisms beyond what can be observed from plant phenotypes and spectroscopic measurements, this method of mass spectrometry-based relative quantification of thylakoid proteins should be applied to Arabidopsis mutants in addition to changes in environmental conditions.

## 6 Thylakoid proteome analysis of photosynthetic mutants: LHCII phosphorylation and proton gradient regulation

### 6.1 Introduction

The bottom-up proteomics strategy used for the work in this thesis allows a descriptive comparison of protein abundance in the thylakoid membrane under different environmental conditions. However, the use of mutants defective in certain photosynthetic processes can help to provide further insights, even when the mutation produces no immediately observable phenotype. Mutants without or with minimal phenotypes may remodel the proteome to compensate for missing proteins or processes, and these changes may be analysed by MS-based proteomics. Proteomics can also be used to study conditionally lethal mutants to find changes that may explain or contribute to the lethality of the mutation under certain conditions. For example, the loss of one protein may cause plant death either by disruption of a single vital process or by dysregulation of signalling pathways leading to broader changes in the proteome.

In Chapter 4, MS-based proteomics was used to quantify the changes in the thylakoid proteome during long-term acclimation to low, moderate and high growth light intensity. Previously it has been reported that the kinase STN7 is required for long term acclimation in *Arabidopsis*, with the *stn7* mutant unable to adjust the PSI/PSII ratio and LHCII/PSII ratio in response to light spectral quality expression (Bonardi et al., 2005; Pesaresi et al., 2009a). The *stn7* plants presented a slightly impaired growth phenotype only when exposed to changing light conditions and a more reduced PQ pool was observed (Grieco et al., 2012; Pesaresi et al., 2009a). Most importantly, *stn7* was incapable of performing state transitions. The phosphatase responsible for state 2 to state 1 transitions – the dissociation of LHCII from PSI and its association with PSII – was later identified as TAP38, also known as PPH1, through generation of *tap38* mutants (Pribil et al., 2010; Shapiguzov et al., 2010). These mutants were impaired in state transitions, being locked in state 2 with an increase in PSI antenna size. However, since the *psal* mutant, which lacks state transitions due to the loss of the major LHCII binding site on PSI, still showed long-term acclimation, the authors speculated that STN7 activity may also be crucial for the operation of a separate signalling pathway that leads to changes in photosynthetic gene expression (Pesaresi et al., 2009a). In addition to LHCB1 and 2, STN7 is also known to phosphorylate a range of other chloroplast proteins including FNR1, ribosomal protein S7, CLPP3 and TSP9 (Fristedt et al., 2008; Schönberg et al., 2017), though which of these targets is involved in the putative signalling mechanism remains unclear.

In Chapter 4, MS analysis found that the abundance of STN7 increased by around 20% in HL while TAP38 decreased by around 30% (Figure 14E). This is a curious result since STN7-dependent phosphorylation of LHCB1 and 2 peaks under short-term low intensity white light exposure, where the excitation imbalance between PSI and PSII is greater (Rintamäki et al., 1997). In addition, under short-

term higher light intensities STN7 becomes inhibited by elevated  $\Delta\text{pH}$  and/or stromal reduction via thioredoxin (FERNYHOUGH et al., 1984; RINTAMÄKI et al., 2000), leading to dephosphorylation of LHCII by TAP38 and increased grana diameters and stacking (RINTAMÄKI et al., 1997; WOOD et al., 2019). Yet, as observed in Chapter 4, grana stacking and diameter is reduced under long-term acclimation suggesting plants acclimated to high light maintain LHCII phosphorylation. The increased abundance of STN7 in high light observed in Chapter 4 would be consistent with this, or alternatively, it may reflect the crucial role of STN7 in phosphorylating its other targets.

In Chapter 5, the thylakoid proteome of *Arabidopsis* grown in an outdoor environment was compared to that of those from a controlled environment growth chamber. *Arabidopsis* mutants lacking the CET protein PGR5, which increased in abundance by 25% in field thylakoids (Figure 24B), grow normally under constant light but die when grown under fluctuating light intensity or in the field (SUORSA et al., 2012). Despite a normal growth phenotype at low light, the *pgr5* mutant showed a low  $\Delta\text{pH}$  phenotype in high light, and thus NPQ and photosynthetic control (Section 1.4.2.2) were strongly impaired, suggesting PGR5-dependent CET plays a crucial role in lumen acidification under these conditions (MUNEKAGE et al., 2002). Plants lacking PGRL1A and B (*pgr1lab*) also show the same phenotype as the *pgr5* mutant (DALCORO et al., 2008) and the two were suggested to function as a ferredoxin-quinone reductase (FQR) (HERTLE et al., 2013). Later work (NANDHA et al., 2007) revealed that *pgr5* plants were ultimately capable of CET at the same level as wild type, but were less readily switched into a CET mode, suggesting the PGR5 and PGRL1 proteins may instead play an indirect regulatory role. Overexpression of PGR5 does not produce changes in electron transfer at steady state but results in delayed chloroplast development and greater induction of NPQ upon high light exposure (OKEGAWA et al., 2007). Plants overexpressing PGR5 have also showed impaired growth initially upon germination and under very low light intensity but once mature, they had greatly increased tolerance to very high light intensity and drought stress (LONG et al., 2008). These observations suggest that PGR5 may be involved in sensing the redox poise of the chloroplast stroma, which is in turn linked to both short- and long-term acclimation.

The aim of this chapter is to use the established proteomic strategy, along with microscopy and native PAGE, to investigate the effect of the absence of TAP38 and STN7 on long-term developmental acclimation to varying light intensity. Relative quantification of the thylakoid proteome is used to investigate differences in the light acclimation strategy in the phosphorylation mutants *stn7* and *tap38* to explore the link between short- and long-term responses to light intensity. Then, the proteome of the *pgr5* mutant is analysed in order to speculate on contributing factors to its lethality in fluctuating light and their relationship to plant survival in a natural environment.

## 6.2 Growth and acclimation of *stn7* and *tap38* to varying light intensity

Col-0 (wild type) and two phosphorylation mutants of this background, *stn7* and *tap38*, Arabidopsis plants were grown with an 8 h photoperiod for 2 weeks under moderate light (ML) then either moved to low light ( $25 \mu\text{mol photons m}^{-2} \text{s}^{-1}$ , LL) or high light ( $600 \mu\text{mol photons m}^{-2} \text{s}^{-1}$ , HL), or kept at ML ( $130 \mu\text{mol photons m}^{-2} \text{s}^{-1}$ ). Representative images of the plants at 6 weeks are shown in Figure 28.

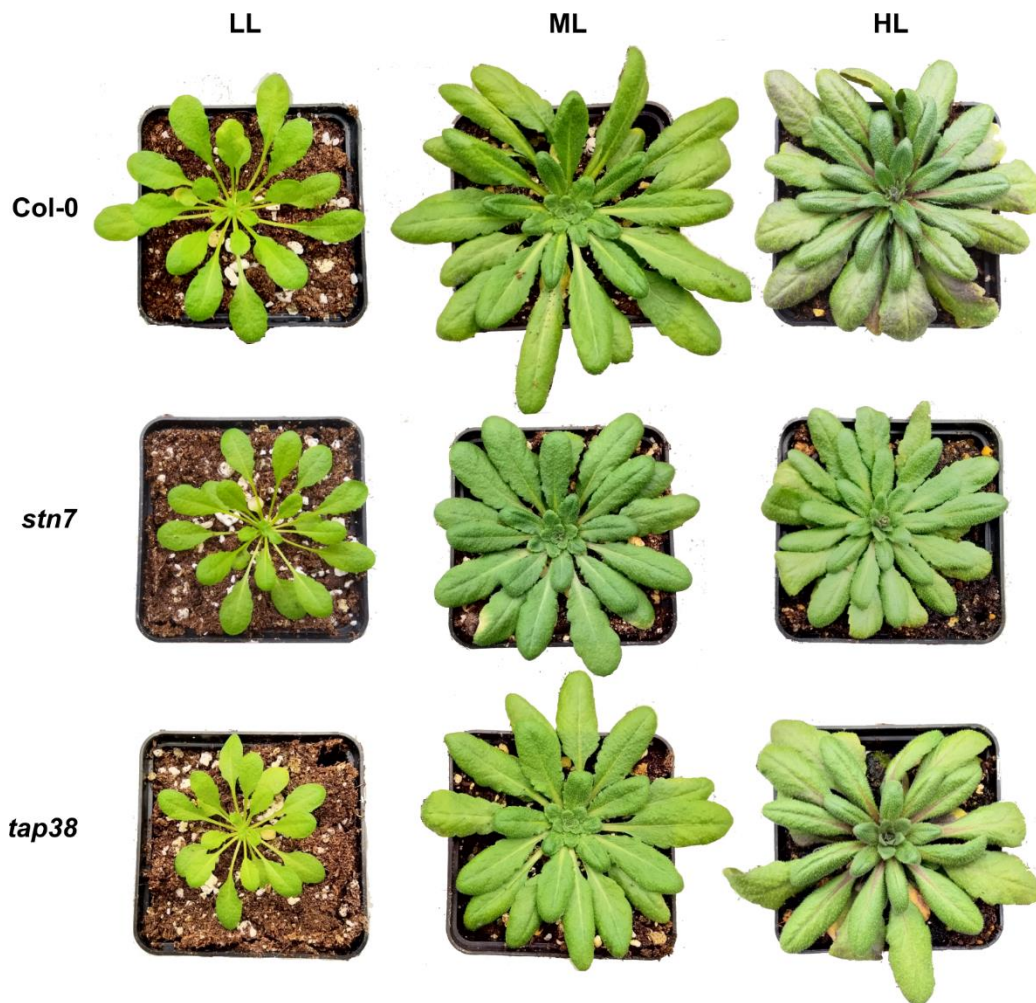


Figure 28: Phosphorylation mutant Arabidopsis plants acclimated to low, moderate and high light intensity. Col-0, *stn7*, and *tap38* Arabidopsis grown for 2 weeks at  $130 \mu\text{mol photons m}^{-2} \text{s}^{-1}$  then 4 weeks at LL ( $25 \mu\text{mol photons m}^{-2} \text{s}^{-1}$ ), ML ( $130 \mu\text{mol photons m}^{-2} \text{s}^{-1}$ ) or HL ( $600 \mu\text{mol photons m}^{-2} \text{s}^{-1}$ ). Photographs were taken on the day on which the HL plants were harvested.

Calculated ratios of chlorophyll *a* to chlorophyll *b* in isolated thylakoids are shown in Table 11. Similarly to the wild type thylakoids acclimated to different light intensities in Chapter 4, the Chl *a/b* ratios of Col-0 plants increased slightly with light intensity. The Chl *a/b* ratios of *stn7* thylakoids, by contrast, increased dramatically from 2.62 in LL to 3.20 in ML. Lack of phosphorylated LHCII associating with PSI in LL may have resulted in low PSI activity, causing increased LHCII synthesis relative to PSII, decreasing the Chl *a/b* ratio. However, the ML Chl *a/b* ratio of *stn7* is similar to that of

Col-0, indicating either fewer LHCII trimers or a lower ratio of PSII to PSI. Surprisingly, the HL *stn7* thylakoids had lower Chl *a/b* ratios than those from the ML plants. The Chl *a/b* ratios of the *tap38* thylakoids, on the other hand, were consistently higher than those from Col-0 and *stn7* plants, suggesting lower levels of LHCII overall and/or a change in PSII/PSI ratio. ML *tap38* thylakoids had the highest Chl *a/b* ratio.

Table 11: Chlorophyll *a/b* ratios of phosphorylation mutants following light acclimation. Ratio of chlorophyll *a* to chlorophyll *b* in isolated Col-0, *stn7* and *tap38* thylakoid membranes from low (LL), moderate (ML) and high (HL) light intensity.

	Chl <i>a</i> /Chl <i>b</i>		
	LL	ML	HL
<b>Col-0</b>	3.00±0.03	3.16±0.08	3.17±0.06
<b><i>stn7</i></b>	2.62±0.06	3.20±0.03	3.02±0.04
<b><i>tap38</i></b>	3.28±0.10	3.64±0.02	3.51±0.05

Since the *stn7* and *tap38* mutations are known to affect the formation of the PSI-LHCI-LHCII supercomplex, clear native PAGE was performed – without Coomassie Blue staining – to better visualise chlorophyll-containing complexes and supercomplexes. For Col-0 plants, the digitonin-solubilised stroma lamellae fractions of the thylakoid samples (Figure 29A) showed less LHCII associating with PSI in HL. In *stn7*, since phosphorylation of LHCII is low, no PSI-LHCI-LHCII supercomplexes were visible, aside from a very faint band in the LL thylakoids. The *tap38* mutant, on the other hand, appeared to contain a much larger number of PSI-LHCI-LHCII supercomplexes than Col-0 in every light condition, presumably arising from constitutively high levels of LHCII phosphorylation seen in this mutant (Pribil et al., 2010). Complexes solubilised from the granal fraction (Figure 29B) were separated by clear native PAGE to visualise PSII supercomplexes. Each genotype appeared capable of forming all of the C<sub>2</sub>S<sub>2</sub>, C<sub>2</sub>S<sub>2</sub>M, and C<sub>2</sub>S<sub>2</sub>M<sub>2</sub> supercomplexes, with LL thylakoids presenting an additional band, corresponding to C<sub>2</sub>S<sub>2</sub>M<sub>2</sub>L. PSII supercomplex formation did not appear to be altered dramatically in the phosphorylation mutants. Comparison of the two gels shows that in LL thylakoids there were fewer complexes solubilised from the stroma lamellae fraction and more complexes solubilised from the grana, suggesting changes in thylakoid stacking. Therefore, unlike the study of Pesaresi et al. (2009), here *stn7* showed changes in the Chl *a/b* ratio and distribution of complexes between the grana and the stroma lamellae that are consistent with an operational, albeit modified, light acclimation response.

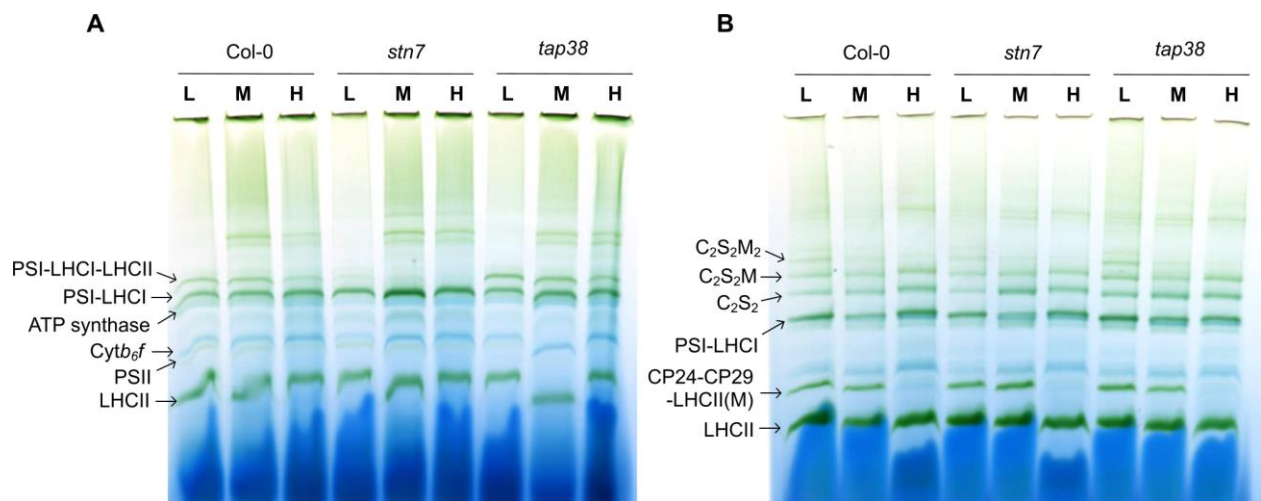


Figure 29: Clear native PAGE analysis of phosphorylation mutants. Clear native PAGE separation of (A) stroma lamellae and (B) grana complexes from Col-0, *stn7*, *tap38* thylakoids from plants acclimated to low (L), moderate (M) and high (H) growth light intensity.

### 6.3 Phosphorylation mutants *stn7* and *tap38* are capable of long term acclimation to light intensity

Thylakoid membranes from Col-0, *stn7* and *tap38* plants grown in LL, ML and HL conditions were prepared for MS analysis as described previously (Chapter 4). Protein digests and MS analyses were performed in three randomised-order batches, grouped by light condition, then all mass spectra were processed together in one batch using MaxQuant. As before, relative protein abundance was calculated using iBAQ, with values normalised to the sum of the core photosynthetic machinery: PSII, PSI, *cytb<sub>6/f</sub>* and ATP synthase. Since MS spectra were acquired at different times, there is greater potential for peptide LC retention time instability or other sources of variability. However, since all other aspects of the procedure such as digestion, LC and MS acquisition methods were consistent for each light condition, the combined data may be used to observe patterns and changes in protein abundance across the entire dataset. Following normalisation and averaging of replicates, proteins identified from the MS data were filtered to include only those thought to be associated with the thylakoid membrane with no missing values and the proteomes were subject to a PCA, implemented in Perseus (Figure 30). Grouping of samples in the PCA showed high similarity between thylakoids acclimated to HL, suggesting that the phosphorylation mutants responded to the high light intensity similarly to the wild type. The proteomes of Col-0 and *tap38* thylakoids grown under LL grouped very closely in the PCA, suggesting that they may respond to low light in a similar way to one another, whereas LL *stn7* was more distinct. The loosest grouping was that of the ML plants. Possibly, the absence of acclimation responses in ML plants may mean that imbalances arising from perturbed LHCII phosphorylation in the mutants have a greater impact on the system.

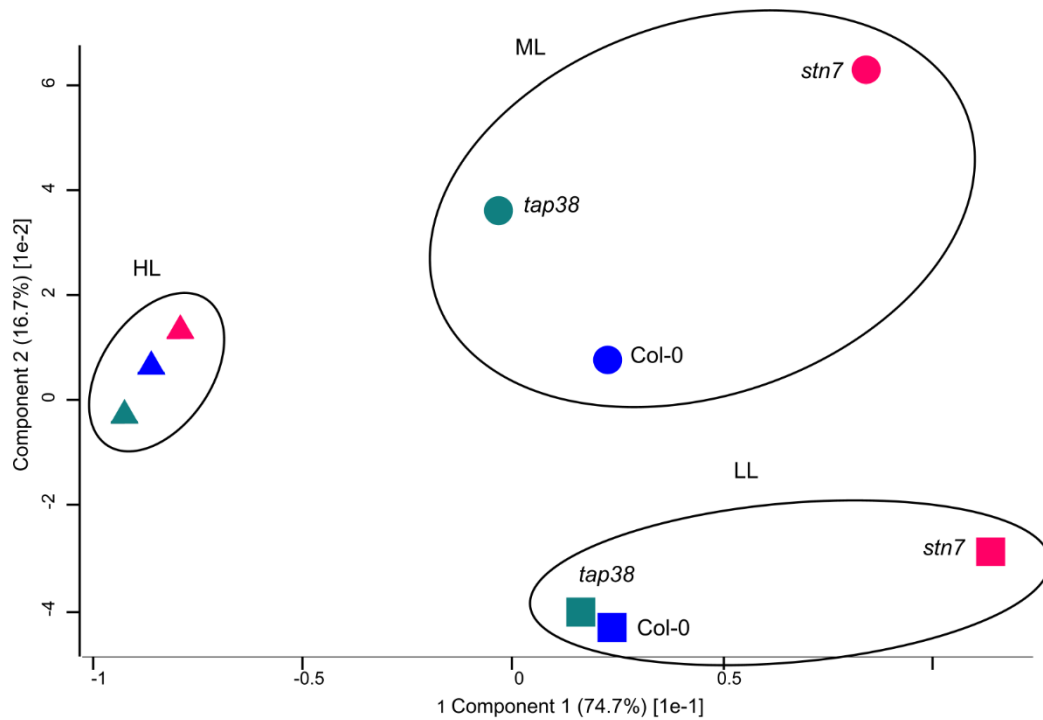


Figure 30: Principle component analysis of MS data to compare phosphorylation mutants. Circles indicate grouping by low light (LL), moderate light (ML) and high light (HL) of Col-0 (blue), *stn7* (pink) and *tap38* (teal) proteomes.

An important consideration is the extent of protein depletion caused by a mutation, so the relative amounts of STN7 and TAP38 compared to the wild type are shown in (Figure 31). The *stn7* mutant contained undetectable amounts of STN7 at ML and only around 2% of its wild-type level at HL. At LL, STN7 was present at a level of around 20% of that seen in Col-0; this may explain the appearance of a faint band corresponding to the PSI-LHCI-LHCII supercomplex seen by clear native PAGE (Figure 29A). The location of the T-DNA insertion in an intron of *stn7* may allow some residual expression in the mutant. Notably, given the proposed role of STN7 in signalling and regulation, STN7 was also significantly depleted in *tap38*, being present at around 35% of wild type levels in all light conditions. If STN7 does indeed act in a signalling cascade to induce changes in gene expression, its depletion in *tap38* could produce similar effects to those of the *stn7* mutation. The same effect was observed, albeit to a much lesser extent, in *stn7*; the loss of STN7 caused a 20-30% reduction in the amount of TAP38. In *tap38*, where the T-DNA insertion is located within the 5' of the gene, the phosphatase was depleted to less than 10% of wild type levels in all light conditions.

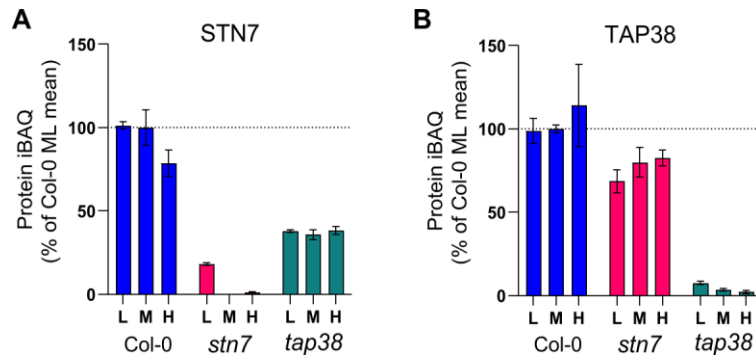


Figure 31: Abundance of STN7 and TAP38 in phosphorylation mutants. MS analysis showing relative abundance of **A**, STN7 and **B**, TAP38 in Col-0, *stn7* and *tap38* thylakoids acclimated to low (L), moderate (M) and high light intensity (H). The bars represent the average of three independent peptide preparations ( $n = 3$ ), derived from a pooled thylakoid sample, which were subject to MS analysis in triplicate in a randomised order and the values averaged. Error bars indicate mean  $\pm$  SD.

The relative abundances of some core multi-subunit complexes are shown in Figure 32. The MS analysis showed that, relative to the core machinery, PSII abundance was fairly consistent across all three genotypes and all three light intensities (Figure 32A). In both *stn7* and *tap38*, the amount of PSI decreased with increasing growth light intensity (Figure 32B). Under ML, both phosphorylation mutants appear to have a lower PSII to PSI ratio than the wild type. It could be expected that in *stn7* thylakoids, since there will be less LHCII associated with PSI and, therefore, lower PSI activity, these plants would increase the number of PSI reaction centres as observed by (Grieco et al., 2012). In *tap38* thylakoids, the lack of phosphatase activity on LHCII increases the number of PSI-LHCI-LHCII supercomplexes (Figure 29A). It could be anticipated that the resulting increase in PSI activity would trigger a decrease in the relative amount of PSI; the opposite is observed in this case. However, the number of LHCII trimers in *tap38* is slightly lower than in Col-0 (Figure 32C), possibly suggesting different mechanisms for regulation of LHCII abundance to those of the PSI/PSII ratio. LHCII trimers generally decreased with increasing growth light intensity across all genotypes. However, plants lacking STN7 changed more dramatically in LHCII abundance, with more trimers than wild type in LL and ML but similar levels as Col-0 and *tap38* when acclimated to HL. The surprisingly similar Chl *a/b* ratios observed between Col-0 and *stn7* grown at ML (Table 11) could be explained by the paralleled increases in LHCII and PSI, which cancel each other out and keep the Chl *a/b* ratios balanced. In LL and ML *stn7* thylakoids also contained more *cytb<sub>6</sub>f* (Figure 32D) overall than Col-0 and *tap38*, while under HL the levels were similar in *stn7* and Col-0 and markedly lower in *tap38*. These data are consistent with the short-term effects of the LHCII phosphorylation mutants on LET activity. For instance, the larger grana in *stn7* were found to slow PQH<sub>2</sub> diffusion between PSII and *cytb<sub>6</sub>f*, slowing LET under low light intensities (Hepworth et al., 2021). The increase in *cytb<sub>6</sub>f* levels in *stn7* under long-term acclimation to LL and ML may reflect an attempt to mitigate this effect. Similarly, *tap38* plants suffer from over-reduction of PSI under high light intensities resulting from their smaller grana that speed up plastocyanin and PQH<sub>2</sub> diffusion (Hepworth et al., 2021), and so the decreased levels of *cytb<sub>6</sub>f* upon

long-term acclimation to HL could represent a ameliorative strategy. ATP synthase increased with growth light intensity, behaving similarly in *stn7* and *tap38*.

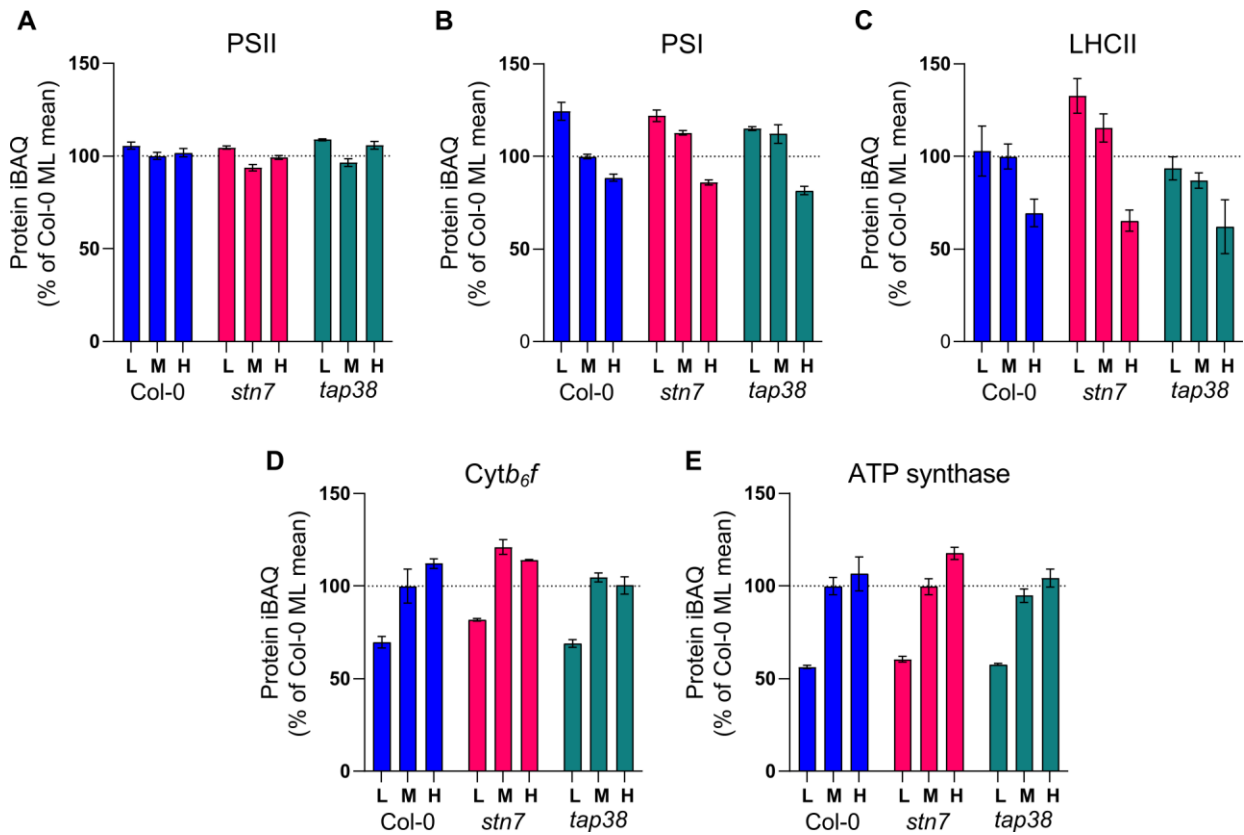


Figure 32: Acclimation-related changes in the abundance of key photosynthetic complexes in phosphorylation mutants. MS analysis showing the relative abundance of **A**, PSII, **B**, PSI, **C**, LHCII, **D**, *cytb<sub>6</sub>/f*, and **E**, ATP synthase from Col-0, *stn7* and *tap38* thylakoids acclimated to low (L), moderate (M) and high light intensity (H). MS data sampling details are as stated in Figure 31.

#### 6.4 Long term changes in thylakoid architecture in *stn7* and *tap38*

Dynamic, short-term changes in thylakoid stacking are controlled primarily by LHCII phosphorylation/dephosphorylation by STN7/TAP38 to balance LET and CET (Wood et al., 2018, 2019). Long-term changes in stacking, as found in Chapter 4, are a result of changes in abundance of CURT1 proteins rather than arising solely from LHCII abundance or phosphorylation. Mutants lacking STN7 or TAP38 are impaired in their short-term thylakoid stacking responses to light intensity, although it is not yet known what effect LHCII phosphorylation has on long-term changes in grana size. Therefore, Col-0, *stn7* and *tap38* Arabidopsis were subjected to EM analysis (Figure 33A-D), to compare the number of membrane layers per granum in LL and HL, and SIM (Figure 33E, F), to determine their grana diameter (measured as grana FWHM) after acclimation to LL, ML and HL.

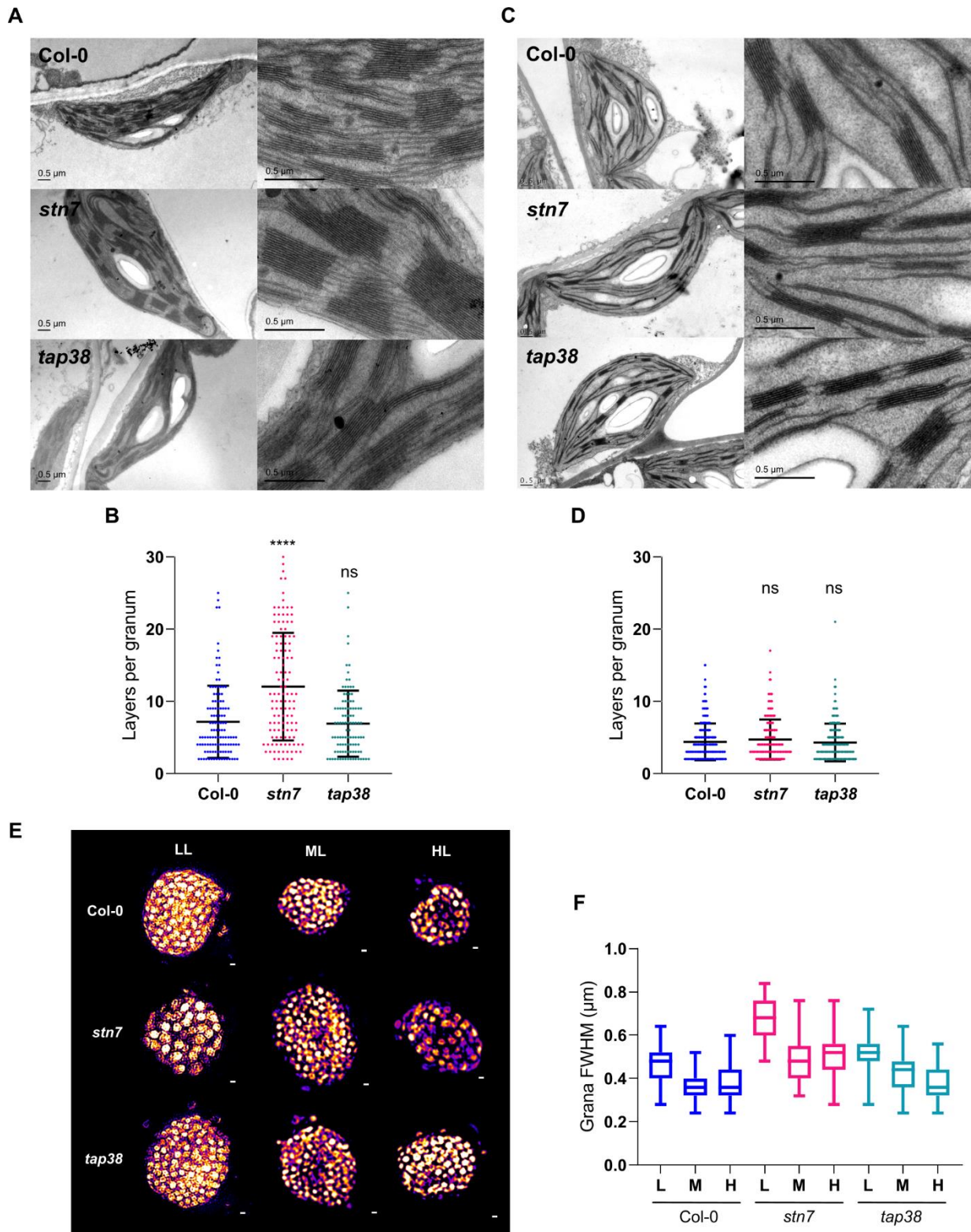


Figure 33: Long-term changes in thylakoid architecture are affected by LHCII phosphorylation. **A**, Thin-section electron micrographs of chloroplasts from Col-0 (top row), stn7 (middle row) and tap38 (bottom row) plants acclimated to LL (scale bar: 0.5  $\mu$ m). **B**, Number of membrane layers per grana stack calculated from electron microscopy images of chloroplasts in Col-0 ( $n = 116$ ), stn7 ( $n = 121$ ) and tap38 ( $n = 102$ ) leaves acclimated to LL (Welch's  $t$ -test. \*\*\*\* $P < 0.0001$ , ns  $> 0.05$ ). **C**, Thin-section electron micrographs of chloroplasts from Col-0 (top row), stn7 (middle row) and tap38 (bottom row) plants acclimated to HL (scale bar: 0.5  $\mu$ m). **D**, Number of membrane layers per grana stack calculated from electron microscopy

images of chloroplasts in Col-0 ( $n = 322$ ), *stn7* ( $n = 192$ ) and *tap38* ( $n = 185$ ) leaves acclimated to HL (Welch's *t*-test,  $ns > 0.05$ ). **E**, SIM images of chloroplasts from a representative 3D SIM image slice from Col-0 (top row), *stn7* (middle row) and *tap38* (bottom row) *Arabidopsis* grown at LL (left column), ML (middle column) and HL (right column). **F**, Box and whisker plots of full width at half-maximum (FWHM) fluorescence intensity of the fluorescent spots (grana,  $n \geq 80$ ) in three-dimensional SIM images of chloroplasts from Col-0, *stn7* and *tap38* *Arabidopsis* grown at low (L), moderate (M) and high light intensity (H).

In wild type *Arabidopsis*, grana decrease in size with increasing growth light intensity, both in grana diameter (Figure 33F) and in the number of membrane layers per granum (Figure 33B, D). In LL, *stn7* chloroplasts contained very large grana with many more layers and a larger diameter than the wild type. This may be explained by the MS data, which showed that the thylakoid membranes of *stn7* plants contained more LHCII trimers (Figure 32C) at LL and ML than the wild type. Since these trimers are unable to form PSI-LHCI-LHCII supercomplexes in the stroma lamellae (Figure 29A), they will accumulate in the grana and increase their size even further. At HL, the *stn7* grana are no different to the wild type in terms of membrane layers (Figure 33D) but they have significantly larger diameters than Col-0 and *tap38* grana. In contrast to the short-term response to light intensity (Wood et al., 2019), grana from *tap38* chloroplasts were no smaller than the wild type at any growth light tested, in terms of either diameter or number of layers. One possible explanation for this may be that changes in the amount of CURT1 (Figure 34A-D) proteins compensate for high levels of LHCII phosphorylation in *tap38*. In HL, *tap38* thylakoids contain around 20% less CURT1A and CURT1B (Figure 34A, B), proteins known to induce membrane curvature and increase stacking. Overall, however, either the CURT1 proteins behave in a similar way in the phosphorylation mutants to in the wild type, or any observed differences are minimal. In contrast to the findings of Chapter 4, neither grana diameter nor membrane layers appear to change in line with CURT1 protein abundance. This suggests that the differences in grana size in *stn7* are mostly a result of LHCII and its phosphorylation state. HL *stn7* plants contain a similar number of LHCII trimers to the wild type, have similar numbers of layers per granum, but have larger grana diameters. Therefore, the larger grana diameter likely result from LHCII phosphorylation specifically. However, the RIQ proteins may reduce the number of layers per granum (Yokoyama et al., 2016). Thylakoids of *stn7* plants grown in HL contained 50% more RIQ1 (Figure 34E) than the wild type, a change that may constrain grana height. They also contained more RIQ2 (Figure 34F) at both LL and HL. Two other proteins with roles in grana stacking, STN8 and CAS (Figure 34G, H), were relatively unaffected in the phosphorylation mutants.

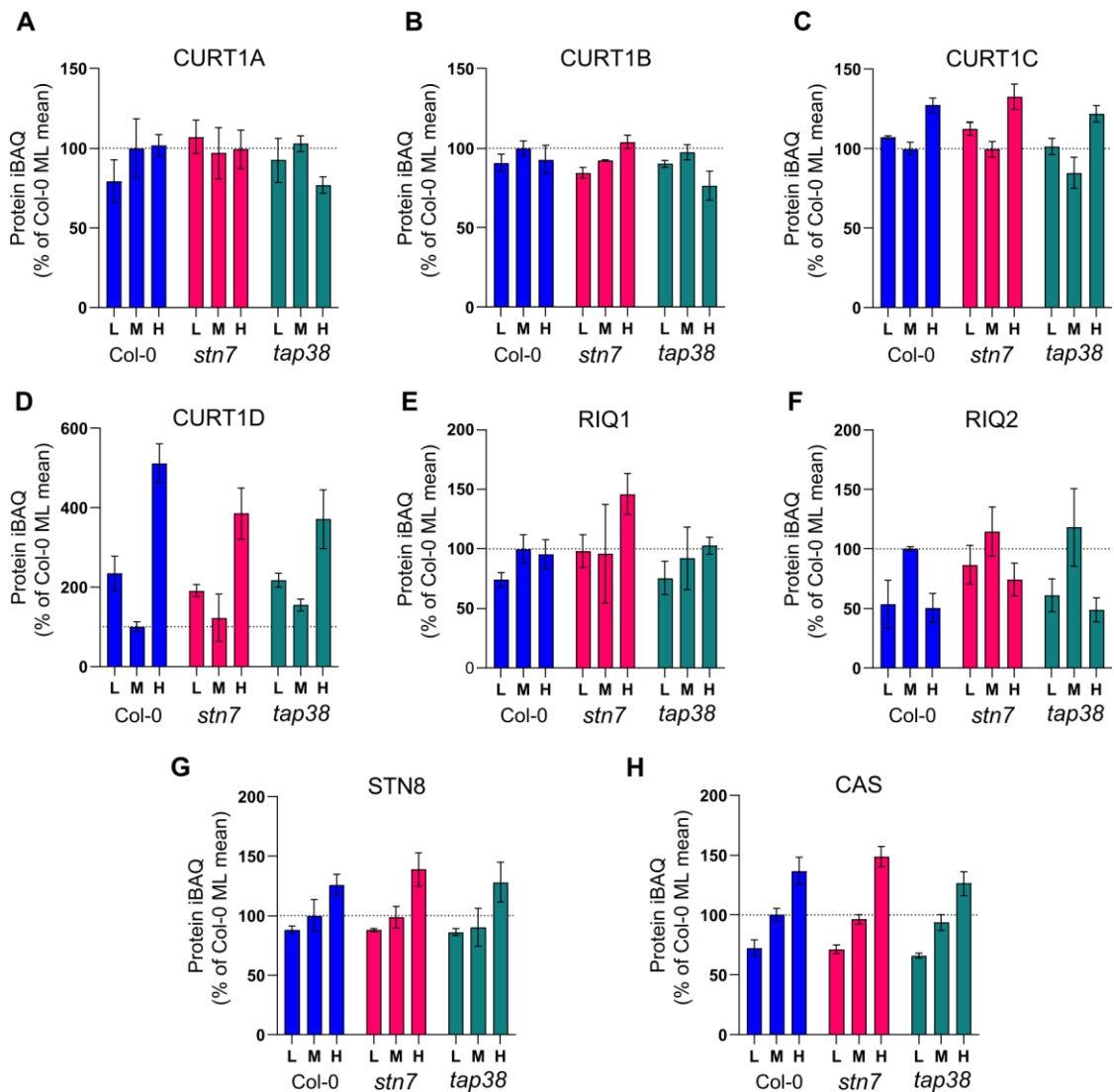


Figure 34: Abundance of proteins involved in thylakoid architecture in phosphorylation mutants. MS analysis showing relative abundance of A-H, CURT1A, CURT1B, CURT1C, CURT1D, RIQ1, RIQ2, STN8 and CAS in Col-0, *stn7* and *tap38* thylakoids acclimated to low (L), moderate (M) and high light intensity (H). Sampling details are as stated in Figure 31.

## 6.5 Electron carrier protein abundance is affected in *stn7* and *tap38*

In addition to the effects of STN7 and TAP38 dependent LHCII (de)phosphorylation on short-term regulation of LET described in Section 6.4, these proteins also affect CET function (Hepworth et al., 2021). LHCII phosphorylation enhances CET under low light conditions where PSI excitation is limiting. Under high light, on the other hand, where the supply of oxidised PQ limits CET, dephosphorylation of LHCII and the larger grana that ensue promote isolation of the stromal pool from PSII. Therefore, changes in thylakoid architecture in *stn7* and *tap38* may be accompanied by differences in the amounts of proteins associated with CET and/or LET. In the wild type, plastocyanin abundance is increased in both LL and HL (Figure 35A), similarly to in Chapter 4. The wild type plants have larger grana in LL so they may increase the amount of plastocyanin to compensate for the longer diffusion distance. HL may also lead to an increase in plastocyanin abundance because of a need for greater

electron transfer capacity. In ML, both phosphorylation mutants have dramatically more plastocyanin than the wild type. They also form larger grana, which could explain the increase in plastocyanin. However, *stn7* and *tap38* plants grown under LL have less plastocyanin than the LL wild type, despite having larger grana. Therefore, grana diameter must not be the only factor determining plastocyanin abundance in LL. Another important electron transfer protein, which was not identified in the MS experiments of the previous chapters, is ferredoxin (Fd). Both isoforms of Fd identified, FD1 (Figure 35B) and FD2 (Figure 35C), also increased dramatically in abundance in the mutants when grown under ML. However, FD1 was not detected at LL conditions in any of the genotypes. The dramatic increase in abundance of these electron carriers in ML may also be linked to grana size, in that it may help to compensate for LET limitation. However, since ferredoxin is a soluble stromal protein that may not be tethered to the thylakoid membrane – as FNR is by TROL and TIC62 – the observed changes may not represent differences in absolute quantities of protein. Rather, the association of ferredoxin with the thylakoid membrane may vary. FNR may better indicate differences in electron transfer in the phosphorylation mutants than Fd, since it may be more consistently associated with the thylakoid membrane. FNR1, which is a target of STN7-dependent phosphorylation (Schönberg et al., 2017), generally increases with light intensity in all genotypes (Figure 35D). Higher FNR1 levels in *stn7* compared to *tap38* suggest phosphorylation of this protein may affect its abundance. In Col-0, contrary to the results of Chapter 4, FNR2 was less abundant in HL than in ML but the phosphorylation mutants increased their FNR2 with growth light intensity (Figure 35E). However, in the wild type, contrary to the results of Chapter 4, FNR2 was less abundant in HL than in ML but the phosphorylation mutants increased their FNR2 with growth light intensity (Figure 35E). The fact that (non-phosphorylated) FNR2 levels were also higher in *stn7* than in *tap38* thylakoids suggests that factors other than FNR phosphorylation related to the altered LET/CET balance in these mutants may regulate FNR1 and 2 abundance. The FNR tethering proteins TIC62 and TROL also generally increase in abundance with growth light intensity in all genotypes (Figure 35F, G) with the highest levels seen in *stn7*, consistent with the elevated FNR1 and 2 levels. Therefore, thylakoids from *stn7* plants generally present increases in the amount of LET proteins, while *tap38* has a slight overall decrease. Since *stn7* has very large grana, and presumably more efficient CET, the slight increase in apparent LET capacity may be an attempt to balance the two electron transfer routes. While *tap38* plants did not have smaller grana, as might be expected, hyperphosphorylation of LHCII and subsequent decrease in the amount of LHCII associated with PSII may reduce PSII activity such that there is less need for a high electron transfer capacity.

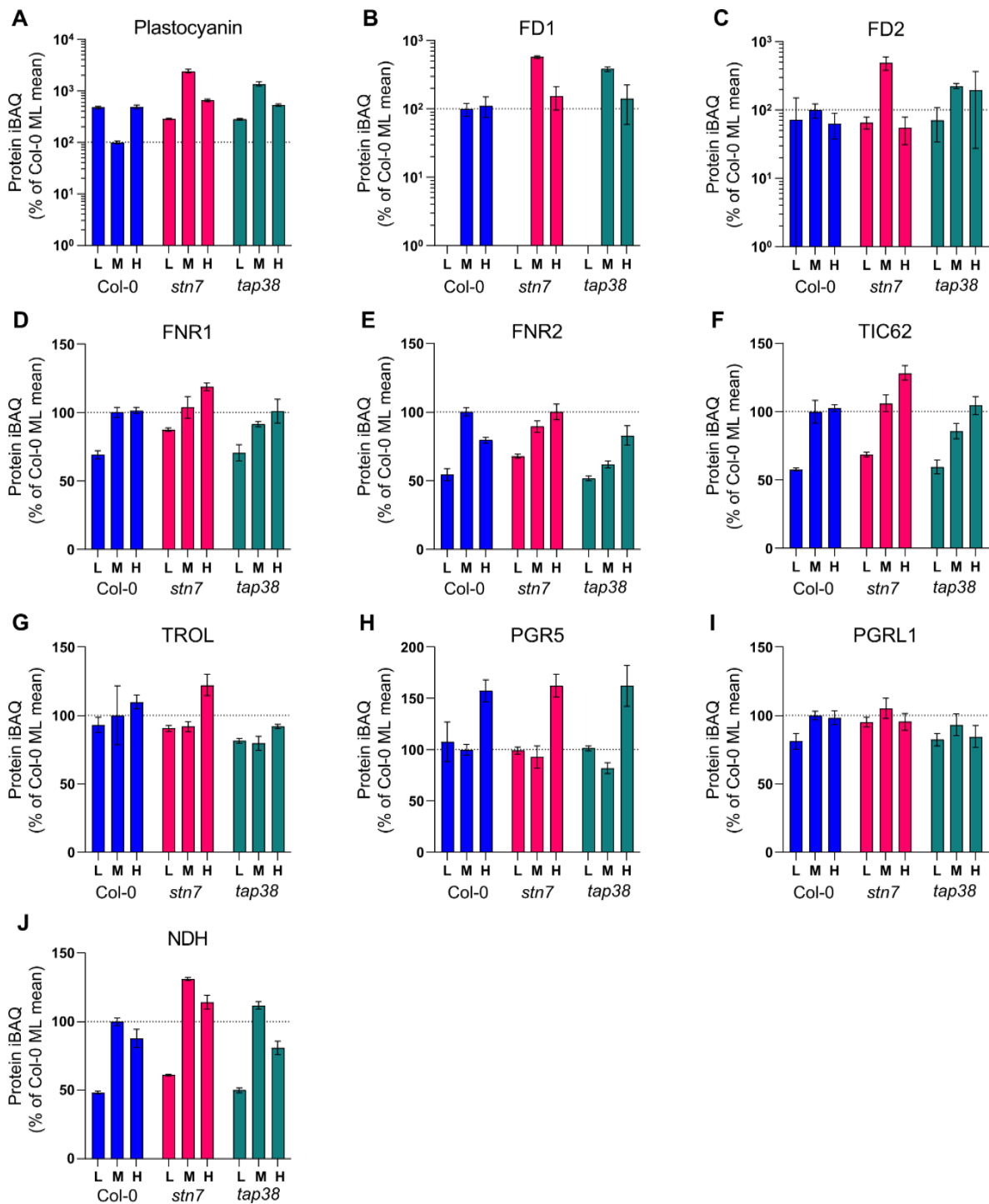


Figure 35: Abundance of electron transfer proteins in phosphorylation mutants. MS analysis showing the relative abundance of A-J, Plastocyanin, ferredoxin 1 (FD1), ferredoxin 2 (FD2), FNR1, FNR2, TIC62, TROL, PGR5, PGRL1 and NDH from Col-0, *stn7* and *tap38* thylakoids acclimated to low (L), moderate (M) and high light intensity (H). MS data sampling details are as stated in Figure 31.

For the CET-related proteins PGR5, PGRL1 and NDH (Figure 35H-J), protein abundance changed with growth light intensity similarly in the phosphorylation mutants to in the wild type. While *stn7* appears to slightly increase its capacity for LET, indicated by slight overall increases in associated proteins, there is no obvious trend with the CET proteins. The abundance of proteins involved in the PGRL1-

mediated pathway of CET does not appear to be affected by LHCII phosphorylation, despite the imbalance this would presumably cause. However, slightly more NDH is present in the *stn7* thylakoids compared to the wild type at each light condition.

## 6.6 Candidate proteins for an STN7-mediated signalling pathway

As in the phosphorylation mutant *stn7*, plants lacking TSP9 are deficient in state transitions. TSP9 is another identified phosphorylation target of STN7 and has been proposed as a link between STN7 and long term acclimation (Fristedt et al., 2008). In particular, it may play a role in acclimation to high light intensity, since exposing mutants lacking TSP9 to high light does not induce expression of a group of signalling proteins that are normally upregulated after high light treatment (Fristedt et al., 2009b). The MS analysis found that TSP9 abundance is influenced by growth light intensity and genotype (2-way ANOVA,  $p = 3.25E-12$ ). In the wild type plants, TSP9 decreased by 30% in HL but was unchanged between LL and ML (Figure 36A). When grown at ML, *stn7* and *tap38* thylakoids contained around 45% and 75% less TSP9, respectively, whereas at LL there was a 30% increase relative to the wild type. At HL, thylakoids of the phosphorylation mutants contained around 60% more TSP9 than the wild type. However, since phosphorylation of TSP9 induces its dissociation from the stromal surface of the thylakoid membrane (Carlberg et al., 2003), these values may represent binding of the protein rather than absolute abundance. If STN7 is responsible for this phosphorylation that leads to release of TSP9 from the membrane, a lack of STN7 in the *stn7* mutant might cause more TSP9 to be retained on the membrane and vice versa for *tap38*. However, both mutations produce a similar effect on the amount of TSP9 quantified.

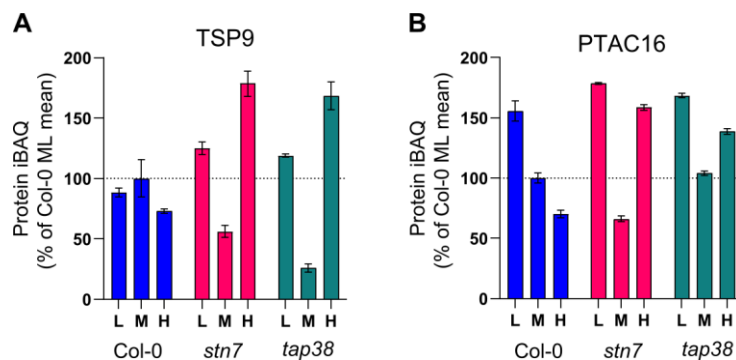


Figure 36: Abundance of potential phosphorylation targets of STN7. MS analysis showing the relative abundance of **A**, TSP9 and **B**, PTAC16 from Col-0, *stn7* and *tap38* thylakoids acclimated to low (L), moderate (M) and high light intensity (H). MS data sampling details are as stated in Figure 31.

Another protein whose abundance was significantly affected by growth light and genotype in an interactive way (2-way ANOVA,  $p = 4.99E-15$ ) was PTAC16 (Figure 36B). Phosphorylation of this protein is dependent on STN7 but it is unclear whether STN7 phosphorylates PTAC16 directly. PTAC16 contains a Rossman fold motif for nucleotide binding and may function in the regulation of chloroplast gene expression by mediating interactions between the thylakoid membrane and the

chloroplast nucleoid (Adamiec et al., 2018; Ingelsson and Vener, 2012). Despite being found to be located on the stromal side of the thylakoid membrane, PTAC16 has also been reported to co-localise with PSII repair-associated luminal proteins DEGP1 and TL18.3 (Zienkiewicz et al., 2012). In wild type plants, PTAC16 decreases with increasing light intensity. However, in *stn7* plants PTAC16 behaves very differently, being present at around 40% less in ML but around 60% higher than the wild type in HL. The *tap38* thylakoids also contained more PTAC16 in HL, but its LL abundance was not affected substantially in either of the mutants. If this protein really is part of a signalling pathway involving STN7, it would appear that other factors are capable of regulating its expression.

### 6.7 The *pgr5* mutant is comparable to wild type in supercomplex formation and grana diameter

Arabidopsis mutants lacking the proton gradient regulation protein PGR5 are highly susceptible to photoinhibition and are unable to grow in a fluctuating light environment. The *pgr5* mutant was subject to proteomic analysis to assess whether this conditional phenotype resulted predominantly from the disruption of a single, essential process, or from dysregulation of signalling pathways leading to more widespread changes in the thylakoid proteome. The *pgr5* mutant used in this experiment is from the *gl-1* genetic background rather than Col-0, so this strain is used as the ‘wild type’ comparison.

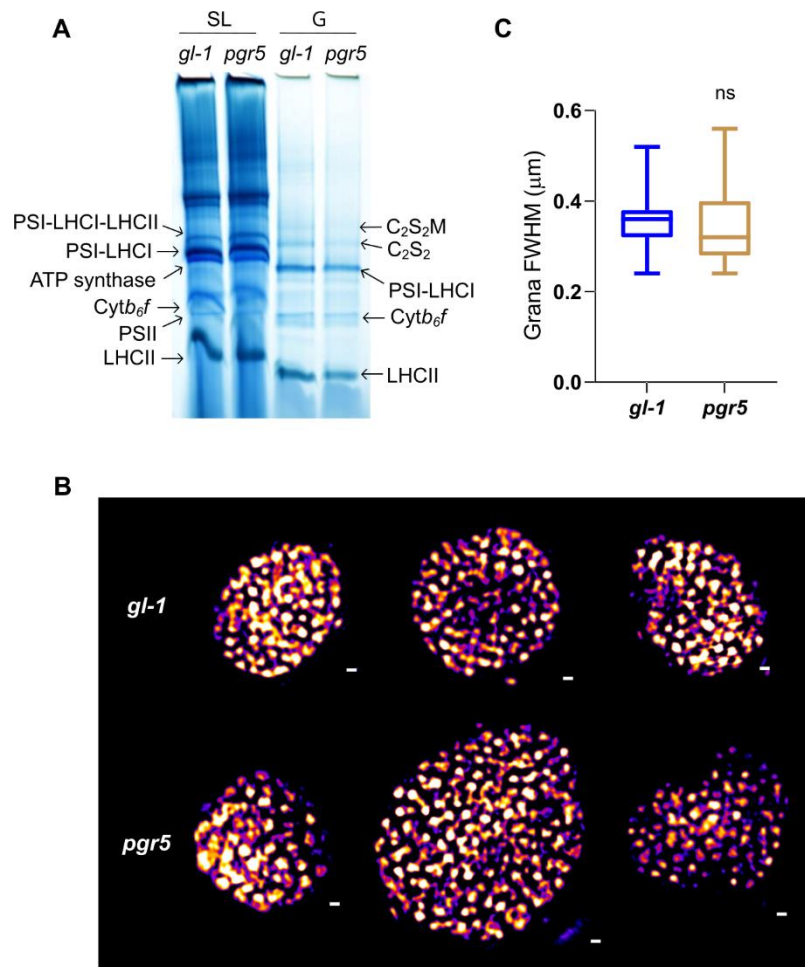


Figure 37: The *pgr5* mutant has similar supercomplex formation and thylakoid architecture to wild type. **A**, BN-PAGE analysis of solubilised stromal lamellae (SL) and granal (G) thylakoid fractions from *gl-1* and *pgr5* plants. **B**, SIM images of chloroplasts from a representative 3D SIM image slice from *gl-1* (top row) and *pgr5* (bottom row) plants. **C**, Full width at half-maximum (FWHM) fluorescence intensity of the fluorescent spots (grana) in three-dimensional SIM images of chloroplasts from *gl-1* ( $n = 81$ ) and *pgr5* ( $n = 104$ ) plants (Welch's *t*-test.  $ns > 0.05$ ).

The *pgr5* and wild type plants were grown at  $150 \mu\text{mol photons m}^{-2} \text{s}^{-1}$  with an 8 h photoperiod for 6 weeks before chloroplasts were prepared for analysis by SIM and thylakoids were isolated for analysis by BN-PAGE and MS. The BN-PAGE (Figure 37A) did not reveal any obvious changes in the stoichiometry of photosynthetic complexes aside from a possible reduction in the number of free LHCII trimers, which fits with the similar Chl *a/b* ratios of the *gl-1* and *pgr5* thylakoids, of 2.94 and 3.05, respectively. The granal fractions of both the mutant and the wild type solubilized poorly in 1%  $\alpha$ -DDM, resulting in poor visualisation of the PSII supercomplexes C<sub>2</sub>S<sub>2</sub> and C<sub>2</sub>S<sub>2</sub>M and an absence of the C<sub>2</sub>S<sub>2</sub>M<sub>2</sub> supercomplex. However, there does appear to be a slight difference in the distribution of complexes between domains; in the *pgr5* thylakoids, a greater proportion of complexes were solubilised from the stroma lamellae than in the wild type. This could suggest a decrease in grana stacking. However, analysis of grana diameter by SIM (Figure 37B, C) did not reveal a significant difference in *pgr5*.

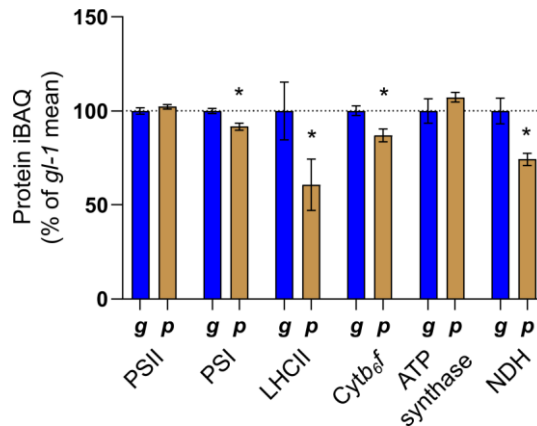


Figure 38: Downregulation of key complexes in *pgr5*. MS analysis showing the relative abundance in *gl-1* (g) and *pgr5* (p) thylakoids of key photosynthetic complexes PSII, PSI, LHCII, Cytb<sub>6</sub>/f, ATP synthase and NDH, expressed as a percentage of the mean in *gl-1*. The bars represent the average of three independent peptide preparations (n = 3), derived from a pooled thylakoid sample, which were subject to MS analysis in triplicate and the values averaged. Error bars indicate mean ± SD. Significant differences between conditions were determined by a modified Welch's t-test (Section 2.9.9, \*q < 0.05).

MS analysis of the key photosynthetic complexes (Figure 38) confirmed the decrease in LHCII abundance observed by BN-PAGE. The number of LHCII trimers in *pgr5* was around 40% less than the wild type, a difference comparable to that of the Field thylakoids (Chapter 5) and more extreme than the LHCII decrease seen in constant HL (Chapter 4). Previously it has been reported (Suorsa et al., 2012) that *pgr5* plants have a 50% reduction in the amount of PSI, even under constant light. This MS analysis, however, found only a very small decrease in the amount of PSI, of only 10%. Suorsa et al. (2012) did not observe any change in the amount of *cytb<sub>6</sub>/f* or NDH. However, this MS analysis reveals a modest (15%) reduction in the amount of *cytb<sub>6</sub>/f* and a 25% decrease in the NDH complex. This is surprising since, as *pgr5* is unable to perform CET via the PGRL1-mediated pathway, one might expect that CET via NDH would be upregulated. Consistent with Suorsa et al. (2012), no difference in the amount of ATP synthase was observed in *pgr5*.

## 6.8 Widespread downregulation of thylakoid protein abundance in *pgr5*

A schematic diagram indicating the ratio of thylakoid proteins in *pgr5* compared to the wild type is shown in (Figure 39). In *pgr5*, where a single amino acid substitution results in instability and degradation of the PGR5 protein (Munekage et al., 2002), the amount of PGR5 detected was depleted to 4% of its wild type level. Overall, this loss of the PGR5 protein results in widespread decreases in proteins related to electron transfer, both linear and cyclic, as well as many related to the regulation of grana stacking, such as CURT1B, CURT1C and CAS. The abundance of RIQ1 and 2 is also lower in the *pgr5* plants. These proteins are thought to decrease grana stacking (Yokoyama et al., 2016), so a lower abundance in the *pgr5* mutant may result in more membrane layers per granum; this has yet to be demonstrated. The dramatic decrease in CP29.3 in *pgr5* is reminiscent of a response to low light, as seen in the previous chapters. A possible function of this protein is to disrupt interactions between PSII

supercomplexes in adjacent membrane layers and facilitate more efficient PSII disassembly and repair, or to reduce binding of M-trimers (Albanese et al., 2017, 2019). However, the overall decrease in LHCII trimer proteins more closely resembles a high light response. In contrast to wild type plants, which keep LHCB3 constant during acclimation to constant high or low light or to natural light (Chapters 4 and 0), *pgr5* had only half as much LHCB3 as *gl-1*. PSI does not dramatically shrink its core antenna, the LHCA proteins, but it may have a reduced ability to bind LHCII trimers. While overall PSI decreases slightly in *pgr5*, there is a more substantial decrease specifically in the amount of PSAH (-65%), the subunit responsible for the interaction between PSI and phosphorylated LHCII. Concomitant loss of LHCB2, which is 50% lower in *pgr5*, and PSAH may represent a compensatory attempt to lower PSI excitation to avoid reaction centre damage.

Ratio *pgr5* vs *gl-1*

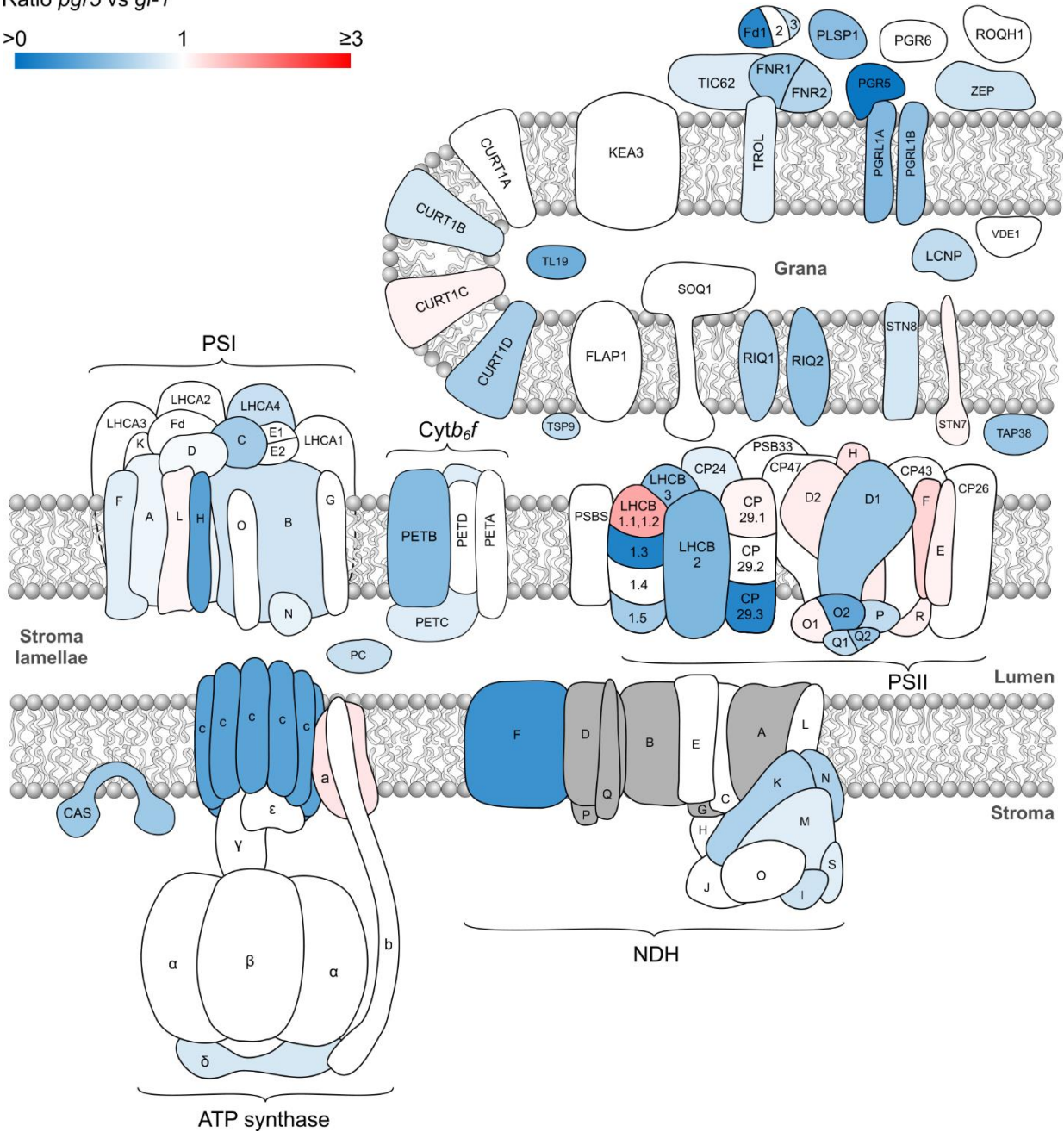


Figure 39: A comparison of the thylakoid proteome in *pgr5* to *gl-1*. Schematic diagram indicating the relative abundance of thylakoid proteins in *pgr5* versus in *gl-1*. Blue proteins are more abundant in *gl-1*, whereas red/pink proteins are more abundant in *pgr5*. Where no significant difference was detected for a quantified protein it is displayed in white. Proteins not identified by MS analysis are shown in grey.

The electron carrier protein plastocyanin (PC) is around 20% less abundant in *pgr5*, and two out of the three Fd isoforms identified are also depleted. FNR decreases by 30-40%, with smaller reductions in its tethering proteins TIC62 and TROL of 15 and 10%, respectively. The loss of PGR5 is also associated with less PGR1. Since mutants lacking the PGR1 protein have a similar phenotype to *pgr5* and the two form a complex (DalCorso et al., 2008), PGR1 is likely redundant in the absence of PGR5. There is no increase in the NDH complex - in fact, there is a decrease – to compensate for the loss of one CET

pathway, which would imply that *pgr5* has very low CET capacity. The depletion of proteins associated with LET to a greater extent, even, than in wild type plants acclimated to LL (Chapter 4) suggests these plants have a very low electron transfer capacity. One might expect that LL levels of electron transfer proteins might delay growth similarly to light restriction. However, previous work on this mutant found it to have wild type levels of both CET and LET under continuous light (Nandha et al., 2007; Okegawa et al., 2007) and a similar growth phenotype (Munekage et al., 2002). Therefore, wild type plants grown at constant ML, and possibly even those acclimated to LL, must have a surplus of electron transfer machinery. These electron transfer proteins must be present at levels higher than is necessary for efficient utilisation of their growth light.

One category of proteins that does not seem particularly affected by the loss of PGR5 is of those involved in the regulation of light harvesting. VDE, PSBS, SOQ1, KEA3 and ROQH1 are present at wild type levels, which would suggest that *pgr5* plants have a normal capacity for NPQ. However, since *pgr5* is deficient in NPQ (Munekage et al., 2002), this supports the idea that it is the inability of *pgr5* to generate sufficient lumen acidification upon high light exposure that impedes NPQ induction.

## 6.9 Downregulation of PSII repair machinery in *pgr5*

One striking result observed is the substantial decrease (around 40%) in the amount of the D1 protein relative to the other transmembrane subunits of the PSII core, which change minimally. The accumulation of PSII subunits without D1 might indicate defects in the PSII repair process. To determine whether depletion of the D1 protein is associated with changes in PSII repair, proteins associated with the PSII repair machinery were quantified and their ratio in *pgr5* to the wild type is shown in Figure 40. The very low relative abundance of the D1 protein would suggest defects in PSII assembly, rather than degradation. In general, however, PSII assembly proteins appear to be present at wild type levels. This includes LPA1 (Peng et al., 2006), LQY1 (Lu et al., 2011), LTO1 (Karamoko et al., 2011), and HCF173, which plays an important role in D1 synthesis (Schult et al., 2007).

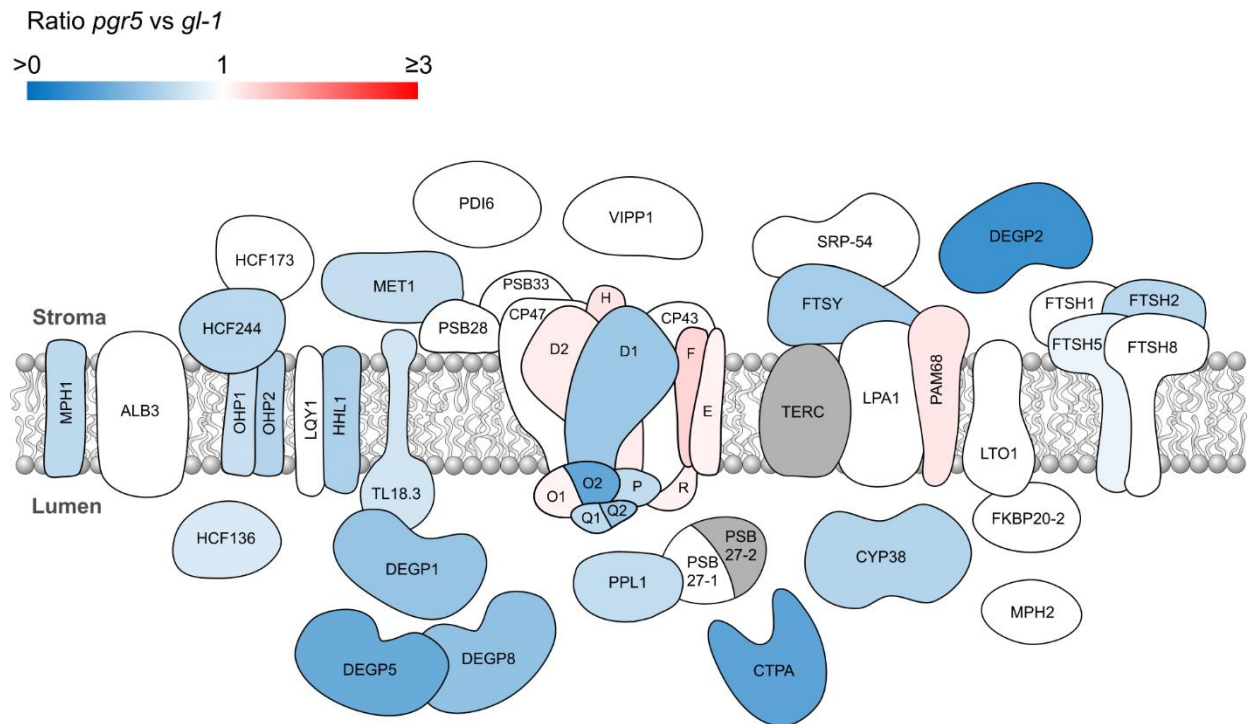


Figure 40: Depletion of PSII repair machinery in *pgr5*. Schematic diagram indicating the relative abundance of PSII repair proteins in *pgr5* versus *gl-1* thylakoids. Blue proteins are more abundant in *gl-1*, whereas red/pink proteins are more abundant in the *pgr5*. Where no significant difference was detected for a quantified protein, it is displayed in white. Proteins not detected in the MS analysis are shown in grey.

DEGP, or Protease Do-like, proteins are serine proteases peripherally associated with the thylakoid membrane (Itzhaki et al., 1998) with roles in the processing of damaged PSII reaction centres. DEGP1, DEGP5 and DEGP8 are located on the luminal side, the latter two forming a heterocomplex. These luminal DEGP proteins increased by 2 to 4-fold in Field plants (Chapter 5) so are likely to be important in fluctuating light. DEGP5, which acts on PSBF, and DEGP8 are most important under stress conditions, whereas DEGP1, the most abundant of these proteases, is most important for normal growth and its absence has a more detrimental effect on growth phenotype (Butenko et al., 2018; Lucinski et al., 2011a). The CTPA protease, also located in the lumen, degrades D1 in PSII repair and is required for normal growth in high light (Shuming et al., 2008). All of these luminal proteases are depleted by between 40 and 60% in *pgr5* thylakoids. DEGP2, located on the stromal side of the thylakoid membrane, is responsible for the initial cleavage of the D1 protein and is upregulated under stress conditions, under which it also degrades the PSII antenna protein LHCB6 (Haußuhl et al., 2001; Lucinski et al., 2011b) whose function is to link the PSII reaction centre to LHCB6 trimers. DEGP2 was greatly depleted in the *pgr5* thylakoids, being present at only 25% of the wild type level. Together, these significant decreases in abundance of proteases responsible for D1 degradation suggest a greatly reduced ability of the mutant to disassemble damaged PSII.

## 6.10 Discussion

It is clear from these MS data that neither STN7 nor TAP38 are essential for long term acclimation to low or high light intensity. Bonardi et al. (2005) first reported an association between the LHCII kinase STN7 and acclimation-related changes in photosystem stoichiometry when they exposed plants to light preferentially exciting either PSI or PSII; this treatment induces state transitions, but likely produces different effects than the light intensity changes used in this work. They found that Chl *a/b* ratios of the thylakoids acclimated to these different light qualities were altered in wild type Arabidopsis but not in *stn7* mutants. Transcriptomics of *stn7* and wild type plants grown in a greenhouse was also performed and revealed widespread downregulation of gene expression in *stn7*. A later study by Pesaresi et al. (2009) also used light preferentially exciting PSI or PSII to assess acclimation-related changes, with immunoblotting, transcription analysis and Chl *a/b* ratios. Plants lacking STN7 did not change their photosystem stoichiometry when exposed to the different light qualities, while the wild type did. To reconcile these studies with the results described in this thesis, it could be that STN7-mediated gene regulation is triggered only by the spectral quality of light, rather than its intensity. However, Tikkanen et al. (2006) did grow *stn7* plants under low, moderate and high light intensity, making their study more comparable to this one. They found that the *stn7* plants did indeed differ in their acclimation responses, with low light *stn7* thylakoids containing less LHCB1 and more PSBS than the wild type. No difference was observed in the transcriptomes of the *stn7* plants, leading the authors to conclude that the STN7-mediated regulation of protein abundance occurred post-transcriptionally. With this new information about how the thylakoid proteomes of these phosphorylation mutants change in response to growth light intensity, it seems unlikely that STN7 plays a major role in adjusting the thylakoid proteome during long-term acclimation. However, a proteomic comparison of thylakoids from *stn7* and *tap38* plants acclimated specifically to PSII or PSI-exciting light wavelengths could reveal a role for STN7 in acclimation to light quality. Since the proteins TSP9 and PTAC16, thought to possibly be involved in gene regulation, behave unexpectedly in the phosphorylation mutants, a signalling role for STN7 cannot be ruled out. However, the data shows that any STN7 involvement in long term acclimation is likely indirect, in that the loss of dynamic grana stacking changes and state transitions perturbs redox-triggered signals, leading to a slightly modified response. It is clear that STN7 is not a key component of the signalling pathway, as suggested by Pesaresi et al. (2009a).

The thylakoid proteome of the *pgr5* mutant was characterised by widespread downregulation of proteins involved in electron transfer, light harvesting and PSII repair. This mutation is lethal in fluctuating light, and the reason for this is understood to be that *pgr5* plants cannot generate sufficient thylakoid lumen acidification upon transition to high light to induce NPQ and photosynthetic control, leading to PSI damage. To preserve PSI, the response of *pgr5* is to downregulate electron transfer. However, these MS data suggests that the loss of proton gradient control has much broader effects. As seen in Chapter 5, plants adapted to fluctuating light massively increase the abundance of proteins involved in PSII repair

and electron transfer – the opposite behaviour to *pgr5*. In addition to the excessive photosystem damage suffered by *pgr5* in fluctuating light, resulting from an absence of NPQ, recovery from that damage is likely to be significantly impaired. Since there is so much disruption to gene regulation even in stress-free conditions, it would be interesting to see whether *pgr5* is capable of acclimating to high or low light in the long term, or whether the induction of these changes in gene expression is dependent on lumenal pH regulation that cannot be achieved in *pgr5*. Considering the normal growth phenotype and the apparently normal electron transfer capacity of *pgr5* under moderate, constant light (Munekage et al., 2002; Nandha et al., 2007; Okegawa et al., 2007), despite its significantly depleted light harvesting and electron transfer machinery, wild type plants must carry out the light reactions at a rate far below their capacity. A surplus of electron transfer proteins likely provides a buffer for changes in environmental conditions, such as sudden increases in light intensity, with photosynthesis ultimately limited by the dark reactions.

Taken together, these quantitative proteomic analyses of photosynthetic mutants highlight the flexibility of photosynthetic gene regulation. It seems clear that even under environmental conditions that do not induce stress responses, the loss of a single protein can result in systemic changes to maintain steady state photosynthesis. When the ability to sense environmental changes is disrupted, as in *pgr5*, signalling and gene expression dysregulation can have unexpected and wide-ranging effects. When studying mutants, combining quantitative proteomics with other techniques can further our understanding of a biological process beyond what can be observed from phenotypes.

## 7 Final summary

The aim of the work described in this thesis was to use mass spectrometry-based proteomics to quantify, for the first time, changes that occur in the Arabidopsis thylakoid membrane proteome upon long-term acclimation to environmental conditions. Proteomics, the study of all proteins in a biological system, is well established in its application to soluble proteomes but less so for membrane proteins because of inherent challenges arising from their biochemical properties. The hydrophobicity of transmembrane domains impedes their extraction and solubilisation, concealing large sections of protein from enzymatic digestion, and a reduced number of lysine and arginine residues means there are fewer cleavage sites for trypsin, the most commonly used protease in proteomics. Digested peptides from transmembrane domains also tend to contain fewer charged residues and thus have poor ionisation efficiency, resulting in low rates of MS detection (Kar et al., 2017). Unsuccessful tryptic digestion and MS analysis of the thylakoid membrane proteome with two well-established methods – in-gel digestion and urea in-solution digestion – and one less common method – digestion in 60% methanol – led to the development of a novel protocol for thylakoid proteomics. Solubilisation of isolated thylakoid membranes and tryptic digestion in the ionic detergent sodium laurate (Lin et al., 2013) facilitated MS identification and relative quantification of a large number of thylakoid proteins investigated in this thesis.

An obvious caveat of MS-based proteomics is that changes in the relative abundance of proteins or lack thereof do not automatically feed into changes in activity, since changes in regulation by post-translational modification or interaction-triggered conformational changes may also play a role. High levels of post-translational modification of a peptide that persist throughout MS sample preparation have the potential to prevent its identification and affect the accuracy of protein quantification. However, inclusion in the database search parameters of as many relevant chemical modifications as computationally feasible should reduce this impact. Regulatory modifications are often present at low levels, and several peptides often contribute to protein quantification. Despite generally broad coverage, some proteins were missing from the dataset, either consistently or occasionally. One of these missing proteins is PBCP, the antagonistic phosphatase of STN8 (Samol et al., 2012). The kinase STN8, which was consistently identified by MS, phosphorylates a number of thylakoid proteins including those within the PSII core and plays a role in the initiation of PSII repair. Quantification of changes in PBCP abundance in response to environmental conditions, as well as in the LHCII phosphorylation mutants *stn7* and *tap38*, could provide further insights into the regulation of PSII phosphorylation and repair. Other proteins, such as CURT1D and LHC1.5, were identified from MS datasets inconsistently, probably because of high sequence identity with their isoforms limiting the number of peptides that can be used for differentiation. Relative quantification of a protein based on, for example, a single unique peptide is likely to be less reliable than that of a protein with no shared tryptic peptide sequences. To improve thylakoid proteome coverage in future experiments, or to increase the quality of the data by

increasing the sequence coverage of already-identified membrane proteins, alternative proteases could be used. Proteases that cleave around hydrophobic residues such as chymotrypsin, which is specific for aromatic residues, have been shown to increase membrane protein identification rate (Fischer and Poetsch, 2006).

Another key issue with mass spectrometry data is that of normalisation to compensate for random variations in sample loading and spectral acquisition patterns. Intensity-based absolute quantification (iBAQ), which relates protein MS intensity to copy number by dividing by the number of theoretical tryptic peptides for that protein (Schwanhäusser et al., 2011), enabled normalisation to the core photosynthetic machinery as well as relative quantification of multi-subunit complexes. The MaxLFQ algorithm (Cox et al., 2014), while used successfully for stoichiometry calculations of the Arabidopsis photosynthetic machinery (McKenzie et al., 2020), was determined to be unsuitable for relative quantification of the thylakoid proteome between light conditions because of differences in data distribution. The method used here, of normalisation to the iBAQ of core photosynthetic complexes, is unaffected by sample complexity, provides a meaningful internal reference for changes in abundance of regulatory proteins, and offers an alternative to immunoblot-based quantification of photosynthetic proteins normalised on a chlorophyll basis.

A focus of the proteomic analysis and key factor in photosynthetic regulation is thylakoid architecture and the proteins that control it. Imaging of chloroplasts by EM and SIM enabled speculation on the relationship between these proteins and thylakoid stacking, both in terms of the number of membrane layers in each granum and the grana diameter, measured as the FWHM of fluorescence intensity of the grana. Larger grana allow more chlorophyll to be packed into a given chloroplast, which creates greater efficiencies in the amount of CBB cycle enzymes and other metabolic machinery associated with a given amount of chlorophyll. A disadvantage of larger grana is the increased diffusion distance for the mobile electron carriers PQ and plastocyanin which slows LET (Wood et al., 2018). In plants acclimated to low light intensity, where grana diameter was larger, the abundance of plastocyanin increased to mitigate this effect. The MS analysis also allowed, for the first time, recognition of the contributions of increased amounts of the CURT1A, CURT1B (Armbruster et al., 2013), RIQ1 and RIQ2 proteins (Yokoyama et al., 2016), which negatively regulate grana size, to the reduced thylakoid stacking seen in plants acclimated to high light intensity in both the growth chamber and the field. Previously, the decreased grana size has generally been solely attributed to the lower levels of LHCII trimers (Anderson et al., 1988; Schöttler and Tóth, 2014; Walters, 2005).

Reducing the distance between the centre of a granum and the stroma lamellae may promote LET, since plastocyanin must diffuse through the densely packed lumen to reach PSI. Damaged PSII also needs to diffuse out into the stroma lamellae to be disassembled and repaired, a process that will benefit from smaller grana diameter. Interestingly, field-grown plants had grana with very few layers but slightly

wider diameters, on average, than those grown at moderate light in a growth chamber. Since the field plants were exposed to much more light, there is likely no need for space efficiency and maximisation of light-harvesting. The slight increase in grana diameter in these plants may not be related to light intensity specifically, since plants grown in constant high light had grana with smaller diameters. Instead, wider grana may promote CET in the field plants, which have substantially more NDH than the plants grown at any constant light intensity. The widespread upregulation of the PSII repair machinery in the outdoor plants may mitigate any detrimental effect of wider grana on PSII repair.

The long-term acclimation-related changes in grana size appear to be somewhat independent of dynamic stacking on the short-term and have different aims. In the short-term, grana size dynamically responds to light intensity in an STN7/TAP38-dependent way via control of LHCII phosphorylation (Wood et al., 2019). Accordingly, grana size is reduced under low/moderate light conditions, when LHCII phosphorylation is at a maximum, whereas it is increased when LHCII is dephosphorylated, in both high light and darkness. It is clear, therefore, that this short-term response to high light exposure behaves quite oppositely to the long-term acclimation response seen here, since low light acclimated plants have larger grana than plants grown under high light. This is not surprising, since the aim of short-term high light responses is generally photoprotection through downregulation of light harvesting and electron transfer, whereas the long-term aim is to restore homeostasis by adjusting the sink capacity of the system to better utilise the increased light level. Indeed, while the phosphorylation mutants *stn7* and *tap38* are unable to adjust grana size on the short term (Wood et al., 2019), they are clearly capable of changing both grana diameter and membrane layers in the long term. Interestingly, field-grown plants had significant reductions in both STN7 and TAP38. Therefore, a comparison of dynamic stacking in outdoor-grown plants to those grown in a controlled environment could reveal whether the field plants are less flexible in their thylakoid architecture.

The MS analysis of the thylakoid proteome in different environmental conditions can be used to infer electron transfer capacity and the balance of LET and CET by relative quantification of the protein components of those pathways. Arabidopsis plants acclimated to constant low light intensity featured grana with larger diameters and increased amounts of PSI, suggesting a greater need for CET relative to LET. However, PGR5 and PGRL1 were no different in abundance to the moderate light plants and NDH was dramatically depleted, despite its purported significance in low light (Yamori et al., 2015). It could be expected that in low light, since there would be less energy going into PSII and fewer electrons moving through the thylakoid membrane, plants would downregulate expression of proteins involved in LET to conserve resources. However, low light plants generally had similar levels of many LET proteins such as FNR1, TIC62 and TROL, and higher plastocyanin abundance. This suggests that the low light plants need to maintain a certain level of LET and hence CO<sub>2</sub> assimilation, as well as PGR5/PGRL1-mediated CET at the expense of ATP production by ATP synthase, which was considerably lower. Downregulation of ATP synthase, along with moderate levels of PGR5/PGRL1,

may be a mechanism to maintain control of lumenal pH, such that induction of photoprotection is not impaired and the dark reactions are provided with enough NADPH.

In terms of electron transfer capacity/requirement, it is interesting to compare the response of the thylakoid proteome to constant high light to that of naturally fluctuating light, which likely reaches intensities much higher than the 800 and 600  $\mu\text{mol photons m}^{-2} \text{ s}^{-1}$  growth lights used for the data of Chapters 4 and 6, respectively. The constant high light plants appeared to favour LET, with dramatic upregulation of many LET-related proteins and grana with smaller diameters. They also appear to have substantially more CET via PGR5/PGRL1, and favour this route over the NDH pathway. If PGR5 serves a regulatory role, as suggested by Johnson and Joliot (2011), then an increase in CET capacity could be instead mediated by the higher amounts of FNR and its membrane tethering proteins TIC62 and TROL. Membrane tethering of FNR has been suggested to regulate the balance between LET and CET by increasing electron flow from Fd to *cyt<sub>b</sub>*f**, with enhanced amounts of tethered FNR found in C4 bundle sheath cells that perform CET (Goss and Hanke, 2014). NDH either increases very slightly in high light plants or is downregulated. In contrast, plants grown in the field have substantially more NDH, increasing the abundance of this complex to a greater extent than PGR5/PGRL1, which increase to a lesser extent than under constant high light. While both routes are important in fluctuating light (Yamori et al., 2016), it would appear that NDH-mediated CET is specifically important in fluctuating light and is not part of a response to high light intensity. Surprisingly, the field plants upregulated expression of LET proteins to a lesser extent than the constant high light plants, despite the higher light irradiances of natural sunlight. It may be that it is more economical for the outdoor plants to invest in protective and regulatory mechanisms, CET included, than to increase electron sink capacity. Indeed, Arabidopsis plants in a natural environment do not benefit from massive vegetative growth; their aim, which is reflected in their growth phenotype, is to flower and reproduce.

The abundance of VDE and ZEP, the enzymes of the xanthophyll cycle that catalyse the interconversion of violaxanthin and zeaxanthin to aid aggregation of LHCII into a dissipative state, appears to be regulated depending on environmental conditions. Plants acclimated to constant light, high or low, favour increasing ZEP relative to VDE and by implication, enhancing de-aggregation of LHCII to quickly restore light harvesting. The plants grown in the field, however, increase the amount of VDE to a greater extent than ZEP. While both the constant high light plants and the field plants upregulate expression of both enzymes, the preference for VDE in the field plants highlights the importance of fast induction of quenching to prevent damage in fluctuating light rather than fast relaxation to restore light harvesting capacity. For low light plants, the doubling of ZEP abundance paired with half as much VDE suggests that fast relaxation of quenching is very important when light is limiting. Increasing both enzymes and, therefore, enhancing zeaxanthin and violaxanthin interconversion in both directions, must be highly beneficial for outdoor-grown plants exposed to variable and rapidly changing light intensities (Hubbart et al., 2018; Kromdijk et al., 2016). While the increase in VDE observed in the field plants is

smaller than that observed in the plants acclimated to constant high light, the lower amount of its substrate – contained within the LHCI trimers – may enhance the effect of this change.

In addition to an enhanced photoprotective capacity via NPQ, many of the key components of the PSII repair cycle also increased in plants acclimated to constant and fluctuating light intensity. An important factor that may enhance PSII repair under high light in the long term is the replacement of LHCB4.1 and 4.2 with the third isoform of CP29, LHCB4.3, which lacks the large C-terminal domain present in the former two isoforms. This isoform increases dramatically in both constant high light and in a natural environment, and decreases in low light acclimated plants and in the *pgr5* mutant. The cryo-EM structure of the C<sub>2</sub>S<sub>2</sub>M<sub>2</sub> supercomplex from spinach shows that the C-terminal domains of LHCB4.1 and 4.2 interact on the stromal side of the complex with CP47, suggesting a role as an anchor (Su et al., 2017). Replacement by LHCB4.3 in the supercomplex would remove this interaction, perhaps allowing more straightforward disassembly of the PSII supercomplex to facilitate either PSII repair or NPQ. These changes in PSII structure and PSII repair cycle machinery may act synergistically with the smaller thylakoid grana and reduced stacking seen in high light plants to enhance the speed of PSII repair, or in the field plants, they may compensate for the detrimental impact of the slightly wider grana on PSII repair.

When comparing the PSII repair machinery of constant high light plants to the field plants, the most obvious difference is that the field plants broadly upregulate PSII repair, whereas the behaviour of the PSII repair machinery of the constant high light plants is more variable, with some decreases observed. While most tended to increase in abundance with growth light intensity, several proteins associated with the repair cycle were upregulated in the low light plants, such as LQY1, PPL1 and FTSH8. This raises questions about what signals lead to their expression to be induced, since it would seem counterintuitive for the plants to produce an incomplete repair machinery or to increase PSII repair capacity under conditions where the risk of reaction centre damage is low. The *pgr5* plants, on the other hand, presented widespread decreases in many PSII repair proteins, while some were unaffected. The expression of proteins that were depleted in this mutant, such as the DEGP proteins and CTPA, may be induced by luminal pH, which is dysregulated in the absence of PGR5. Similarly to a wild type low light response, LHCB4.3 decreased substantially, despite a decrease in LHCI reminiscent of a high light response. Overall, the broad range of protein depletions seen in *pgr5* does hint at a more complex function of PGR5. An investigation of the thylakoid proteome of *pgr5* plants acclimated to different light intensities, or other non-lethal environmental conditions known to affect photosynthetic gene expression, could determine whether the mutant is able to perform long term acclimation. A comparison with mutants lacking PGRL1 – or another protein that perturbs the proton gradient – could reveal whether the disruption observed here is a result of luminal pH or whether PGR5 has a specific signalling or regulatory role.

Given the demonstrable importance of acclimation to plant fitness in nature (Athanasidou et al., 2010), work of this kind could be used to inform future efforts to manipulate this process for crop improvement. Several of the proteins up-regulated in high light and in the field, such as VDE, PSBS and *cytb<sub>6</sub>f*, have recently been targeted for overexpression in crop plants with the aim of increasing yield to augment global food production (Kromdijk et al., 2016; Simkin et al., 2017). Extension of this approach to include some of the other proteins identified here that change in abundance may open up new avenues for yield improvement. If the end goal of plant photosynthesis research is its translation into positive outcomes for agriculture and biotechnology, any hypotheses surrounding photosynthetic mechanisms should be considered within the context of natural or agricultural environmental conditions. The comparison of the thylakoid proteomes of Arabidopsis plants grown in a controlled, growth chamber environment to a 'field' environment aimed to contextualise the features of the long-term response to light intensity. While thylakoids isolated from the field plants most closely resembled the constant high light acclimated thylakoids in terms of proteome remodelling, several differences in the response were observed. These range from the FNR tethering protein TROL, which was upregulated only in the field, to the electron carrier plastocyanin, which was present in the field thylakoids at the same level as in constant moderate light but upregulated in constant high light. More work is required to unravel which specific environmental factors produce these differences, be they fluctuating light from moving cloud cover, differences between the light spectrum of artificial lighting and the sun, the gradual transition between night and daylight, low temperatures, variable humidity, and/or simply a higher maximum light intensity. However, these massively variable factors are also the reason for the use of controlled environment growth chambers, and the reason why this field experiment can never be reproduced exactly. Another caveat of this experiment is the structural and size differences between Arabidopsis and most crop plants. While the leaves of Arabidopsis, arranged in a characteristic rosette shape, will absorb a largely similar amount of light to one another, the leaves of maize or rice plants will form a canopy as they grow, shading most of the plant from direct sunlight. Understory leaves, and the chloroplasts within them, will experience a very different light environment to those in full sun, dealing with both low light and intense sunflecks from leaf movement in the wind. Any genetic manipulation of a crop plant would ideally enhance photosynthesis in the whole plant if it were to improve yields. However, despite these factors complicating photosynthetic research in a field environment, proteomics seems a good option since it takes a snapshot of the abundance of all quantifiable proteins involved in many different processes. A whole-system analysis, rather than measurement of a single protein or process, has the potential to inform about the integration of all photosynthetic mechanisms. If this kind of proteomic approach can be widened to include stromal photosynthetic proteins involved in carbon assimilation, combined with transcriptomics and metabolomics, we can begin to unravel the complex regulatory networks that lead to optimisation of photosynthesis in a changing environment.

In conclusion, the work described in this thesis shows that relative quantification by label-free MS-based proteomics can be used to study photosynthetic acclimation, providing detailed insight into how the many interconnected regulatory and photoprotective processes work together. Arabidopsis plants grown in light limiting conditions prioritise economics, with a simplified photosynthetic machinery focusing on light harvesting, fast relaxation of NPQ, and PGR5/PGRL1-mediated CET. High light acclimated plants focus on increasing their capacity for LET flux, NPQ induction and PSII repair. Constant, controlled high light causes plants to preferentially enhance CET via the PGR5/PGRL1 pathway, whereas the NDH-dependent CET pathway is favoured in plants grown in natural light and weather conditions. The data also show that the LHCII kinase STN7 is not required for long-term acclimation to light intensity. While STN7 and TAP38 control thylakoid architecture in the short term by LHCII (de)phosphorylation, long term changes in grana size are determined by the abundance of the CURT1 proteins and LHCII. Ultimately, the proteomic strategy used here could be applied to many more questions to further our understanding of the complex and dynamic system that is the thylakoid membrane, revealing targets for future genetic manipulation to improve crop yields and increase global food production.

## Bibliography

- Adamiec, M., Misztal, L., Kosicka, E., Paluch-Lubawa, E., and Luciński, R. (2018). *Arabidopsis thaliana* *egy2* mutants display altered expression level of genes encoding crucial photosystem II proteins. *J. Plant Physiol.* *231*, 155–167.
- Adams, W.W., Watson, A.M., Mueh, K.E., Amiard, V., Turgeon, R., Ebbert, V., Logan, B.A., Combs, A.F., and Demmig-Adams, B. (2007). Photosynthetic acclimation in the context of structural constraints to carbon export from leaves. *Photosynth. Res.* *94*, 455–466.
- Aebersold, R., and Mann, M. (2003). Mass spectrometry-based proteomics. *Nature* *422*, 198–207.
- Albanese, P., Manfredi, M., Meneghesso, A., Marengo, E., Saracco, G., Barber, J., Morosinotto, T., and Pagliano, C. (2016). Dynamic reorganization of photosystem II supercomplexes in response to variations in light intensities. *Biochim. Biophys. Acta - Bioenerg.* *1857*, 1651–1660.
- Albanese, P., Melero, R., Engel, B.D., Grinzato, A., Manfredi, M., Chiodoni, A., Vargas, J., Sánchez, C.Ó., Marengo, E., Saracco, G., et al. (2017). Pea PSII-LHCII supercomplexes form pairs by making connections across the stromal gap. *Sci. Rep.* *7*, 1–16.
- Albanese, P., Manfredi, M., Re, A., Marengo, E., Saracco, G., and Pagliano, C. (2018). Thylakoid proteome modulation in pea plants grown at different irradiances: quantitative proteomic profiling in a non-model organism aided by transcriptomic data integration. *Plant J.* *96*, 786–800.
- Albanese, P., Manfredi, M., Marengo, E., Saracco, G., and Pagliano, C. (2019). Structural and functional differentiation of the light-harvesting protein Lhcb4 during land plant diversification. *Physiol. Plant.* *166*, 336–350.
- Albertsson, P.Å. (2001). A quantitative model of the domain structure of the photosynthetic membrane. *Trends Plant Sci.* *6*, 349–354.
- Albertsson, P.A., Andreasson, E., Stefansson, H., and Wollenberger, L. (1994). Fractionation of Thylakoid Membrane. *Methods Enzymol.* *228*, 469–482.
- Alfonso-garrido, J., Garcia-calvo, E., and Luque-garcia, J.L. (2015). Sample preparation strategies for improving the identification of membrane proteins by mass spectrometry. *Anal. Bioanal. Chem.* *407*, 4893–4905.
- Amstutz, C.L., Fristedt, R., Schultink, A., Merchant, S.S., Niyogi, K.K., and Malnoë, A. (2020). An atypical short-chain dehydrogenase–reductase functions in the relaxation of photoprotective qH in *Arabidopsis*. *Nat. Plants* *6*, 154–166.
- Andaluz, S., López-Millán, A.-F., De las Rivas, J., Aro, E.-M., Abadía, J., and Abadía, A. (2006). Proteomic profiles of thylakoid membranes and changes in response to iron deficiency. *Photosynth.*

Res. 89, 141–155.

Anderson, J.M. (1986). Photoregulation of the composition, function and structure of thylakoid membranes. *Annu. Rev. Plant. Physiol.* 37, 93–136.

Anderson, J., Chow, W., and Goodchild, D. (1988). Thylakoid Membrane Organisation in Sun/Shade Acclimation. *Aust. J. Plant Physiol.* 15, 11–26.

Anderson, J.M., Horton, P., Kim, E.-H., and Chow, W.S. (2012). Towards elucidation of dynamic structural changes of plant thylakoid architecture. *Philos. Trans. R. Soc. Lond. B. Biol. Sci.* 367, 3515–3524.

Andersson, B., and Anderson, J.M. (1980). Lateral heterogeneity in the distribution of chlorophyll-protein complexes of the thylakoid membranes of spinach chloroplasts. *Biochim. Biophys. Acta* 593, 427–440.

Andersson, U., Heddad, M., and Adamska, I. (2003). Light stress-induced one-helix protein of the chlorophyll a/b-binding family associated with photosystem I. *Plant Physiol.* 132, 811–820.

Armbruster, U., Labs, M., Pribil, M., Viola, S., Xu, W., Scharfenberg, M., Hertle, A.P., Rojahn, U., Jensen, P.E., Rappaport, F., et al. (2013). Arabidopsis CURVATURE THYLAKOID1 Proteins Modify Thylakoid Architecture by Inducing Membrane Curvature. *Plant Cell* 25, 2661–2678.

Armbruster, U., Carrillo, L.R., Venema, K., Pavlovic, L., Schmidtman, E., Kornfeld, A., Jahns, P., Berry, J.A., Kramer, D.M., and Jonikas, M.C. (2014). Ion antiport accelerates photosynthetic acclimation in fluctuating light environments. *Nat. Commun.* 5, 1–8.

Aro, E.M., Virgin, I., and Andersson, B. (1993). Photoinhibition of Photosystem II. Inactivation, protein damage and turnover. *BBA - Bioenerg.* 1143, 113–134.

Athanasiou, K., Dyson, B.C., Webster, R.E., and Johnson, G.N. (2010). Dynamic acclimation of photosynthesis increases plant fitness in changing environments. *Plant Physiol.* 152, 366–373.

Austin, J.R., and Staehelin, L.A. (2011). Three-Dimensional Architecture of Grana and Stroma Thylakoids of Higher Plants as Determined by Electron Tomography. *Plant Physiol.* 155, 1601–1611.

Bailey, S., Walters, R.G., Jansson, S., and Horton, P. (2001). Acclimation of *Arabidopsis thaliana* to the light environment: The existence of separate low light and high light responses. *Planta* 213, 794–801.

Bailey, S., Horton, P., and Walters, R.G. (2004). Acclimation of *Arabidopsis thaliana* to the light environment: The relationship between photosynthetic function and chloroplast composition. *Planta* 218, 793–802.

- Ballottari, M., Dall'Osto, L., Morosinotto, T., and Bassi, R. (2007). Contrasting behavior of higher plant photosystem I and II antenna systems during acclimation. *J. Biol. Chem.* 282, 8947–8958.
- Bellafiore, S., Barneche, F., Peltier, G., and Rochaix, J.-D. (2005). State transitions and light adaptation require chloroplast thylakoid protein kinase STN7. *Nature* 433, 892–895.
- Benson, S.L., Maheswaran, P., Ware, M.A., Hunter, C.N., Horton, P., Jansson, S., Ruban, A. V., and Johnson, M.P. (2015). An intact light harvesting complex I antenna system is required for complete state transitions in *Arabidopsis*. *Nat. Plants* 1, 15176.
- Benz, J.P., Stengel, A., Lintala, M., Lee, Y.-H., Weber, A., Philippar, K., Gügel, I.L., Kaieda, S., Ikegami, T., Mulo, P., et al. (2009). *Arabidopsis* Tic62 and Ferredoxin-NADP(H) Oxidoreductase Form Light-Regulated Complexes That Are Integrated into the Chloroplast Redox Poise. *Plant Cell* 21, 3965–3983.
- Bergantino, E., Segalla, A., Brunetta, A., Teardo, E., Rigoni, F., Giacometti, G.M., and Szabò, I. (2003). Light- and pH-dependent structural changes in the PsbS subunit of photosystem II. *Proc. Natl. Acad. Sci. U. S. A.* 100, 15265–15270.
- Berry, S., and Rumberg, B. (1996). H<sup>+</sup>/ATP coupling ratio at the unmodulated CF<sub>0</sub>CF<sub>1</sub>-ATP synthase determined by proton flux measurements. *Biochim. Biophys. Acta - Bioenerg.* 1276, 51–56.
- van Bezouwen, L.S., Caffarri, S., Kale, R.S., Kouřil, R., Thunnissen, A.-M.W.H., Oostergetel, G.T., and Boekema, E.J. (2017). Subunit and chlorophyll organization of the plant photosystem II supercomplex. *Nat. Plants* 3, 1–11.
- Boardman, N.K. (1977). Comparative Photosynthesis of Sun and Shade Plants. *Annu. Rev. Plant Physiol.* 28, 355–377.
- Bonardi, V., Pesaresi, P., Becker, T., Schleiff, E., Wagner, R., Pfannschmidt, T., Jahns, P., and Leister, D. (2005). Photosystem II core phosphorylation and photosynthetic acclimation require two different protein kinases. *Nature* 437, 1–4.
- Brooks, M.D., Sylak-Glassman, E.J., Fleming, G.R., and Niyogi, K.K. (2013). A thioredoxin-like/ $\beta$ -propeller protein maintains the efficiency of light harvesting in *Arabidopsis*. *Proc. Natl. Acad. Sci. U. S. A.* 110, E2733–E2740.
- Brutnell, T.P., Wang, L., Swartwood, K., Goldschmidt, A., Jackson, D., Zhu, X.G., Kellogg, E., and van Eck, J. (2010). *Setaria viridis*: A model for C<sub>4</sub> photosynthesis. *Plant Cell* 22, 2537–2544.
- Buchert, F., Mosebach, L., Gäbelein, P., and Hippler, M. (2020). PGR5 is required for efficient Q cycle in the cytochrome b<sub>6</sub>f complex during cyclic electron flow. *Biochem. J.* 477, 1631–1650.
- Burkey, K.O. (1993). Effect of growth irradiance on plastocyanin levels in barley. *Photosynth. Res.* 36,

103–110.

Butenko, Y., Lin, A., Naveh, L., Kupervaser, M., Levin, Y., Reich, Z., and Adam, Z. (2018). Differential Roles of the Thylakoid Lumenal Deg Protease. *Plant Physiol.* *178*, 1065–1080.

Caffarri, S., Kouřil, R., Kereïche, S., Boekema, E.J., and Croce, R. (2009). Functional architecture of higher plant photosystem II supercomplexes. *EMBO J.* *28*, 3052–3063.

Carlberg, I., Hansson, M., Kieselbach, T., Schro, W.P., Andersson, B., and Vener, A. V (2003). A novel plant protein undergoing light-induced phosphorylation and release from the photosynthetic thylakoid membranes. *Proc. Natl. Acad. Sci.* *100*, 757–762.

Carol, P., Stevenson, D., Bisanz, C., Breitenbach, J., Sandmann, G., Mache, R., Coupland, G., Kuntz, M., Moléculaire, D.G., Fourier, U.J., et al. (1999). Mutations in the Arabidopsis Gene IMMUTANS Cause a Variegated Phenotype by Inactivating a Chloroplast Terminal Oxidase Associated with Phytoene Desaturation. *Plant Cell* *11*, 57–68.

Chaux, F., Peltier, G., and Johnson, X. (2015). A security network in PSI photoprotection: regulation of photosynthetic control, NPQ and O<sub>2</sub> photoreduction by cyclic electron flow. *Front. Plant Sci.* *6*, 1–7.

Cho, L.-H., Yoon, J., and An, G. (2017). The control of flowering time by environmental factors. *Plant J.* *90*, 708–719.

Chory, J., Ecker, J.R., Briggs, S., Caboche, M., Coruzzi, G.M., Cook, D., Dangl, J., Grant, S., Guerinot, M. Lou, Henikoff, S., et al. (2000). National Science Foundation-Sponsored Workshop Report: “The 2010 Project” Functional Genomics and the Virtual Plant. A Blueprint for Understanding How Plants Are Built and How to Improve Them. *Plant Physiol.* *123*, 423–425.

Chow, W., and Anderson, J. (1987). Photosynthetic Responses of *Pisum sativum* to an Increase in Irradiance During Growth II. Thylakoid Membrane Components. *Aust. J. Plant Physiol.* *14*, 9–19.

Chow, W., and Hope, A. (1987). The Stoichiometries of Supramolecular Complexes in Thylakoid Membranes From Spinach Chloroplasts. *Funct. Plant Biol.* *14*, 21–28.

Chow, W., Qian, L., Goodchild, D., and Anderson, J.M. (1988). Photosynthetic acclimation of *Alocasia macrorrhiza* (L.) G. Don to growth irradiance: Structure, function and composition of chloroplasts. *Aust. J. Plant Physiol.* *15*, 107–122.

Chuartzman, S.G., Nevo, R., Shimoni, E., Charuvi, D., Kiss, V., Ohad, I., Brumfeld, V., and Reich, Z. (2008). Thylakoid membrane remodeling during state transitions in Arabidopsis. *Plant Cell* *20*, 1029–1039.

Correa-Galvis, V., Poschmann, G., Melzer, M., Stühler, K., and Jahns, P. (2016). PsbS interactions

involved in the activation of energy dissipation in Arabidopsis. *Nat. Plants* 2, 1–8.

Cox, J., and Mann, M. (2008). MaxQuant enables high peptide identification rates, individualized p.p.b.-range mass accuracies and proteome-wide protein quantification. *Nat. Biotechnol.* 26, 1367–1372.

Cox, J., Hein, M.Y., Lubner, C.A., Paron, I., Nagaraj, N., and Mann, M. (2014). Accurate proteome-wide label-free quantification by delayed normalization and maximal peptide ratio extraction, termed MaxLFQ. *Mol. Cell. Proteomics* 13, 2513–2526.

Crepin, A., and Caffarri, S. (2015). The specific localizations of phosphorylated Lhcb1 and Lhcb2 isoforms reveal the role of Lhcb2 in the formation of the PSI-LHCII supercomplex in Arabidopsis during state transitions. *Biochim. Biophys. Acta - Bioenerg.* 1847, 1539–1548.

Crepin, A., Kučerová, Z., Kosta, A., Durand, E., and Caffarri, S. (2020). Isolation and characterization of a large photosystem I–light-harvesting complex II supercomplex with an additional Lhca1–a4 dimer in Arabidopsis. *Plant J.* 3, 1–12.

Cutolo, E., Parvin, N., Ruge, H., Pirayesh, N., Roustan, V., Weckwerth, W., Teige, M., Grieco, M., Larosa, V., and Vothknecht, U.C. (2019). The High Light Response in Arabidopsis Requires the Calcium Sensor Protein CAS, a Target of STN7- and STN8-Mediated Phosphorylation. *Front. Plant Sci.* 10, 1–15.

DalCorso, G., Pesaresi, P., Masiero, S., Aseeva, E., Schünemann, D., Finazzi, G., Joliot, P., Barbato, R., and Leister, D. (2008). A Complex Containing PGRL1 and PGR5 Is Involved in the Switch between Linear and Cyclic Electron Flow in Arabidopsis. *Cell* 132, 273–285.

Dale, A.M.P., and Causton, D.R. (1992). Use of the Chlorophyll a/b Ratio as a Bioassay for the Light Environment of a Plant. *Funct. Ecol.* 6, 190–196.

Damkjær, J.T., Kereš, S., Johnson, M.P., Kovacs, L., Kiss, A.Z., Boekema, E.J., Ruban, A. V, Horton, P., and Jansson, S. (2009). The Photosystem II Light-Harvesting Protein Lhcb3 Affects the Macrostructure of Photosystem II and the Rate of State Transitions in Arabidopsis. *21*, 3245–3256.

Daum, B., Nicastro, D., McIntosh, J.R., and Kuhlbrandt, W. (2010). Arrangement of Photosystem II and ATP Synthase in Chloroplast Membranes of Spinach and Pea. *Plant Cell* 22, 1299–1312.

Day, D.A., Ryrie, I.J., and Fuad, N. (1984). Investigations of the role of the main light-harvesting chlorophyll-protein complex in thylakoid membranes. Reconstitution of depleted membranes from intermittent-light-grown plants with the isolated complex. *J. Cell Biol.* 98, 163–172.

Dittrich, J., Becker, S., Hecht, M., and Ceglarek, U. (2015). Sample preparation strategies for targeted proteomics via proteotypic peptides in human blood using liquid chromatography tandem mass

spectrometry. *Proteomics - Clin. Appl.* 9, 5–16.

Drissi, R., Dubois, M.L., and Boisvert, F.M. (2013). Proteomics methods for subcellular proteome analysis. *FEBS J.* 280, 5626–5634.

Endow, J.K., and Inoue, K. (2013). Stable complex formation of thylakoidal processing peptidase and PGRL1. *FEBS Lett.* 587, 2226–2231.

Erik, P., Bassi, R., Boekema, E.J., Dekker, J.P., Jansson, S., Leister, D., Robinson, C., and Vibe, H. (2007). Structure, function and regulation of plant photosystem I. *Biochim. Biophys. Acta* 1767, 335–352.

Ermakova, M., Lopez-Calcano, P.E., Raines, C.A., Furbank, R.T., and Caemmerer, S. von (2019). Overexpression of the Rieske FeS protein of the Cytochrome b6f complex increases C4 photosynthesis. *Commun. Biol.* 314, 1–12.

Fabre, B., Lambour, T., Bouyssié, D., Menneteau, T., Monsarrat, B., Burlet-Schiltz, O., and Bousquet-Dubouch, M.P. (2014). Comparison of label-free quantification methods for the determination of protein complexes subunits stoichiometry. *EuPA Open Proteomics* 4, 82–86.

Fan, D.Y., Hope, A.B., Smith, P.J., Jia, H., Pace, R.J., Anderson, J.M., and Chow, W.S. (2007). The stoichiometry of the two photosystems in higher plants revisited. *Biochim. Biophys. Acta - Bioenerg.* 1767, 1064–1072.

Fernyhough, P., Horton, P., and Foyer, C. (1984). Regulation of Light Harvesting Chlorophyll a/b Binding Protein (LHCP) Phosphorylation in Intact Maize Mesophyll Chloroplasts. In *Advances in Photosynthesis Research*, (Springer Netherlands), pp. 299–302.

Ferro, M., Brugière, S., Salvi, D., Seigneurin-Berny, D., Court, M., Moyet, L., Ramus, C., Miras, S., Mellal, M., Le Gall, S., et al. (2010). AT\_CHLORO, a Comprehensive Chloroplast Proteome Database with Subplastidial Localization and Curated Information on Envelope Proteins. *Mol. Cell. Proteomics* 9, 1063–1084.

Fischer, F., and Poetsch, A. (2006). Protein cleavage strategies for an improved analysis of the membrane proteome. *Proteome Sci.* 4, 1–12.

Flannery, S.E., Hepworth, C., Wood, W.H.J., Pastorelli, F., Hunter, C.N., Dickman, M.J., Jackson, P.J., and Johnson, M.P. (2021). Developmental acclimation of the thylakoid proteome to light intensity in *Arabidopsis*. *Plant J.* 105, 223–244.

Foyer, C.H. (2018). Reactive oxygen species, oxidative signaling and the regulation of photosynthesis. *Environ. Exp. Bot.* 154, 134–142.

Foyer, C., and Noctor, G. (2005). Redox Homeostasis and Antioxidant Signaling: A Metabolic Interface

- between Stress Perception and Physiological Responses. *Plant Cell* *17*, 1866–1875.
- Frenkel, M., Bellafiore, S., Rochaix, J., and Jansson, S. (2007). Hierarchy amongst photosynthetic acclimation responses for plant fitness. *Physiol. Plant.* *129*, 455–459.
- Frenkel, M., Johansson Jänkämpää, H., Moen, J., and Jansson, S. (2008). An illustrated gardener's guide to transgenic *Arabidopsis* field experiments. *New Phytol.* *180*, 545–555.
- Friso, G., Giacomelli, L., Ytterberg, A.J., Peltier, J., Rudella, A., Sun, Q., and Wijk, K.J. Van (2004). In-Depth Analysis of the Thylakoid Membrane Proteome of *Arabidopsis thaliana* Chloroplasts: New Proteins, New Functions, and a Plastid Proteome Database. *Plant Cell* *16*, 478–499.
- Fristedt, R., Carlberg, I., Zygadlo, A., Scheller, H.V., and Vener, A. V. (2008). Involvement of TSP9 Phosphoprotein in Balancing the Photosynthetic Light Harvesting Process in *Arabidopsis thaliana*. *Photosynth. Energy from Sun* 1009–1012.
- Fristedt, R., Willig, A., Granath, P., Crèvecoeur, M., Rochaix, J.-D., and Vener, A. V. (2009a). Phosphorylation of Photosystem II Controls Functional Macroscopic Folding of Photosynthetic Membranes in *Arabidopsis*. *Plant Cell* *21*, 3950–3964.
- Fristedt, R., Carlberg, I., Zygadlo, A., Piippo, M., Nurmi, M., Aro, E.M., Scheller, H.V., and Vener, A. V. (2009b). Intrinsically unstructured phosphoprotein TSP9 regulates light harvesting in *Arabidopsis thaliana*. *Biochemistry* *48*, 499–509.
- Galetskiy, D., Susnea, I., Reiser, V., Adamska, I., and Przybylski, M. (2008). Structure and Dynamics of Photosystem II Light-Harvesting Complex Revealed by High-Resolution FTICR Mass Spectrometric Proteome Analysis. *J. Am. Soc. Mass Spectrom.* *19*, 1004–1013.
- Galka, W.P., Santabarbara, S., Thu, T., Khuong, H., Degand, H., Morsomme, P., Jennings, R.C., Boekema, E.J., Caffarri, S., Galka, P., et al. (2012). Functional Analyses of the Plant Photosystem I–Light-Harvesting Complex II Supercomplex Reveal That Light-Harvesting Complex II Loosely Bound to Photosystem II Is a Very Efficient Antenna for Photosystem I in State II. *Plant Cell* *24*, 2963–2978.
- Gamez-Arjona, F.M., Raynaud, S., Ragel, P., and Mérida, Á. (2014). Starch synthase 4 is located in the thylakoid membrane and interacts with plastoglobule-associated proteins in *Arabidopsis*. *Plant J.* *80*, 305–316.
- Garab, G., Lohner, K., Laggner, P., and Farkas, T. (2000). Self-regulation of the lipid content of membranes by non-bilayer lipids: A hypothesis. *Trends Plant Sci.* *5*, 489–494.
- Ghosh, R., Gilda, J.E., and Gomes, A. V (2014). Accuracy of Western Blots. *Expert Rev. Proteomics* *11*, 549–560.
- Giacomelli, L., Rudella, A., and Wijk, K.J. Van (2006). High Light Response of the Thylakoid

Proteome in Arabidopsis Wild Type and the Ascorbate-Deficient Mutant *vtc2-2*. A Comparative Proteomics Study. *Plant Physiol.* *141*, 685–701.

Gjindali, A., Herrmann, H.A., Schwartz, J.M., Johnson, G.N., and Calzadilla, P.I. (2021). A Holistic Approach to Study Photosynthetic Acclimation Responses of Plants to Fluctuating Light. *Front. Plant Sci.* *12*, 1–20.

Gomez, S.M., Nishio, J.N., Faull, K.F., and Whitelegge, J.P. (2002). The Chloroplast Grana Proteome Defined by Intact Mass Measurements from Liquid Chromatography Mass Spectrometry. *Mol. Cell. Proteomics* *1*, 46–59.

Goral, T.K., Johnson, M.P., Brain, A.P.R., Kirchhoff, H., Ruban, A. V., and Mullineaux, C.W. (2010). Visualizing the mobility and distribution of chlorophyll proteins in higher plant thylakoid membranes: effects of photoinhibition and protein phosphorylation. *Plant J.* *62*, 948–959.

Goss, T., and Hanke, G. (2014). The End of the Line: Can Ferredoxin and Ferredoxin NADP(H) Oxidoreductase Determine the Fate of Photosynthetic Electrons? *Curr. Protein Pept. Sci.* *15*, 385–393.

Gray, G.R., Savitch, L. V., Ivanov, A.G., and Huner, N.P.A. (1996). Photosystem II excitation pressure and development of resistance to photoinhibition: II. Adjustment of photosynthetic capacity in winter wheat and winter rye. *Plant Physiol.* *110*, 61–71.

Grieco, M., Tikkanen, M., Paakkarinen, V., Kangasjarvi, S., and Aro, E.-M. (2012). Steady-state phosphorylation of light-harvesting complex II proteins preserves Photosystem I under fluctuating white light. *Plant Physiol.* *160*, 1896–1910.

Hahn, A., Vonck, J., Mills, D.J., Meier, T., and Kuhlbrandt, W. (2018). Structure, mechanism, and regulation of the chloroplast ATP synthase. *Science* (80-. ). *360*, 1–8.

Hajirezaei, M.R., Peisker, M., Tschiersch, H., Palatnik, J.F., Valle, E.M., Carrillo, N., and Sonnewald, U. (2002). Small changes in the activity of chloroplastic NADP<sup>+</sup>-dependent ferredoxin oxidoreductase lead to impaired plant growth and restrict photosynthetic activity of transgenic tobacco plants. *Plant J.* *29*, 281–293.

Hansson, M., and Vener, A. V (2003). Identification of Three Previously Unknown in Vivo Protein Phosphorylation Sites in Thylakoid Membranes of *Arabidopsis thaliana*. *Mol. Cell. Proteomics* *2*, 550–559.

Hansson, M., Dupuis, T., Strömquist, R., Andersson, B., Vener, A. V., and Carlberg, I. (2007). The mobile thylakoid phosphoprotein TSP9 interacts with the light-harvesting complex II and the peripheries of both photosystems. *J. Biol. Chem.* *282*, 16214–16222.

Haußuhl, K., Andersson, B., and Adamska, I. (2001). A chloroplast DegP2 protease performs the

primary cleavage of the photodamaged D1 protein in plant photosystem II. *EMBO J.* *20*, 713–722.

Hepworth, C., Wood, W.H.J., Emrich-Mills, T.Z., Proctor, M.S., Casson, S., and Johnson, M.P. (2021). Dynamic thylakoid stacking and state transitions work synergistically to avoid acceptor-side limitation of photosystem I. *Nat. Plants* *7*, 87–98.

Herbstova, M., Tietz, S., Kinzel, C., Turkina, M. V., and Kirchhoff, H. (2012). Architectural switch in plant photosynthetic membranes induced by light stress. *Proc. Natl. Acad. Sci.* *109*, 20130–20135.

Hertle, A.P., Blunder, T., Wunder, T., Pesaresi, P., Pribil, M., Armbruster, U., and Leister, D. (2013). PGRL1 Is the Elusive Ferredoxin-Plastoquinone Reductase in Photosynthetic Cyclic Electron Flow. *Mol. Cell* *49*, 511–523.

Hey, D., and Grimm, B. (2018). ONE-HELIX PROTEIN2 (OHP2) is required for the stability of OHP1 and assembly factor HCF244 and is functionally linked to PSII biogenesis. *Plant Physiol.* *177*, 1453–1472.

Hooper, C.M., Castleden, I.R., Tanz, S.K., Aryamanesh, N., and Millar, A.H. (2017). SUBA4: The interactive data analysis centre for Arabidopsis subcellular protein locations. *Nucleic Acids Res.* *45*, D1064–D1074.

Hubbart, S., Smillie, I.R.A., Heatley, M., Swarup, R., Foo, C.C., Zhao, L., and Murchie, E.H. (2018). Enhanced thylakoid photoprotection can increase yield and canopy radiation use efficiency in rice. *Commun. Biol.* *1*, 1–12.

Huner, N.P.A., Maxwell, D.P., Gray, G.R., Savitch, L. V., Kroi, M., Ivanov, A.G., and Falk, S. (1996). Sensing environmental temperature change through imbalances between energy supply and energy consumption: Redox state of photosystem II. *Physiol. Plant.* *98*, 358–364.

Hutin, C., Nussaume, L., Moise, N., Moya, I., Kloppstech, K., and Havaux, M. (2003). Early light-induced proteins protect Arabidopsis from photooxidative stress. *Proc. Natl. Acad. Sci. U. S. A.* *100*, 4921–4926.

Ingelsson, B., and Vener, A. V (2012). Phosphoproteomics of Arabidopsis chloroplasts reveals involvement of the STN7 kinase in phosphorylation of nucleoid protein pTAC16. *FEBS Lett.* *586*, 1265–1271.

Ishihara, S., Takabayashi, A., Ido, K., Endo, T., Ifuku, K., and Sato, F. (2007). Distinct Functions for the Two PsbP-Like Proteins PPL1 and PPL2 in the Chloroplast Thylakoid Lumen of Arabidopsis. *Plant Physiol.* *145*, 668–679.

Itzhaki, H., Naveh, L., Lindahl, M., Cook, M., and Adam, Z. (1998). Identification and Characterization of DegP, a Serine Protease Associated with the Luminal Side of the Thylakoid Membrane. *J. Biol.*

Chem. 273, 7094–7098.

Jahns, P., Graf, M., Munekage, Y., and Shikanai, T. (2002). Single point mutation in the Rieske iron-sulfur subunit of cytochrome b6/f leads to an altered pH dependence of plastoquinol oxidation in *Arabidopsis*. *FEBS Lett.* 519, 99–102.

Järvi, S., Suorsa, M., and Aro, E.M. (2015). Photosystem II repair in plant chloroplasts - Regulation, assisting proteins and shared components with photosystem II biogenesis. *Biochim. Biophys. Acta - Bioenerg.* 1847, 900–909.

Jin, H., Liu, B., Luo, L., Feng, D., Wang, P., Liu, J., Da, Q., He, Y., Qi, K., Wang, J., et al. (2014). HYPERSENSITIVE TO HIGH LIGHT1 Interacts with LOW QUANTUM YIELD OF PHOTOSYSTEM III and Functions in Protection of Photosystem II from Photodamage in *Arabidopsis*. *Plant Cell* 26, 1213–1229.

Jin, Y., Chen, S., Fan, X., Song, H., Li, X., Xu, J., and Qian, H. (2017). Diuron treatment reveals the different roles of two cyclic electron transfer pathways in photosystem II in *Arabidopsis thaliana*. *Pestic. Biochem. Physiol.* 137, 15–20.

Johnson, G.N. (2007). Cyclic Electron Transport. *Encycl. Life Sci.* 1–5.

Johnson, M.P. (2016). An overview of photosynthesis. *Essays Biochem.* 60, 255–273.

Johnson, M.P., and Wientjes, E. (2020). The relevance of dynamic thylakoid organisation to photosynthetic regulation. *Biochim. Biophys. Acta - Bioenerg.* 1861, 148039.

Johnson, M.P., Goral, T.K., Duffy, C.D.P., Brain, A.P.R., Mullineaux, C.W., and Ruban, A. V. (2011). Photoprotective Energy Dissipation Involves the Reorganization of Photosystem II Light-Harvesting Complexes in the Grana Membranes of Spinach Chloroplasts. *Plant Cell* 23, 1468–1479.

Johnson, M.P., Vasilev, C., Olsen, J.D., and Hunter, C.N. (2014). Nanodomains of Cytochrome *b6/f* and Photosystem II Complexes in Spinach Grana Thylakoid Membranes. *Plant Cell* 26, 3051–3061.

Joliot, P., and Johnson, G.N. (2011). Regulation of cyclic and linear electron flow in higher plants. *Proc. Natl. Acad. Sci.* 108, 13317–13322.

Jurić, S., Hazler-Pilepić, K., Tomašić, A., Lepeduš, H., Jeličić, B., Puthiyaveetil, S., Bionda, T., Vojta, L., Allen, J.F., Schleiff, E., et al. (2009). Tethering of ferredoxin:NADP<sup>+</sup> oxidoreductase to thylakoid membranes is mediated by novel chloroplast protein TROL. *Plant J.* 60, 783–794.

Kanervo, E., Suorsa, M., and Aro, E. (2005). Functional flexibility and acclimation of the thylakoid membrane. *Photochem. Photobiol. Sci.* 4, 1072–1080.

Kar, U.K., Simonian, M., and Whitelegge, J.P. (2017). Integral membrane proteins: bottom-up, top-

down and structural proteomics. *Expert Rev. Proteomics* 14, 715–723.

Karamoko, M., Cline, S., Redding, K., Ruiz, N., and Hamel, P.P. (2011). Lumen Thiol Oxidoreductase1, a Disulfide Bond-Forming Catalyst, Is Required for the Assembly of Photosystem II in Arabidopsis. *Plant Cell* 23, 4462–4475.

Kern, J., and Renger, G. (2007). Photosystem II: Structure and mechanism of the water:plastoquinone oxidoreductase. *Photosynth. Res.* 94, 183–202.

Kieselbach, T., Bystedt, M., Hynds, P., Robinson, C., and Schroder, W.P. (2000). A peroxidase homologue and novel plastocyanin located by proteomics to the Arabidopsis chloroplast thylakoid lumen. *FEBS Lett.* 480, 271–276.

Kirchhoff, H. (2014). Diffusion of molecules and macromolecules in thylakoid membranes. *Biochim. Biophys. Acta - Bioenerg.* 495–502.

Kirchhoff, H., Horstmann, S., and Weis, E. (2000). Control of the photosynthetic electron transport by PQ diffusion microdomains in thylakoids of higher plants. *Biochim. Biophys. Acta - Bioenerg.* 1459, 148–168.

Kleffmann, T., Russenberger, D., Von Zychlinski, A., Christopher, W., Sjölander, K., Gruissem, W., and Baginsky, S. (2004). The *Arabidopsis thaliana* chloroplast proteome reveals pathway abundance and novel protein functions. *Curr. Biol.* 14, 354–362.

Kono, M., Yamori, W., Suzuki, Y., and Terashima, I. (2017). Photoprotection of PSI by far-red light against the fluctuating light-induced photoinhibition in *Arabidopsis thaliana* and field-grown plants. *Plant Cell Physiol.* 58, 35–45.

Koskela, M.M., Brünje, A., Ivanauskaite, A., Grabsztunowicz, M., Lassowskat, I., Neumann, U., Dinh, T. V, Sindlinger, J., Schwarzer, D., Wirtz, M., et al. (2018). Chloroplast Acetyltransferase NSI Is Required for State Transitions in Arabidopsis. *Plant Cell* 30, 1695–1709.

Koskela, M.M., Brünje, A., Ivanauskaite, A., Lopez, L.S., Schneider, D., Detar, R.A., Henning, H., Iris, K., and Paula, F. (2020). Comparative analysis of thylakoid protein complexes in state transition mutants *nsi* and *stn7*: focus on PSI and LHCI. *Photosynth. Res.*

Kouřil, R., Wientjes, E., Bultema, J.B., Croce, R., and Boekema, E.J. (2013). High-light vs. low-light: Effect of light acclimation on photosystem II composition and organization in *Arabidopsis thaliana*. *Biochim. Biophys. Acta - Bioenerg.* 1827, 411–419.

Kovinich, N., Kayanja, G., Chanoca, A., Riedl, K., Otegui, M.S., and Grotewold, E. (2014). Not all anthocyanins are born equal: distinct patterns induced by stress in Arabidopsis. *Planta* 240, 931–940.

Kowalewska, Ł., Suski, S., Garstka, M., and Mostowska, A. (2016). Three-Dimensional Visualization

of the Tubular-Lamellar Transformation of the Internal Plastid Membrane Network during Runner Bean Chloroplast Biogenesis. *Plant Cell* 28, 875–891.

Kowalewska, L., Bykowski, M., and Mostowska, A. (2019). Spatial organization of thylakoid network in higher plants. *Bot. Lett.* 166, 326–343.

Kramer, D.M., and Evans, J.R. (2011). The Importance of Energy Balance in Improving Photosynthetic Productivity. *Plant Physiol.* 155, 70–78.

Kromdijk, J., Glowacka, K., Leonelli, L., Gabilly, S.T., Iwai, M., Niyogi, K.K., and Long, S.P. (2016). Improving photosynthesis and crop productivity by accelerating recovery from photoprotection. *Science.* 354, 857–862.

Külheim, C., Ågren, J., and Jansson, S. (2002). Rapid regulation of light harvesting and plant fitness in the field. *Science.* 297, 91–93.

Kyle, D.J., Staehelin, L.A., and Arntzen, C.J. (1983). Lateral Mobility of the Light-Harvesting Complex in Chloroplast Membranes Controls Excitation Energy Distribution in Higher Plants. *Arch. Biochem. Biophys.* 222, 527–541.

Laganowsky, A., Gómez, S.M., Whitelegge, J.P., and Nishio, J.N. (2009). Hydroponics on a chip: Analysis of the Fe deficient Arabidopsis thylakoid membrane proteome. *J. Proteomics* 72, 397–415.

Leoni, C., Pietrzykowska, M., Kiss, A.Z., Suorsa, M., Ceci, L.R., and Aro, E. (2013). Very rapid phosphorylation kinetics suggest a unique role for Lhcb2 during state transitions in Arabidopsis. 236–246.

Li, Y., Liu, B., Zhang, J., Kong, F., Zhang, L., Meng, H., Li, W., Rochaix, J.D., Li, D., and Peng, L. (2019). OHP1, OHP2, and HCF244 form a transient functional complex with the photosystem II reaction center. *Plant Physiol.* 179, 195–208.

Li, Z., Wakao, S., Fischer, B.B., and Niyogi, K.K. (2009). Sensing and Responding to Excess Light. *Annu. Rev. Plant Biol.* 60, 239–260.

Lin, Y., Huo, L., Liu, Z., Li, J., Liu, Y., He, Q., Wang, X., and Liang, S. (2013). Sodium Laurate, a Novel Protease- and Mass Spectrometry-Compatible Detergent for Mass Spectrometry-Based Membrane Proteomics. *PLoS One* 8.

Liu, J., and Last, R.L. (2017). A chloroplast thylakoid lumen protein is required for proper photosynthetic acclimation of plants under fluctuating light environments. *Proc. Natl. Acad. Sci. U. S. A.* 114, E8110–E8117.

Liu, C., Willmund, F., Whitelegge, J.P., Hawat, S., Knapp, B., Lodha, M., and Schroda, M. (2005). J-Domain Protein CDJ2 and HSP70B Are a Plastidic Chaperone Pair That Interacts with Vesicle-

Inducing Protein in Plastids 1. *Mol. Biol. Cell* 16, 1165.

Liu, W., Tu, W., Liu, Y., Sun, R., Liu, C., and Yang, C. (2016). The N-terminal domain of Lhcb proteins is critical for recognition of the LHCB kinase. *BBA - Bioenerg.* 1857, 79–88.

Liu, X., Zhou, Y., Xiao, J., and Bao, F. (2018). Effects of chilling on the structure, function and development of chloroplasts. *Front. Plant Sci.* 871, 1–10.

Long, T.A., Okegawa, Y., Shikanai, T., Schmidt, G.W., and Covert, S.F. (2008). Conserved role of PROTON GRADIENT REGULATION 5 in the regulation of PSI cyclic electron transport. *Planta* 228, 907–918.

Lu, Y., Hall, D.A., and Last, R.L. (2011). A Small Zinc Finger Thylakoid Protein Plays a Role in Maintenance of Photosystem II in *Arabidopsis thaliana*. *Plant Cell* 23, 1861–1875.

Lucinski, R., Misztal, L., Samardakiewicz, S., and Jackowski, G. (2011a). Involvement of Deg5 protease in wounding-related disposal of PsbF apoprotein. *Plant Physiol. Biochem.* 49, 311–320.

Lucinski, R., Misztal, L., Samardakiewicz, S., and Jackowski, G. (2011b). The thylakoid protease Deg2 is involved in stress-related degradation of the photosystem II light-harvesting protein Lhcb6 in *Arabidopsis thaliana*. *New Phytol.* 192, 74–86.

Lundquist, P.K., Poliakov, A., Bhuiyan, N.H., Zybaïlov, B., Sun, Q., and Wijk, K.J. Van (2012). The Functional Network of the Arabidopsis Plastoglobule Proteome Based on Quantitative Proteomics and Genome-Wide Coexpression Analysis. *Plant Physiol.* 158, 1172–1192.

Lundquist, P.K., Poliakov, A., Giacomelli, L., Friso, G., Appel, M., McQuinn, R.P., Krasnoff, S.B., Rowland, E., Ponnala, L., Sun, Q., et al. (2013). Loss of Plastoglobule Kinases ABC1K1 and ABC1K3 Causes Conditional Degreening, Modified Prenyl-Lipids, and Recruitment of the Jasmonic Acid Pathway. *Plant Cell* 25, 1818–1839.

Malmberg, R.L., Held, S., Waits, A., and Mauricio, R. (2005). Epistasis for fitness-related quantitative traits in *Arabidopsis thaliana* grown in the field and in the greenhouse. *Genetics* 171, 2013–2027.

Malnoë, A., Schultink, A., Shahrabi, S., Rumeau, D., Havaux, M., and Niyogi, K.K. (2018). The Plastid Lipocalin LCNP Is Required for Sustained Photoprotective Energy Dissipation in Arabidopsis. *Plant Cell* 30, 196–208.

Malone, L.A., Qian, P., Mayneord, G.E., Hitchcock, A., Farmer, D.A., Thompson, R.F., Swainsbury, D.J.K., Ranson, N.A., Hunter, C.N., and Johnson, M.P. (2019). Cryo-EM structure of the spinach cytochrome *b<sub>6</sub>f* complex at 3.6 Å resolution. *Nature* 575, 535–542.

Malone, L.A., Proctor, M.S., Hitchcock, A., Hunter, C.N., and Johnson, M.P. (2021). Cytochrome *b<sub>6</sub>f* – Orchestrator of photosynthetic electron transfer. *Biochim. Biophys. Acta - Bioenerg.* 1862, 148380.

- Mann, C.C. (1999). Genetic Engineers Aim to Soup Up Crop Photosynthesis. *Science*. 283, 314–316.
- Martin, W., Goremykin, V., and Hansmann, S. (1998). Gene transfer to the nucleus and the evolution of chloroplasts. *393*, 162–165.
- Martinis, J., Glauser, G., Valimareanu, S., Stettler, M., Zeeman, S.C., and Yamamoto, H. (2014). ABC1K1/PGR6 kinase: a regulatory link between photosynthetic activity and chloroplast metabolism. *Plant J.* 77, 269–283.
- Matsubara, S., and Chow, W.S. (2004). Populations of photoinactivated photosystem II reaction centers characterized by chlorophyll a fluorescence lifetime in vivo. *Proc. Natl. Acad. Sci.* 101, 18234–18239.
- Mazor, Y., Borovikova, A., and Nelson, N. (2015). The structure of plant photosystem I super-complex at 2.8 Å resolution. *Elife* 4, 1–18.
- McFadden, G.I., and Van Dooren, G.G. (2004). Evolution: Red algal genome affirms a common origin of all plastids. *Curr. Biol.* 14, 514–516.
- McKenzie, S.D., Ibrahim, I.M., Aryal, U.K., and Puthiyaveetil, S. (2020). Stoichiometry of protein complexes in plant photosynthetic membranes. *Biochim. Biophys. Acta - Bioenerg.* 1861, 148141.
- Melis, A. (1991). Dynamics of photosynthetic membrane composition and function. *BBA - Bioenerg.* 1058, 87–106.
- Michel, H., Griffin, P.R., Shabanowitz, J., Hunt, D.F., and Bennett, J. (1991). Tandem mass spectrometry identifies sites of three post-translational modifications of spinach light-harvesting chlorophyll protein II: Proteolytic cleavage, acetylation, and phosphorylation. *J. Biol. Chem.* 266, 17584–17591.
- Miller, M.A.E., O’Cualain, R., Selley, J., Knight, D., Karim, M.F., Hubbard, S.J., and Johnson, G.N. (2017). Dynamic Acclimation to High Light in *Arabidopsis thaliana* Involves Widespread Reengineering of the Leaf Proteome. *Front. Plant Sci.* 8, 1–15.
- Mishra, Y., Johansson Jänkänpää, H., Kiss, A.Z., Funk, C., Schröder, W.P., and Jansson, S. (2012). *Arabidopsis* plants grown in the field and climate chambers significantly differ in leaf morphology and photosystem components. *BMC Plant Biol.* 12, 6.
- Miyake, C. (2010). Alternative Electron Flows (Water–Water Cycle and Cyclic Electron Flow Around PSI) in Photosynthesis: Molecular Mechanisms and Physiological Functions. *Plant Cell Physiol.* 51, 1951–1963.
- Moore, S.M., Hess, S.M., and Jorgenson, J.W. (2016). Extraction, Enrichment, Solubilization, and Digestion Techniques for Membrane Proteomics. *J. Proteome Res.* 15, 1243–1252.

- Munekage, Y., Hojo, M., Endo, T., Tasaka, M., and Shikanai, T. (2002). PGR5 Is Involved in Cyclic Electron Flow around Photosystem I and Is Essential for Photoprotection in Arabidopsis. *Cell* 110, 361–371.
- Munekage, Y., Hashimoto, M., Miyake, C., Tomizawa, K.-I., Endo, T., Tasaka, M., and Shikanai, T. (2004). Cyclic electron flow around photosystem I is essential for photosynthesis. *Nature* 579–582, 361–371.
- Murchie, E.H., and Horton, P. (1997). Acclimation of photosynthesis to irradiance and spectral quality in British plant species: Chlorophyll content, photosynthetic capacity and habitat preference. *Plant, Cell Environ.* 20, 438–448.
- Murchie, E.H., and Ruban, A. V. (2020). Dynamic non-photochemical quenching in plants: from molecular mechanism to productivity. *Plant J.* 101, 885–896.
- Myouga, F., Takahashi, K., Tanaka, R., Nagata, N., Kiss, A.Z., Funk, C., Nomura, Y., Nakagami, H., Jansson, S., and Shinozaki, K. (2018). Stable accumulation of photosystem II requires ONE-HELIX PROTEIN1 (OHP1) of the light harvesting-like family. *Plant Physiol.* 176, 2277–2291.
- Nacir, H., and Bréhélin, C. (2013). When proteomics reveals unsuspected roles: the plastoglobule example. *Front. Plant Sci.* 4, 1–8.
- Nandha, B., Finazzi, G., Joliot, P., Hald, S., and Johnson, G.N. (2007). The role of PGR5 in the redox poisoning of photosynthetic electron transport. *BBA* 1767, 1252–1259.
- Nath, K., Jajoo, A., Sharma, R., Timilsina, R., Shin, Y., Aro, E., Gil, H., and Lee, C. (2013). Towards a critical understanding of the photosystem II repair mechanism and its regulation during stress conditions. *FEBS Lett.* 587, 3372–3381.
- Nawrocki, W.J., Bailleul, B., Picot, D., Cardol, P., Rappaport, F., Wollman, F.A., and Joliot, P. (2019). The mechanism of cyclic electron flow. *Biochim. Biophys. Acta - Bioenerg.* 1860, 433–438.
- Nelson, C.J., Alexova, R., Jacoby, R.P., and Harvey Millar, A. (2014). Proteins with high turnover rate in barley leaves estimated by proteome analysis combined with in planta isotope labeling. *Plant Physiol.* 166, 91–108.
- Niedermaier, S., Schneider, T., Bahl, M.O., Matsubara, S., and Huesgen, P.F. (2020). Photoprotective Acclimation of the Arabidopsis thaliana Leaf Proteome to Fluctuating Light. *Front. Genet.* 11, 1–15.
- Norén, H., Svensson, P., Stegmark, R., Funk, C., Adamska, I., and Andersson, B. (2003). Expression of the early light-induced protein but not the PsbS protein is influenced by low temperature and depends on the developmental stage of the plant in field-grown pea cultivars. *Plant, Cell Environ.* 26, 245–253.
- Okegawa, Y., Long, T.A., Iwano, M., Takayama, S., Kobayashi, Y., Covert, S.F., and Shikanai, T.

(2007). A Balanced PGR5 Level is Required for Chloroplast Development and Optimum Operation of Cyclic Electron Transport Around Photosystem I. *Plant Cell Physiol.* *48*, 1462–1471.

Van Oudenhove, L., and Devreese, B. (2013). A review on recent developments in mass spectrometry instrumentation and quantitative tools advancing bacterial proteomics. *Appl. Microbiol. Biotechnol.* *97*, 4749–4762.

Pagliano, C., Nield, J., Marsano, F., Pape, T., Barera, S., Saracco, G., and Barber, J. (2014). Proteomic characterization and three-dimensional electron microscopy study of PSII-LHCII supercomplexes from higher plants. *Biochim. Biophys. Acta - Bioenerg.* *1837*, 1454–1462.

Pan, X., Ma, J., Su, X., Cao, P., Chang, W., Liu, Z., Zhang, X., and Li, M. (2018). Structure of the maize photosystem I supercomplex with light-harvesting complexes I and II. *Science (80-. )*. *360*, 1109–1113.

Pandey, A., Andersen, J.S., and Mann, M. (2000). Use of Mass Spectrometry to Study Signaling Pathways. *Sci. Signal.* *2000*, 1–12.

Peltier, J.-B., Emanuelsson, O., Kalume, D.E., Ytterberg, A.J., Friso, G., Rudella, A., Liberles, D.A., Soderberg, L., Roepstorff, P., von Heijne, G., et al. (2002). Central Functions of the Lumenal and Peripheral Thylakoid Proteome of *Arabidopsis* Determined by Experimentation and Genome-Wide Prediction. *Plant Cell* *14*, 211–236.

Peltier, J.-B., Ytterberg, A.J., Sun, Q., and Wijk, K.J. Van (2004). New Functions of the Thylakoid Membrane Proteome of *Arabidopsis thaliana* Revealed by a Simple, Fast, and Versatile Fractionation Strategy. *J. Biol. Chem.* *279*, 49367–49383.

Peltier, J., Cai, Y., Sun, Q., Zabrouskov, V., Giacomelli, L., Rudella, A., Ytterberg, A.J., Rutschow, H., and Wijk, K.J. Van (2006). The Oligomeric Stromal Proteome of *Arabidopsis thaliana* Chloroplasts. 114–133.

Peng, L., Ma, J., Chi, W., Guo, J., Zhu, S., Lu, Q., Lu, C., and Zhang, L. (2006). LOW PSII ACCUMULATION1 Is Involved in Efficient Assembly of Photosystem II in *Arabidopsis thaliana*. *Plant Cell* *18*, 955–969.

Peng, L., Fukao, Y., Fujiwara, M., Takami, T., and Shikanai, T. (2009). Efficient operation of NAD(P)H dehydrogenase requires supercomplex formation with photosystem I via minor LHCI in *Arabidopsis*. *Plant Cell* *21*, 3623–3640.

Perkins, D.N., Pappin, D.J.C., Creasy, D.M., and Cottrell, J.S. (1999). Probability-based protein identification by searching sequence databases using mass spectrometry data. *Electrophoresis* *20*, 3551–3567.

- Pesaresi, P., Hertle, A., Pribil, M., Kleine, T., Wagner, R., Strissel, H., Lhnatowicz, A., Bonardi, V., Scharfenberg, M., Schneider, A., et al. (2009a). Arabidopsis STN7 kinase provides a link between short- and long-term photosynthetic acclimation. *Plant Cell* 21, 2402–2423.
- Pesaresi, P., Scharfenberg, M., Weigel, M., Granlund, I., Schroder, W.P., Finazzi, G., Rappaport, F., Masiero, S., Furini, A., Jahns, P., et al. (2009b). Mutants, Overexpressors, and Interactors of Arabidopsis Plastocyanin Isoforms: Revised Roles of Plastocyanin in Photosynthetic Electron Flow and Thylakoid Redox State. *Mol. Plant* 2, 236–248.
- Pescheck, F., and Bilger, W. (2019). High impact of seasonal temperature changes on acclimation of photoprotection and radiation-induced damage in field grown Arabidopsis thaliana. *Plant Physiol. Biochem.* 134, 129–136.
- Peter, G.F., and Thornber, J.P. (1991). Biochemical Composition and Organization of Higher Plant Photosystem II Light-harvesting Pigment-Proteins. *J. Biol. Chem.* 266, 16745–16754.
- Petersen, J., Förster, K., Turina, P., and Gräber, P. (2012). Comparison of the H<sup>+</sup>/ATP ratios of the H<sup>+</sup>-ATP synthases from yeast and from chloroplast. *Proc. Natl. Acad. Sci.* 109, 11150–11155.
- Petersen, K., Schöttler, M.A., Karcher, D., Thiele, W., and Bock, R. (2011). Elimination of a group II intron from a plastid gene causes a mutant phenotype. *Nucleic Acids Res.* 39, 5181–5192.
- Pfannschmidt, T., Nilsson, A., Tullberg, A., Link, G., and Allen, J.F. (1999). Direct transcriptional control of the chloroplast genes psbA and psaAB adjusts photosynthesis to light energy distribution in plants. *IUBMB Life* 48, 271–276.
- Pietrzykowska, M., Suorsa, M., Semchonok, D.A., Tikkanen, M., Boekema, E.J., Aro, E.-M., and Jansson, S. (2014). The Light-Harvesting Chlorophyll a/b Binding Proteins Lhcb1 and Lhcb2 Play Complementary Roles during State Transitions in Arabidopsis. *Plant Cell* 26, 3646–3660.
- Piller, L.E., Glauser, G., Kessler, F., and Besagni, C. (2014). Role of plastoglobules in metabolite repair in the tocopherol redox cycle. *Front. Plant Sci.* 5, 1–10.
- Poorter, H., Fiorani, F., Pieruschka, R., Wojciechowski, T., van der Putten, W.H., Kleyer, M., Schurr, U., and Postma, J. (2016). Pampered inside, pestered outside? Differences and similarities between plants growing in controlled conditions and in the field. *New Phytol.* 212, 838–855.
- Porra, R.J., Thompson, W.A., and Kriedemann, P.E. (1989). Determination of accurate extinction coefficients and simultaneous equations for assaying chlorophylls a and b extracted with four different solvents: verification of the concentration of chlorophyll standards by atomic absorption spectroscopy. *Biochim. Biophys. Acta* 975, 384–394.
- Pralon, T., Shanmugabalaji, V., Longoni, P., Glauser, G., Ksas, B., Collombat, J., Desmeules, S.,

- Havaux, M., Finazzi, G., and Kessler, F. (2019). Plastoquinone homeostasis by Arabidopsis proton gradient regulation 6 is essential for photosynthetic efficiency. *Commun. Biol.* 2, 1–11.
- Pribil, M., Pesaresi, P., Hertle, A., Barbato, R., and Leister, D. (2010). Role of plastid protein phosphatase TAP38 in LHCII dephosphorylation and thylakoid electron flow. *PLoS Biol.* 8.
- Pribil, M., Sandoval-ibáñez, O., Xu, W., Sharma, A., Labs, M., Liu, Q., Galgenmuller, C., Schneider, T., Wessels, M., Matsubara, S., et al. (2018). Fine-Tuning of Photosynthesis Requires CURVATURE THYLAKOID1-Mediated Thylakoid Plasticity. *Plant Physiol.* 176, 2351–2364.
- Puthiyaveetil, S., Kavanagh, T.A., Cain, P., Sullivan, J.A., Newell, C.A., Gray, J.C., Robinson, C., Giezen, M. Van Der, Rogers, M.B., and Allen, J.F. (2008). The ancestral symbiont sensor kinase CSK links photosynthesis with gene expression in chloroplasts. *Proc. Natl. Acad. Sci.* 105, 10061–10066.
- Puthiyaveetil, S., Tsabari, O., Lowry, T., Lenhart, S., Lewis, R.R., Reich, Z., and Kirchhoff, H. (2014). Compartmentalization of the protein repair machinery in photosynthetic membranes. *Proc. Natl. Acad. Sci.* 111, 15839–15844.
- Qin, X., Suga, M., Kuang, T., and Shen, J.R. (2015). Structural basis for energy transfer pathways in the plant PSI-LHCI supercomplex. *Science.* 348, 989–995.
- Reiland, S., Finazzi, G., Endler, A., Willig, A., Baerenfaller, K., Grossmann, J., Gerrits, B., Rutishauser, D., Gruissem, W., Rochaix, J.D., et al. (2011). Comparative phosphoproteome profiling reveals a function of the STN8 kinase in fine-tuning of cyclic electron flow (CEF). *Proc. Natl. Acad. Sci. U. S. A.* 108, 12955–12960.
- Rintamäki, E., Salonent, M., Suoranta, U.M., Carlberg, I., Andersson, B., and Aro, E.M. (1997). Phosphorylation of light-harvesting complex II and photosystem II core proteins shows different irradiance-dependent regulation in vivo. *J. Biol. Chem.* 272, 30476–30482.
- Rintamäki, E., Martinsuo, P., Pursiheimo, S., and Aro, E.M. (2000). Cooperative regulation of light-harvesting complex II phosphorylation via the plastoquinol and ferredoxin-thioredoxin system in chloroplasts. *Proc. Natl. Acad. Sci. U. S. A.* 97, 11644–11649.
- Rossini, S., Casazza, A.P., Engelmann, E.C.M., Havaux, M., Jennings, R.C., and Soave, C. (2006). Suppression of Both ELIP1 and ELIP2 in Arabidopsis Does Not Affect Tolerance to Photoinhibition and Photooxidative Stress. *Plant Physiol.* 141, 1264–1273.
- Rosso, D., Bode, R., Li, W., Krol, M., Saccon, D., Wang, S., Schillaci, L.A., Rodermel, S.R., Maxwell, D.P., and Hüner, N.P.A. (2009). Photosynthetic redox imbalance governs leaf sectoring in the *Arabidopsis thaliana* variegation mutants immutans, spotty, var1, and var2. *Plant Cell* 21, 3473–3492.
- Ruban, A. V. (2016). Nonphotochemical Chlorophyll Fluorescence Quenching: Mechanism and

- Effectiveness in Protecting Plants from Photodamage. *Plant Physiol.* 170, 1903–1916.
- Ruban, A. V (2009). Plants in light. *Commun. Integr. Biol.* 2, 50–55.
- Ruban, A. V., and Johnson, M.P. (2009). Dynamics of higher plant photosystem cross-section associated with state transitions. *Photosynth. Res.* 99, 173–183.
- Ruban, A. V., Johnson, M.P., and Duffy, C.D.P. (2012). The photoprotective molecular switch in the photosystem II antenna. *Biochim. Biophys. Acta - Bioenerg.* 1817, 167–181.
- Rumberg, B., Reinwald, E., Schröder, H., and Siggel, U. (1968). Correlation between Electron Flow, Proton Translocation and Phosphorylation in Chloroplasts. *Naturwissenschaften* 55, 77–79.
- Sacharz, J., Giovagnetti, V., Ungerer, P., Mastroianni, G., and Ruban, A. V. (2017). The xanthophyll cycle affects reversible interactions between PsbS and light-harvesting complex II to control non-photochemical quenching. *Nat. Plants* 3, 16225.
- Samol, I., Shapiguzov, A., Ingelsson, B., Fucile, G., Crèvecoeur, M., Vener, A. V., Rochaix, J.D., and Goldschmidt-Clermont, M. (2012). Identification of a photosystem II phosphatase involved in light acclimation in *Arabidopsis*. *Plant Cell* 24, 2596–2609.
- Sato, R., Kono, M., Harada, K., Ohta, H., Takaichi, S., and Masuda, S. (2017). Fluctuating-Light-Acclimation Protein1, conserved in oxygenic phototrophs, regulates H<sup>+</sup> homeostasis and non-photochemical quenching in chloroplasts. *Plant Cell Physiol.* 58, 1622–1630.
- Scheltema, R.A., Hauschild, J.-P., Lange, O., Hornburg, D., Denisov, E., Kuehn, A., Makarov, A., Mann, M., Performance, H., Chromatography, L., et al. (2014). The Q Exactive HF, a Benchtop Mass Spectrometer with a Pre-filter, High Performance Quadrupole and an Ultra-High Field Orbitrap Analyzer. *Mol. Cell. Proteomics* 3698–3708.
- Schneider, A., Steinberger, I., Strissel, H., Kunz, H.H., Manavski, N., Meurer, J., Burkhard, G., Jarzombski, S., Schünemann, D., Geimer, S., et al. (2014). The *Arabidopsis* Tellurite resistance C protein together with ALB3 is involved in photosystem II protein synthesis. *Plant J.* 78, 344–356.
- Schönberg, A., Rödiger, A., Mehwald, W., Galonska, J., Christ, G., Helm, S., Thieme, D., Majovsky, P., Hoehenwarter, W., and Baginsky, S. (2017). Identification of STN7/STN8 kinase targets reveals connections between electron transport, metabolism and gene expression. *Plant J.* 90, 1176–1186.
- Schöttler, M.A., and Tóth, S.Z. (2014). Photosynthetic complex stoichiometry dynamics in higher plants: environmental acclimation and photosynthetic flux control. *Front. Plant Sci.* 5, 188.
- Schreiber, U. (1986). Detection of rapid induction kinetics with a new type of high-frequency modulated chlorophyll fluorometer. *Photosynth. Res.* 9, 261–272.

- Schubert, M., Petersson, U.A., Haas, B.J., Funk, C., Schröder, W.P., and Kieselbach, T. (2002). Proteome map of the chloroplast lumen of *Arabidopsis thaliana*. *J. Biol. Chem.* *277*, 8354–8365.
- Schult, K., Meierhoff, K., Paradies, S., Toller, T., Wolff, P., and Westhoff, P. (2007). The Nuclear-Encoded Factor HCF173 Is Involved in the Initiation of Translation of the *psbA* mRNA in *Arabidopsis thaliana*. *Plant Cell* *19*, 1329–1346.
- Schumann, T., Paul, S., Melzer, M., Dörmann, P., and Jahns, P. (2017). Plant Growth under Natural Light Conditions Provides Highly Flexible Short-Term Acclimation Properties toward High Light Stress. *Front. Plant Sci.* *8*, 1–18.
- Schwahnhäuser, B., Busse, D., Li, N., Dittmar, G., Schuchhardt, J., Wolf, J., Chen, W., and Selbach, M. (2011). Global quantification of mammalian gene expression control. *Nature* *473*, 337–342.
- Seiler, F., Soll, J., and Bölder, B. (2017). Comparative Phenotypal and Molecular Analyses of *Arabidopsis* Grown under Fluorescent and LED Light. *Plants* *6*, 24.
- Selinski, J., and Scheibe, R. (2019). Malate valves: old shuttles with new perspectives. *Plant Biol.* *21*, 21–30.
- Semchuk, N.M., Lushchak, O. V., Falk, J., Krupinska, K., and Lushchak, V.I. (2009). Inactivation of genes, encoding tocopherol biosynthetic pathway enzymes, results in oxidative stress in outdoor grown *Arabidopsis thaliana*. *Plant Physiol. Biochem.* *47*, 384–390.
- Shapiguzov, A., Ingelsson, B., Samol, I., Andres, C., Kessler, F., Rochaix, J.-D., Vener, A. V, and Goldschmidt-Clermont, M. (2010). The PPH1 phosphatase is specifically involved in LHCII dephosphorylation and state transitions in *Arabidopsis*. *Proc. Natl. Acad. Sci. U. S. A.* *107*, 4782–4787.
- Shapiguzov, A., Chai, X., Fucile, G., Longoni, P., Zhang, L., and Rochaix, J.D. (2016). Activation of the Stt7/STN7 Kinase through dynamic interactions with the cytochrome *b6/f* complex. *Plant Physiol.* *171*, 82–92.
- Sheng, X., Watanabe, A., Li, A., Kim, E., Song, C., Murata, K., Song, D., Minagawa, J., and Liu, Z. (2019). Structural insight into light harvesting for photosystem II in green algae. *Nat. Plants* *5*, 1320–1330.
- Shikanai, T. (2016). Chloroplast NDH: A different enzyme with a structure similar to that of respiratory NADH dehydrogenase. *Biochim. Biophys. Acta - Bioenerg.* *1857*, 1015–1022.
- Shikanai, T., Munekage, Y., Shimizu, K., Endo, T., and Hashimoto, T. (1999). Identification and characterization of *Arabidopsis* mutants with reduced quenching of chlorophyll fluorescence. *Plant Cell Physiol.* *40*, 1134–1142.
- Shimakawa, G., and Miyake, C. (2018). Changing frequency of fluctuating light reveals the molecular

- mechanism for P700 oxidation in plant leaves. *Plant Direct* 2, 1–11.
- Shuming, Y.I.N., Xuwu, S.U.N., and Lixin, Z. (2008). An Arabidopsis *ctpA* homologue is involved in the repair of photosystem II under high light. *Chinese Sci. Bull.* 53, 1021–1026.
- Simkin, A.J., McAusland, L., Lawson, T., and Raines, C.A. (2017). Overexpression of the rieskeFeS protein increases electron transport rates and biomass yield. *Plant Physiol.* 175, 134–145.
- Simon, L.M., Kotormán, M., Garab, G., and Laczkó, I. (2001). Structure and Activity of  $\alpha$ -Chymotrypsin and Trypsin in Aqueous Organic Media. *Biochem. Biophys. Res. Commun.* 280, 1367–1371.
- Smith, W.K., Vogelmann, T.C., DeLucia, E.H., Bell, D.T., and Shepherd, K.A. (1997). Leaf Form and Photosynthesis. *Bioscience* 47, 785–793.
- Somerville, C., and Koornneef, M. (2002). A fortunate choice: the history of Arabidopsis as a model plant. *Nat. Rev.* 3, 3–9.
- Stirbet, A., Lazár, D., Guo, Y., and Govindjee (2019). Photosynthesis: Basics, History, and Modeling. *Ann. Bot.* 1–27.
- Strand, D.D., Fisher, N., and Kramer, D.M. (2017). The higher plant plastid NAD(P)H dehydrogenase-like complex (NDH) is a high efficiency proton pump that increases ATP production by cyclic electron flow. *J. Biol. Chem.* 292, 11850–11860.
- Strand, D.D., D’Andrea, L., and Bock, R. (2019). The plastid NAD(P)H dehydrogenase-like complex: Structure, function and evolutionary dynamics. *Biochem. J.* 476, 2743–2756.
- Su, X., Ma, J., Wei, X., Cao, P., Zhu, D., Chang, W., Liu, Z., Zhang, X., and Li, M. (2017). Structure and assembly mechanism of plant C2S2M2-type PSII-LHCII supercomplex. *Science.* 357, 815–820.
- Suorsa, M. (2015). Cyclic electron flow provides acclimatory plasticity for the photosynthetic machinery under various environmental conditions and developmental stages. *Front. Plant Sci.* 6, 1–8.
- Suorsa, M., Järvi, S., Grieco, M., Nurmi, M., Pietrzykowska, M., Rantala, M., Kangasjärvi, S., Paakkarinen, V., Tikkanen, M., Jansson, S., et al. (2012). PROTON GRADIENT REGULATION5 is essential for proper acclimation of Arabidopsis photosystem I to naturally and artificially fluctuating light conditions. *Plant Cell* 24, 2934–2948.
- Suorsa, M., Grieco, M., Järvi, S., Gollan, P.J., Kangasjärvi, S., Tikkanen, M., and Aro, E. (2013). PGR5 ensures photosynthetic control to safeguard photosystem I under fluctuating light conditions. *Plant Signal. Behav.* 8, 167–172.
- Suorsa, M., Rantala, M., Mamedov, F., Lespinasse, M., Trotta, A., Grieco, M., Vuorio, E., Tikkanen,

- M., Järvi, S., and Aro, E.M. (2015). Light acclimation involves dynamic re-organization of the pigment-protein megacomplexes in non-appressed thylakoid domains. *Plant J.* *84*, 360–373.
- Swainston, N., Jameson, D., and Carroll, K. (2011). A QconCAT informatics pipeline for the analysis, visualization and sharing of absolute quantitative proteomics data. *Proteomics* *11*, 329–333.
- Swarbreck, D., Wilks, C., Lamesch, P., Berardini, T.Z., Garcia-Hernandez, M., Foerster, H., Li, D., Meyer, T., Muller, R., Ploetz, L., et al. (2008). The Arabidopsis Information Resource (TAIR): Gene structure and function annotation. *Nucleic Acids Res.* *36*, 1009–1014.
- Tanaka, A., and Makino, A. (2009). Photosynthetic Research in Plant Science. *Plant Cell Physiol.* *50*, 681–683.
- Theis, J., and Schroda, M. (2016). Revisiting the photosystem II repair cycle. *Plant Signal. Behav.* *11*, 1–8.
- Thimijan, R.W., and Heins, R.D. (1983). Photometric, Radiometric, and Quantum Light Units of Measure: A Review of Procedures for Interconversion. *HortScience* *18*, 818–820.
- Tikhonov, A.N. (2014). Plant Physiology and Biochemistry The cytochrome *b<sub>6</sub>f* complex at the crossroad of photosynthetic electron transport pathways. *Plant Physiol. Biochem.* *81*, 163–183.
- Tikkanen, M., and Aro, E.M. (2014). Integrative regulatory network of plant thylakoid energy transduction. *Trends Plant Sci.* *19*, 10–17.
- Tikkanen, M., Piippo, M., Suorsa, M., Sirpiö, S., Mulo, P., Vainonen, J., Vener, A. V., Allahverdiyeva, Y., and Aro, E.-M. (2006). State transitions revisited - A buffering system for dynamic low light acclimation of Arabidopsis. *Plant Mol. Biol.* *62*, 779–793.
- Tikkanen, M., Nurmi, M., Kangasjärvi, S., and Aro, E.M. (2008). Core protein phosphorylation facilitates the repair of photodamaged photosystem II at high light. *Biochim. Biophys. Acta - Bioenerg.* *1777*, 1432–1437.
- Tikkanen, M., Grieco, M., Kangasjärvi, S., and Aro, E.-M. (2010). Thylakoid Protein Phosphorylation in Higher Plant Chloroplasts Optimizes Electron Transfer under Fluctuating Light. *Plant Physiol.* *152*, 723–735.
- Tikkanen, M., Mekala, N.R., and Aro, E. (2014). Photosystem II photoinhibition-repair cycle protects Photosystem I from irreversible damage. *BBA - Bioenerg.* *1837*, 210–215.
- Timperio, A.M., Huber, C.G., and Zolla, L. (2004). Separation and identification of the light harvesting proteins contained in grana and stroma thylakoid membrane fractions. *J. Chromatogr. A* *1040*, 73–81.
- Timperio, A.M., D'Amici, G.M., Barta, C., Loreto, F., and Zolla, L. (2007). Proteomics, pigment

composition, and organization of thylakoid membranes in iron-deficient spinach leaves. *J. Exp. Bot.* *58*, 3695–3710.

Tomizioli, M., Lazar, C., Brugie, S., Burger, T., Salvi, D., Gatto, L., Moyet, L., Breckels, L.M., Hesse, A., Lilley, K.S., et al. (2014). Deciphering Thylakoid Sub-compartments using a Mass Spectrometry-based Approach. *Mol. Cell. Proteomics* *13*, 2147–2167.

Townsend, A.J., Retkute, R., Chinnathambi, K., Randall, J.W.P., Foulkes, J., Carmo-Silva, E., and Murchie, E.H. (2018). Suboptimal acclimation of photosynthesis to light in wheat Canopies. *Plant Physiol.* *176*, 1233–1246.

Trinh, M.D.L., Sato, R., and Masuda, S. (2019). Genetic characterization of a *flap1* null mutation in *Arabidopsis npq4* and *pgr5* plants suggests that the regulatory role of FLAP1 involves the control of proton homeostasis in chloroplasts. *Photosynth. Res.* *139*, 413–424.

Trotta, A., Bajwa, A.A., Mancini, I., Paakkarinen, V., Pribil, M., and Aro, E.M. (2019). The role of phosphorylation dynamics of curvature thylakoid 1B in plant thylakoid membranes. *Plant Physiol.* *181*, 1615–1631.

Tyanova, S., Temu, T., Sinitcyn, P., Carlson, A., Hein, M.Y., Geiger, T., Mann, M., and Cox, J. (2016). The Perseus computational platform for comprehensive analysis of (prote)omics data. *Nat. Methods* *13*, 731–740.

Välikangas, T., Suomi, T., and Elo, L.L. (2018). A systematic evaluation of normalization methods in quantitative label-free proteomics. *Brief. Bioinform.* *19*, 1–11.

Vener, A. V. (2007). Environmentally modulated phosphorylation and dynamics of proteins in photosynthetic membranes. *1767*, 449–457.

Vener, A. V., Van Kan, P.J.M., Rich, P.R., Ohad, I., and Andersson, B. (1997). Plastoquinol at the quinol oxidation site of reduced cytochrome *bf* mediates signal transduction between light and protein phosphorylation: Thylakoid protein kinase deactivation by a single-turnover flash. *Proc. Natl. Acad. Sci. U. S. A.* *94*, 1585–1590.

Vener, A. V., Rokka, A., Fulgosi, H., Andersson, B., and Hermann, R.G. (1999). A cyclophilin-regulated PP2A-like protein phosphatase in thylakoid membranes of plant chloroplasts. *Biochemistry* *38*, 14955–14965.

Vener, A. V., Harms, A., Sussman, M.R., and Vierstra, R.D. (2001). Mass Spectrometric Resolution of Reversible Protein Phosphorylation in Photosynthetic Membranes of *Arabidopsis thaliana*. *J. Biol. Chem.* *276*, 6959–6966.

Violet-Chabrand, S., Matthews, J.S.A., Simkin, A.J., Raines, C.A., and Lawson, T. (2017). Importance

- of Fluctuations in Light on Plant Photosynthetic Acclimation. *Plant Physiol.* *173*, 2163–2179.
- Walters, R.G. (2005). Towards an understanding of photosynthetic acclimation. *J. Exp. Bot.* *56*, 435–447.
- Walters, R.G., and Horton, P. (1994). Acclimation of *Arabidopsis thaliana* to the light environment: Changes in composition of the photosynthetic apparatus. *Planta* *195*, 248–256.
- Wang, J., Yu, Q., Xiong, H., Wang, J., Chen, S., Yang, Z., and Dai, S.D. (2016a). Proteomic insight into the response of *Arabidopsis* chloroplasts to darkness. *PLoS One* *11*, 1–24.
- Wang, Y., Ji, K., Shen, S., and Chen, H. (2016b). Probing molecular events associated with early development of thylakoid membranes by comparative proteomics and low temperature fluorescence. *J. Proteomics* *143*, 401–415.
- Ware, M.A., Belgio, E., and Ruban, A. V. (2015). Photoprotective capacity of non-photochemical quenching in plants acclimated to different light intensities. *Photosynth. Res.* *126*, 261–274.
- Weisz, D.A., Johnson, V.M., Niedzwiedzki, D.M., Shinn, M.K., Liu, H., Klitzke, C.F., Gross, M.L., Blankenship, R.E., Lohman, T.M., and Pakrasi, H.B. (2019). A novel chlorophyll protein complex in the repair cycle of photosystem II. *Proc. Natl. Acad. Sci. U. S. A.* *116*, 21907–21913.
- West, K.R., and Wiskich, J.T. (1968). Photosynthetic Control by Isolated Pea Chloroplasts. *Biochem. J.* *109*, 527–532.
- Whitelegge, J.P. (2003). Thylakoid membrane proteomics. *Photosynth. Res.* *78*, 265–277.
- Wientjes, E., Van Amerongen, H., and Croce, R. (2013a). Quantum yield of charge separation in photosystem II: Functional effect of changes in the antenna size upon light acclimation. *J. Phys. Chem. B* *117*, 11200–11208.
- Wientjes, E., Van Amerongen, H., and Croce, R. (2013b). LHCII is an antenna of both photosystems after long-term acclimation. *Biochim. Biophys. Acta - Bioenerg.* *1827*, 420–426.
- Wiese, S., Reidegeld, K.A., Meyer, H.E., and Warscheid, B. (2007). Protein labeling by iTRAQ: A new tool for quantitative mass spectrometry in proteome research. *Proteomics* *7*, 340–350.
- Wituszyńska, W., Gałazka, K., Rusaczonek, A., Vanderauwera, S., Van Breusegem, F., and Karpiński, S. (2013). Multivariable environmental conditions promote photosynthetic adaptation potential in *Arabidopsis thaliana*. *J. Plant Physiol.* *170*, 548–559.
- Wood, W.H.J., Mayneord, G.E., Hobbs, J.K., Barnett, S.F.H., Huang, X., MacGregor-Chatwin, C., Hunter, C.N., and Johnson, M.P. (2018). Dynamic thylakoid stacking regulates the balance between linear and cyclic photosynthetic electron transfer. *Nat. Plants* *4*, 116–127.

- Wood, W.H.J., Barnett, S.F.H., Flannery, S., Hunter, C.N., and Johnson, M.P. (2019). Dynamic Thylakoid Stacking Is Regulated by LHCII Phosphorylation but Not Its interaction with PSI. *Plant Physiol.* *180*, 2152–2166.
- Wu, X., Oh, M.H., Schwarz, E.M., Larue, C.T., Sivaguru, M., Imai, B.S., Yau, P.M., Ort, D.R., and Huber, S.C. (2011). Lysine acetylation is a widespread protein modification for diverse proteins in *Arabidopsis*. *Plant Physiol.* *155*, 1769–1778.
- Yadav, K.N.S., Semchonok, D.A., Nosek, L., Kouřil, R., Fucile, G., Boekema, E.J., and Eichacker, L.A. (2017). Supercomplexes of plant photosystem I with cytochrome *b<sub>6</sub>f*, light-harvesting complex II and NDH. *Biochim. Biophys. Acta - Bioenerg.* *1858*, 12–20.
- Yamori, W., and Shikanai, T. (2016). Physiological Functions of Cyclic Electron Transport Around Photosystem I in Sustaining Photosynthesis and Plant Growth. *Annu. Rev. Plant Biol.* *67*, 81–106.
- Yamori, W., Shikanai, T., and Makino, A. (2015). Photosystem i cyclic electron flow via chloroplast NADH dehydrogenase-like complex performs a physiological role for photosynthesis at low light. *Sci. Rep.* *5*, 1–9.
- Yamori, W., Makino, A., and Shikanai, T. (2016). A physiological role of cyclic electron transport around photosystem I in sustaining photosynthesis under fluctuating light in rice. *Sci. Rep.* *6*, 1–12.
- Yin, Z.H., and Johnson, G.N. (2000). Photosynthetic acclimation of higher plants to growth in fluctuating light environments. *Photosynth. Res.* *63*, 97–107.
- Yin, L., Vener, A. V., and Spetea, C. (2015). The membrane proteome of stroma thylakoids from *Arabidopsis thaliana* studied by successive in-solution and in-gel digestion. *Physiol. Plant.* *154*, 433–446.
- Yokoyama, R., Yamamoto, H., Kondo, M., Takeda, S., Ifuku, K., Fukao, Y., Kamei, Y., Nishimura, M., and Shikanai, T. (2016). Grana-Localized Proteins, RIQ1 and RIQ2, Affect the Organization of Light-Harvesting Complex II and Grana Stacking in *Arabidopsis*. *Plant Cell* *28*, 2261–2275.
- Youssef, A., Laizet, Y., Block, M.A., Maréchal, E., Alcaraz, J., Larson, T.R., Pontier, D., Gaffe, J., and Kuntz, M. (2010). Plant lipid-associated fibrillin proteins condition jasmonate production under photosynthetic stress. *Plant J.* *61*, 436–445.
- Zancani, M., Braidot, E., Filippi, A., and Lippe, G. (2020). Mitochondrion Structural and functional properties of plant mitochondrial F-ATP synthase. *Mitochondrion* *53*, 178–193.
- Zhang, N., Chen, R., Young, N., Wishart, D., Winter, P., Weiner, J.H., and Li, L. (2007). Comparison of SDS- and methanol-assisted protein solubilization and digestion methods for *Escherichia coli* membrane proteome analysis by 2-D LC-MS/MS. *Proteomics* *7*, 484–493.

- Zhang, Y., Wen, Z., Washburn, M.P., and Florens, L. (2015). Improving label-free quantitative proteomics strategies by distributing shared peptides and stabilizing variance. *Anal. Chem.* 87, 4749–4756.
- Zhao, L., Cong, X., Zhai, L., Hu, H., Xu, J.Y., Zhao, W., Zhu, M., Tan, M., and Ye, B.C. (2020a). Comparative evaluation of label-free quantification strategies. *J. Proteomics* 215, 103669.
- Zhao, Y., Yu, H., Zhou, J.M., Smith, S.M., and Li, J. (2020b). Malate Circulation: Linking Chloroplast Metabolism to Mitochondrial ROS. *Trends Plant Sci.* 25, 446–454.
- Zienkiewicz, M., Ferenc, A., Wasilewska, W., and Romanowska, E. (2012). High light stimulates Deg1-dependent cleavage of the minor LHCII antenna proteins CP26 and CP29 and the PsbS protein in *Arabidopsis thaliana*. *Planta* 235, 279–288.
- Zybailov, B., Rutschow, H., Friso, G., Rudella, A., Emanuelsson, O., Sun, Q., and van Wijk, K.J. (2008). Sorting signals, N-terminal modifications and abundance of the chloroplast proteome. *PLoS One* 3, 1–19.

## Appendices

Table 12: Relative abundance of thylakoid-associated proteins in acclimation. Details of the 401 MS-quantified thylakoid proteins from Arabidopsis plants acclimated to LL, ML and HL, including functional category, protein/gene name, description, UniProtKB identifier, TAIR ID and abundance ratios. Proteins with altered abundance in different light irradiances were identified by a modified one-way ANOVA ( $q < 0.05$ ). Significant proteins were subjected to further statistical analysis to determine significant changes between light conditions by a modified Welch's *t*-test ( $q < 0.05$ ). Median protein iBAQ values for each light condition were used for the calculation of ratios in ML versus LL, HL versus ML, and HL versus LL.

Category	Protein/ gene name	Description	UniProtKB accession	TAIR ID	ANOVA Sig.	ANOVA q-value	ML vs LL			HL vs ML			HL vs LL		
							Ratio	Sig.	q-value	Ratio	Sig.	q-value	Ratio	Sig.	q-value
Assembly	At4g28740	LOW PSII ACCUMULATION-like protein	F4JM22	At4g28740	+	0	1.89	+	0.00425714	1.47	+	0.0138269	2.77	+	0.00190354
Assembly	At5g48790	LOW PSII ACCUMULATION protein	Q94F50;Q9FKB7	AT5G48790	+	0.000548246	2.45	+	0.0146449	1.23	+	0.521021	3.02		0.0037861
Assembly	CCB1	Protein COFACTOR ASSEMBLY OF COMPLEX C SUBUNIT B CCB1	Q9LSE4	AT3G26710	+	0	1.73	+	0.00211236	1.74	+	0.00124771	3.01	+	0.00048
Assembly	CCB2	Protein COFACTOR ASSEMBLY OF COMPLEX C SUBUNIT B CCB2	Q9FJ81	At5g52110		0.144816	0.94			1.05			0.99		
Assembly	CCS1	Cytochrome c biogenesis protein CCS1	Q9XIA4	AT1G49380	+	0.00100103	1.70	+	0.00616034	0.92	+	0.8618	1.57		0.00757212
Assembly	DAC	AT3g17930/MEB5_15	Q94BY7	AT3g17930		0.18787	1.35			0.61			0.82		
Assembly	FFC	Signal recognition particle 54 kDa protein	P37107	AT5G03940	+	0	3.68	+	0.0024381	1.51	+	0.0166541	5.57	+	0.00265502
Assembly	HCF101	Fe-S cluster assembly factor HCF101	Q6STH5	AT3G24430	+	0	4.82	+	0.00064	1.91	+	0.00754515	9.20	+	0.00155634
Assembly	HCF136	Photosystem II stability/assembly factor HCF136	A0A1P8BG37;O82660	AT5G23120	+	3.31492E-05	1.15	+	0.0176034	1.21	+	0.012017	1.39	+	0.00279595
Assembly	HCF164	Thioredoxin-like protein HCF164	O23166	AT4G37200	+	0	0.22	+	0.00217822	0.48	+	0.16094	0.10		0
Assembly	HCF244	NAD(P)-binding Rossmann-fold superfamily protein	O65502	AT4G35250	+	0.000228723	1.08	+	0.0328889	1.34	+	0.0111622	1.44	+	0.00330579
Assembly	LPA2	Protein LOW PSII ACCUMULATION 2	F4KDA6	At5g51545	+	0	0.33	+	0.00138365	0.66	+	0.0620043	0.22		0.000670807
Assembly	LPA3	Protein LOW PSII ACCUMULATION 3	Q8H0W0	AT1G73060	+	0	2.00	+	0.00714911	1.18	+	0.0416115	2.37	+	0.000580645
Assembly	MPH2	Thylakoid luminal 16.5 kDa protein	A0A1P8B5G9;A0A1P8B5H3;O22773	AT4G02530	+	0	1.74	+	0	0.84	+	0.00568935	1.47	+	0.00167851
Assembly	PPD1	PsbP domain-containing protein 1	O23403	AT4G15510	+	0	5.16	+	0	1.35	+	0.000830189	6.96	+	0
Assembly	SECE1	Preprotein translocase subunit SECE1	O23342	AT4G14870	+	0.00276625	1.37	+	0.0145155	1.00	+	0.874498	1.38		0.00556074
Assembly	Y3IP1	Ycf3-interacting protein 1	Q9LU01	AT5G44650	+	0.00058661	1.77	+	0.0135187	1.12	+	0.442039	1.98		0.00492193
Assembly	YCF4	Photosystem I assembly protein Ycf4	P56788	ATCG00520	+	0	1.48	+	0.00277778	1.35	+	0.00469691	2.01	+	0.000907563
ATP synthase	ATPA	ATP synthase subunit alpha	P56757	ATCG00120	+	0	1.80	+	0.001375	1.07	+	0.12719	1.92		0.00219092
ATP synthase	ATPB	ATP synthase subunit beta	P19366	ATCG00480	+	0	1.51	+	0.00294118	1.17	+	0.0217596	1.76	+	0.00216718

ATP synthase	ATPC1	ATP synthase gamma chain 1	Q01908	AT4G04640	+	0	1.41	+	0.00679675	1.29	+	0.0120511	1.82	+	0.00074598 <sub>1</sub>
ATP synthase	ATPD	ATP synthase subunit delta	Q9SSS9	AT4G09650	+	0	1.97	+	0.00207353	1.01	+	0.595902	1.99		0.00190048
ATP synthase	ATPE	ATP synthase epsilon chain	P09468	ATCG00470	+	0	2.01	+	0.00813043	1.21	+	0.355931	2.44		0.00218409
ATP synthase	ATPF	ATP synthase subunit b	P56759	ATCG00130	+	0	1.59	+	0.00289947	1.38	+	0.0246682	2.18	+	0.00307475
ATP synthase	ATPH	ATP synthase subunit c	P56760	ATCG00140	+	0.00752636	95.78		0.0683314	0.78	+	0.58236	75.00		0.00192208
ATP synthase	ATPI	ATP synthase subunit a	P56758	ATCG00150	+	0.014835	0.92		0.781644	1.39		0.0803954	1.28		0.0603482
ATP synthase	PDE334	AT4g32260/F10M6_100	Q42139	AT4G32260	+	0.000264591	0.73	+	0.0123134	1.52	+	0	1.11	+	0.0153777
Carbon fixation	BCA1	Beta carbonic anhydrase 1	A0A1I9LQB3;P27140	AT3G01500	+	0	2.22	+	0.00066666 <sub>7</sub>	3.44	+	0	7.64	+	0.00062069
Carbon fixation	GAPA2	Glyceraldehyde-3-phosphate dehydrogenase GAPA2	A0A1P8APR6;Q9LPW0;F4HNZ6	AT1G12900	+	0	1.53		0.054043	2.78	+	0	4.25	+	0.0005625
Carbon fixation	RBCL	Ribulose bisphosphate carboxylase large chain	O03042	ATCG00490	+	0	1.60	+	0.00740713	2.97	+	0	4.77	+	0.00057446 <sub>8</sub>
Carbon fixation	RBCS-1A	Ribulose bisphosphate carboxylase small chain 1A	P10795	AT1G67090	+	0	3.95	+	0.00399038	2.25	+	0	8.91	+	0.00070129 <sub>9</sub>
Carbon fixation	RBCS-2B	Ribulose bisphosphate carboxylase small chain	B3H5S2;F4KA76;P10797;P10798	AT5G38410	+	0	2.01	+	0.0043653	3.87	+	0	7.76	+	0.00072483 <sub>2</sub>
Carbon fixation	RCA	Ribulose bisphosphate carboxylase/oxygenase activase	F4IVZ7;P10896	AT2G39730	+	0	3.65	+	0	3.45	+	0	12.62	+	0.00055958 <sub>5</sub>
Chloroplast replication	FTSZ1	Cell division protein FtsZ homolog 1	Q42545	AT5G55280	+	0	2.57	+	0.00293834	2.77	+	0	7.12	+	0
Chloroplast replication	FTSZ2-1	Cell division protein FtsZ homolog 2-1	A0A1P8AXD8;O82533	AT2G36250	+	0.000518349	10.34	+	0.0184518	1.02	+	0.596157	10.55		0.00169283
Chloroplast replication	FTSZ2-2	Cell division protein FtsZ homolog 2-2	A0A1I9LSJ8;Q9LXJ0	AT3G52750	+	0	3.18	+	0.00706641	3.18	+	0	10.11	+	0.00054
Chloroplast replication	GC1	Epimerase family protein SDR39U1 homolog	A0A1P8B167;Q9SJU9	AT2G21280	+	0	3.93	+	0.0070397	2.33	+	0.0159285	9.16	+	0.00342156
Chlororespiration	PIFI	Post-illumination chlorophyll fluorescence increase	B3H4M0;F4J037;F4J034;Q9LVZ5;F4J036	At3g15840	+	0.000970954	1.77	+	0.00418735	0.60		0.0227909	1.06	+	0.85156
Cytochrome b6f	PETA	Cytochrome f	P56771	ATCG00540	+	0.000229947	1.20	+	0.0205413	1.18	+	0.00863422	1.42	+	0.00065322 <sub>6</sub>
Cytochrome b6f	PETB	Cytochrome b6	P56773	ATCG00720	+	0	2.54	+	0.0011828	1.25	+	0.0153567	3.18	+	0
Cytochrome b6f	PETC	Cytochrome b6-f complex subunit 4	P56774	ATCG00730	+	3.27869E-05	1.53	+	0.004	0.97	+	0.508149	1.48		0.00073417 <sub>7</sub>
Cytochrome b6f	PETD	Cytochrome b6-f complex iron-sulfur subunit	Q9ZR03	AT4G03280	+	0.00964253	0.90		0.741347	1.17	+	0.0206618	1.05	+	0.0446101
DNA/RNA	At1g07660	Histone H4	P59259;A8MRV1	AT1G07660	+	0	3.65	+	0.00199293	1.96	+	0.00467148	7.15	+	0.00164007
DNA/RNA	At2g21530	SMAD/FHA domain-containing protein	Q8GWP4	AT2G21530	+	0	5.28	+	0.0181538	1.55	+	0.0188235	8.21	+	0.00164925
DNA/RNA	At2g24420	DNA repair ATPase-like protein	Q9ZQ26	AT2G24420	+	0	3.91	+	0.0126	3.08	+	0.00203261	12.07	+	0.00044081 <sub>6</sub>

DNA/RNA	At4g02725	Spindle pole body-associated protein	Q6DBF6	AT4G02725	+	0.00423041	1.22	+	0.00955184	0.53		0.0382787	0.65	+	0.221794
DNA/RNA	CCR1	Glycine-rich RNA-binding protein 8	Q03251	AT4G39260	+	0	2.82	+	0.00259941	2.86	+	0.00182336	8.06	+	0.000776978
DNA/RNA	CCR2	Glycine-rich RNA-binding protein 7	F4IHK9;Q03250	AT2G21660	+	0	4.91	+	0.000857143	1.19	+	0.311099	5.83		0.00239403
DNA/RNA	CP29A	29 kDa ribonucleoprotein	F4JAF3;Q43349	AT3G53460	+	0.000545852	8.61	+	0.0155762	1.48	+	0.0187371	12.76	+	0.00766427
DNA/RNA	CP29B	RNA-binding protein CP29B	Q9ZUU4	AT2G37220	+	0	2.15	+	0.00130178	1.42	+	0.00129524	3.05	+	0.000923077
DNA/RNA	CP31A	31 kDa ribonucleoprotein	Q04836	AT4G24770	+	0	1.24		0.367297	7.01	+	0	8.67	+	0.000377622
DNA/RNA	GYRA	Probable DNA gyrase subunit A/mitochondrial	Q9CAF6	AT3G10690	+	0.000033195	2.90	+	0.0214252	4.77	+	0.00587175	13.83	+	0.00240841
DNA/RNA	H2B	Histone H2B.9	Q9LZ45;Q9ZUS0;Q9LZT0;Q9FFC0;Q9LQQ4;P40283;O23629;Q9SI96;Q9SF55;Q9LFF6	AT1G07790	+	0	2.66	+	0.00112941	1.98	+	0	5.27	+	0
DNA/RNA	IF3-2	Translation initiation factor IF-3	O82234	AT2G24060	+	0	3.98		0.953134	1.78		0.00338767	7.09	+	0.963258
DNA/RNA	IF3-4	Translation initiation factor IF-3	F4JQD8;Q94B52	AT4G30690	+	0.00270439	1.83	+	0.0101735	1.84	+	0.0305968	3.38	+	0.00724364
DNA/RNA	MFP1	MAR-binding filament-like protein 1	Q9LW85	AT3G16000	+	0.00658867	1.03		0.431332	1.25	+	0.131651	1.29		0.0036875
DNA/RNA	PTAC16	Protein PLASTID TRANSCRIPTIONALLY ACTIVE 16	Q9STF2	AT3G46780	+	0.0218533	1.09		0.0915348	0.96	+	0.849131	1.05		0.0408654
DNA/RNA	RAT5	Probable histone H2AXb	Q9S9K7;O04848;Q9LD28;O81826;Q9LHQ5;Q9C681;Q9C944;Q9FJE8;Q94F49	AT1G51060	+	0	2.24	+	0.00412933	2.12	+	0	4.77	+	0
DNA/RNA	rpoA	DNA-directed RNA polymerase subunit alpha	P56762	ATCG00740	+	0	3.09	+	0.0013913	2.19	+	0	6.75	+	0
DNA/RNA	TUFA	Elongation factor Tu	P17745	AT4G20360	+	0	3.13	+	0.000979592	2.46	+	0.00214536	7.68	+	0.00080798
Electron transfer	LFNR1	Ferredoxin--NADP reductase, leaf isozyme 2	C0Z2A8;Q8W493	AT1G20020	+	0	1.04		0.431486	1.47	+	0	1.53	+	0.000715232
Electron transfer	LFNR2	Ferredoxin--NADP reductase, leaf isozyme 1	F4JZ46;Q9FKW6	AT5G66190	+	0	1.31	+	0.012543	1.72	+	0.00101608	2.25	+	0.000603352
Electron transfer	NDC1	Alternative NAD(P)H-ubiquinone oxidoreductase C1/mitochondrial	Q8GXR9	AT5G08740	+	0	1.83	+	0.00124675	1.58	+	0.00103607	2.89	+	0
Electron transfer	PC	Plastocyanin major isoform	P42699	AT1G20340	+	0	0.38	+	0.0024	1.40	+	0.00435229	0.53	+	0.0009
Electron transfer	PGR5	Protein PROTON GRADIENT REGULATION 5	Q9SL05	AT2G05620	+	0.00327831	1.04		0.469274	1.29	+	0.0278794	1.34	+	0.0287396

Electron transfer	PGR6	Uncharacterized aarF domain-containing protein kinase At4g31390	A0A1P8B7P6;Q8RWG1	AT4G31390	+	0	2.13	+	0.00195708	2.07	+	0.00426565	4.42	+	0.00161314	
Electron transfer	PGRL1A	PGR5-like protein 1A	A0A2H1ZEN5;Q8H112	AT4G22890		0.0712756	1.10			1.00			1.10			
Electron transfer	PGRL1B	PGR5-like protein 1B	F4JPU9;Q8GYC7	AT4G11960	+	0	0.97		0.904894	2.09	+	0.00279263	2.03	+	0.00164618	
Electron transfer	TIC62	Protein TIC 62	Q8H0U5	AT3G18890	+	0	1.13		0.169821	1.73	+	0.00875272	1.96	+	0.00075	
Electron transfer	TROL	Rhodanese-like domain-containing protein 4	A0A1P8B8J7;Q9M158	AT4G01050		0.190312	1.00			1.08			1.08			
Ion channel	BASS2	Sodium/pyruvate cotransporter BASS2	Q1EBV7	AT2G26900	+	0	1.91	+	0.0124227	1.85	+	0.00463799	3.54	+	0.000373702	
Ion channel	DIT2-1	Dicarboxylate transporter 2.1	Q9FMF7	AT5G64290	+	0.000562836	1.78	+	0.0149123	6.79	+	0.0284954	12.11	+	0.0134322	
Ion channel	KEA3	K(+) efflux antiporter 3	Q9M0Z3	At4g04850	+	0.00411742	1.10		0.135338	1.43	+	0.345159	1.58		0.00277586	
Ion channel	MNJ8.18	LOW protein: ammonium transporter 1-like protein	Q93Z11	AT5G37360	+	0.0417981	1.29		0.233213	1.03		0.951605	1.33		0.0546197	
Ion channel	TIC110	Protein TIC110	Q8LPR9	AT1G06950	+	0	6.86	+	0.00140127	3.38	+	0	23.15	+	0	
Kinase/phosphatase	At3g59780	Rhodanese/Cell cycle control phosphatase superfamily protein	F4J9G2	At3g59780	+	0.00264453	1.11	+	0.01023	1.02	+	0.480317	1.13		0.0152551	
Kinase/phosphatase	At5g35170	Adenylate kinase 5	F4JYC0;Q8VYL1	AT5G35170	+	0.00042623	1.05		0.841712	1.98	+	0.0153316	2.07	+	0.00469479	
Kinase/phosphatase	PGK1	Phosphoglycerate kinase	Q9LD57;F4J3L1;P50318	AT1G56190	+	0	2.21	+	0.00419718	2.37	+	0	5.22	+	0.000696697	
LHCI	LHCA1	Chlorophyll a-b binding protein 6	A8MS75;F4JE43;F4JE46;Q01667	AT3G54890	+	0.000299492	0.75	+	0.00375979	0.99	+	0.85363	0.74		0.00179242	
LHCI	LHCA2	Photosystem I chlorophyll a/b-binding protein 2	Q9SYW8	AT3G61470	+	0.0146161	0.64		0.171294	1.02		0.55719	0.66		0.0596132	
LHCI	LHCA3	Photosystem I chlorophyll a/b-binding protein 3-1	Q9SY97	AT1G61520	+	0.0496279	0.89		0.479397	0.97		0.521503	0.86		0.133689	
LHCI	LHCA4	Chlorophyll a-b binding protein 4	P27521	AT3G47470		0.0519547	1.07			0.90			0.96			
LHCI	LHCA6	Photosystem I chlorophyll a/b-binding protein 6	Q8LCQ4	AT1G19150		0.107135	0.80			1.18			0.94			
LHCII	LHCB1.1;LHCB1.2;LHCB1.3	Chlorophyll a-b binding protein 1	P04778	AT1G29910	+	0.000936524	1.00			1	0.71	+	0.0111787	0.71	+	0.00249633
LHCII	LHCB1.4	Chlorophyll a-b binding protein	Q39142	AT2G34430	+	0.00412133	0.90		0.0603084	0.90	+	0.308081	0.82		0.00446231	
LHCII	LHCB2	Chlorophyll a-b binding protein 2	A0A1I9LMB4;A0A1P8AZ91;Q9S7J7;Q9SHR7;Q9XF87	AT2G05070	+	3.33333E-05	0.91		0.0700303	0.81	+	0.00552014	0.73	+	0.00102326	
LHCII	LHCB3	Chlorophyll a-b binding protein 3	Q9S7M0	AT5G54270	+	0.0471068	0.92		0.0923777	1.23		0.220176	1.13		1	
LHCII	LHCB4.1 (CP29.1)	Chlorophyll a-b binding protein CP29.1	Q07473	AT5G01530	+	0.00022842	0.79	+	0.0166331	0.84	+	0.0240475	0.66	+	0.000433735	
LHCII	LHCB4.2 (CP29.2)	Chlorophyll a-b binding protein CP29.2	Q9XF88	AT3G08940	+	0	0.84	+	0.00128655	0.89	+	0	0.75	+	0.000782609	
LHCII	LHCB4.3 (CP29.3)	Chlorophyll a-b binding protein CP29.3	F4IGY6;Q9S7W1	AT2G40100	+	0	59.88	+	0.00493246	3.36	+	0	200.90	+	0.000822335	

LHCII	LHCB5 (CP26)	Chlorophyll a-b binding protein CP26	Q9XF89	AT4G10340	+	0	0.58	+	0.00165714	0.96	+	0.409292	0.56		0.00164784
LHCII	LHCB6 (CP24)	Chlorophyll a-b binding protein	Q9LQM2	AT1G15820	+	0.00166499	1.04	+	0.0321802	0.87	+	0.0114875	0.90	+	0.0470835
LHC-like	LiI3.1	Light-harvesting complex-like protein 3 isotype 1	Q9SYX1	AT4G17600	+	0	1.45	+	0.00435535	1.51	+	0.00255158	2.18	+	0.000850394
LHC-like	LiI3.2	Light-harvesting complex-like protein 3 isotype 2	Q6NKS4	AT5G47110	+	0.000448075	1.17	+	0.0180533	1.30	+	0.0196655	1.53	+	0.00191276
LHC-like	OHP1	High-light-induced protein	O81208	AT5G02120	+	0.00323151	1.49	+	0.00709333	0.79	+	0.833783	1.17		0.0329187
LHC-like	OHP2	Light-harvesting complex-like protein OHP2	Q9FEC1	AT1G34000		0.0975212	1.06			0.97			1.03		
Light harvesting regulation	PSBS	Photosystem II 22 kDa protein	F4IEG8;Q9XF91	AT1G44575	+	0	1.40	+	0.010764	1.55	+	0.00221189	2.18	+	0.000760656
Light harvesting regulation	SOQ1	Protein SUPPRESSOR OF QUENCHING 1	Q8VZ10	AT1G56500	+	0	0.96		0.794043	1.43	+	0.00226455	1.37	+	0.000391304
Light harvesting regulation	STN7	Serine/threonine-protein kinase STN7	Q9S713	AT1G68830	+	0.0013885	1.02		0.905568	1.12	+	0.0303242	1.14	+	0.000457627
Light harvesting regulation	STN8	Serine/threonine-protein kinase STN8	Q9LZV4	AT5G01920	+	0.00133741	1.04		1	1.23	+	0.00755779	1.27	+	0.00602927
Light harvesting regulation	TAP38	Protein phosphatase 2C 57	P49599	AT4G27800	+	0.0146029	1.09		0.359691	0.68		0.0779103	0.74		0.0586
Light harvesting regulation	TSP9	Thylakoid soluble phosphoprotein	Q9SD66	AT3G47070		0.0785744	1.01			0.98			0.99		
Light harvesting regulation	VDE1	Violaxanthin de-epoxidase	Q39249	AT1G08550	+	0	2.39	+	0.00112245	0.98	+	0.418534	2.35		0.000782609
Light harvesting regulation	ZEP	Zeaxanthin epoxidase	Q9FGC7	AT5G67030	+	0	0.48	+	0.00210448	1.48	+	0.0161818	0.71	+	0.0032967
NDH	NDHC	NAD(P)H-quinone oxidoreductase subunit 3	P56751	ATCG00440	+	0	3.54	+	0.00765441	0.81	+	0.447727	2.87		0.000631579
NDH	NDHE	NAD(P)H-quinone oxidoreductase subunit 4L	P26289	ATCG01070	+	0.00534836	0.81		0.38303	0.89	+	0.0738824	0.72		0.0244846
NDH	NDHF	NAD(P)H-quinone oxidoreductase subunit 5	P56752	ATCG01010	+	7.57781E-05	2.95	+	0.0042673	0.87	+	0.390894	2.56		0.000857143
NDH	NDHH	NAD(P)H-quinone oxidoreductase subunit H	P56753	ATCG01110	+	0.000390129	3.61	+	0.012788	1.23	+	0.766953	4.44		0.00342623
NDH	NDHI	NAD(P)H-quinone oxidoreductase subunit I	P56755	ATCG01090	+	0	1.43	+	0.00167308	1.32	+	0.0335169	1.89	+	0.002526
NDH	NDHJ	NAD(P)H-quinone oxidoreductase subunit J	P56754	ATCG00420	+	0.000546448	1.40	+	0.00963238	1.34	+	0.0524017	1.87		0.00367792
NDH	NDHK	NAD(P)H-quinone oxidoreductase subunit K	P56756	ATCG00430	+	0.000513636	1.25		0.172554	1.33	+	0.0256835	1.67	+	0.000676385
NDH	NDHM	NAD(P)H-quinone oxidoreductase subunit M	Q2V2S7	AT4G37925	+	0.00984644	1.53	+	0.0329415	0.85	+	0.962763	1.30		0.0298237
NDH	NDHN	NAD(P)H-quinone oxidoreductase subunit N	Q9LVM2	AT5G58260	+	0	2.19	+	0.00261493	0.93	+	0.99029	2.03		0.000648
NDH	NDHO	NAD(P)H-quinone oxidoreductase subunit O	Q9S829	AT1G74880	+	0	2.35	+	0.00117073	1.26	+	0.000814815	2.96	+	0
NDH	NDHS	NAD(P)H-quinone oxidoreductase subunit S	Q9T0A4	AT4G23890	+	0.000525967	0.92		0.989479	2.08	+	0.00822967	1.91	+	0.0030575
NDH	NDHT	NAD(P)H-quinone oxidoreductase subunit T	Q9SMS0	AT4G09350	+	0.0458405	0.89		0.801725	1.58		0.183754	1.41		0.137611
NDH	NDHU	NAD(P)H-quinone oxidoreductase subunit U	Q84VQ4	AT5G21430	+	3.32871E-05	1.66	+	0.00168116	1.23	+	0.0284041	2.05	+	0.0028
NDH	PNSB1	Photosynthetic NDH subunit of subcomplex B 1	Q9S9N6	AT1G15980	+	0.000511312	1.12		0.135382	1.23	+	0.0196416	1.38	+	0.000792176

NDH	PNSB2	Photosynthetic NDH subunit of subcomplex B 2	F4I890;F4I891;Q94AQ8	AT1G64770	+	0.0348127	1.15		0.0623793	1.17		0.75782	1.34		0.111569
NDH	PNSB3	Photosynthetic NDH subunit of subcomplex B 3	Q9LU21	AT3G16250	+	0.000107817	1.67	+	0.0123847	1.35	+	0.0190465	2.25	+	0.00083505 <sub>2</sub>
NDH	PNSB4	Photosynthetic NDH subunit of subcomplex B 4	A0A1P8AS98;F4IC6;Q8RXS1	AT1G18730	+	0.0022549	2.03	+	0.0152642	0.69	+	0.19433	1.41		0.028854
NDH	PNSB5	Photosynthetic NDH subunit of subcomplex B 5	Q9FG89	AT5G43750	+	0.0315784	0.77		0.171105	1.24		0.126785	0.96		0.900314
NDH	PNSL1	Photosynthetic NDH subunit of luminal location 1	O80634	AT2G39470	+	0.000488479	1.22	+	0.00914286	1.05	+	0.328525	1.29		0.0015536
NDH	PNSL2	Photosynthetic NDH subunit of luminal location 2	Q9XI73	AT1G14150	+	0	2.67	+	0.00164151	1.05	+	0.148598	2.79		0
NDH	PNSL3	Photosynthetic NDH subunit of luminal location 3	Q9SGH4	AT3G01440	+	0.00137652	1.44	+	0.00157466	1.09	+	0.668601	1.56		0.0129725
NDH	PNSL4	Photosynthetic NDH subunit of luminal location 4	F4JW56;Q9SCY3	AT4G39710	+	0	1.58	+	0.00115663	1.17	+	0.062831	1.85		0.00303621
NDH	PNSL5	Photosynthetic NDH subunit of luminal location 5	Q9ASS6	AT5G13120	+	0.0442667	0.74		0.613749	1.31		0.0990709	0.97		0.355345
Other/unknown	AAC1	ADP,ATP carrier protein 1	P31167	AT3G08580	+	0	6.58	+	0	2.97	+	0	19.54	+	0
Other/unknown	AAC2	ADP,ATP carrier protein 2	P40941	AT5G13490		1	5.38			10.25			55.19		
Other/unknown	accD	Acetyl-coenzyme A carboxylase carboxyl transferase subunit beta	P56765	ATCG00500	+	0	2.32	+	0.00375	2.65	+	0	6.15	+	0.00086631
Other/unknown	AOC2	Allene oxide cyclase 2	Q9LS02	AT3G25770	+	0	7.76	+	0.00067132 <sub>9</sub>	1.01	+	0.652621	7.83		0.00072809
Other/unknown	APG3	Peptide chain release factor APG3	Q8RX79	AT3G62910	+	0	3.30	+	0.0101252	2.73	+	0.00185507	9.01	+	0.00045188 <sub>3</sub>
Other/unknown	APXT	L-ascorbate peroxidase T	A0A1P8APU0;Q42593	AT1G77490		0.067934	1.08			1.05			1.13		
Other/unknown	At1g24360	3-oxoacyl-[acyl-carrier-protein] reductase	P33207	AT1G24360	+	0	10.90	+	0	10.36	+	0	112.9 <sub>6</sub>	+	0.00041538 <sub>5</sub>
Other/unknown	At1g33810	Zinc finger/BTB domain protein	Q8L9M8	AT1G33810	+	0	11.69	+	0.00883099	2.90	+	0.00440074	33.94	+	0.00166164
Other/unknown	At1g52510	Alpha/beta-Hydrolases superfamily protein	Q8VZ57;F4ICZ4	AT1G52510	+	0	4.89	+	0.0012973	1.41	+	0	6.88	+	0
Other/unknown	At1g54520	Myelin-associated oligodendrocyte basic protein	Q8RWI0	At1g54520	+	0.000302177	2.03	+	0.014956	1.44	+	0.0739581	2.93		0.00049315 <sub>1</sub>
Other/unknown	At1g72640	NAD(P)-binding Rossmann-fold superfamily protein	A0A1P8AVW7;F4IDE8;Q6NMC1;A0A1P8AW09	AT1G72640	+	0.000370192	6.10	+	0.0103694	2.04	+	0.0108546	12.43	+	0.00187639
Other/unknown	At1g73110	p-loop containing nucleoside triphosphate hydrolases superfamily protein	A0A1P8ATD8;Q9AST9	AT1G73110	+	0.000227213	5.35	+	0.00374026	2.69	+	0.0166332	14.36	+	0.004595
Other/unknown	At1g78915	Tetratricopeptide repeat (TPR)-like superfamily protein	Q8GWV1;F4IBX4;F4IBX5	AT1G78915	+	0.00271081	1.94	+	0.00947119	1.16	+	0.351733	2.24		0.0182405
Other/unknown	At2g05310	Expressed protein	Q9SJ31	AT2G05310	+	0.00593657	0.68	+	0.0244265	1.04	+	0.882871	0.71		0.0213909
Other/unknown	At2g17972	Transmembrane protein	Q8S8K0	AT2G17972	+	0.00164257	1.32		0.0501988	1.26	+	0.12011	1.65		0.0214146
Other/unknown	At2g27290	FAM210B-like protein, putative (DUF1279)	Q9XIN6	AT2G27290	+	0.00349285	0.42	+	0.00280899	1.24		0.278379	0.52		0.0686667
Other/unknown	At2g27680	NAD(P)-linked oxidoreductase superfamily protein	Q9ZUX0	AT2G27680	+	0	4.11	+	0.00076190 <sub>5</sub>	1.66	+	0.00788852	6.84	+	0.00143667

Other/unknown	At2g41040	Uncharacterized methyltransferase At2g41040	Q0WPT7	AT2G41040	+	0	2.97	+	0.0021283	2.57	+	0.00217259	7.63	+	0.00072
Other/unknown	At3g43540	Initiation factor 4F subunit	F4I256;Q9M236	AT3G43540	+	0	1.97	+	0.00652066	1.81	+	0.00206763	3.58	+	0.000516746
Other/unknown	At3g61870	Plant/protein	F4IX01;Q9M277	AT3G61870	+	0.000854167	1.02		0.720525	1.32	+	0.0159277	1.35	+	0.00250368
Other/unknown	At4g28025	Uncharacterized protein At4g28025	F4JKG2;Q9C5F3	AT4G28025	+	0.0054794	1.53	+	0.0477639	1.39	+	0.265525	2.12		0.0047182
Other/unknown	At5g08680	ATP synthase subunit beta-2	P83484;P83483;Q9C5A9	AT5G08670	+	0	1.79	+	0.0214821	3.18	+	0.00841762	5.69	+	0.00157857
Other/unknown	At5g14910	Heavy metal transport/detoxification superfamily protein	Q93VK7	AT5G14910	+	0	3.27	+	0.00110553	1.67	+	0.0028186	5.45	+	0.000648045
Other/unknown	At5g51010	Rubredoxin-like superfamily protein	Q9FI47	AT5G51010	+	0	0.26	+	0.000695652	4.31		0	1.12	+	0.652608
Other/unknown	CAC3	Acetyl-coenzyme A carboxylase carboxyl transferase subunit alpha	Q9LD43	AT2G38040	+	0	2.99	+	0.00189262	2.41	+	0	7.19	+	0.000420233
Other/unknown	CAS	Calcium sensing receptor	A0A1P8BCX7;Q9FN48	AT5G23060	+	0	1.40	+	0.00168421	1.66	+	0.00448393	2.32	+	0.000645418
Other/unknown	CHL	Chloroplastic lipocalin, AtCHL	Q9STS7	AT3G47860	+	0.000509009	0.66	+	0.0036	0.58	+	0.161876	0.38		0.005164
Other/unknown	DiT1	Dicarboxylate transporter 1	B3H4S6;Q9LXV3	AT5G12860	+	0	1.57	+	0.00491106	3.27	+	0	5.15	+	0
Other/unknown	EMB3003	Dihydrolipoyllysine-residue acetyltransferase component 5 of pyruvate dehydrogenase complex	Q9C8P0	AT1G34430	+	0.0377319	0.74		0.498675	1.61		0.214549	1.20		0.310207
Other/unknown	F13A11.2	Inner membrane localized protein	Q9C7S3	AT1G42960	+	0.000566486	4.28	+	0.00397129	3.87	+	0.0332262	16.57	+	0.0116536
Other/unknown	F16M2_10	AT3g63160/F16M2_10	Q9M1X3	AT3G63160	+	0.0246916	0.89		0.984318	1.31		0.127187	1.16		0.0720168
Other/unknown	F1N21.10	Probable lactoylglutathione lyase, chloroplast	Q8W593	AT1G67280	+	0	2.46	+	0	1.65	+	0.0086072	4.06	+	0.000855446
Other/unknown	F24J8.11	F24J8.11 protein	Q9LPK9	AT1G21500	+	0.00643494	0.41		0.103184	0.39	+	0.0924256	0.16		0.0430065
Other/unknown	F26O13.150	Transmembrane protein	Q9SCZ8	AT3G51510		0.0688361	0.77			1.52			1.16		
Other/unknown	F4P12_170	2,3-bisphosphoglycerate-independent phosphoglycerate mutase	Q9LFH1;F4JAF4	AT3G53470	+	0	1.32	+	0.0193279	1.40	+	0.00975191	1.85	+	0
Other/unknown	F6N7.27	Uncharacterized protein PAM68-like	Q9LTD9	AT5G52780	+	0.004377	2.87		0.0912511	1.03	+	0.673104	2.97		0.0376466
Other/unknown	FAB2	Acyl-[acyl-carrier-protein] desaturase	F4IS32;O22832;Q9LF04;Q9M879	AT2G43710	+	0	9.58	+	0.00720309	4.14	+	0	39.68	+	0.000376307
Other/unknown	FBA1	Fructose-bisphosphate aldolase	F4IGL5;F4IGL7;Q9SJJ4	AT2G01140	+	0	1.76	+	0.00312632	2.96	+	0	5.20	+	0
Other/unknown	FBA2	Fructose-bisphosphate aldolase	F4JUU5;Q944G9	AT4G38970	+	0	2.06	+	0.00096	1.76	+	0.00453818	3.63	+	0.000649299
Other/unknown	GDCST	Aminomethyltransferase	A0A2H1ZEA9;O65396	AT1G11860	+	0	13.84	+	0.0036272	3.66	+	0	50.63	+	0.000640884
Other/unknown	GER3	Germin-like protein subfamily 3 member 3	P94072	AT5G20630	+	0	2.71	+	0.00420706	2.28	+	0.0166751	6.19	+	0.00355435
Other/unknown	GLDP1	Glycine dehydrogenase (decarboxylating) 1	Q94B78;B3H5Y8	AT4G33010	+	0	16.49	+	0.00222047	3.18	+	0.00432847	52.39	+	0.00157295

Other/unknown	GLN2	Glutamine synthetase/mitochondrial	Q43127	AT5G35630	+	0	1.17		0.156391	2.21	+	0.00260993	2.58	+	0.000659878
Other/unknown	GLO1	(S)-2-hydroxy-acid oxidase GLO1	Q2V3V9;Q9LRR9;A8MS37;B3H4B8	AT3G14420	+	0	3.80	+	0.00274608	3.39	+	0.00125153	12.90	+	0.00077512
Other/unknown	LOX2	Lipoxygenase 2	P38418;A0A119LPH1	AT3G45140	+	0	7.09	+	0.00162712	1.53	+	0	10.86	+	0
Other/unknown	LTA2	Dihydrolipoylysine-residue acetyltransferase component 4 of pyruvate dehydrogenase complex	Q9SQI8	AT3G25860	+	0	1.43		0.225062	1.98	+	0.00126316	2.82	+	0.00081203
Other/unknown	LTA3	Dihydrolipoylysine-residue acetyltransferase component 1 of pyruvate dehydrogenase complex	F4J5T2;Q0WQF7	AT3G52200	+	0	2.39	+	0.00208118	2.58	+	0.0055493	6.18	+	0.00167003
Other/unknown	MBB18.5	Alpha/beta-Hydrolases superfamily protein	Q9FFW9;F4KBJ3	AT5G38520	+	0.00333906	1.17	+	0.0125122	1.13	+	0.26276	1.32		0.0137904
Other/unknown	MJC20.18	Uncharacterized protein At5g42070	Q8RWR9	AT5G42070	+	0	1.71	+	0.0108312	2.77	+	0	4.73	+	0
Other/unknown	TL17	Thylakoid luminal 17.4 kDa protein	A0A1P8BAQ0;F4JX83;P81760	AT5G53490	+	0.000560428	0.35	+	0.0211322	0.87	+	0.135101	0.30		0.00806198
Other/unknown	MQB2.4	Integral membrane HPP family protein	F4K7S5;Q8GZ51	AT5G62720	+	0.0013591	7.79	+	0.000635762	1.49	+	0.275996	11.59		0.0287808
Other/unknown	MRO11.7	GPI-anchored adhesin-like protein	A0A1P8BAU8;Q9FF91	AT5G23890	+	0	14.32	+	0	2.67	+	0.00466306	38.20	+	0.00100763
Other/unknown	MTG13.11	Low-density receptor-like protein	A8MS48;Q8H0X5	AT5G16660	+	0.00128425	1.43	+	0.0264481	2.48	+	0.0572805	3.54		0.0134629
Other/unknown	MVA3.2	Alpha/beta-Hydrolases superfamily protein	Q9FN84	AT5G17670	+	0.0132826	5.02	+	0.0214536	0.73		0.516409	3.66		0.0619767
Other/unknown	NAGK	Acetylglutamate kinase	Q9SCL7	AT3G57560	+	0	2.51	+	0.000744186	1.45	+	0.00849289	3.65	+	0.000731377
Other/unknown	OEP161	Outer envelope pore protein 16-1	Q9ZV24	AT2G28900	+	0.000107962	0.89		0.998102	2.05	+	0.00334118	1.82	+	0.00178654
Other/unknown	PLGG1	Plastidal glycolate/glycerate translocator 1	Q9FVQ4	AT1G32080	+	0	5.20	+	0.00187654	2.34	+	0.00216162	12.18	+	0.000733032
Other/unknown	PLR1	Pyridoxal reductase	Q56Y42	AT5G53580	+	0.000301405	2.67	+	0.00569492	0.97	+	0.806618	2.58		0.00372142
Other/unknown	PMDH2	Malate dehydrogenase	F4KDZ4;Q9ZP05;A0A1P8BBQ0;A8MRP1;B3H560	AT5G09660	+	0	5.55	+	0.00204484	6.20	+	0.00177778	34.38	+	0.0008
Other/unknown	PTAC5	Protein disulfide isomerase pTAC5	A0A1P8B4I3;A1A6M1	AT4G13670	+	0.000371084	1.59		0.0808037	1.85	+	0.0133388	2.93	+	0.00450761
Other/unknown	RPI3	Probable ribose-5-phosphate isomerase 3	Q9S726	AT3G04790	+	0	2.15	+	0.00881547	2.40	+	0.00100958	5.16	+	0.000455696
Other/unknown	STR10	Rhodanese-like domain-containing protein 10	Q9SR92	AT3G08920	+	0.00323773	1.19	+	0.0124037	0.72		0.0157873	0.86	+	0.895821
Other/unknown	STR11	Rhodanese-like domain-containing protein 11	Q0WWT7	At4g24750	+	0	1.15	+	0.00213636	1.25	+	0.0153516	1.44	+	0.00245636
Other/unknown	STR14	Rhodanese-like domain-containing protein 14	Q94A65	AT4G27700	+	0.000392435	1.37	+	0.0102736	1.10	+	0.0426534	1.50	+	0.00161609
Other/unknown	STR4A	Rhodanese-like domain-containing protein 4A	Q56XR7	AT3G25480	+	0.000378844	1.74	+	0.00109091	1.23	+	0.173032	2.14		0.00517037
Other/unknown	STR9	Rhodanese-like domain-containing protein 9	O48529	AT2G42220	+	0.000346299	0.77	+	0.00195156	0.96	+	0.993986	0.74		0.0030661
Other/unknown	T10O22.3	Microbial collagenase	Q9LM40	AT1G18060	+	0	2.32	+	0	2.21	+	0.0118486	5.13	+	0.0025

Other/unknown	T4M8.15	Uncharacterized protein At2g03420/T4M8.15	Q9ZQ78	AT2G03420	+	0.000389215	1.63	+	0.00780987	0.80	+	0.0279398	1.30	+	0.00759036
Other/unknown	T6G15.50	Transmembrane protein	Q9T0H1	AT4G13500	+	0.0304206	0.88		0.0756678	1.21		0.135547	1.06		0.891633
Other/unknown	TIC214	Protein TIC 214	P56785	ATCG01130	+	0.000559232	0.03	+	0.0240783	2.84	+	0.016819	0.10	+	0.016528
Other/unknown	TIC55	Protein TIC 55	Q9SK50	AT2G24820	+	0	1.94	+	0.00472566	2.84	+	0	5.50	+	0.00065454 5
Other/unknown	TL15A	Thylakoid luminal 15 kDa protein 1	O22160	AT2G44920	+	0.0152793	1.58		0.0617851	1.00	+	0.982024	1.58		0.0356757
Other/unknown	TL17.9	Thylakoid luminal 17.9 kDa protein	Q9SW33	AT4G24930	+	0.000298734	1.97	+	0.0105455	1.10	+	0.898362	2.17		0.00241203
Other/unknown	TL19	Thylakoid luminal 19 kDa protein	P82658	At3g63540		0.05655	1.39			0.80			1.10		
Other/unknown	TL20.3	Thylakoid luminal protein TL20.3	A0A178W1 Q3;B6EUA5; Q8H1Q1	AT1G12250	+	0.000570806	1.55	+	0.0124932	1.06	+	1	1.65		0.00170154
Other/unknown	TPT	Triose phosphate/phosphate translocator TPT	A0A219HYB 6;A0A219HZ H3;A0A219I 0W9;Q9ZSR 7	AT5G46110	+	0	0.86		0.0972318	2.36	+	0	2.03	+	0
Other/unknown	YCF37	Homolog of Synechocystis YCF37	O64835	AT2G23670	+	0	1.03		0.38867	1.24	+	0.00291959	1.28	+	0.00070948
Pigment synthesis	CAO	Chlorophyllide a oxygenase	Q9MBA1	AT1G44446	+	0.00240313	1.31	+	0.0124552	1.26		0.947679	1.65		0.864886
Pigment synthesis	CHLD	Magnesium-chelatase subunit ChLD	Q9SJE1	AT1G08520	+	0	8.04	+	0.00417757	3.53	+	0	28.35	+	0
Pigment synthesis	CHLG	Chlorophyll synthase	Q38833	AT3G51820	+	0.0224486	1.03		0.65232	1.61		0.0603415	1.65		0.222501
Pigment synthesis	CHLH	Magnesium-chelatase subunit ChIH	A8MR05;Q9 FNBO	AT5G13630	+	0	4.11	+	0.00197403	2.11	+	0.0012439	8.68	+	0.00085039 4
Pigment synthesis	CHL1	Magnesium-chelatase subunit ChII	P16127;Q5X F33	AT4G18480	+	0	3.52	+	0	2.01	+	0	7.07	+	0
Pigment synthesis	CHLM	Magnesium protoporphyrin IX methyltransferase	A0A1P8B4G 1;Q9SW18	AT4G25080	+	0	0.69	+	0.00290698	0.91	+	0.317456	0.63		0.00068644 1
Pigment synthesis	CHLP	Geranylgeranyl diphosphate reductase	Q9CA67	AT1G74470	+	0	2.16	+	0.00157377	1.29	+	0.00222917	2.79	+	0.00051428 6
Pigment synthesis	CRD1	Magnesium-protoporphyrin IX monomethyl ester [oxidative] cyclase	F4J0U9;Q9 M591	AT3G56940	+	0	1.98	+	0.00120879	1.26	+	0.0053975	2.49	+	0.00051923 1
Pigment synthesis	CYP97B3	Cytochrome P450 97B3	O23365	AT4G15110	+	0	2.39	+	0.00289855	1.50	+	0.0109021	3.59	+	0.00074121 4
Pigment synthesis	CYP97C1	Carotene epsilon-monoxygenase	Q6TBX7	At3g53130	+	0	3.18	+	0.00133333	1.30	+	0.0158074	4.12	+	0.00084816 8
Pigment synthesis	DVR	Divinyl chlorophyllide a 8-vinyl-reductase	Q1H537	AT5G18660	+	0	1.94	+	0.00364557	1.42	+	0.00278621	2.75	+	0.00075348 8
Pigment synthesis	FC2	Ferrochelatase	F41MT3;O04 921	AT2G30390	+	0.000230254	2.54	+	0.00366412	0.72	+	0.0257136	1.84	+	0.00314365
Pigment synthesis	GUN4	Tetrapyrrole-binding protein	Q9LX31	AT3G59400	+	0	3.24	+	0.00271739	1.44	+	0.00970898	4.65	+	0.00069230 8
Pigment synthesis	HCAR	7-hydroxymethyl chlorophyll a reductase	Q8GS60	AT1G04620	+	0.00335187	0.60		0.10381	0.60	+	0.126912	0.36		0.00460652

Pigment synthesis	LUT5	Protein LUTEIN DEFICIENT 5	Q93VK5	AT1G31800	+	0.00034717	3.93		0.0571116	1.86	+	0.0122297	7.30	+	0.00239046
Pigment synthesis	PAO	Pheophorbide a oxygenase	Q9FYC2	AT3G44880	+	0.00056833	1.36	+	0.00612159	1.04	+	0.351328	1.42		0.00314799
Pigment synthesis	PDS	15-cis-phytoene desaturase/chromoplastic	Q07356	AT4G14210	+	0.000564655	1.06		0.383086	1.24	+	0.0317098	1.31	+	0.00050704 2
Pigment synthesis	PORB	Protochlorophyllide reductase B	P21218	AT4G27440	+	0	1.87	+	0.00265455	0.59	+	0.00441713	1.11	+	0.0458435
Pigment synthesis	PORC	Protochlorophyllide reductase C	F412F8;O48741	AT1G03630	+	0.000571429	1.65	+	0.0213968	1.08	+	0.991948	1.78		0
Pigment synthesis	PPOX1	Protoporphyrinogen oxidase 1	P55826	AT4G01690	+	0	1.60	+	0.00069064 7	1.15	+	0.0485109	1.84	+	0.0024048
Pigment synthesis	YCF54	EMBRYO DEFECTIVE 3143	Q9LVM3	AT5G58250	+	0	2.79	+	0.00164929	1.22	+	0.0263823	3.39	+	0.00069379
Plastoglobule	ABC1K3	Uncharacterized aarF domain-containing protein kinase At1g79600	Q9MA15	AT1G79600	+	0	1.77	+	0.0275792	2.49	+	0	4.40	+	0.00083076 9
Plastoglobule	At1g06690	Uncharacterized oxidoreductase At1g06690	Q94A68	AT1G06690	+	0	8.61	+	0.00234146	1.63	+	0.0235244	14.04	+	0.00248175
Plastoglobule	At1g32220	Uncharacterized protein At1g32220	Q9FVR6	AT1G32220	+	0	1.27		0.30756	2.52	+	0.00213466	3.19	+	0.0019252
Plastoglobule	At1g54570	Acyltransferase-like protein At1g54570	Q9ZVN2	AT1G54570	+	0	1.88	+	0.0211604	3.61	+	0.00445028	6.77	+	0.00101538
Plastoglobule	At1g71810	Uncharacterized aarF domain-containing protein kinase At1g71810	Q94BU1	AT1G71810	+	0	3.22	+	0.00065306 1	1.73	+	0.00254622	5.58	+	0.00073804 1
Plastoglobule	At2g34460	Uncharacterized protein At2g34460	Q8H124	AT2G34460	+	0	1.46	+	0.00901718	1.46	+	0.00322244	2.13	+	0
Plastoglobule	At4g13200	Uncharacterized protein At4g13200	Q8LDV3	AT4G13200	+	0	0.96		0.117342	2.13	+	0	2.04	+	0.001625
Plastoglobule	At5g05200	Uncharacterized aarF domain-containing protein kinase At5g05200	Q9ASX5	AT5G05200	+	0	2.58		0.546423	10.51	+	0.00976687	27.16	+	0.00375597
Plastoglobule	CCD4	Probable carotenoid cleavage dioxygenase 4	O49675	AT4G19170	+	0.00833119	0.80		0.657728	1.55	+	0.0519135	1.24		0.00849763
Plastoglobule	CSP41B	Chloroplast stem-loop binding protein of 41 kDa b	A0A1P8ATL2;Q9SA52	AT1G09340	+	0	1.59	+	0.0037555	3.20	+	0	5.07	+	0
Plastoglobule	CYP74A	Allene oxide synthase	Q96242	AT5G42650	+	0	1.06	+	0.0405617	1.94	+	0	2.06	+	0.00040909 1
Plastoglobule	PAP1	Probable plastid-lipid-associated protein 1	O81439	AT4G04020	+	0	1.14	+	0.0496595	5.13	+	0	5.83	+	0.00053731 3
Plastoglobule	PAP10	Probable plastid-lipid-associated protein 10	Q8W4F1	AT2G46910	+	0	3.10	+	0.00438532	2.29	+	0	7.09	+	0.00068842 7
Plastoglobule	PAP11	Probable plastid-lipid-associated protein 11	O81304	AT4G00030	+	0.000448598	3.07	+	0.031609	1.12	+	0.177779	3.44		0.00070282
Plastoglobule	PAP12	Probable plastid-lipid-associated protein 12	Q8LAP6	AT1G51110	+	0	1.24	+	0.00213592	1.46	+	0.0020271	1.80	+	0.00074311 9
Plastoglobule	PAP13	Probable plastid-lipid-associated protein 13	A8MRU9;F4IM05;Q8S9M1	AT2G42130	+	0.000972973	0.26	+	0.0181285	4.29		0.0118832	1.13	+	0.884335
Plastoglobule	PAP2	Probable plastid-lipid-associated protein 2	O49629	AT4G22240	+	0	2.06	+	0.00075	4.11	+	0	8.46	+	0
Plastoglobule	PAP3	Probable plastid-lipid-associated protein 3	O82291	AT2G35490	+	0	1.40	+	0.0027027	2.23	+	0.00209291	3.12	+	0.00074141 9
Plastoglobule	PAP4	Probable plastid-lipid-associated protein 4	Q9LU85	AT3G26070	+	0	0.89		0.430368	1.79	+	0.00102597	1.59	+	0.00068354 4

Plastoglobule	PAP5	Probable plastid-lipid-associated protein 5	A0A1I9LP70;Q6DBN2	AT3G26080	+	0.000382609	1.30		0.457346	1.53	+	0.117468	1.98		0.000624277
Plastoglobule	PAP6	Probable plastid-lipid-associated protein 6	A0A1I9LQU3;A0A1I9LQU5;Q9LW57	AT3G23400	+	0	1.44	+	0.00271207	1.21	+	0.0026755	1.74	+	0.000675
Plastoglobule	PAP8	Probable plastid-lipid-associated protein 8	F4K2P2;Q941D3	AT5G19940	+	0.00572123	1.25	+	0.0125619	0.96	+	0.579242	1.19		0.0302826
Plastoglobule	PAP9	Probable plastid-lipid-associated protein 9	Q9M2P7	AT3G58010	+	0.000819328	0.60	+	0.0204858	0.87	+	0.226697	0.52		0.00143396
Plastoglobule	PLAT1	PLAT domain-containing protein 1	O65660	AT4G39730	+	0	2.27	+	0.007192	3.02	+	0	6.85	+	0.000668588
Plastoglobule	PSY	PHYTOENE SYNTHASE	F4KGX7;P37271	AT5G17230	+	0.00081761	5.97	+	0.0163699	0.52	+	0.066836	3.13		0.000736508
Plastoglobule	T22K18.4	Heme-binding-like protein At3g10130	Q9SR77	AT3G10130	+	0	2.42	+	0.002256	1.78	+	0.0193382	4.29	+	0.00303199
Plastoglobule	VTE1	Tocopherol cyclase	Q94FY7	AT4G32770	+	0	1.95	+	0.00717534	1.98	+	0	3.88	+	0.000794118
Protease	ARASP2	Probable membrane metalloprotease ARASP2	O23053	AT1G05140	+	0.000262211	2.28	+	0.00712046	0.41		0.00436832	0.93	+	0.769658
Protease	At2g21960	Expressed protein	Q9SJ03	AT2G21960	+	0.000517755	1.44	+	0.010612	0.97	+	0.388234	1.40		0.00304045
Protease	CLPP4	ATP-dependent Clp protease proteolytic subunit 4	Q94B60	AT5G45390	+	0	3.60	+	0.000888889	2.72	+	0.0159072	9.80	+	0.00375099
Protease	EGY2	Probable zinc metalloprotease EGY2	F4K0T6;F4K0T7;Q9FFK3	AT5G05740	+	0.00348952	1.69	+	0.032415	0.81	+	0.802079	1.37		0.00914151
Protease	SPPA	Serine protease SPPA	A0A1P8AUG2;Q9C9C0	AT1G73990	+	0.00334545	1.11		0.756751	1.26	+	0.0478554	1.41	+	0.0229392
Protein folding	At3g12345	FKBP-type peptidyl-prolyl cis-trans isomerase	Q9LHH3	AT3G12345	+	0.00195432	1.52		0.0617116	1.33	+	0.051632	2.02		0.0117878
Protein folding	CLPB3	Chaperone protein ClpB3	Q9LF37	AT5G15450	+	0	4.34	+	0.00918291	8.43	+	0.00633616	36.60	+	0.00250737
Protein folding	CLPC1	Chaperone protein ClpC1	Q9FI56;F4JF64;Q9SXJ7	AT3G48870	+	0	3.37	+	0.00219455	2.54	+	0	8.57	+	0.000446281
Protein folding	CLPP5	ATP-dependent Clp protease proteolytic subunit 5	Q9S834	AT1G02560	+	0.0005	2.51	+	0.00378325	2.13	+	0.0384811	5.35	+	0.00885478
Protein folding	CPN21	20 kDa chaperonin	O65282	AT5G20720	+	0	4.49	+	0.00216092	2.08	+	0.00216709	9.34	+	0.000736364
Protein folding	CPN60A1	Chaperonin 60 subunit alpha 1	P21238	AT2G28000	+	0	2.65	+	0.00952	4.46	+	0.00152663	11.82	+	0.000687898
Protein folding	CYP26-2	Peptidyl-prolyl cis-trans isomerase CYP26-2	A0A1P8APN5;F4HTT6	At1g74070	+	0	1.93	+	0.000806723	1.51	+	0.0121582	2.91	+	0.00165886
Protein folding	CYP28	Peptidyl-prolyl cis-trans isomerase CYP28	A0A1P8B9P2;O65220	At5g35100	+	0	2.55	+	0.00107843	1.78	+	0	4.53	+	0.00187937
Protein folding	CYP37	Peptidyl-prolyl cis-trans isomerase CYP37	A0A1I9LQ22;A0A1I9LQ23;P82869	AT3G15520	+	0.000515393	1.54	+	0.00857754	1.17	+	0.0538578	1.81		0.00602192
Protein folding	DJA5	AT4g39960/T5J17_130	Q940V1	AT4G39960	+	0.000449123	3.45	+	0.00199127	1.55	+	0.0493739	5.34	+	0.00759952
Protein folding	DJA7	Molecular chaperone Hsp40/DnaJ family protein	A0A1P8ART2;Q0WN54	AT1G80030		0.125866	0.56			1.59			0.89		
Protein folding	FKBP16-3	Peptidyl-prolyl cis-trans isomerase FKBP16-3	A0A1P8B252;O22870	AT2G43560		0.398858	1.26			1.12			1.42		
Protein folding	FKBP16-4	Peptidyl-prolyl cis-trans isomerase FKBP16-4	Q9SR70	AT3G10060	+	0.000376068	1.98	+	0.00432579	0.93	+	0.457923	1.84		0.001631

Protein folding	FKBP17-2	Peptidyl-prolyl cis-trans isomerase FKBP17-2	Q9LDY5	AT1G18170	+	0.000469767	0.68	+	0.0181793	1.77		0.00153571	1.20	+	0.787775
Protein folding	HSP70-3	Heat shock 70 kDa protein 3	O65719	AT1G16030	+	0	3.25	+	0.00121519	3.31	+	0	10.78	+	0
Protein folding	HSP70-6	Heat shock 70 kDa protein 6	Q9STW6	AT4G24280	+	0	2.24	+	0.00216923	2.61	+	0.00104636	5.84	+	0.000830769
Protein folding	TIG	Trigger factor-like protein TIG	Q8S9L5	AT5G55220	+	0.000503902	2.70	+	0.00755473	2.60	+	0.0339978	7.02	+	0.00910928
Protein translocation	SCY1	Preprotein translocase subunit SCY1	Q38885	AT2G18710	+	0.000505593	0.55	+	0.0145799	2.15		0.00560854	1.18	+	0.0645497
Protein translocation	SECA1	Protein translocase subunit SecA	A0A1P8B485;F4JG57;Q9SYI0	AT4G01800	+	0	2.42	+	0.00372816	1.95	+	0	4.72	+	0
Protein translocation	TATB	Sec-independent protein translocase protein TATB	Q9XH75	AT5G52440	+	0.0256527	0.86		0.0667556	1.08		0.949121	0.93		0.0668596
Protein translocation	TATC	Sec-independent protein translocase protein TATC	Q9SJV5	AT2G01110	+	0	1.58	+	0.00961616	1.48	+	0.00775658	2.34	+	0
PSI	PSAA	Photosystem I P700 chlorophyll a apoprotein A1	P56766	ATCG00350	+	0	0.69	+	0.00476786	0.97	+	0.801698	0.67		0.00165333
PSI	PSAB	Photosystem I P700 chlorophyll a apoprotein A2	P56767	ATCG00340	+	0	0.65	+	0.00226506	0.83	+	0.00175824	0.54	+	0.000780723
PSI	PSAC	Photosystem I iron-sulfur center	P62090	ATCG01060	+	0.000470314	0.74	+	0.00294624	1.24	+	0.0121373	0.92	+	0.0215088
PSI	PSAD	Photosystem I reaction center subunit II	Q9S7H1;Q9SA56	AT1G03130	+	0.000507295	1.01		0.83935	0.79	+	0.0153717	0.80	+	0.00081
PSI	PSAE1	Photosystem I reaction center subunit IV A	Q9S831	AT4G28750	+	0	0.59	+	0.00277008	0.72	+	0.00271749	0.42	+	0.000682105
PSI	PSAE2	Photosystem I reaction center subunit IV B	Q9S714	AT2G20260	+	0.000510158	0.70	+	0.0101415	1.09	+	0.95443	0.76		0.00472409
PSI	PSAF	Photosystem I reaction center subunit III	Q9SHE8	AT1G31330		0.111129	1.04			0.96			1.00		
PSI	PSAG	Photosystem I reaction center subunit V	Q9S7N7	AT1G55670	+	0.000268068	0.80	+	0.00716335	0.96	+	0.376987	0.77		0.00243399
PSI	PSAH	Photosystem I reaction center subunit VI	Q9SUI6;Q9SUI7	AT1G52230		0.143118	1.01			0.98			0.99		
PSI	PSAK	Photosystem I reaction center subunit psaK	Q9SUI5	AT1G30380	+	0	0.45	+	0.00196516	1.02	+	0.580263	0.46		0
PSI	PSAL	Photosystem I reaction center subunit XI	A0A1P8B6D0;Q9SUI4	AT4G12800	+	0	0.67	+	0.00193151	0.82	+	0.0155607	0.55	+	0
PSI	PSAN	Photosystem I reaction center subunit N	P49107	AT5G64040	+	0	0.60	+	0.0011	0.86	+	0.0284368	0.52	+	0.000721604
PSI	PSAO	Photosystem I subunit O	Q949Q5	AT1G08380	+	0.00281897	2.05	+	0.0186137	0.68		0.0223866	1.40	+	0.16226
PSII	PSB33	Rieske (2Fe-2S) domain-containing protein	Q9C9I7	AT1G71500	+	0.00198419	1.20		0.0664338	1.10	+	0.529311	1.32		0.000380282
PSII	PSBA (D1)	Photosystem II protein D1	P83755	ATCG00020		0.0606603	1.10			1.30			1.43		
PSII	PSBB (CP47)	Photosystem II CP47 reaction center protein	P56777	ATCG00680	+	0	1.69	+	0.0019322	0.94	+	0.0453025	1.59	+	0.000695279
PSII	PSBC (CP43)	Photosystem II CP43 reaction center protein	P56778	ATCG00280	+	0	0.80	+	0.00224701	0.95	+	0.210432	0.76		0.000661224
PSII	PSBD (D2)	Photosystem II D2 protein	P56761	ATCG00270		0.0588452	0.86			1.09			0.94		
PSII	PSBE	Cytochrome b559 subunit alpha	P56779	ATCG00580	+	0.00194851	1.03	+	0.0263806	0.92		0.0082825	0.95	+	0.189118
PSII	PSBF	Cytochrome b559 subunit beta	P62095	ATCG00570	+	0.000511891	1.66	+	0.00570701	0.74		0.0072605	1.23	+	0.449161
PSII	PSBH	Photosystem II reaction center protein H	P56780	ATCG00710	+	0.0124646	0.84		0.0774759	1.05	+	0.964663	0.88		0.0139158

PSII	PSBO1	Oxygen-evolving enhancer protein 1-1	P23321	AT5G66570	+	0.00981153	0.96	+	0.0195477	0.95	+	0.784429	0.91		0.0337965
PSII	PSBO2	Oxygen-evolving enhancer protein 1-2	Q9S841	AT3G50820	+	0.00195045	0.98		0.792399	1.13	+	0.0284245	1.11	+	0.0159059
PSII	PSBP1	Oxygen-evolving enhancer protein 2-1	Q42029	AT1G06680	+	0.01266	0.95		0.742237	0.84		0.139161	0.80		0.0575522
PSII	PSBQ1	Oxygen-evolving enhancer protein 3-1	Q9XFT3	AT4G21280	+	0.000393832	0.81	+	0.00468421	1.16	+	0.0127308	0.94	+	0.0208657
PSII	PSBQ2	Oxygen-evolving enhancer protein 3-2	Q41932	AT4G05180	+	0	0.48	+	0	0.62	+	0.00082397	0.30	+	0
PSII	PSBR	Photosystem II 10 kDa polypeptide	P27202	AT1G79040		0.0508935	1.06			0.95			1.01		
PSII	PSBT	Photosystem II 5 kDa protein	A0A1I9LS90;Q39195	AT3G21055	+	0.000262887	0.64	+	0.0120247	0.70	+	0.0160515	0.45	+	0.00304895
PSII repair	ALB3	Inner membrane protein ALBINO3	F4IJM1;Q8LBP4	AT2G28800	+	0.00548968	0.52		0.0665761	1.01	+	0.587055	0.53		0.0286769
PSII repair	CYP38	Peptidyl-prolyl cis-trans isomerase CYP38	Q9SSA5	AT3G01480	+	0	1.04		0.988442	0.65	+	0.00127103	0.68	+	0.000372414
PSII repair	DEGP1	Protease Do-like 1	O22609	AT3G27925	+	0	2.22	+	0.00171429	1.05	+	0.723816	2.32		0.000734694
PSII repair	FKBP20-2	Peptidyl-prolyl cis-trans isomerase FKBP20-2	A0A1I9LRJ6;Q0WRJ7	AT3G60370		0.0562962	2.56			0.39			1.00		
PSII repair	FTSH1	ATP-dependent zinc metalloprotease FTSH 1	Q39102	AT1G50250		0.111556	0.73			1.23			0.90		
PSII repair	FTSH2	ATP-dependent zinc metalloprotease FTSH 2	A0A1P8AXC1;O80860	AT2G30950	+	0	1.81	+	0.00147692	1.10	+	0.0401644	1.98	+	0
PSII repair	FTSH5	ATP-dependent zinc metalloprotease FTSH 5	Q9FH02	AT5G42270	+	0	1.59	+	0.00263855	1.12	+	0.0557728	1.78		0.00217391
PSII repair	FTSH8	ATP-dependent zinc metalloprotease FTSH 8	Q8W585	AT1G06430	+	0.00133878	0.73	+	0.00475724	1.33		0.0158475	0.97	+	0.871393
PSII repair	FTSY	Cell division protein FtsY homolog	O80842	AT2G45770	+	0	3.79	+	0.0101742	3.47	+	0.00260086	13.17	+	0.000650602
PSII repair	HHL1	Protein HHL1	Q8LDL0	At1g67700	+	0	1.89		0.0852815	2.14	+	0.0134497	4.06	+	0.000651911
PSII repair	HSP70-7	Heat shock 70 kDa protein 7	Q9LTX9	AT5G49910	+	0	2.82	+	0.00127907	2.35	+	0.00289571	6.64	+	0.000786408
PSII repair	LPA1	Protein LOW PSII ACCUMULATION 1	Q9SRY4	AT1G02910	+	0.000265971	1.99	+	0.0027375	1.00	+	0.356319	2.00		0.00192834
PSII repair	LQY1	Protein disulfide-isomerase LQY1	Q8GSJ6	AT1G75690	+	0.000857741	0.63	+	0.00104348	1.42		0.0480131	0.90	+	0.323332
PSII repair	MET1	Protein MET1	Q94BS2	AT1G55480	+	0.000266667	2.16	+	0.0089863	1.81	+	0.0254782	3.91	+	0.00368606
PSII repair	MPH1	Protein MAINTENANCE OF PSII UNDER HIGH LIGHT 1	Q9FL44	AT5G07020	+	0	1.47	+	0.0122945	1.32	+	0.0147632	1.93	+	0.00165058
PSII repair	PPL1	PsbP-like protein 1	P82538	AT3G55330	+	0.00422642	0.65	+	0.00118919	1.23		0.370068	0.80		0.0999916
PSII repair	PSB27-1	Photosystem II repair protein PSB27-H1	Q9LR64	AT1G03600	+	0.000302564	0.59	+	0.00289182	1.19	+	0.294315	0.70		0.0030618
PSII repair	TL18.3	UPF0603 protein At1g54780	Q9ZVL6	AT1G54780	+	0.00194659	0.85	+	0.0205876	1.14		0.0142563	0.97	+	0.0612839
PSII repair	VIPP1	Membrane-associated protein VIPP1	A0A178W0D3;O80796	AT1G65260	+	0.00277162	1.47	+	0.0382266	1.18	+	0.203054	1.75		0.0080716
Redox regulation	At1g14345	NAD(P)-linked oxidoreductase superfamily protein	Q949S6	AT1G14345	+	0.00114933	1.48	+	0.00267073	1.22	+	0.34957	1.80		0.0103063
Redox regulation	At1g50450	Saccharopine dehydrogenase	Q94BZ0	AT1G50450	+	0.000374241	1.37	+	0.00204348	1.81	+	0.0259626	2.49	+	0.00555392
Redox regulation	At3g02730	Thioredoxin F1	Q9XFH8	AT3G02730	+	0	1.68	+	0.0163463	1.96	+	0	3.30	+	0.000459574

Redox regulation	ATHM2	Thioredoxin M2	F4JG94;Q9SEU8	AT4G03520	+	0.000374696	1.91	+	0.00973026	1.19	+	0.0268265	2.27	+	0.00276395
Redox regulation	BAS1	2-Cys peroxiredoxin BAS1	Q96291	AT3G11630	+	0	3.38	+	0.0128743	4.90	+	0	16.55	+	0
Redox regulation	CITRX	Thioredoxin-like protein CITRX	Q9M7X9	AT3G06730	+	3.28767E-05	2.95	+	0.000657534	1.82	+	0.0305222	5.37	+	0.0036827
Redox regulation	ENH1	Rubredoxin family protein	A8MSF2;Q9FFJ2	AT5G17170	+	0.00170971	0.76	+	0.00829496	1.76		0.0187141	1.33	+	0.104733
Redox regulation	F20D21.31	Rubredoxin-like superfamily protein	Q9SLI4	AT1G54500	+	0.0314504	1.13		0.505424	1.03	+	0.529025	1.16		0.0264246
Redox regulation	MCK7.20	Malate dehydrogenase	Q8H1E2;F4KEX3	AT5G58330	+	0	3.23	+	0.00231148	2.11	+	0	6.80	+	0.000439024
Redox regulation	MDH	Malate dehydrogenase	Q9SN86	AT3G47520	+	0	4.61	+	0.00158182	2.11	+	0.00292562	9.74	+	0.00065587
Redox regulation	MED24.18	Thioredoxin family protein	Q940I2	AT5G03880	+	0.000033241	0.86		0.0746405	1.34	+	0.00176309	1.15	+	0.00470647
Redox regulation	PRXQ	Peroxiredoxin Q	A0A1I9LR27;F4JBC9;Q9LU86	AT3G26060	+	0	1.93	+	0.00424703	2.39	+	0.00434432	4.61	+	0.00193464
Redox regulation	TRXM1	Thioredoxin M1	Q48737	AT1G03680	+	0.00797419	0.80		0.0643619	1.50		0.0467807	1.19	+	0.203297
Redox regulation	TRXM4	Thioredoxin M4	Q9SEU6	AT3G15360	+	0.0154923	1.52	+	0.00144737	1.36		0.823904	2.07		0.0859979
Ribosome	PSRP2	30S ribosomal protein 2	Q8VYM4	AT3G52150	+	0	1.83	+	0.00260714	2.09	+	0.00348162	3.82	+	0.0015814
Ribosome	PSRP5	50S ribosomal protein 5	Q9LER7	AT3G56910	+	3.30579E-05	1.17		0.0604929	1.44	+	0.008256	1.69	+	0.000463519
Ribosome	RPL1	50S ribosomal protein L1	Q9LY66;F4J296	AT3G63490	+	0	1.65	+	0.00474667	1.94	+	0	3.20	+	0
Ribosome	RPL10	50S ribosomal protein L10	Q9FY50	AT5G13510	+	0	2.00	+	0.00205091	2.02	+	0	4.04	+	0
Ribosome	RPL11	50S ribosomal protein L11	Q9MAP3	AT1G32990	+	0	2.11	+	0.00648049	2.26	+	0.00218926	4.77	+	0.00103327
Ribosome	RPL12A	50S ribosomal protein L12-1	P36212;P36210	AT3G27830	+	0	1.99	+	0.00800729	2.25	+	0	4.49	+	0.000722741
Ribosome	RPL14	50S ribosomal protein L14	P56792	ATCG00780	+	0	1.70	+	0.0022381	1.82	+	0.000758621	3.11	+	0.00072973
Ribosome	RPL15	50S ribosomal protein L15	P25873	AT3G25920	+	0	2.07	+	0.00965174	1.53	+	0.00215617	3.17	+	0.0005
Ribosome	RPL16	50S ribosomal protein L16	P56793	ATCG00790	+	0	3.03	+	0.00109453	1.64	+	0.0226427	4.96	+	0.00178069
Ribosome	RPL17	50S ribosomal protein L17	Q9M385	AT3G54210	+	0	1.61	+	0.00111675	2.19	+	0	3.54	+	0.000692308
Ribosome	RPL18	50S ribosomal protein L18	Q9SX68	AT1G48350	+	0	1.67	+	0.00379259	1.74	+	0.0121027	2.92	+	0.00279191
Ribosome	RPL21	50S ribosomal protein L21	P51412	AT1G35680	+	0	3.20	+	0.00917483	1.57	+	0.00273589	5.03	+	0.000738854
Ribosome	RPL23-A	50S ribosomal protein L23	P61845	ATCG00840	+	0	2.06	+	0.000738462	2.10	+	0.0171144	4.31	+	0.00330124
Ribosome	RPL24	50S ribosomal protein L24	P92959;F4K1S8	AT5G54600	+	0.00304725	0.57		0.204521	2.55	+	0.0162825	1.46	+	0.0157438
Ribosome	RPL27	50S ribosomal protein L27	Q9FLN4	AT5G40950	+	0.00109804	0.86		0.461402	1.79	+	0.0104727	1.53	+	0.00445671

Ribosome	RPL29	50S ribosomal protein L29	Q9FJP3	AT5G65220	+	0.000397129	1.94	+	0.0185882	1.88	+	0.0170932	3.64	+	0.00451334
Ribosome	RPL2-A	50S ribosomal protein L2	P56791	ATCG00830	+	0.00295367	1.15		0.16977	1.65	+	0.103622	1.90		0.00366129
Ribosome	RPL31	50S ribosomal protein L31	Q9FWS4	AT1G75350	+	0.00592551	1.91		0.273359	1.24	+	0.344796	2.37		0.000596685
Ribosome	RPL3A	50S ribosomal protein L3-1	Q9SKX4	AT2G43030	+	0	2.21	+	0.0038209	1.73	+	0	3.83	+	0.000367347
Ribosome	RPL4	50S ribosomal protein L4	Q2V4Q4;Q3EDH2;O50061	AT1G07320	+	0	2.54	+	0	1.85	+	0	4.71	+	0
Ribosome	RPL5	50S ribosomal protein L5	O04603	AT4G01310	+	0	1.99	+	0.00488985	2.01	+	0.0101763	4.00	+	0.00215054
Ribosome	RPL6	50S ribosomal protein L6	O23049	AT1G05190	+	0	1.86	+	0.00377396	2.13	+	0	3.97	+	0
Ribosome	RPL9	50S ribosomal protein L9	P25864	AT3G44890	+	0	2.68	+	0.00724514	1.47	+	0.00261771	3.94	+	0.000654545
Ribosome	RPS10	30S ribosomal protein S10	Q9LK61	At3g13120	+	0.000500554	2.89	+	0.0105786	2.18	+	0.0397019	6.31	+	0.00848757
Ribosome	RPS11	30S ribosomal protein S11	P56802	ATCG00750	+	0	1.64	+	0.0027933	1.50	+	0.0025678	2.47	+	0.000664756
Ribosome	RPS13	30S ribosomal protein S13	P42732;B3H631	AT5G14320	+	0	2.16	+	0.000648649	1.20	+	0.0620703	2.60		0.0018944
Ribosome	RPS15	30S ribosomal protein S15	P56805	ATCG01120	+	0	2.62	+	0.00131507	1.99	+	0.00277346	5.22	+	0.000755245
Ribosome	RPS17	30S ribosomal protein S17	P16180	AT1G79850	+	0	1.42	+	0.0027248	1.87	+	0.00582131	2.65	+	0.00203145
Ribosome	RPS18	30S ribosomal protein S18	P56807	ATCG00650	+	0.000563441	3.30	+	0.0174479	0.99	+	0.795453	3.26		0.00379461
Ribosome	RPS19	30S ribosomal protein S19	P56808	ATCG00820	+	0	2.14	+	0.0184011	1.67	+	0.0122126	3.57	+	0
Ribosome	RPS2	30S ribosomal protein S2	P56797	ATCG00160	+	0	1.83	+	0.00162617	2.00	+	0	3.67	+	0
Ribosome	RPS20	30S ribosomal protein S20	Q9ASV6	AT3G15190	+	0	1.25	+	0.026516	1.65	+	0.00979692	2.06	+	0
Ribosome	RPS3	30S ribosomal protein S3	P56798	ATCG00800	+	0	1.88	+	0.00220736	1.69	+	0	3.17	+	0
Ribosome	RPS4	30S ribosomal protein S4	P56799	ATCG00380	+	0	1.84	+	0.00743503	1.31	+	0.0158274	2.41	+	0
Ribosome	RPS5	30S ribosomal protein S5	P93014	AT2G33800	+	0	2.16	+	0.00525106	1.32	+	0.0273953	2.85	+	0
Ribosome	RPS6	30S ribosomal protein S6 alpha	A0A1P8AV66;Q8VY91	At1g64510	+	0.000268775	1.97	+	0.00452252	2.11	+	0.0160308	4.14	+	0.0045019
Ribosome	RPS8	30S ribosomal protein S8	P56801	ATCG00770	+	3.26975E-05	1.99	+	0.0102904	3.69	+	0.0133369	7.34	+	0.00393862
Ribosome	RPS9	30S ribosomal protein S9	Q9XJ27	AT1G74970	+	0.00189851	1.14		0.295032	1.56	+	0.0356013	1.78	+	0.00926488
Starch	BAM3	Beta-amylase 3	O23553	At4g17090	+	0	12.10	+	0.00168932	2.48	+	0.00104983	29.94	+	0.000635616
Starch	GBSS1	Granule-bound starch synthase 1/amyloplastic	Q9MAQ0	AT1G32900	+	0.00037931	6.34	+	0.0106792	0.48	+	0.0257741	3.05	+	0.00421456
Starch	SS1	Starch synthase 1/amyloplastic	Q9FNF2	AT5G24300	+	0.000371532	1.69	+	0.0392826	2.86	+	0.0158677	4.85	+	0.0050495
Stress responsive	ABC1K8	Protein ACTIVITY OF BC1 COMPLEX KINASE 8	Q93Y08	AT5G64940	+	0	2.73	+	0.0230092	3.73	+	0	10.19	+	0.00072956
Stress responsive	ALDH3I1	Aldehyde dehydrogenase family 3 member I1	F4JKM4;A0A1P8B7C0;Q8W033;A0A1P8B7C2	AT4G34240	+	0	1.88	+	0.00964865	1.38	+	0.013585	2.59	+	0.000676409
Stress responsive	APE1	Acclimation of photosynthesis to environment	A0A219HZL6;Q2HIR7	AT5G38660	+	0.000501109	1.23	+	0.0175219	1.02	+	0.781551	1.25		0.000586957

Stress responsive	AT5g02160	Transmembrane protein	Q9FPH2	AT5G02160	+	0	0.36	+	0.000842105	0.71	+	0.0128098	0.26	+	0.000637363
Stress responsive	CLH1	Chlorophyllase-1	O22527	AT1G19670	+	0	1.19		0.449178	8.88	+	0.00559858	10.54	+	0.00248902
Stress responsive	F11M15.26	At1g51400/F5D21_10	Q9SYE2	AT1G51400	+	0	0.35	+	0.00101053	0.81	+	0.0496555	0.28	+	0.000824427
Stress responsive	FLU	Protein FLUORESCENT IN BLUE LIGHT	F4JFR1;F4JFR2;Q940U6	AT3G14110	+	0.000606955	0.97		1	1.35	+	0.00906667	1.31	+	0.00307042
Stress responsive	LIR1	Light-regulated protein 1	Q96500	At3g26740	+	0.000489607	1.19	+	0.00275472	0.75		0.00776936	0.89	+	0.924333
Stress responsive	PPD3	PsbP domain-containing protein 3	Q9S720	AT1G76450	+	0.000394299	1.63	+	0.0172023	1.10	+	0.0750972	1.80		0.00203465
Stress responsive	PPD4	PsbP domain-containing protein 4	O49292	AT1G77090	+	0	1.11		0.485389	1.67	+	0.00324194	1.86	+	0.00064986
Stress responsive	PPD6	PsbP domain-containing protein 6	Q9LXX5	AT3G56650	+	0.00889991	1.57	+	0.0102403	1.00		0.75297	1.57		0.106364
Stress responsive	SHM1	Serine hydroxymethyltransferase 1	Q9SZJ5;Q94C74	AT4G37930	+	0	9.90	+	0.00487931	4.42	+	0	43.75	+	0.000727273
Stress responsive	TL29	Thylakoid luminal 29 kDa protein	A0A1P8B8W6;A0A1P8B8Y3;P82281	AT4G09010	+	0	1.86	+	0.000768	1.10	+	0.0909659	2.06		0.0021875
Thylakoid architecture	CURT1A	Protein CURVATURE THYLAKOID 1A	O04616	AT4G01150	+	0.000508436	1.01		0.507067	1.38	+	0.0141481	1.40	+	0.000663934
Thylakoid architecture	CURT1B	Protein CURVATURE THYLAKOID 1B	Q8LCA1	AT2G46820	+	0.0021063	1.14		0.572179	1.27	+	0.0230263	1.45	+	0.00304469
Thylakoid architecture	CURT1C	Protein CURVATURE THYLAKOID 1C	Q9M812	AT1G52220		0.107072	0.92			1.02			0.93		
Thylakoid architecture	FZL	Probable transmembrane GTPase FZO-like	A0A1P8AUL2;A0A1P8AUL4;Q1KPV0	AT1G03160	+	0.000264935	0.95		0.890851	2.11	+	0.00274214	2.00	+	0.00159855
Thylakoid architecture	PLSP1	Chloroplast processing peptidase	A0A1I9LMR3;Q8HOW1	AT3G24590	+	0.01092	1.15	+	0.0421871	1.22		0.227251	1.41		0.0586624
Thylakoid architecture	RIQ1	Reduced induction of non-photochemical quenching1	Q9SD79	AT5G08050	+	0	1.14		0.336925	1.67	+	0.00567944	1.91	+	0.000389892
Thylakoid architecture	RIQ2	Reduced induction of non-photochemical quenching2	Q94F10	AT1G74730	+	0.000390588	0.74	+	0.0118949	2.31	+	0.0121446	1.71	+	0.0118802
Thylakoid architecture	THF1	Protein THYLAKOID FORMATION 1	Q9SKT0	AT2G20890	+	0.0132706	1.12		0.077565	1.22	+	0.644534	1.36		0.0274342

Table 13: Relative abundance of thylakoid-associated proteins in the Field versus the Lab. Details of the 439 MS-quantified thylakoid proteins from Arabidopsis plants grown outdoors versus in a controlled environment, including functional category, protein/gene name, description, UniProtKB identifier, TAIR ID and abundance ratios. Significant changes were identified by a modified Welch's t-test ( $q < 0.05$ ). Median protein iBAQ values were used for the calculation of ratios.

Category	Protein/ gene name	Description	UniProtKB accession	TAIR ID	Ratio Field vs Lab	Welch's t-test sig.	Welch's t-test q-value
Assembly	ALB4	ALBINO3-like protein 1	F4I9A9;Q9FYL3	AT1G24490	1.80	+	0.00208295
Assembly	At4g28740	LOW PSII ACCUMULATION-like protein	F4JM22	AT4G28740	2.12	+	0
Assembly	At5g48790	LOW PSII ACCUMULATION protein	Q94F50;Q9FKB7	AT5G48790	1.41	+	0.0216884
Assembly	CCB1	Protein COFACTOR ASSEMBLY OF COMPLEX C SUBUNIT B CCB1	Q9LSE4	AT3G26710	1.43	+	0.0278453
Assembly	CCB2	Protein COFACTOR ASSEMBLY OF COMPLEX C SUBUNIT B CCB2	Q9FJ81	AT5G52110	1.30		0.173796
Assembly	CCS1	Cytochrome c biogenesis protein CCS1	Q9XIA4	AT1G49380	1.19		0.39718
Assembly	DAC		Q94BY7	AT3G17930	1.21	+	0.0396022
Assembly	FFC		P37107	AT5G03940	2.10	+	0
Assembly	HCF101	Fe-S cluster assembly factor HCF101	Q6STH5	AT3G24430	5.16	+	0
Assembly	HCF136	Photosystem II stability/assembly factor HCF136	A0A1P8BG37;O82660	AT5G23120	1.96	+	0
Assembly	HCF164	Thioredoxin-like protein HCF164	O23166	AT4G37200	1.22	+	0.00867532
Assembly	HCF244	NAD(P)-binding Rossmann-fold superfamily protein	O65502	AT4G35250	1.64	+	0.00481967
Assembly	LPA2	Protein LOW PSII ACCUMULATION 2	F4KDA6	AT5G51545	0.72	+	0.00178
Assembly	LPA3	Protein LOW PSII ACCUMULATION 3	Q8HOW0	AT1G73060	1.27	+	0.0215662
Assembly	MPH2	Thylakoid luminal 16.5 kDa protein	A0A1P8B5H3;O22773;A0A1P8B5G9	AT4G02530	0.97		0.995271
Assembly	PPD1	PsbP domain-containing protein 1	O23403	AT4G15510	1.57	+	0.00457588
Assembly	Y3IP1	Ycf3-interacting protein 1	Q9LU01	AT5G44650	1.58	+	0.00131915
Assembly	YCF4	Photosystem I assembly protein Ycf4	P56788	AtCg00520	1.47	+	0
ATP synthase	ATPA	ATP synthase subunit alpha	P56757	ATCG00120	1.43	+	0
ATP synthase	ATPB	ATP synthase subunit beta	P19366	ATCG00480	1.35	+	0
ATP synthase	ATPC1	ATP synthase gamma chain 1	Q01908	AT4G04640	1.25	+	0.000898551
ATP synthase	ATPD	ATP synthase subunit delta	Q9SSS9	AT4G09650	1.33	+	0.00494118
ATP synthase	ATPE	ATP synthase epsilon chain	P09468	ATCG00470	1.41	+	0.00146746
ATP synthase	ATPF	ATP synthase subunit b	P56759	ATCG00130	1.45	+	0.00110714
ATP synthase	ATPH	ATP synthase subunit c	P56760	ATCG00140	0.43		0.930208
ATP synthase	ATPI	ATP synthase subunit a	P56758	ATCG00150	1.40	+	0.00149398
ATP synthase	PDE334		Q42139	AT4G32260	1.35	+	0.00802649
Carbon fixation	BCA1	Beta carbonic anhydrase 1	P27140;A0A119LQB3	AT3G01500	2.82	+	0
Carbon fixation	RBCL	Ribulose bisphosphate carboxylase large chain	O03042	AtCg00490	2.42	+	0
Carbon fixation	RBCS-1A	Ribulose bisphosphate carboxylase small chain 1A	P10795	AT1G67090	3.60	+	0
Carbon fixation	RBCS-1B	Ribulose bisphosphate carboxylase small chain 1B	P10796	AT5G38430	3.30	+	0

Carbon fixation	RBCS-2B	Ribulose biphosphate carboxylase small chain 3B	P10798;P10797;F4KA76;B3H5S2	AT5G38410;AT5G38420	3.77	+	0
Carbon fixation	RCA	Ribulose biphosphate carboxylase/oxygenase activase	P10896;F4IVZ7	AT2G39730	3.51	+	0
Chloroplast replication	FTSZ1	Cell division protein FtsZ homolog 1	Q42545	AT5G55280	2.28	+	0.00571429
Chloroplast replication	FTSZ2-1	Cell division protein FtsZ homolog 2-1	A0A1P8AXD8;O82533	AT2G36250	2.41	+	0
Chloroplast replication	FTSZ2-2	Cell division protein FtsZ homolog 2-2	Q9LXJ0;A0A1I9LSJ8	AT3G52750	10.94	+	0.00100813
Chlororespiration	PIFI	Post-illumination chlorophyll fluorescence increase	B3H4M0;F4J037;F4J034;Q9LVZ5;F4J036	AT3G15840	1.37	+	0.00474194
Cytochrome b6f	PETA	Cytochrome f	P56771	ATCG00540	1.64	+	0.00642807
Cytochrome b6f	PETB	Cytochrome b6	P56773	ATCG00720	1.49	+	0.007125
Cytochrome b6f	PETC	Cytochrome b6-f complex subunit 4	P56774	ATCG00730	1.42	+	0
Cytochrome b6f	PETD	Cytochrome b6-f complex iron-sulfur subunit	Q9ZR03	AT4G03280	1.38	+	0
DNA/RNA	At2g21530		Q8GWP4	AT2G21530	2.65	+	0.00797368
DNA/RNA	At2g24420		Q9ZQ26	AT2G24420	1.74	+	0.000918519
DNA/RNA	CCR1		Q03251;F4JVC0;F4JVC1;F4JVB9	AT4G39260	3.20	+	0
DNA/RNA	CCR2		F4IHK9;Q03250	AT2G21660	4.07	+	0.00145029
DNA/RNA	CP29A	29 kDa ribonucleoprotein	F4JAF3;Q43349	AT3G53460	1.68	+	0.00565056
DNA/RNA	CP29B	RNA-binding protein CP29B	Q9ZUU4	AT2G37220	1.79	+	0.00536882
DNA/RNA	CP31A	31 kDa ribonucleoprotein	Q04836	AT4G24770	1.49	+	0
DNA/RNA	F16M2_10		Q9M1X3	AT3G63160	1.82	+	0
DNA/RNA	PTAC16	Protein PLASTID TRANSCRIPTIONALLY ACTIVE 16	Q9STF2	AT3G46780	0.90	+	0.00216268
DNA/RNA	rpoA	DNA-directed RNA polymerase subunit alpha	P56762	AtCg00740	1.25	+	0.00455814
DNA/RNA	TUFA	Elongation factor Tu	P17745	AT4G20360	2.83	+	0
Electron transfer	LFNR1	Ferredoxin--NADP reductase, leaf isozyme 2	Q8W493;C0Z2A8	AT1G20020	1.14	+	0.00111712
Electron transfer	LFNR2	Ferredoxin--NADP reductase, leaf isozyme 1	Q9FKW6;F4JZ46	AT5G66190	1.30	+	0.00213208
Electron transfer	NDC1	Alternative NAD(P)H-ubiquinone oxidoreductase C1/mitochondrial	Q8GXR9	AT5G08740	2.60	+	0
Electron transfer	PC	Plastocyanin major isoform	P42699	AT1G20340	0.89		0.104465
Electron transfer	PETE	Plastocyanin minor isoform	A0A1P8APR2;P11490	AT1G76100	1.94		0.974821
Electron transfer	PGR5	Protein PROTON GRADIENT REGULATION 5	Q9SL05	AT2G05620	1.25	+	0.00206393
Electron transfer	PGR6	Uncharacterized aarF domain-containing protein kinase At4g31390	Q8RWG1;A0A1P8B7P6	AT4G31390	3.41	+	0
Electron transfer	PGRL1A	PGR5-like protein 1A	Q8H112;A0A2H1ZEN5	AT4G22890	1.14	+	0.0301978
Electron transfer	PGRL1B	PGR5-like protein 1B	F4JPU9;Q8GYC7	AT4G11960	1.65	+	0.00445763
Electron transfer	TIC62	Protein TIC 62	Q8H0U5	AT3G18890	1.40	+	0.00412444
Electron transfer	TROL	Rhodanese-like domain-containing protein 4	A0A1P8B8J7;Q9M158	AT4G01050	1.44	+	0.0100685
Ion channel	DIT2-1	Dicarboxylate transporter 2.1	Q9FMF7	AT5G64290	2.45	+	0.00487967

Ion channel	KEA3	K(+) efflux antiporter 3	Q9M0Z3	AT4G04850	1.51	+	0
Ion channel	MNJ8.18	LOW protein: ammonium transporter 1-like protein	Q93Z11	AT5G37360	0.85		0.0633439
Kinase/phosphatase	At3g59780	Rhodanese/Cell cycle control phosphatase superfamily protein	F4J9G2	AT3G59780	1.43	+	0.00150303
Kinase/phosphatase	At5g35170	Adenylate kinase 5	F4JYC0;Q8VYL1	AT5G35170	1.68	+	0
Kinase/phosphatase	PGK1	Phosphoglycerate kinase	F4I3L1;P50318	AT1G56190	3.47	+	0
Kinase/phosphatase	PGK1	Phosphoglycerate kinase 1	Q9LD57	AT3G12780	2.39	+	0
LHCI	LHCA1	Chlorophyll a-b binding protein 6	A8MS75;Q01667; F4JE46;F4JE43	AT3G54890	1.02		0.867552
LHCI	LHCA2	Photosystem I chlorophyll a/b-binding protein 2	Q9SYW8	AT3G61470	0.97		0.876333
LHCI	LHCA3	Photosystem I chlorophyll a/b-binding protein 3-1	Q9SY97	AT1G61520	0.83	+	0.0120356
LHCI	LHCA4	Chlorophyll a-b binding protein 4	P27521	AT3G47470	0.90	+	0.0252661
LHCI	LHCA6	Photosystem I chlorophyll a/b-binding protein 6	Q8LCQ4	AT1G19150	0.67		1
LHCII	LHCB1.1;LHCB 1.2	Chlorophyll a-b binding protein 2	Q8VZ87;P0CJ48	AT1G29910	0.67	+	0
LHCII	LHCB1.3	Chlorophyll a-b binding protein 1	P04778	AT1G29930	1.13	+	0.021812
LHCII	LHCB1.4	Chlorophyll a-b binding protein	Q39142	AT2G34430	0.23	+	0
LHCII	LHCB1.5	Chlorophyll a-b binding protein	Q39141	AT2G34420	1.12		1
LHCII	LHCB2	Chlorophyll a-b binding protein 2	Q9S7J7;Q9SHR7; Q9XF87;A0A1I9L MB4;A0A1P8AZ91	AT2G05070;AT2G 05100;AT3G27690	0.79	+	0.0109235
LHCII	LHCB3	Chlorophyll a-b binding protein 3	Q9S7M0	AT5G54270	0.95		0.104436
LHCII	LHCB4.1 (CP29.1)	Chlorophyll a-b binding protein CP29.1	Q07473	AT5G01530	1.11	+	0.00144186
LHCII	LHCB4.2 (CP29.2)	Chlorophyll a-b binding protein CP29.2	Q9XF88	AT3G08940	0.80	+	0
LHCII	LHCB4.3 (CP29.3)	Chlorophyll a-b binding protein CP29.3	Q9S7W1;F4IGY6	AT2G40100	5.43	+	0.00913924
LHCII	LHCB5 (CP26)	Chlorophyll a-b binding protein CP26	Q9XF89	AT4G10340	0.98		0.104166
LHCII	LHCB6 (CP24)	Chlorophyll a-b binding protein	Q9LMQ2	AT1G15820	0.89	+	0
LHC-like	Lil3.1	Light-harvesting complex-like protein 3 isotype 1	Q9SYX1	AT4G17600	1.40	+	0.00187368
LHC-like	Lil3.2	Light-harvesting complex-like protein 3 isotype 2	Q6NKS4	AT5G47110	1.21	+	0.00623656
LHC-like	OHP1	High-light-induced protein	O81208	AT5G02120	1.57	+	0.00476113
LHC-like	OHP2	Light-harvesting complex-like protein OHP2	Q9FEC1	AT1G34000	0.85	+	0.00209259
Light regulation	harvesting LCNP		Q9STS7	AT3G47860	1.25	+	0.00260633
Light regulation	harvesting PSBS	Photosystem II 22 kDa protein	Q9XF91;F4IEG8	AT1G44575	1.93	+	0
Light regulation	harvesting ROQH1		Q8GYZ0;F4JSP1	AT4G31530	2.14	+	0
Light regulation	harvesting SOQ1	Protein SUPPRESSOR OF QUENCHING 1	Q8VZ10	AT1G56500	1.37	+	0
Light regulation	harvesting STN7	Serine/threonine-protein kinase STN7	Q9S713	AT1G68830	0.61	+	0.00408811

Light regulation	harvesting	STN8	Serine/threonine-protein kinase STN8	Q9LZV4	AT5G01920	1.64	+	0.00455411
Light regulation	harvesting	TAP38	Protein phosphatase 2C 57	P49599	AT4G27800	0.70	+	0.00466667
Light regulation	harvesting	TSP9	Thylakoid soluble phosphoprotein	Q9SD66	AT3G47070	1.79	+	0.00210233
Light regulation	harvesting	VDE1	Violaxanthin de-epoxidase	Q39249	AT1G08550	1.60	+	0.00207339
Light regulation	harvesting	ZEP	Zeaxanthin epoxidase	Q9FGC7	AT5G67030	1.28	+	0.00794754
NDH		NDHC	NAD(P)H-quinone oxidoreductase subunit 3	P56751	ATCG00440	3.92	+	0.0260559
NDH		NDHE	NAD(P)H-quinone oxidoreductase subunit 4L	P26289	ATCG01070	1.33	+	0.004704
NDH		NDHF	NAD(P)H-quinone oxidoreductase subunit 5	P56752	ATCG01010	1.62		0.135282
NDH		NDHH	NAD(P)H-quinone oxidoreductase subunit H	P56753	ATCG01110	1.67	+	0.000843537
NDH		NDHI	NAD(P)H-quinone oxidoreductase subunit I	P56755	ATCG01090	1.93	+	0.00816162
NDH		NDHJ	NAD(P)H-quinone oxidoreductase subunit J	P56754	ATCG00420	1.08		0.799712
NDH		NDHK	NAD(P)H-quinone oxidoreductase subunit K	P56756	ATCG00430	1.28	+	0.00810702
NDH		ndhL		Q9CAC5	AT1G70760	1.72	+	0.00114815
NDH		NDHM	NAD(P)H-quinone oxidoreductase subunit M	Q2V2S7	AT4G37925	1.17	+	0.0119294
NDH		NDHN	NAD(P)H-quinone oxidoreductase subunit N	Q9LVM2	AT5G58260	1.43	+	0.00534848
NDH		NDHO	NAD(P)H-quinone oxidoreductase subunit O	Q9S829	AT1G74880	2.52	+	0.0109571
NDH		NDHS	NAD(P)H-quinone oxidoreductase subunit S	Q9T0A4	AT4G23890	2.65	+	0.000826667
NDH		NDHT	NAD(P)H-quinone oxidoreductase subunit T	Q9SMS0	AT4G09350	2.20	+	0.0309699
NDH		NDHU	NAD(P)H-quinone oxidoreductase subunit U	Q84VQ4	AT5G21430	1.35	+	0
NDH		PNSB1	Photosynthetic NDH subunit of subcomplex B 1	Q9S9N6	AT1G15980	1.58	+	0.00501538
NDH		PNSB2	Photosynthetic NDH subunit of subcomplex B 2	Q94AQ8;F4I891;F4I890	AT1G64770	1.29	+	0.00459389
NDH		PNSB3	Photosynthetic NDH subunit of subcomplex B 3	Q9LU21	AT3G16250	1.47	+	0.00258296
NDH		PNSB4	Photosynthetic NDH subunit of subcomplex B 4	A0A1P8AS98;F4I CC6;Q8RXS1	AT1G18730	0.73	+	0.00585507
NDH		PNSB5	Photosynthetic NDH subunit of subcomplex B 5	Q9FG89	AT5G43750	1.42		0.586973
NDH		PNSL1	Photosynthetic NDH subunit of luminal location 1	O80634	AT2G39470	1.42	+	0.00186387
NDH		PNSL2	Photosynthetic NDH subunit of luminal location 2	Q9XI73	AT1G14150	1.82	+	0.010759
NDH		PNSL3	Photosynthetic NDH subunit of luminal location 3	Q9SGH4	AT3G01440	1.04		0.225556
NDH		PNSL4	Photosynthetic NDH subunit of luminal location 4	F4JW56;Q9SCY3	AT4G39710	1.46	+	0.00567164
NDH		PNSL5	Photosynthetic NDH subunit of luminal location 5	Q9ASS6	AT5G13120	0.76	+	0.00173659
Other/unknown		AAC1		P31167	AT3G08580	2.88	+	0.000946565
Other/unknown		AAC2		P40941	AT5G13490	4.05		1
Other/unknown		AOC2		Q9LS02	AT3G25770	2.21	+	0
Other/unknown		APG3	Peptide chain release factor APG3	Q8RX79	AT3G62910	4.06	+	0.00569288
Other/unknown		APXT	L-ascorbate peroxidase T	A0A1P8APU0;Q42593	AT1G77490	1.09	+	0.0109908

Other/unknown	At1g07660		P59259;A8MRV1	AT2G28740	2.73	+	0
Other/unknown	At1g18060		Q9LM40	AT1G18060	2.49	+	0.00705155
Other/unknown	At1g24360		P33207	AT1G24360	1.97	+	0.0119646
Other/unknown	At1g33810	Zinc finger/BTB domain protein	Q8L9M8	AT1G33810	2.19	+	0.00096875
Other/unknown	At1g52510		Q8VZ57;F4ICZ4	AT1G52510	2.08	+	0.00112727
Other/unknown	At1g73110		Q9AST9;A0A1P8A TD8	AT1G73110	4.43	+	0.00105085
Other/unknown	At1g78915		Q8GVV1;F4IBX4; F4IBX5	AT1G78915	1.34	+	0.00459375
Other/unknown	At2g03420		Q9ZQ78	AT2G03420	0.76		0.656275
Other/unknown	At2g27290	FAM210B-like protein, putative (DUF1279)	Q9XIN6	AT2G27290	1.09		0.0664737
Other/unknown	At2g27680		Q9ZUX0	AT2G27680	2.23	+	0
Other/unknown	At3g14420		Q9LRR9;A8MS37; B3H4B8;Q2V3V9	AT3G14420	3.39	+	0
Other/unknown	At3g61870	Plant/protein	F4IX01;Q9M277	AT3G61870	1.63	+	0
Other/unknown	At4g02725		Q6DBF6	AT4G02725	3.78	+	0.00925641
Other/unknown	At5g14910	Heavy metal transport/detoxification superfamily protein	Q93VK7	AT5G14910	1.92	+	0.000861111
Other/unknown	At5g16660		A8MS48;Q8H0X5	AT5G16660	1.25	+	0.00556777
Other/unknown	At5g42070		Q8RWR9	AT5G42070	1.23		0.192904
Other/unknown	At5g51010		Q9FI47	AT5G51010	2.54	+	0.00461176
Other/unknown	BASS2		Q1EBV7	AT2G26900	2.16	+	0.00171154
Other/unknown	CAC3		Q9LD43	AT2G38040	1.82	+	0
Other/unknown	CAS	Calcium sensing receptor	Q9FN48;A0A1P8B CX7	AT5G23060	1.25	+	0.00181633
Other/unknown	F11M15.26		Q9SXE2	AT1G51400	0.58	+	0
Other/unknown	F13A11.2		Q9C7S3	AT1G42960	2.33	+	0
Other/unknown	F24J8.11		Q9LPK9	AT1G21500	2.37		0.262458
Other/unknown	FAB2	Acyl-[acyl-carrier-protein] desaturase	F4IS32;O22832	AT2G43710	3.36	+	0.00710035
Other/unknown	FBA1	Fructose-bisphosphate aldolase	Q9ZU52	AT2G01140	2.23	+	0.0212457
Other/unknown	FBA1	Fructose-bisphosphate aldolase	Q9SJU4;F4IGL5; F4IGL7	AT2G21330	2.69	+	0
Other/unknown	FBA2	Probable fructose-bisphosphate aldolase 2	Q944G9;F4JUJ5	AT4G38970	2.12	+	0
Other/unknown	FLAP1	Fluctuating light acclimation protein 1	Q8RWI0	AT1G54520	1.52	+	0.00782313
Other/unknown	GAPA2		A0A1P8APR6;Q9L PW0;F4HNZ6	AT1G12900	1.92	+	0
Other/unknown	GC1		A0A1P8B167;Q9S JU9	AT2G21280	2.67	+	0
Other/unknown	GDCST		A0A2H1ZEA9;O65 396	AT1G11860	1.41	+	0.000905109
Other/unknown	GER3		P94072	AT5G20630	2.86	+	0.00113761
Other/unknown	GLDP1		Q94B78;B3H5Y8	AT4G33010	2.92	+	0.00483951
Other/unknown	GLN2	Glutamine synthetase/mitochondrial	Q43127	AT5G35630	2.10	+	0.00183505

Other/unknown	GYRA		Q9CAF6	AT3G10690	2.05	+	0
Other/unknown	HSP70-3		O65719	AT3G09440	3.30	+	0.00449573
Other/unknown	LGUC		Q8W593	AT1G67280	2.87	+	0.00145882
Other/unknown	LOX2	Lipoxygenase 2	P38418;A0A1I9LP H1	AT3G45140	2.29	+	0
Other/unknown	LTA2	Dihydrolipoyllysine-residue acetyltransferase component 4 of pyruvate dehydrogenase complex	Q9SQI8	AT3G25860	2.14	+	0.00562963
Other/unknown	LTA3	Dihydrolipoyllysine-residue acetyltransferase component 1 of pyruvate dehydrogenase complex	F4J5T2;Q0WQF7	AT3G52200	1.53	+	0.00453448
Other/unknown	MFP1		Q9LW85	AT3G16000	1.26	+	0.00928617
Other/unknown	MNC6.3	Thylakoid luminal 17.4 kDa protein	F4JX83;A0A1P8B AQ0;P81760	AT5G53490	1.21	+	0.0148304
Other/unknown	MRO11.7	GPI-anchored adhesin-like protein	A0A1P8BAU8;Q9 FF91	AT5G23890	2.94	+	0.00141714
Other/unknown	MXK3.17		Q93Y08	AT5G64940	1.21		0.177944
Other/unknown	NAGK		Q9SCL7	AT3G57560	2.40	+	0.00140909
Other/unknown	OEP161		Q9ZV24	AT2G28900	3.00	+	0
Other/unknown	PLGG1		Q9FVQ4	AT1G32080	2.90	+	0.017314
Other/unknown	PMDH2	Malate dehydrogenase	F4KDZ4;Q9ZP05; A0A1P8BBQ0;A8 MRP1;B3H560	AT5G09660	2.60	+	0
Other/unknown	PPD2	PsbP domain-containing protein 2	Q8VY52	AT2G28605	3.80		0.972829
Other/unknown	PPD5	PsbP domain-containing protein 5	A0A178U9N5;P82 715	AT5G11450	1.97	+	0.000815789
Other/unknown	PPD7	PsbP domain-containing protein 7	F4J7A7;A0A1I9LQ E7	AT3G05410	1.63	+	0.00214218
Other/unknown	PRXII		Q949U7	AT3G52960	2.21	+	0
Other/unknown	PTAC5	Protein disulfide isomerase pTAC5	A0A1P8B4I3;A1A6 M1	AT4G13670	2.57	+	0.00614841
Other/unknown	RAT5		Q9LD28;O81826; Q9C681	AT5G54640	2.02	+	0.0465067
Other/unknown	RPI3		Q9S726	AT3G04790	2.30		0.978054
Other/unknown	SHM1		Q9SZJ5	AT4G37930	2.82	+	0
Other/unknown	STR10	Rhodanese-like domain-containing protein 10	Q9SR92	AT3G08920	1.12		0.0690184
Other/unknown	STR11	Rhodanese-like domain-containing protein 11	Q0WWT7	AT4G24750	1.01		0.827885
Other/unknown	STR14	Rhodanese-like domain-containing protein 14	Q94A65	AT4G27700	1.95	+	0.0333842
Other/unknown	STR9	Rhodanese-like domain-containing protein 9	O48529	AT2G42220	0.71	+	0.00172816
Other/unknown	T6G15.50		Q9T0H1	AT4G13500	1.24	+	0.046385
Other/unknown	TAAC	Thylakoid ADP,ATP carrier protein	Q9M024	AT5G01500	1.31	+	0.0109851
Other/unknown	TL15A	Thylakoid luminal 15 kDa protein 1	O22160	AT2G44920	1.05		0.0571353
Other/unknown	TL15B	Thylakoid luminal 15.0 kDa protein 2	Q9LVV5	AT5G52970	2.55	+	0.008
Other/unknown	TL17.9	Thylakoid luminal 17.9 kDa protein	Q9SW33	AT4G24930	1.66	+	0.00472289
Other/unknown	TL19	Thylakoid luminal 19 kDa protein	P82658	AT3G63540	1.23	+	0.00619217

Other/unknown	TL20.3	Thylakoid lumenal protein TL20.3	B6EUA5;Q8H1Q1; A0A178W1Q3	AT1G12250	1.30		0.0875521
Other/unknown	TPT		A0A219HYB6;A0A 219HZH3;A0A219I 0W9;Q9ZSR7	AT5G46110	2.40	+	0.000855172
Other/unknown	TRL22		Q8LCT3	AT4G29670	4.56	+	0.0199075
Other/unknown	YCF37	Homolog of Synechocystis YCF37	O64835	AT2G23670	1.66	+	0
Pigment synthesis	CHLD	Magnesium-chelatase subunit ChLD	Q9SJE1	AT1G08520	3.46	+	0
Pigment synthesis	CHLG	Chlorophyll synthase	Q38833	AT3G51820	1.04		0.729631
Pigment synthesis	CHLH	Magnesium-chelatase subunit ChH	Q9FNB0;A8MR05	AT5G13630	1.81	+	0.00178894
Pigment synthesis	CHLI1	Magnesium-chelatase subunit ChII	P16127	AT4G18480	3.58	+	0.00259459
Pigment synthesis	CHLI1	Magnesium-chelatase subunit ChII	Q5XF33	AT5G45930	1.65	+	0.0357065
Pigment synthesis	CHLM	Magnesium protoporphyrin IX methyltransferase	A0A1P8B4G1;Q9 SW18	AT4G25080	1.03		0.969714
Pigment synthesis	CHLP	Geranylgeranyl diphosphate reductase	Q9CA67	AT1G74470	1.32	+	0.00177114
Pigment synthesis	CRD1	Magnesium-protoporphyrin IX monomethyl ester [oxidative] cyclase	Q9M591;F4J0U9	AT3G56940	1.13	+	0.00873203
Pigment synthesis	CYP97B3	Cytochrome P450 97B3	O23365	AT4G15110	1.27	+	0.012
Pigment synthesis	CYP97C1	Carotene epsilon-monooxygenase	Q6TBX7	AT3G53130	1.28		0.0660686
Pigment synthesis	DVR	Divinyl chlorophyllide a 8-vinyl-reductase	Q1H537	AT5G18660	1.03		0.7156
Pigment synthesis	FC2	Ferrochelatase-2	F4IMT3;O04921	AT2G30390	1.89	+	0.0147872
Pigment synthesis	HCAR	7-hydroxymethyl chlorophyll a reductase	Q8GS60	AT1G04620	1.52	+	0.0048
Pigment synthesis	LUT5	Protein LUTEIN DEFICIENT 5	Q93VK5	AT1G31800	1.18	+	0.018342
Pigment synthesis	NOL	Chlorophyll(ide) b reductase NOL	Q8LEU3	AT5G04900	1.37	+	0.0216271
Pigment synthesis	PAO	Pheophorbide a oxygenase	Q9FYC2	AT3G44880	3.48	+	0.000992
Pigment synthesis	PDS	15-cis-phytoene desaturase/chromoplastic	Q07356	AT4G14210	1.08		0.950155
Pigment synthesis	PORB	Protochlorophyllide reductase B	P21218	AT4G27440	0.28	+	0.00096124
Pigment synthesis	PORC	Protochlorophyllide reductase C	F4I2F8;O48741	AT1G03630	0.84	+	0.00671777
Pigment synthesis	PPOX1	Protoporphyrinogen oxidase 1	P55826	AT4G01690	1.10		0.105082
Pigment synthesis	PPOX2	Protoporphyrinogen oxidase 2/mitochondrial	Q8S9J1;A0A1P8B E58;A0A1P8BE27	AT5G14220	4.46	+	0.00784983
Pigment synthesis	VTE3		Q9LY74	AT3G63410	2.70	+	0
Pigment synthesis	YCF54		Q9LVM3	AT5G58250	1.29	+	0.011018
Pigment synthesis	ZDS1		Q38893	AT3G04870	4.04	+	0.00621429
Plastoglobule	ABC1K3	Uncharacterized aarF domain-containing protein kinase At1g79600	Q9MA15	AT1G79600	2.86	+	0
Plastoglobule	At1g06690		Q94A68	AT1G06690	5.87	+	0.00468526
Plastoglobule	At1g26090		Q6DYE4	AT1G26090	4.53	+	0.00587636
Plastoglobule	At1g32220	Uncharacterized protein At1g32220	Q9FVR6	AT1G32220	3.33	+	0.000953846
Plastoglobule	At1g54570	Acyltransferase-like protein At1g54570	Q9ZVN2	AT1G54570	8.89	+	0.00134054
Plastoglobule	At1g71810	Uncharacterized aarF domain-containing protein kinase At1g71810	Q94BU1	AT1G71810	3.25	+	0.00162092
Plastoglobule	At1g78140		Q8LBV4	AT1G78140	4.00	+	0.0044766
Plastoglobule	At2g34460	Uncharacterized protein At2g34460	Q8H124	AT2G34460	1.99	+	0

Plastoglobule	At2g41040		Q0WPT7	AT2G41040	4.69	+	0.00464822
Plastoglobule	At3g07700		B9DGY1;F4JFM1	AT3G07700	5.67	+	0.000832215
Plastoglobule	At3g24190		Q9LRN0	AT3G24190	6.51	+	0.00157962
Plastoglobule	At3g27110		A0A178VFN4;Q9LSC4;A0A1I9LM40;A0A1I9LM41	AT3G27110	5.00	+	0.00707586
Plastoglobule	At4g13200	Uncharacterized protein At4g13200	Q8LDV3	AT4G13200	2.15	+	0
Plastoglobule	At5g05200	Uncharacterized aarF domain-containing protein kinase At5g05200	Q9ASX5	AT5G05200	6.55	+	0.00133333
Plastoglobule	CCD4	Probable carotenoid cleavage dioxygenase 4	O49675	AT4G19170	1.60	+	0
Plastoglobule	CSP41B	Chloroplast stem-loop binding protein of 41 kDa b	A0A1P8ATL2;Q9SA52	AT1G09340	1.80	+	0.00179798
Plastoglobule	CYP74A	Allene oxide synthase	Q96242	AT5G42650	1.29	+	0
Plastoglobule	PAP1	Probable plastid-lipid-associated protein 1	O81439	AT4G04020	5.19	+	0.00103333
Plastoglobule	PAP10	Probable plastid-lipid-associated protein 10	Q8W4F1	AT2G46910	3.51	+	0.0070274
Plastoglobule	PAP11	Probable plastid-lipid-associated protein 11	O81304	AT4G00030	1.68	+	0.00813423
Plastoglobule	PAP12	Probable plastid-lipid-associated protein 12	Q8LAP6	AT1G51110	1.60	+	0.0107245
Plastoglobule	PAP13	Probable plastid-lipid-associated protein 13	Q8S9M1;F4IM05;A8MRU9	AT2G42130	2.13	+	0.00153086
Plastoglobule	PAP2	Probable plastid-lipid-associated protein 2	O49629	AT4G22240	5.76	+	0.00142529
Plastoglobule	PAP3	Probable plastid-lipid-associated protein 3	O82291	AT2G35490	2.55	+	0.0013262
Plastoglobule	PAP4	Probable plastid-lipid-associated protein 4	Q9LU85	AT3G26070	1.93	+	0
Plastoglobule	PAP5	Probable plastid-lipid-associated protein 5	A0A1I9LP70;Q6DBN2	AT3G26080	2.44		0.108206
Plastoglobule	PAP6	Probable plastid-lipid-associated protein 6	Q9LW57;A0A1I9LQU5;A0A1I9LQU3	AT3G23400	2.03	+	0
Plastoglobule	PAP8	Probable plastid-lipid-associated protein 8	Q941D3;F4K2P2	AT5G19940	0.54	+	0.000932331
Plastoglobule	PAP9	Probable plastid-lipid-associated protein 9	Q9M2P7	AT3G58010	1.90	+	0
Plastoglobule	PLAT1	PLAT domain-containing protein 1	O65660	AT4G39730	2.36	+	0
Plastoglobule	PSY	PHYTOENE SYNTHASE	F4KGX7;P37271	AT5G17230	1.05		0.957052
Plastoglobule	VTE1	Tocopherol cyclase	Q94FY7	AT4G32770	3.39	+	0.00140113
Plastoglobule			Q9SR77	AT3G10130	2.72	+	0.000976378
Plastoglobule			Q9LW26	AT3G26840	4.31	+	0.0049
Plastoglobule			Q9M236;F4IZ56	AT3G43540	2.73	+	0.0108571
Protease	ARASP2		O23053	AT1G05140	1.05		0.378496
Protease	At2g21960		Q9SJ03	AT2G21960	1.55	+	0.00184456
Protease	CLPP4		Q94B60	AT5G45390	1.39	+	0.0230225
Protease	CLPP5		Q9S834	AT1G02560	2.98	+	0.0319891
Protease	EGY2		F4K0T6;F4K0T7;Q9FFK3	AT5G05740	1.30	+	0.0107578
Protease	FTSH11	ATP-dependent zinc metalloprotease FTSH 11/mitochondrial	Q9FGM0	AT5G53170	3.14	+	0

Protease	FTSH12	ATP-dependent zinc metalloprotease FTSH 12	A0A1P8ARD2;Q9SAJ3;A0A1P8ARE4	AT1G79560	4.65	+	0
Protease	FTSH9	ATP-dependent zinc metalloprotease FTSH 9	Q9FIM2	AT5G58870	6.80	+	0.00185417
Protease	SPPA	Serine protease SPPA	Q9C9C0;A0A1P8AUG2	AT1G73990	4.27	+	0.00451502
Protein folding	At3g12345	FKBP-type peptidyl-prolyl cis-trans isomerase	Q9LHH3	AT3G12345	1.49	+	0.00138547
Protein folding	CLPB3	Chaperone protein ClpB3	Q9LF37	AT5G15450	5.07	+	0.00161039
Protein folding	CPN21	20 kDa chaperonin	O65282	AT5G20720	1.92	+	0.00410619
Protein folding	CPN60A1	Chaperonin 60 subunit alpha 1	P21238	AT2G28000	3.44	+	0
Protein folding	CYP26-2	Peptidyl-prolyl cis-trans isomerase CYP26-2	F4HTT6;A0A1P8APN5	AT1G74070	1.61	+	0.0108902
Protein folding	CYP28	Peptidyl-prolyl cis-trans isomerase CYP28	A0A1P8B9P2;O65220	AT5G35100	2.56	+	0.00155975
Protein folding	CYP37	Peptidyl-prolyl cis-trans isomerase CYP37	P82869;A0A1I9LQ22;A0A1I9LQ23	AT3G15520	1.80	+	0.00573585
Protein folding	DJA5		Q940V1;Q9SJJ7	AT4G39960	2.10	+	0.00589781
Protein folding	DJA7		A0A1P8ART2;Q0WN54	AT1G80030	2.06	+	0.00478049
Protein folding	FKBP13	Peptidyl-prolyl cis-trans isomerase FKBP13	Q9SCY2	AT5G45680	2.90	+	0.00107826
Protein folding	FKBP16-3	Peptidyl-prolyl cis-trans isomerase FKBP16-3	A0A1P8B252;O22870	AT2G43560	1.23	+	0.00908176
Protein folding	FKBP16-4	Peptidyl-prolyl cis-trans isomerase FKBP16-4	Q9SR70	AT3G10060	1.52	+	0.00215238
Protein folding	FKBP17-2	Peptidyl-prolyl cis-trans isomerase FKBP17-2	Q9LDY5	AT1G18170	1.17		0.482104
Protein folding	FKBP18	Peptidyl-prolyl cis-trans isomerase FKBP18	A0A1P8APZ5;Q9LM71	AT1G20810	2.84	+	0.00104202
Protein folding	FKBP19	Peptidyl-prolyl cis-trans isomerase FKBP19	Q9LYR5;A0A1R7T3F4	AT5G13410	3.04	+	0
Protein folding	HSP70-6	Heat shock 70 kDa protein 6	Q9STW6	AT4G24280	1.86		0.0862768
Protein folding	TIG	Trigger factor-like protein TIG	Q8S9L5	AT5G55220	3.13	+	0.0017451
Protein translocation	CLPC1		Q9FI56	AT5G50920	3.34	+	0
Protein translocation	SCY1	Preprotein translocase subunit SCY1	Q38885	AT2G18710	1.44	+	0.00777027
Protein translocation	SECA1	Protein translocase subunit SecA	A0A1P8B485;Q9SYI0;F4JG57	AT4G01800	1.88	+	0.0049205
Protein translocation	TATA	Sec-independent protein translocase protein TATA	Q9LKU2	AT5G28750	0.85		0.764232
Protein translocation	TATB	Sec-independent protein translocase protein TATB	Q9XH75	AT5G52440	1.22	+	0.0148739
Protein translocation	TATC	Sec-independent protein translocase protein TATC	Q9SJV5	AT2G01110	1.48	+	0.00176238
Protein translocation	TIC110		Q8LPR9	AT1G06950	3.54	+	0.0016
Protein translocation	TIC55		Q9SK50	AT2G24820	3.33	+	0
PSI	PSAA	Photosystem I P700 chlorophyll a apoprotein A1	P56766	ATCG00350	0.79	+	0
PSI	PSAB	Photosystem I P700 chlorophyll a apoprotein A2	P56767	ATCG00340	0.72	+	0.00134783
PSI	PSAC	Photosystem I iron-sulfur center	P62090	ATCG01060	0.67	+	0.00105983

PSI	PSAD	Photosystem I reaction center subunit II-2	Q9SA56;Q9S7H1	AT1G03130;AT4G02770	0.72	+	0.00560886
PSI	PSAE1	Photosystem I reaction center subunit IV A	Q9S831	AT4G28750	0.65	+	0
PSI	PSAE2	Photosystem I reaction center subunit IV B	Q9S714	AT2G20260	0.89		0.212192
PSI	PSAF	Photosystem I reaction center subunit III	Q9SHE8	AT1G31330	0.82	+	0.00135519
PSI	PSAG	Photosystem I reaction center subunit V	Q9S7N7	AT1G55670	0.80	+	0
PSI	PSAH	Photosystem I reaction center subunit VI-1	Q9SUI7;Q9SUI6	AT1G52230;AT3G16140	0.90	+	0.0408257
PSI	PSAK	Photosystem I reaction center subunit psak	Q9SUI5	AT1G30380	0.82	+	0.0107915
PSI	PSAL	Photosystem I reaction center subunit XI	A0A1P8B6D0;Q9SUI4	AT4G12800	0.81	+	0
PSI	PSAN	Photosystem I reaction center subunit N	P49107	AT5G64040	0.72	+	0
PSI	PSAO	Photosystem I subunit O	Q949Q5	AT1G08380	0.85		0.683176
PSII	PSB28	Photosystem II reaction center PSB28 protein	F4JM05;Q8W0Y8	AT4G28660	2.23	+	0
PSII	PSB33	Rieske (2Fe-2S) domain-containing protein	Q9C9I7	AT1G71500	1.60	+	0
PSII	PSBA (D1)	Photosystem II protein D1	P83755	ATCG00020	1.01		0.13957
PSII	PSBB (CP47)	Photosystem II CP47 reaction center protein	P56777	ATCG00680	1.12		0.835847
PSII	PSBC (CP43)	Photosystem II CP43 reaction center protein	P56778	ATCG00280	0.98		0.896823
PSII	PSBD (D2)	Photosystem II D2 protein	P56761	ATCG00270	1.05		0.883602
PSII	PSBE	Cytochrome b559 subunit alpha	P56779	ATCG00580	1.00		0.728399
PSII	PSBF	Cytochrome b559 subunit beta	P62095	ATCG00570	0.95	+	0.0106914
PSII	PSBH	Photosystem II reaction center protein H	P56780	ATCG00710	1.13		0.296312
PSII	PSBO1	Oxygen-evolving enhancer protein 1-1	P23321	AT5G66570	0.97	+	0.00808
PSII	PSBO2	Oxygen-evolving enhancer protein 1-2	Q9S841	AT3G50820	1.01		0.55003
PSII	PSBP1	Oxygen-evolving enhancer protein 2-1	Q42029	AT1G06680	1.00		0.615862
PSII	PSBQ1	Oxygen-evolving enhancer protein 3-1	Q9XFT3	AT4G21280	1.08	+	0.00462992
PSII	PSBQ2	Oxygen-evolving enhancer protein 3-2	Q41932	AT4G05180	0.56	+	0
PSII	PSBR	Photosystem II 10 kDa polypeptide	P27202	AT1G79040	0.23		0.731128
PSII	PSBT	Photosystem II 5 kDa protein	A0A1I9LS90;Q39195	AT3G21055	0.90	+	0.0262507
PSII repair	ALB3	Inner membrane protein ALBINO3	F4IJM1;Q8LBP4	AT2G28800	1.21	+	0.0207564
PSII repair	CTPA1		F4KHG6	AT5G46390	1.89	+	0.00870358
PSII repair	CYP38	Peptidyl-prolyl cis-trans isomerase CYP38	Q9SSA5	AT3G01480	1.02		0.789096
PSII repair	DEG5		A0A1P8B644;A0A1P8B643;Q9SEL7	AT4G18370	2.49	+	0.00108772
PSII repair	DEG8		F4KFV6;Q9LU10	AT5G39830	3.77	+	0.00583394
PSII repair	DEGP1	Protease Do-like 1	O22609	AT3G27925	2.16	+	0.00137778
PSII repair	DEGP2	Protease Do-like 2	B3H581;O82261	AT2G47940	0.85		0.999228
PSII repair	F17F16.7	Protein HIGH CHLOROPHYLL FLUORESCENCE PHENOTYPE 173	A0A1P8AWY1;Q8W4D6;A0A1P8AWU9	AT1G16720	2.01	+	0.00136264

PSII repair	FKBP20-2	Peptidyl-prolyl cis-trans isomerase FKBP20-2	A0A1I9LRJ6;Q0W RJ7	AT3G60370	1.83	+	0.00617021
PSII repair	FTSH1	ATP-dependent zinc metalloprotease FTSH 1	Q39102	AT1G50250	1.72	+	0
PSII repair	FTSH2	ATP-dependent zinc metalloprotease FTSH 2	A0A1P8AXC1;O80 860	AT2G30950	1.75	+	0.00457391
PSII repair	FTSH5	ATP-dependent zinc metalloprotease FTSH 5	Q9FH02	AT5G42270	1.66	+	0
PSII repair	FTSH8	ATP-dependent zinc metalloprotease FTSH 8	Q8W585	AT1G06430	2.20	+	0.00261818
PSII repair	FTSY		O80842	AT2G45770	3.81	+	0
PSII repair	HHL1	Protein HHL1	Q8LDL0	AT1G67700	1.40	+	0.0270444
PSII repair	HSP70-7		Q9LTX9	AT5G49910	2.34	+	0
PSII repair	LPA1	Protein LOW PSII ACCUMULATION 1	Q9SRY4	AT1G02910	1.23	+	0.0109524
PSII repair	LQY1	Protein disulfide-isomerase LQY1	Q8GSJ6	AT1G75690	1.54	+	0.0107267
PSII repair	LTO1	Thiol-disulfide oxidoreductase LTO1	A0A1P8B950;Q8L 540	AT4G35760	1.62	+	0
PSII repair	MET1	Protein MET1	Q94BS2	AT1G55480	1.97	+	0.00461404
PSII repair	MPH1	Protein MAINTENANCE OF PSII UNDER HIGH LIGHT 1	Q9FL44	AT5G07020	1.26	+	0.000849315
PSII repair	PAM68	Protein PAM68	A0A1P8B8D1;O49 668	AT4G19100	1.48	+	0.00106897
PSII repair	PDI6	Protein disulfide isomerase-like 1-2	Q9SRG3	AT1G77510	1.99	+	0.0275789
PSII repair	PPL1	PsbP-like protein 1	P82538	AT3G55330	1.79	+	0.000879433
PSII repair	PSB27-1	Photosystem II repair protein PSB27-H1	Q9LR64	AT1G03600	1.16		0.436786
PSII repair	PSB27-2	Photosystem II D1 precursor processing protein PSB27-H2	A0A1P8ASY3;Q9Z VZ9	AT1G05385	1.93	+	0.00503475
PSII repair	ROC4		F4IX28;F4IX26;P3 4791	AT3G62030	1.07		0.715257
PSII repair	RubA	Rubredoxin-like superfamily protein	Q9SLI4	AT1G54500	1.43	+	0.0395772
PSII repair	SRP-54A		A8MSA9;P49967	AT1G48900	1.66	+	0.00911041
PSII repair	TERC		A0A1P8BDK4;F4J ZG9	AT5G12130	1.41	+	0.000867133
PSII repair	TL18.3	UPF0603 protein At1g54780	Q9ZVL6	AT1G54780	1.20	+	0
PSII repair	VIPP1	Membrane-associated protein VIPP1	A0A178W0D3;O8 0796	AT1G65260	1.43	+	0.00805316
Redox regulation	At1g14345	NAD(P)-linked oxidoreductase superfamily protein	Q949S6	AT1G14345	1.62	+	0.0015122
Redox regulation	At1g50450	Saccharopine dehydrogenase	Q94BZ0	AT1G50450	2.95	+	0.00155
Redox regulation	ATHM2	Thioredoxin M2	Q9SEU8;F4JG94	AT4G03520	1.82	+	0
Redox regulation	BAS1	2-Cys peroxiredoxin BAS1	Q96291	AT3G11630	2.47	+	0.000821192
Redox regulation	BAS1B		Q9C5R8;A0A1P8 BD74	AT5G06290	3.10	+	0.0202075
Redox regulation	CITRX	Thioredoxin-like protein CITRX	Q9M7X9	AT3G06730	1.44	+	0.00182564
Redox regulation	ENH1	Rubredoxin family protein	Q9FFJ2;A8MSF2	AT5G17170	1.89	+	0.0048595
Redox regulation	FSD3	Superoxide dismutase [Fe] 3	Q9FMX0	AT5G23310	0.94		1
Redox regulation	MCK7.20	Malate dehydrogenase	Q8H1E2;F4KEX3	AT5G58330	2.36	+	0

Redox regulation	MDH	Malate dehydrogenase	Q9SN86	AT3G47520	2.39	+	0
Redox regulation	MED24.18	Thioredoxin family protein	Q940I2	AT5G03880	1.22	+	0.00945455
Redox regulation	NTRC	NADPH-dependent thioredoxin reductase 3	O22229	AT2G41680	4.84	+	0
Redox regulation	PRXQ	Peroxiredoxin Q	A0A1I9LR27;F4JB C9;Q9LU86	AT3G26060	2.47	+	0
Redox regulation	TRXF1		Q9XFH8	AT3G02730	56.14		0.970862
Redox regulation	TRXM1	Thioredoxin M1	O48737	AT1G03680	1.66	+	0.00357143
Redox regulation	TRXM4	Thioredoxin M4	Q9SEU6	AT3G15360	1.76	+	0
Ribosome	PSRP2	30S ribosomal protein 2	Q8VYM4	AT3G52150	2.22	+	0
Ribosome	PSRP5	50S ribosomal protein 5	Q9LER7	AT3G56910	1.90	+	0.00558824
Ribosome	PSRP6		A0A1P8BCP6;Q9 FKP0	AT5G17870	3.52	+	0.0205057
Ribosome	RPL1	50S ribosomal protein L1	Q9LY66;F4J296	AT3G63490	2.06	+	0.00115888
Ribosome	RPL10	50S ribosomal protein L10	Q9FY50	AT5G13510	2.10	+	0
Ribosome	RPL11	50S ribosomal protein L11	Q9MAP3	AT1G32990	2.20	+	0.000984127
Ribosome	RPL12A	50S ribosomal protein L12-3	P36212;P36210	AT3G27830;AT3G 27850	2.77	+	0.00102479
Ribosome	RPL13		Q9SYL9	AT1G78630	1.22	+	0.0394703
Ribosome	RPL14	50S ribosomal protein L14	P56792	AtCg00780	1.84	+	0
Ribosome	RPL15	50S ribosomal protein L15	P25873	AT3G25920	2.06	+	0
Ribosome	RPL16	50S ribosomal protein L16	P56793	AtCg00790	2.45	+	0.000892086
Ribosome	RPL17	50S ribosomal protein L17	Q9M385	AT3G54210	1.71	+	0.00499617
Ribosome	RPL18	50S ribosomal protein L18	Q9SX68	AT1G48350	1.71	+	0
Ribosome	RPL19-1		Q8W463	AT4G17560	2.33		0.0513404
Ribosome	RPL21	50S ribosomal protein L21	P51412	AT1G35680	1.80	+	0.00101639
Ribosome	rpl22	50S ribosomal protein L22	P56795	AtCg00810	0.99		0.981351
Ribosome	RPL23-A	50S ribosomal protein L23	P61845	AtCg00840	2.12	+	0.00137017
Ribosome	RPL24	50S ribosomal protein L24	P92959	AT5G54600	1.53	+	0.009425
Ribosome	RPL27	50S ribosomal protein L27	Q9FLN4	AT5G40950	2.06	+	0.000911765
Ribosome	RPL29	50S ribosomal protein L29	Q9FJP3	AT5G65220	1.78	+	0.00212207
Ribosome	RPL2-A	50S ribosomal protein L2	P56791	AtCg00830	1.94	+	0
Ribosome	RPL31	50S ribosomal protein L31	Q9FWS4	AT1G75350	1.74	+	0.00922684
Ribosome	RPL3A	50S ribosomal protein L3-1	Q9SKX4	AT2G43030	1.97	+	0
Ribosome	RPL4	50S ribosomal protein L4	Q2V4Q4;Q3EDH2; O50061	AT1G07320	1.71	+	0.00901935
Ribosome	RPL5	50S ribosomal protein L5	O04603	AT4G01310	2.15	+	0.000925373
Ribosome	RPL6	50S ribosomal protein L6	O23049	AT1G05190	2.13	+	0
Ribosome	RPL9	50S ribosomal protein L9	P25864	AT3G44890	2.47	+	0
Ribosome	RPS10	30S ribosomal protein S10	Q9LK61	AT3G13120	2.56	+	0.00180711
Ribosome	RPS11	30S ribosomal protein S11	P56802	AtCg00750	1.83	+	0.000939394

Ribosome	rps12-A	30S ribosomal protein S12	P62126	AtCg00065;AtCg01230;AtCg00905	2.00	+	0.00175369
Ribosome	RPS13	30S ribosomal protein S13	P42732	AT5G14320	1.99	+	0
Ribosome	rps14	30S ribosomal protein S14	P56804	AtCg00330	2.31	+	0.0290909
Ribosome	RPS15	30S ribosomal protein S15	P56805	AtCg01120	1.86	+	0.00919745
Ribosome	RPS17	30S ribosomal protein S17	P16180	AT1G79850	2.24	+	0
Ribosome	RPS18	30S ribosomal protein S18	P56807	AtCg00650	1.95	+	0
Ribosome	RPS19	30S ribosomal protein S19	P56808	AtCg00820	2.03	+	0.00779661
Ribosome	RPS2	30S ribosomal protein S2	P56797	AtCg00160	1.93	+	0.00147619
Ribosome	RPS20	30S ribosomal protein S20	Q9ASV6	AT3G15190	2.16	+	0.00158974
Ribosome	RPS3	30S ribosomal protein S3	P56798	AtCg00800	1.62	+	0.00674126
Ribosome	RPS4	30S ribosomal protein S4	P56799	AtCg00380	1.78	+	0.000885714
Ribosome	RPS5	30S ribosomal protein S5	P93014	AT2G33800	1.50	+	0.0049771
Ribosome	RPS6	30S ribosomal protein S6 alpha	A0A1P8AV66;Q8VY91	AT1G64510	1.89	+	0.00916825
Ribosome	RPS7	Ribosomal protein S7	A0A2P2CLF5;P92557	AT2G07696	1.94		0.987819
Ribosome	rps7-A	30S ribosomal protein S7	P61841	AtCg00900;AtCg01240	1.92	+	0.001
Ribosome	RPS8	30S ribosomal protein S8	P56801	AtCg00770	1.82	+	0.00156962
Ribosome	RPS9	30S ribosomal protein S9	Q9XJ27	AT1G74970	1.62	+	0
Ribosome	RRP31	30S ribosomal protein 3-1	A8MQL0;Q9SX22	AT1G68590	2.40	+	0.00581295
Starch	BAM3	Beta-amylase 3	O23553	AT4G17090	3.28	+	0.00148503
Starch	GBSS1	Granule-bound starch synthase 1/amyloplastic	Q9MAQ0	AT1G32900	32.99	+	0.00139326
Starch	SS1	Starch synthase 1/amyloplastic	Q9FNF2	AT5G24300	4.99	+	0
Starch	SS2	Starch synthase 2/amyloplastic	Q9MAC8	AT3G01180	30.27	+	0.000837838
Starch	SS3	Starch synthase 3/amyloplastic	F4IAG1;F4IAG2	AT1G11720	2.11	+	0.02175
Stress responsive	APE1	Acclimation of photosynthesis to environment	Q2HIR7;A0A219HZL6	AT5G38660	1.36	+	0
Stress responsive	AT5g02160		Q9FPH2	AT5G02160	0.57	+	0.00109735
Stress responsive	CLH1	Chlorophyllase-1	O22527	AT1G19670	15.85	+	0.000873239
Stress responsive	FLU	Protein FLUORESCENT IN BLUE LIGHT	F4JFR2;F4JFR1;Q940U6	AT3G14110	1.28	+	0.0397089
Stress responsive	LIR1	Light-regulated protein 1	Q96500	AT3G26740	1.04		0.0709843
Stress responsive	PPD3	PsbP domain-containing protein 3	Q9S720	AT1G76450	1.65	+	0.00143353
Stress responsive	PPD4	PsbP domain-containing protein 4	O49292	AT1G77090	1.82	+	0.00152147
Stress responsive	PPD6	PsbP domain-containing protein 6	Q9LXX5	AT3G56650	1.29	+	0.00864725
Stress responsive	TL29	Thylakoid luminal 29 kDa protein	A0A1P8B8W6;A0A1P8B8Y3;P82281	AT4G09010	1.27	+	0.00612676
Thylakoid architecture	CURT1A	Protein CURVATURE THYLAKOID 1A	O04616	AT4G01150	1.76	+	0.00211215
Thylakoid architecture	CURT1B	Protein CURVATURE THYLAKOID 1B	Q8LCA1	AT2G46820	1.22	+	0.00154037

Thylakoid architecture	CURT1C	Protein CURVATURE THYLAKOID 1C	Q9M812	AT1G52220	1.03		0.787229
Thylakoid architecture	CURT1D	Protein CURVATURE THYLAKOID 1D	A0A1P8B4V5;Q8LDD3	AT4G38100	1.38		0.397845
Thylakoid architecture	FZL	Probable transmembrane GTPase FZO-like	A0A1P8AUL4;Q1KPV0;A0A1P8AUL2	AT1G03160	1.59	+	0.00496203
Thylakoid architecture	PLSP1	Chloroplast processing peptidase	A0A1I9LMR3;Q8H0W1	AT3G24590	2.20	+	0.0108242
Thylakoid architecture	RIQ1	Reduced induction of non-photochemical quenching1	Q9SD79	AT5G08050	1.61	+	0.0018836
Thylakoid architecture	RIQ2	Reduced induction of non-photochemical quenching2	Q94F10	AT1G74730	1.71	+	0.00171981
Thylakoid architecture	THF1	Protein THYLAKOID FORMATION 1	Q9SKT0	AT2G20890	1.60	+	0

Table 14: Relative abundance of thylakoid-associated proteins in light-acclimated phosphorylation mutants. Details of the 447 MS-quantified thylakoid proteins from Col-0, stn7 and tap38 Arabidopsis plants grown at LL, ML and HL, including functional category, protein/gene name, description, UniProtKB identifier, TAIR ID and abundance ratios relative to Col-0 at ML. Proteins with altered abundance light irradiance (Light) or Genotype were identified by two-way ANOVA ( $p < 0.05$ ). Median protein iBAQ values were used for the calculation of ratios.

Category	Protein/ gene name	Description	UniProtKB accession	TAIR ID	Ratio relative to ML Col-0									Two-way ANOVA p- value Genotype	Two-way ANOVA p- value Light	Two-way ANOVA p- value Interaction
					LL Col-0	ML Col-0	HL Col-0	LL stn7	ML stn7	HL stn7	LL tap38	ML tap38	HL tap38			
Assembly	ALB4	ALBINO3-like protein 1	F4I9A9;Q9FYL3	AT1G24490	1.24	1	1.48	1.17	1.72	2.03	1.03	1.67	1.22	0.0090376 <sub>1</sub>	0.0022592	0.0117548
Assembly	At3g17930		Q94BY7	AT3G17930	0.79	1	1.55	0.61	1.20	1.78	0.87	1.59	1.30	0.120806	9.44E-08	0.0008925 <sub>73</sub>
Assembly	At4g28740		F4JM22	AT4G28740	0.67	1	1.41	0.84	1.17	1.77	0.69	0.86	1.06	5.65E-05	1.43E-08	0.0250456
Assembly	At5g48790		Q94F50;Q9FKB7	AT5G48790	0.98	1	1.24	1.28	0.89	1.20	1.25	0.93	1.22	0.654362	0.0002790 <sub>06</sub>	0.142975
Assembly	CCB1		Q9LSE4	AT3G26710	0.65	1	1.13	0.77	1.03	1.37	0.64	0.85	1.06	2.95E-05	2.80E-11	0.0160635
Assembly	CCS1	Cytochrome c biogenesis protein CCS1	Q9XIA4	AT1G49380	0.90	1	2.07	1.34	1.91	1.88	1.28	1.82	1.15	0.0037224 <sub>2</sub>	0.0001605 <sub>2</sub>	0.0014810 <sub>5</sub>
Assembly	CEST		Q9LU01	AT5G44650	0.62	1	1.71	0.69	1.28	2.04	0.63	1.22	1.48	5.21E-06	6.01E-16	4.31E-06
Assembly	F23E12.190		O65502	AT4G35250	0.87	1	0.97	1.05	1.13	1.24	0.91	0.99	0.92	1.47E-06	0.0211402	0.0388592
Assembly	FFC	Signal recognition particle 54 kDa protein	P37107	AT5G03940	0.81	1	1.35	1.06	0.94	2.51	0.62	1.12	1.34	4.47E-09	7.22E-14	3.54E-09
Assembly	HCF101	Fe-S cluster assembly factor HCF101	Q6STH5	AT3G24430	0.32	1	1.17	0.77	0.46	1.73	0.48	0.53	0.57	2.02E-05	2.23E-07	3.62E-06
Assembly	HCF136	Photosystem II stability/assembly factor HCF136	O82660;A0A1P8BG37	AT5G23120	1.04	1	1.53	1.31	1.62	1.74	1.26	1.24	1.48	2.90E-11	3.77E-12	3.00E-06
Assembly	HCF164	Thioredoxin-like protein HCF164	O23166	AT4G37200	0.73	1	0.95	0.86	1.22	1.11	0.72	1.09	0.81	0.0329372	1.58E-05	0.335606
Assembly	HCF208		Q9FJ81	AT5G52110	0.98	1	1.32	1.05	1.25	1.11	0.82	1.05	1.01	0.037713	0.0625774	0.108695
Assembly	LPA2	Protein LOW PSII ACCUMULATION 2	F4KDA6	AT5G51545	0.53	1	0.74	0.51	1.53	0.83	0.50	1.44	0.75	0.0433447	3.68E-07	0.0213195
Assembly	LPA3	Protein LOW PSII ACCUMULATION 3	Q8H0W0	AT1G73060	1.29	1	1.21	1.48	1.02	2.36	1.31	0.94	2.10	0.0044505 <sub>9</sub>	1.33E-06	0.0380471
Assembly	PPD1	PsbP domain-containing protein 1	O23403	AT4G15510	0.71	1	3.76	1.12	3.49	5.93	0.77	2.44	4.31	7.20E-05	7.93E-10	0.026366
Assembly	ycf4	Photosystem I assembly protein Ycf4	P56788	AtCg00520	0.70	1	1.32	0.81	1.25	1.81	0.86	1.08	1.39	8.22E-06	6.74E-13	0.0004472 <sub>98</sub>
Assembly	TL16.5	Thylakoid luminal 16.5 kDa protein	A0A1P8B5H3;O22773;A0A1P8B5G9	AT4G02530	1.03	1	0.76	1.07	0.46	0.97	0.95	0.54	0.75	0.0045477	5.40E-07	6.87E-06
ATP synthase	atpA	ATP synthase subunit alpha	P56757	ATCG00120	0.58	1	1.22	0.59	1.00	1.31	0.60	0.99	1.15	0.114644	3.51E-15	0.198899
ATP synthase	atpB	ATP synthase subunit beta	P19366	ATCG00480	0.59	1	0.99	0.61	0.99	1.12	0.57	0.99	0.97	1.21E-05	1.87E-19	7.75E-05
ATP synthase	ATPC1	ATP synthase gamma chain 1	Q01908	AT4G04640	0.65	1	0.86	0.70	1.12	1.01	0.63	0.92	1.02	0.0171392	3.26E-09	0.654635
ATP synthase	ATPD	ATP synthase subunit delta	Q9SSS9	AT4G09650	0.62	1	0.92	0.69	0.75	1.08	0.70	0.71	0.86	0.0760841	7.47E-08	0.0002455 <sub>4</sub>
ATP synthase	atpE	ATP synthase epsilon chain	P09468	ATCG00470	0.63	1	1.14	0.70	1.12	1.27	0.68	1.01	1.10	0.0003587 <sub>08</sub>	1.87E-13	0.143885
ATP synthase	atpF	ATP synthase subunit b	P56759	ATCG00130	0.53	1	1.31	0.61	1.34	1.67	0.51	1.13	1.18	0.557403	4.33E-05	0.752902

ATP synthase	atpH	ATP synthase subunit c	P56760	ATCG00140	0.03	1	0.16	0.42	0.68	0.25	0.26	0.18	0.27	0.505542	0.0541759	0.0498448
ATP synthase	atpI	ATP synthase subunit a	P56758	ATCG00150	0.73	1	0.34	0.95	0.80	0.82	0.72	0.85	0.63	0.0870473	0.0035816 <sub>1</sub>	0.0360638
ATP synthase	F10M6.100		Q42139	AT4G32260	0.55	1	1.14	0.56	0.57	1.24	0.56	0.59	1.02	0.0223413	8.18E-09	0.0015893 <sub>1</sub>
Carbon fixation	BCA1	Beta carbonic anhydrase 1	A0A119LQB3;P27140	AT3G01500	0.48	1	1.29	0.93	0.99	1.73	0.44	0.84	1.12	2.31E-12	2.26E-16	1.41E-07
Carbon fixation	rbcL	Ribulose biphosphate carboxylase large chain	O03042	ATCG00490	0.74	1	2.68	0.49	2.49	3.20	0.53	2.08	2.39	2.23E-11	1.73E-21	9.59E-13
Carbon fixation	RBCS-1A	Ribulose biphosphate carboxylase small chain 1A	P10795	AT1G67090	0.72	1	2.91	0.62	2.93	4.34	0.62	1.94	3.94	0.0127518	1.82E-09	0.0859096
Carbon fixation	RBCS-3B	Ribulose biphosphate carboxylase small chain 3B	P10798;P10797;B3H5S2;F4KA76	AT5G38410;AT5G38420	0.78	1	2.45	0.54	2.34	3.56	0.55	1.89	2.60	2.28E-10	4.46E-19	1.32E-09
Carbon fixation	RCA	Ribulose biphosphate carboxylase/oxygenase activase	P10896;F4IVZ7	AT2G39730	0.29	1	1.35	0.69	0.50	1.69	0.34	0.67	0.93	1.60E-14	4.09E-22	2.43E-16
Chloroplast replication	FTSZ1	Cell division protein FtsZ homolog 1	Q42545	AT5G55280	0.71	1	1.25	1.35	0.30	2.78	1.00	0.65	1.01	0.0001865 <sub>99</sub>	4.30E-06	0.0001189 <sub>21</sub>
Chloroplast replication	FTSZ2-1	Cell division protein FtsZ homolog 2-1	A0A1P8AXD8;O82533	AT2G36250	0.77	1	2.08	1.33	0.33	2.44	0.93	0.73	1.24	6.92E-05	2.98E-11	1.04E-06
Chlororespiration	PIFI		B3H4M0;F4J037;F4J034;Q9LVZ5;F4J036	AT3G15840	0.91	1	1.08	1.23	1.45	1.38	0.89	1.44	1.25	0.0006404 <sub>46</sub>	0.0036178 <sub>9</sub>	0.171208
Cytochrome b6f	petA	Cytochrome f	P56771	ATCG00540	0.66	1	1.15	0.79	1.21	1.07	0.66	1.03	1.03	5.00E-06	2.03E-14	0.0002085 <sub>64</sub>
Cytochrome b6f	petB	Cytochrome b6	P56773	ATCG00720	0.80	1	1.06	1.10	0.99	1.41	0.79	1.09	1.10	0.0014277 <sub>6</sub>	0.0003759 <sub>68</sub>	0.195827
Cytochrome b6f	petC	Cytochrome b6-f complex iron-sulfur subunit	Q9ZR03	AT4G03280	0.75	1	1.15	0.87	1.33	1.24	0.72	1.11	0.99	0.0001529 <sub>65</sub>	1.83E-08	0.0844564
Cytochrome b6f	petD	Cytochrome b6-f complex subunit 4	P56774	AT4G03280	0.79	1	1.28	0.83	1.05	1.31	0.74	1.20	1.32	0.3186	1.51E-06	0.501627
DNA/RNA	At1g08880	Probable histone H2AXb	Q9S9K7;O04848	At1g08880	0.77	1	4.96	0.92	1.14	3.44	0.59	2.20	4.59	0.291725	1.71E-08	0.160714
DNA/RNA	At2g21530		Q8GWP4	AT2G21530	0.41	1	0.81	0.48	1.82	1.19	0.95	0.98	0.53	2.92E-07	6.79E-09	7.64E-08
DNA/RNA	At2g24420		Q9ZQ26	AT2G24420	0.59	1	2.79	0.54	0.52	2.35	0.44	0.92	1.96	0.0002746 <sub>93</sub>	3.32E-16	0.0002186 <sub>05</sub>
DNA/RNA	At5g22880	Histone H2B.10	Q9FFC0	At5g22880	1.26	1	7.08	1.32	1.43	6.10	1.10	2.66	6.55	0.0132685	1.88E-16	0.0006488 <sub>48</sub>
DNA/RNA	At5g27670	Probable histone H2A.5	Q94F49	At5g27670	0.96	1	4.85	1.14	3.41	3.26	0.66	3.41	5.14	0.426846	3.31E-05	0.0621754
DNA/RNA	CP29A	29 kDa ribonucleoprotein	Q43349;F4JAF3	AT3G53460	2.65	1	10.72	6.12	15.05	14.18	3.43	11.92	9.75	4.02E-07	5.77E-08	9.06E-06
DNA/RNA	CP29B	RNA-binding protein CP29B	Q9ZUU4	AT2G37220	0.62	1	1.14	1.37	2.58	1.72	0.89	1.61	0.90	4.47E-12	2.17E-10	1.65E-06
DNA/RNA	CP31A	31 kDa ribonucleoprotein	Q04836	AT4G24770	0.20	1	1.07	0.24	1.25	1.75	0.21	2.47	1.38	4.07E-11	4.84E-18	9.80E-13
DNA/RNA	GYRA	Probable DNA gyrase subunit A/mitochondrial	Q9CAF6	AT3G10690	0.99	1	6.68	1.43	1.99	7.42	1.13	2.92	5.13	0.0022221 <sub>5</sub>	4.48E-16	2.65E-06
DNA/RNA	H2AV	Probable histone H2A variant 3	Q9C944;Q9SII0;O23628;F4JT33;Q9T0H7	AT1G52740	1.16	1	5.87	1.14	1.74	4.49	0.65	3.99	4.46	0.0387322	1.09E-11	5.54E-06
DNA/RNA	H2B	Histone H2B.7	Q9LZT0;O23629;Q9LZ45	At5g02570	1.01	1	8.59	1.47	2.59	15.71	1.10	2.80	14.54	0.832065	0.0001495 <sub>4</sub>	0.976384
DNA/RNA	RBG7	Glycine-rich RNA-binding protein 7	Q03250;F4IHK9	AT2G21660	1.75	1	8.44	2.24	2.44	6.69	2.25	3.93	4.60	0.352227	9.12E-17	6.67E-12

DNA/RNA	RBG8	Glycine-rich RNA-binding protein 8	Q03251;F4JVC0; F4JVC1;F4JVB9	AT4G39260	0.64	1	3.59	0.55	1.36	3.16	0.53	2.86	1.84	0.644783	2.54E-10	8.67E-07
DNA/RNA	rpoA	DNA-directed RNA polymerase subunit alpha	P56762	AtCg00740	1.16	1	3.56	1.22	1.88	4.05	1.11	2.34	3.38	0.0018409 9	3.45E-14	0.0004189 85
DNA/RNA	T10C21.40	Translation initiation factor IF-3	Q94B52;F4JQD8	At4g30690	0.75	1	0.66	0.66	1.21	0.94	0.61	1.43	1.15	0.0365418	0.0001699 92	0.107588
DNA/RNA	T6H20.190		Q9STF2	AT3G46780	1.54	1	0.71	1.77	0.65	1.57	1.68	1.04	1.38	2.73E-12	3.02E-19	4.99E-15
DNA/RNA	TUFA	Elongation factor Tu	P17745	AT4G20360	0.50	1	0.94	0.82	1.03	1.48	0.49	1.02	1.09	1.24E-10	4.41E-15	1.19E-07
Electron transfer	DRT112	Plastocyanin major isoform	P42699	AT1G20340	4.86	1	4.90	2.94	24.97	6.38	2.90	13.68	5.29	1.38E-12	1.46E-14	1.99E-14
Electron transfer	FD2	Ferredoxin-2	P16972	AT1G60950	0.35	1	0.57	0.67	5.94	0.49	0.67	2.64	2.71	0.0075580 1	4.35E-05	0.0003776 91
Electron transfer	LFNR1	Ferredoxin--NADP reductase, leaf isozyme 1	Q9FKW6;F4JZ46	AT5G66190	0.69	1	1.03	0.90	1.04	1.21	0.73	0.93	0.98	4.98E-06	2.65E-10	0.131695
Electron transfer	LFNR2	Ferredoxin--NADP reductase, leaf isozyme 2	Q8W493;C0Z2A 8	AT1G20020	0.53	1	0.79	0.67	0.88	0.97	0.51	0.61	0.81	1.41E-08	9.32E-12	4.43E-07
Electron transfer	NDC1	Alternative NAD(P)H-ubiquinone oxidoreductase C1/mitochondrial	Q8GXR9	AT5G08740	0.64	1	2.46	0.86	1.10	2.51	0.72	1.15	2.58	0.0578948	4.60E-17	0.488565
Electron transfer	PGR5	Protein PROTON GRADIENT REGULATION 5	Q9SL05	AT2G05620	1.04	1	1.57	1.02	1.01	1.73	1.04	0.85	1.74	0.509359	4.01E-10	0.505547
Electron transfer	PGR6	Uncharacterized aarF domain-containing protein kinase At4g31390	Q8RWG1;A0A1P 8B7P6	AT4G31390	0.86	1	3.62	1.03	1.65	3.37	1.09	1.55	3.04	0.108657	1.11E-13	0.0190423
Electron transfer	PGRL1A	PGR5-like protein 1A	Q8H112;A0A2H1 ZEN5	AT4G22890	0.75	1	0.93	0.90	1.03	0.94	0.77	0.91	0.84	0.0023973 3	0.0001745 98	0.185758
Electron transfer	PGRL1B	PGR5-like protein 1B	Q8GYC7;F4JPU 9	AT4G11960	2.57	1	3.99	2.45	2.03	2.76	2.45	2.20	3.09	0.757931	3.21E-07	0.0013572 6
Electron transfer	STR4	Rhodanese-like domain-containing protein 4	A0A1P8B8J7;Q9 M158	AT4G01050	0.98	1	1.21	0.97	0.99	1.30	0.88	0.85	1.00	0.0004690 03	0.0001591 21	0.167979
Electron transfer	TIC62	Protein TIC 62	Q8H0U5	AT3G18890	0.60	1	1.07	0.70	1.08	1.29	0.62	0.86	1.05	2.40E-06	2.87E-13	0.0106738
Ion channel	At5g37360		Q93Z11	AT5G37360	0.64	1	0.99	0.76	0.98	1.22	0.72	0.90	0.81	0.646428	0.0143895	0.728811
Ion channel	DIT2-1	Dicarboxylate transporter 2.1	Q9FMF7	AT5G64290	0.56	1	1.16	0.63	1.10	2.00	0.42	1.07	0.80	0.0179034	1.05E-05	0.0772914
Ion channel	KEA3	K(+) efflux antiporter 3	Q9M0Z3	AT4G04850	1.28	1	2.68	1.14	1.27	2.76	1.41	0.95	2.32	0.0533837	1.38E-12	0.0053462 7
Kinase/phosphatase	At3g59780		F4J9G2	AT3G59780	1.06	1	1.33	1.13	1.15	1.40	1.09	1.07	1.11	2.93E-05	8.73E-08	9.73E-05
Kinase/phosphatase	At5g35170	Adenylate kinase 5	F4JYC0;Q8VYL1	AT5G35170	0.04	1	0.13	0.02	0.76	0.34	0.03	0.85	0.09	0.332231	3.84E-11	0.0213068
Kinase/phosphatase	PGK1	Phosphoglycerate kinase 1	Q9LD57	AT3G12780	0.60	1	1.02	1.29	0.93	1.24	0.67	0.90	0.70	4.77E-10	0.0003530 05	5.46E-08
LHCI	LHCA1	Chlorophyll a-b binding protein 6	A8MS75;Q01667	AT3G54890	1.33	1	1.03	1.25	1.23	1.03	1.19	1.30	0.90	0.0676009	2.78E-08	6.22E-06
LHCI	Lhca2		Q9SYW8	AT3G61470;A T5G28450	1.29	1	1.05	1.35	1.09	0.83	1.07	0.80	0.67	0.106166	0.0003230 37	0.423524
LHCI	LHCA3		Q9SY97	AT1G61520	1.10	1	0.88	1.10	0.41	0.84	1.05	0.43	0.88	4.22E-07	8.81E-12	7.78E-08
LHCI	LHCA4	Chlorophyll a-b binding protein 4	P27521	AT3G47470	0.94	1	0.68	1.07	0.88	0.78	0.95	0.79	0.67	0.214458	1.47E-06	0.170655
LHCI	LHCA5	Photosystem I chlorophyll a/b-binding protein 5	Q9C639	At1g45474	0.41	1	0.78	2.33	1.35	1.12	2.40	1.17	0.82	0.0811702	0.0150423	0.211182
LHCI	LHCA6		Q8LCQ4	AT1G19150	0.42	1	0.42	0.47	1.22	0.44	0.75	1.02	0.46	0.472531	9.80E-05	0.355015
LHCII	Lhb1B1		Q39142	AT2G34430	1.93	1	0.43	2.13	0.81	0.45	1.39	0.96	0.37	8.34E-07	1.03E-17	1.84E-07

LHCII	Lhb1B2		Q39141	AT2G34420	0.94	1	0.58	1.27	1.22	0.65	0.91	0.88	0.57	9.20E-06	1.90E-09	0.0377002
LHCII	LHCB1.2;LHCB1.1	Chlorophyll a-b binding protein 3	Q8VZ87;P0CJ48	AT1G29910	0.83	1	0.92	1.30	1.26	0.64	0.96	0.88	0.89	0.0780214	0.00501281	0.027888
LHCII	LHCB1.3	Chlorophyll a-b binding protein 1	P04778	AT1G29930	1.20	1	1.17	1.92	1.66	1.76	1.06	0.97	0.81	1.13E-12	0.00282328	0.00686231
LHCII	LHCB2.2		Q9S7J7;Q9SHR7;Q9XF87;A0A119LMB4;A0A1P8AZ91	AT2G05070;AT2G05100;AT3G27690	1.27	1	0.83	1.54	0.98	0.78	1.20	0.98	0.69	0.00123948	1.68E-12	0.00237087
LHCII	LHCB3*1		Q9S7M0	AT5G54270	0.99	1	0.69	1.14	1.12	0.73	0.86	1.06	0.60	0.0252179	9.28E-07	0.724102
LHCII	LHCB4.1	Chlorophyll a-b binding protein CP29.1	Q07473	AT5G01530	1.11	1	0.97	1.13	1.00	1.08	1.12	0.96	1.00	0.146833	0.00056015	0.195216
LHCII	LHCB4.2	Chlorophyll a-b binding protein CP29.2	Q9XF88	AT3G08940	1.23	1	0.88	1.17	0.90	0.90	1.18	0.83	0.90	0.113556	7.15E-10	0.0355893
LHCII	LHCB4.3	Chlorophyll a-b binding protein CP29.3	Q9S7W1;F4IGY6	AT2G40100	0.02	1	2.63	0.02	1.64	3.14	0.01	1.23	3.53	0.37777	1.55E-09	0.871757
LHCII	LHCB5	Chlorophyll a-b binding protein CP26	Q9XF89	AT4G10340	0.65	1	0.78	0.74	0.93	0.79	0.65	1.13	0.64	0.986901	7.42E-06	0.336285
LHCII	LHCB6		Q9LMQ2	AT1G15820	1.16	1	1.00	1.28	1.07	1.05	1.05	1.00	0.85	1.63E-05	4.34E-07	0.0344755
LHC-like	At5g47110		Q6NKS4	AT5G47110	0.96	1	1.08	1.33	1.44	1.59	1.20	1.17	1.12	0.00345295	0.623602	0.734225
LHC-like	HLIP	High-light-induced protein	O81208	AT5G02120	1.28	1	0.80	1.84	2.05	1.59	1.60	1.33	1.09	0.00028527	0.329519	0.504836
LHC-like	Lil3:1		Q9SYX1	AT4G17600	0.68	1	1.61	0.89	1.71	1.67	0.78	1.57	1.29	7.80E-05	3.89E-10	0.000126039
LHC-like	T15K4.5		Q9FEC1	AT1G34000	0.96	1	0.78	1.06	0.83	1.08	1.00	0.77	0.83	0.0223813	0.0457448	0.254377
Light harvesting regulation	At1g56500		Q8VZ10	AT1G56500	0.90	1	1.20	1.04	1.36	1.45	0.91	1.19	1.23	2.63E-06	6.68E-09	0.144565
Light harvesting regulation	At4g31530		Q8GYZ0;F4JSP1	AT4G31530	0.65	1	1.35	1.18	0.67	1.73	0.77	0.69	0.89	1.19E-07	6.46E-10	8.44E-08
Light harvesting regulation	CHL	Chloroplastic lipocalin	Q9STS7	AT3G47860	1.62	1	1.92	1.93	0.97	1.72	1.63	1.19	1.46	0.154168	4.81E-10	0.00224156
Light harvesting regulation	PPH1	Protein phosphatase 2C 57	P49599	AT4G27800	0.97	1	1.14	0.72	0.83	0.80	0.07	0.04	0.02	5.25E-14	0.231996	0.27269
Light harvesting regulation	PSBS	Photosystem II 22 kDa protein	Q9XF91;F4IEG8	AT1G44575	0.84	1	1.43	1.03	1.13	1.79	0.88	0.92	1.33	1.02E-10	2.02E-16	7.17E-05
Light harvesting regulation	STN8	Serine/threonine-protein kinase STN8	Q9LZV4	AT5G01920	0.86	1	1.24	0.84	0.94	1.34	0.82	0.88	1.21	0.42916	2.97E-07	0.732281
Light harvesting regulation	TSP9	Thylakoid soluble phosphoprotein	Q9SD66	AT3G47070	0.97	1	0.80	1.35	0.63	1.90	1.29	0.26	1.79	3.08E-07	1.37E-13	3.25E-12
Light harvesting regulation	VDE1	Violaxanthin de-epoxidase	Q39249	AT1G08550	1.68	1	2.89	1.57	3.74	2.96	1.35	2.31	2.32	1.60E-10	4.19E-12	1.57E-11
Light harvesting regulation	ZEP	Zeaxanthin epoxidase	Q9FGC7	AT5G67030	0.75	1	0.69	0.84	1.15	0.83	0.76	1.10	0.57	0.00193797	8.83E-11	0.105383
NDH	FKBP16-2	Photosynthetic NDH subunit of lumenal location 4	F4JW56;Q9SCY3	AT4G39710	0.61	1	1.08	0.79	1.16	1.40	0.70	0.95	1.20	2.59E-07	9.93E-13	0.0105867
NDH	NDF6	Photosynthetic NDH subunit of subcomplex B 4	A0A1P8AS98;F4ICC6;Q8RXS1	AT1G18730	0.37	1	1.23	0.68	1.17	1.16	0.59	1.02	1.01	0.00685423	3.10E-10	0.0896358

NDH	ndhA	NAD(P)H-quinone oxidoreductase subunit 1	Q37165	AtCg01100	0.45	1	0.48	0.59	0.75	0.76	0.55	0.73	0.50	0.515621	0.0010037 2	0.354756
NDH	ndhC	NAD(P)H-quinone oxidoreductase subunit 3	P56751	ATCG00440	0.61	1	1.06	1.12	0.98	1.50	0.96	1.46	1.27	0.0424713	0.0055928 1	0.598243
NDH	ndhE	NAD(P)H-quinone oxidoreductase subunit 4L	P26289	ATCG01070	0.40	1	0.87	0.46	1.22	1.02	0.39	1.04	0.83	1.70E-05	2.36E-14	0.156161
NDH	ndhF	NAD(P)H-quinone oxidoreductase subunit 5	P56752	ATCG01010	0.31	1	0.54	0.43	0.71	0.83	0.31	0.46	0.45	0.0161426	0.0003083 32	0.0396594
NDH	ndhH	NAD(P)H-quinone oxidoreductase subunit H	P56753	ATCG01110	0.48	1	1.08	0.64	1.03	1.54	0.50	1.03	0.98	0.0004302 02	1.24E-10	0.0018788
NDH	ndhI	NAD(P)H-quinone oxidoreductase subunit I	P56755	ATCG01090	0.42	1	0.84	0.58	1.44	1.14	0.43	1.17	0.56	3.38E-05	3.43E-10	0.0099787 9
NDH	ndhJ	NAD(P)H-quinone oxidoreductase subunit J	P56754	ATCG00420	0.59	1	0.96	0.68	1.74	1.30	0.61	1.29	0.83	2.21E-07	4.08E-11	0.0002554 34
NDH	ndhK	NAD(P)H-quinone oxidoreductase subunit K	P56756	ATCG00430	0.44	1	0.86	0.56	1.47	1.00	0.41	1.13	0.79	1.02E-07	1.38E-14	0.0005279 67
NDH	ndhL	NAD(P)H-quinone oxidoreductase subunit L	Q9CAC5	AT1G70760	0.72	1	1.10	0.91	1.03	1.48	0.79	1.16	1.00	0.0001094 11	2.18E-07	0.0024225 6
NDH	ndhM	NAD(P)H-quinone oxidoreductase subunit M	Q2V2S7	AT4G37925	0.42	1	0.72	0.49	1.44	1.05	0.36	1.23	0.62	2.56E-07	1.60E-13	0.0001570 98
NDH	ndhN	NAD(P)H-quinone oxidoreductase subunit N	Q9LVM2	AT5G58260	0.53	1	1.13	0.75	1.47	1.37	0.58	1.24	1.06	2.82E-07	1.55E-12	0.0570438
NDH	ndhO	NAD(P)H-quinone oxidoreductase subunit O	Q9S829	AT1G74880	0.48	1	0.65	0.56	1.20	0.81	0.46	1.09	0.71	0.0027049	7.09E-10	0.555166
NDH	ndhS	NAD(P)H-quinone oxidoreductase subunit S	Q9T0A4	AT4G23890	0.57	1	0.73	0.59	1.02	0.99	0.54	1.17	0.73	0.372521	2.21E-06	0.267926
NDH	ndhT	NAD(P)H-quinone oxidoreductase subunit T	Q9SMS0	AT4G09350	0.28	1	1.18	0.68	2.26	1.98	0.30	1.15	1.02	0.0004789 94	4.01E-05	0.381194
NDH	ndhU	NAD(P)H-quinone oxidoreductase subunit U	Q84VQ4	AT5G21430	0.49	1	0.89	0.65	1.15	1.22	0.51	0.95	0.83	5.43E-05	9.25E-10	0.162424
NDH	PNSB1	Photosynthetic NDH subunit of subcomplex B 1	Q9S9N6	AT1G15980	0.48	1	1.00	0.63	1.16	1.21	0.53	1.05	0.91	2.70E-06	5.70E-13	0.0708959
NDH	PNSB2	Photosynthetic NDH subunit of subcomplex B 2	Q94AQ8;F4I891; F4I890	AT1G64770	0.37	1	0.42	0.54	1.29	0.79	0.49	0.85	0.35	4.56E-05	1.84E-09	0.0701517
NDH	PNSB3	Photosynthetic NDH subunit of subcomplex B 3	Q9LU21	AT3G16250	0.35	1	1.03	0.42	1.65	1.07	0.34	1.28	0.87	0.0010928 2	8.43E-12	0.0057126 8
NDH	PNSB5	Photosynthetic NDH subunit of subcomplex B 5	Q9FG89	AT5G43750	0.56	1	0.76	0.77	1.30	0.76	0.55	1.26	0.60	0.0019257 5	2.74E-09	0.0281667
NDH	PNSL1	Photosynthetic NDH subunit of luminal location 1	O80634	AT2G39470	0.44	1	0.74	0.62	0.97	0.83	0.48	0.77	0.76	0.0055828 8	5.78E-09	0.0445443
NDH	PNSL2	Photosynthetic NDH subunit of luminal location 2	Q9XI73	AT1G14150	0.47	1	0.93	0.62	1.01	1.08	0.57	0.80	0.85	1.26E-05	5.79E-12	0.0011670 9
NDH	PNSL3	Photosynthetic NDH subunit of luminal location 3	Q9SGH4	AT3G01440	0.33	1	1.02	0.55	1.04	1.58	0.36	0.69	0.92	1.09E-06	1.36E-11	0.0041104 8
NDH	PNSL5	Photosynthetic NDH subunit of luminal location 5	Q9ASS6	AT5G13120	0.60	1	0.78	0.64	1.41	1.07	0.53	1.27	0.63	5.97E-06	8.17E-11	0.0038492 7
Other/unknown	AAC1	ADP,ATP carrier protein 1	P31167	AT3G08580	0.78	1	4.35	0.73	0.85	3.72	0.61	1.03	3.47	3.21E-07	1.05E-23	3.68E-07
Other/unknown	AAC2	ADP,ATP carrier protein 2	P40941	AT5G13490	0.56	1	3.23	0.43	2.55	3.29	0.39	3.05	2.67	0.053128	2.28E-09	0.0167767
Other/unknown	accD	Acetyl-coenzyme A carboxylase carboxyl transferase subunit beta	P56765	AtCg00500	1.40	1	3.28	2.67	1.69	4.05	1.37	2.47	3.10	0.123486	0.0001663 26	0.0544717

Other/unknown	ALDH3I1	Aldehyde dehydrogenase family 3 member I1	A0A1P8B7C0;Q8W033;A0A1P8B7C2;F4JKM4	At4g34240	0.81	1	1.57	1.01	1.48	2.09	0.84	0.83	1.35	7.08E-05	1.64E-07	0.136693
Other/unknown	AOC2	Allene oxide cyclase 2	Q9LSO2	AT3G25770	0.16	1	1.54	0.14	1.31	2.03	0.21	1.07	1.15	7.72E-07	8.90E-18	3.23E-07
Other/unknown	APG3	Peptide chain release factor APG3	Q8RX79	AT3G62910	0.38	1	2.27	0.94	0.77	2.86	0.49	0.90	1.60	2.26E-05	8.80E-12	2.46E-05
Other/unknown	APXT	L-ascorbate peroxidase T	A0A1P8APU0;Q42593	AT1G77490;AT2G18140;AT2G18150	0.90	1	1.11	1.28	1.42	1.13	1.10	1.45	0.96	3.56E-05	9.74E-05	0.000972305
Other/unknown	At1g07660	Histone H4	P59259;A8MRV1	AT2G28740	2.05	1	9.10	2.02	1.49	7.75	1.60	1.48	8.17	0.0855903	8.83E-21	0.00219187
Other/unknown	At1g12250	Thylakoid lumenal protein At1g12250	Q8H1Q1;B6EUA5;A0A178W1Q3	AT1G12250	0.86	1	0.82	0.78	1.80	1.16	0.72	1.02	0.91	3.75E-09	2.68E-10	3.18E-07
Other/unknown	At1g18060		Q9LM40	AT1G18060	0.36	1	1.51	0.29	0.90	1.75	0.42	0.75	1.47	0.170274	1.29E-12	0.017731
Other/unknown	At1g52510		Q8VZ57;F4ICZ4	AT1G52510	0.23	1	1.08	0.52	0.83	1.34	0.33	0.87	0.90	2.15E-05	1.47E-14	2.43E-06
Other/unknown	At1g54520		Q8RWI0	AT1G54520	1.00	1	1.05	1.47	1.61	1.59	1.07	1.15	1.21	5.13E-07	0.415831	0.820405
Other/unknown	At1g72640	NAD(P)-binding Rossmann-fold superfamily protein	F4IDE8;Q6NMC1;A0A1P8AVW7;A0A1P8AW09	At1g72640	0.78	1	3.15	1.20	1.58	3.49	0.80	1.44	2.82	0.171899	1.25E-09	0.648691
Other/unknown	At1g78915		Q8GWV1;F4IBX4;F4IBX5	AT1G78915	0.95	1	1.50	0.97	0.90	2.06	1.07	0.87	1.45	0.0254132	5.68E-10	0.0016535
Other/unknown	At2g05310		Q9SJ31	At2g05310	1.46	1	1.08	1.56	0.86	0.99	1.24	0.97	0.72	0.117846	8.62E-06	0.167522
Other/unknown	At2g27290		Q9XIN6	AT2G27290	1.71	1	1.60	1.60	0.99	1.70	1.62	0.91	1.45	0.320876	5.83E-06	0.787473
Other/unknown	At2g27680		Q9ZUX0	AT2G27680	0.32	1	0.84	0.85	0.33	1.34	0.44	0.53	0.40	2.15E-05	3.23E-05	1.67E-08
Other/unknown	At4g02725		Q6DBF6	AT4G02725	1.75	1	1.92	1.51	1.66	1.69	1.68	1.91	1.87	0.00123005	0.00170278	0.000116284
Other/unknown	At4g28025		F4JKG2;Q9C5F3	At4g28025	0.34	1	2.25	0.42	1.47	2.18	0.98	0.92	1.93	0.740531	6.94E-08	0.0729771
Other/unknown	At5g08680	ATP synthase subunit beta-1	P83483;P83484;Q9C5A9	At5g08680	0.48	1	1.53	0.46	1.00	1.02	0.46	0.96	1.46	0.40535	8.16E-05	0.852129
Other/unknown	At5g14910		Q93VK7	AT5G14910	0.60	1	1.76	0.75	2.32	2.37	0.53	2.31	1.71	3.03E-07	6.52E-12	4.63E-06
Other/unknown	At5g16660		A8MS48;Q8H0X5	AT5G16660	1.74	1	2.21	1.45	1.40	2.84	1.02	1.32	1.87	0.0127918	2.52E-06	0.0148315
Other/unknown	At5g23890		Q9FF91;A0A1P8BAU8	AT5G23890	1.30	1	12.66	1.55	3.26	10.20	0.85	3.78	8.05	0.0170821	2.14E-18	3.02E-08
Other/unknown	At5g38520	Alpha/beta-Hydrolases superfamily protein	Q9FFW9;F4KBJ3	At5g38520	0.51	1	0.77	0.60	1.07	0.80	0.51	0.90	0.71	0.0406624	2.83E-08	0.378313
Other/unknown	At5g42070		Q8RWR9	AT5G42070	0.61	1	1.94	0.70	2.28	2.15	0.46	1.36	1.91	1.10E-05	5.35E-12	0.000372211
Other/unknown	At5g51010		Q9FI47	AT5G51010	2.45	1	1.91	2.38	1.88	1.93	1.89	1.59	2.08	0.00540137	1.82E-08	7.24E-05
Other/unknown	At5g52780	Uncharacterized protein PAM68-like	Q9LTD9	At5g52780	0.76	1	1.24	0.81	1.22	1.36	0.70	1.15	0.93	0.00942389	0.000158888	0.153898
Other/unknown	At5g53490	Thylakoid lumenal 17.4 kDa protein	A0A1P8BAQ0;F4JX83;P81760	AT5G53490	2.65	1	1.33	2.12	3.08	1.72	2.04	1.11	1.37	7.96E-10	4.55E-09	1.70E-10
Other/unknown	BASS2	Sodium/pyruvate cotransporter BASS2	Q1EBV7	AT2G26900	1.67	1	3.59	2.08	1.61	4.23	1.49	1.75	2.92	0.00969216	4.41E-11	0.00180229

Other/unknown	CAC3	Acetyl-coenzyme A carboxylase carboxyl transferase subunit alpha	Q9LD43	AT2G38040	1.22	1	2.27	1.58	1.65	2.92	1.04	1.79	2.20	1.43E-07	5.89E-14	4.25E-06
Other/unknown	CAS	Calcium sensing receptor	Q9FN48;A0A1P8BCX7	AT5G23060	0.70	1	1.38	0.71	0.98	1.47	0.67	0.93	1.29	0.0169075	3.57E-13	0.154082
Other/unknown	DiT1	Dicarboxylate transporter 1	B3H4S6;Q9LXV3	AT5G12860	0.79	1	1.87	1.36	0.72	1.82	0.83	0.60	1.93	0.634112	0.00173277	0.765257
Other/unknown	EMB3003	Dihydropolyllysine-residue acetyltransferase component 5 of pyruvate dehydrogenase complex	Q9C8P0	AT1G34430	0.84	1	1.28	1.49	1.49	2.12	1.10	1.28	1.41	2.64E-07	7.93E-05	0.0522718
Other/unknown	F11M15.26		Q9SYE2	AT1G51400	1.14	1	0.64	0.90	0.80	0.69	0.93	0.74	0.74	0.0103685	8.53E-06	0.00719593
Other/unknown	F13A11.2		Q9C7S3	AT1G42960	0.62	1	2.98	0.77	1.25	3.53	0.59	1.81	2.12	0.0505255	2.24E-12	6.66E-05
Other/unknown	F16M2_10		Q9M1X3	AT3G63160	0.34	1	0.83	0.47	0.66	0.90	0.37	0.74	0.52	7.50E-05	2.84E-09	3.92E-05
Other/unknown	F17F16.7		A0A1P8AWY1;Q8W4D6;A0A1P8AWU9	AT1G16720	0.94	1	1.44	1.16	1.86	1.94	0.96	1.75	1.61	1.01E-07	2.65E-09	0.000376322
Other/unknown	F21F14.40		Q9M277;F4IX01	AT3G61870	1.63	1	2.06	1.59	1.39	2.11	1.47	1.22	1.83	0.00135807	1.26E-11	0.00546634
Other/unknown	F24J8.11		Q9LPK9	AT1G21500	0.01	1	0.11	0.01	0.73	0.25	0.02	0.73	0.16	0.981834	1.27E-09	0.353395
Other/unknown	F26O13.150		Q9SCZ8	AT3G51510	0.68	1	0.76	0.57	0.99	0.71	0.52	0.62	0.41	0.0025372	0.000167194	0.567515
Other/unknown	F4P12_170	2,3-bisphosphoglycerate-independent phosphoglycerate mutase	Q9LFH1;F4JAF4	At3g53470	0.85	1	1.13	1.04	0.75	1.27	0.89	1.03	1.03	0.55618	0.0710758	0.210937
Other/unknown	FBA1	Probable fructose-bisphosphate aldolase 1	Q9SJU4;F4IGL5;F4IGL7	AT2G21330	0.36	1	2.66	0.62	2.40	2.72	0.38	1.76	2.27	9.97E-13	3.15E-22	1.00E-11
Other/unknown	FBA2	Probable fructose-bisphosphate aldolase 2	Q944G9;F4JUJ5	AT4G38970	0.41	1	1.85	0.89	1.45	1.89	0.47	1.12	1.59	1.00E-10	3.00E-18	5.13E-05
Other/unknown	FBA3	Probable fructose-bisphosphate aldolase 3	Q9ZU52	AT2G01140	1.92	1	16.28	1.17	3.65	11.55	1.04	5.14	12.56	0.586589	1.20E-13	0.00166737
Other/unknown	GAPA2	Glyceraldehyde-3-phosphate dehydrogenase GAPA2	Q9LPW0;A0A1P8APR6;F4HNZ6	AT1G12900	0.89	1	3.57	0.62	3.65	4.35	0.65	1.93	3.74	4.25E-13	2.08E-21	4.54E-13
Other/unknown	GC1	Epimerase family protein SDR39U1 homolog	A0A1P8B167;Q9SJU9	AT2G21280	0.63	1	2.96	0.96	1.41	3.41	0.59	1.53	2.22	0.00819888	1.65E-13	0.00383257
Other/unknown	GDCST	Aminomethyltransferase	A0A2H1ZE9;O65396	AT1G11860	2.56	1	6.78	1.30	3.94	5.76	1.04	3.21	8.06	0.00384524	2.29E-16	7.87E-09
Other/unknown	GLDP1	Glycine dehydrogenase (decarboxylating) 1	Q94B78;B3H5Y8	AT4G33010	0.56	1	7.73	0.37	3.93	6.58	0.32	2.40	7.43	3.09E-05	5.09E-23	2.73E-11
Other/unknown	GLN2	Glutamine synthetase/mitochondrial	Q43127	AT5G35630	0.60	1	0.67	1.40	0.60	0.86	0.58	0.56	0.45	8.20E-15	1.29E-09	3.22E-15
Other/unknown	GLO1	Peroxisomal (S)-2-hydroxy-acid oxidase GLO1	Q9LRR9;A8MS37;B3H4B8;Q2V3V9	AT3G14420	1.76	1	4.13	1.38	2.95	4.48	0.85	2.19	4.86	7.61E-06	2.54E-17	5.26E-08
Other/unknown	HSP70-3	Heat shock 70 kDa protein 3	O65719	AT3G09440	1.48	1	3.30	1.63	0.66	3.04	1.16	1.59	2.35	0.0013455	1.05E-17	5.26E-10
Other/unknown	LOX2	Lipoxygenase 2	P38418;A0A119LPH1	AT3G45140	0.18	1	1.25	0.17	1.15	1.38	0.17	0.96	1.06	1.32E-10	5.98E-25	4.42E-08
Other/unknown	LTA2	Dihydropolyllysine-residue acetyltransferase component 4 of pyruvate dehydrogenase complex	Q9SQI8	AT3G25860	2.35	1	2.00	3.25	1.44	3.11	2.34	1.20	2.79	4.84E-07	1.61E-11	0.0100709
Other/unknown	LTA3	Dihydropolyllysine-residue acetyltransferase component 1 of pyruvate dehydrogenase complex	F4J5T2;Q0WQF7	AT3G52200	3.31	1	7.42	2.73	1.96	6.13	2.09	2.00	8.07	0.00731411	1.16E-16	1.96E-05
Other/unknown	MFP1	MAR-binding filament-like protein 1	Q9LW85	AT3G16000	1.21	1	1.43	1.17	0.89	2.00	1.06	1.19	1.53	0.015496	1.36E-11	2.22E-06

Other/unknown	MVA3.2	Alpha/beta-Hydrolases superfamily protein	Q9FN84	At5g17670	0.36	1	1.98	0.61	1.23	2.61	0.57	0.70	2.62	0.0449738	2.65E-10	0.238555
Other/unknown	MXK3.17		Q93Y08	AT5G64940	1.07	1	3.44	1.25	1.39	3.64	1.09	1.36	2.38	0.000258775	1.26E-14	2.08E-05
Other/unknown	OEP161	Outer envelope pore protein 16-1	Q9ZV24	AT2G28900	1.09	1	2.36	1.24	0.54	2.07	1.01	0.75	1.76	0.0095773	8.27E-12	0.00381193
Other/unknown	PLGG1	Plastidal glycolate/glycerate translocator 1	Q9FVQ4	AT1G32080	0.33	1	2.31	0.72	0.94	2.81	0.33	1.24	1.62	5.17E-08	1.46E-18	1.13E-09
Other/unknown	PMDH2	Malate dehydrogenase	F4KDZ4;Q9ZP05;A0A1P8BBQ0;A8MRP1;B3H560	AT5G09660	0.46	1	1.85	0.53	1.11	2.41	0.33	0.94	1.68	5.68E-09	1.27E-19	3.42E-06
Other/unknown	PPD5	PsbP domain-containing protein 5	A0A178U9N5;P82715	AT5G11450	0.84	1	1.15	1.01	1.80	1.79	0.77	1.64	1.51	0.00648147	3.39E-05	0.0230847
Other/unknown	PPD7	PsbP domain-containing protein 7	F4J7A7	AT3G05410	1.07	1	1.21	0.92	0.89	1.76	1.03	1.10	1.09	0.227649	0.0123615	0.0369155
Other/unknown	PRXIIIE	Peroxisome oxidoreductin-2E	Q949U7	AT3G52960	0.90	1	0.77	1.20	2.01	1.04	0.73	0.91	0.80	7.24E-06	0.000138632	0.00058597
Other/unknown	PTAC5		A1A6M1;A0A1P8B4I3	AT4G13670	0.36	1	1.98	0.56	2.21	4.03	0.43	1.79	1.60	5.77E-07	1.01E-10	4.06E-06
Other/unknown	RAT5	Histone H2A.6	Q9LD28;O81826;Q9C681	AT5G54640	1.50	1	6.88	1.57	1.23	5.48	1.28	2.19	6.03	0.0228474	1.75E-18	3.26E-05
Other/unknown	RPI3	Probable ribose-5-phosphate isomerase 3	Q9S726	AT3G04790	0.85	1	1.45	1.54	1.52	1.73	0.96	1.56	0.77	0.0329181	0.64544	0.0140254
Other/unknown	SHM1	Serine hydroxymethyltransferase 1	Q9SZJ5	AT4G37930	0.53	1	5.53	0.35	3.29	5.66	0.27	2.04	5.14	3.68E-09	1.90E-23	8.65E-11
Other/unknown	STR10	Rhodanese-like domain-containing protein 10	Q9SR92	AT3G08920	1.45	1	0.88	1.43	1.19	1.21	1.28	1.02	1.05	0.000783875	1.95E-07	0.0175735
Other/unknown	STR11	Rhodanese-like domain-containing protein 11	Q0WWT7	AT4G24750	1.18	1	1.08	1.10	0.84	1.03	1.14	0.83	0.89	0.00114099	1.95E-05	0.0464787
Other/unknown	STR4A	Rhodanese-like domain-containing protein 4A	Q56XR7	At3g25480	1.57	1	1.98	1.73	1.36	2.50	1.74	1.21	1.71	0.0107987	1.44E-05	0.0656255
Other/unknown	STR9	Rhodanese-like domain-containing protein 9	O48529	AT2G42220	1.23	1	1.40	1.16	1.05	1.17	1.17	1.27	1.35	0.000557337	9.99E-06	0.000168061
Other/unknown	T6G15.50		Q9T0H1	AT4G13500	1.27	1	1.17	1.58	1.13	0.84	1.19	1.03	0.65	0.00387215	5.18E-05	0.0327247
Other/unknown	TIC110	Protein TIC110	Q8LPR9	AT1G06950	0.62	1	3.78	0.94	1.32	4.93	0.59	1.79	2.49	1.16E-07	2.15E-17	4.10E-09
Other/unknown	TIC214	Protein TIC 214	P56785	AtCg01000;AtCg01130	2.02	1	6.35	1.71	0.77	3.98	1.17	1.34	3.78	0.0180589	2.47E-07	0.05762
Other/unknown	TIC55	Protein TIC 55	Q9SK50	AT2G24820	0.68	1	2.78	0.89	1.07	2.80	0.60	1.23	1.78	9.24E-07	1.59E-17	1.38E-07
Other/unknown	TL15	Thylakoid lumenal 15 kDa protein 1	O22160	AT2G44920	6.29	1	3.01	2.87	26.45	6.24	3.35	8.19	4.61	1.22E-13	1.36E-13	2.69E-15
Other/unknown	TL17.9	Thylakoid lumenal 17.9 kDa protein	Q9SW33	AT4G24930	2.30	1	2.12	2.05	4.77	3.31	1.90	2.58	3.24	5.75E-05	0.0236887	0.000361493
Other/unknown	TL19	Thylakoid lumenal 19 kDa protein	P82658	AT3G63540	3.13	1	2.34	2.28	3.47	2.76	2.03	2.07	2.38	1.73E-05	0.503323	6.69E-08
Other/unknown	TPT	Triose phosphate/phosphate translocator TPT	A0A219HYB6;A0A219HZH3;A0A219J0W9;Q9ZSR7	AT5G46110	1.36	1	1.95	1.65	0.69	2.06	0.97	0.85	1.53	9.21E-05	3.34E-11	0.000285547
Other/unknown	YCF37		O64835	AT2G23670	0.97	1	1.77	1.06	0.76	1.73	0.97	0.38	1.53	1.43E-06	1.02E-14	6.44E-05
Other/unknown		3-oxoacyl-[acyl-carrier-protein] reductase	P33207	AT1G24360	5.90	1	5.73	4.12	2.77	5.72	3.02	3.21	6.08	0.866121	2.75E-10	3.17E-06
Other/unknown			Q8L9M8	AT1G33810	0.93	1	3.66	1.44	0.70	6.15	0.84	1.43	4.06	0.00548256	4.01E-13	0.000885226
Other/unknown		Probable lactoylglutathione lyase, chloroplast	Q8W593	AT1G67280	0.63	1	1.66	1.28	0.91	1.89	0.67	0.68	0.81	3.36E-09	2.63E-10	8.01E-07

Other/unknown			Q9AST9;A0A1P8 ATD8	AT1G73110	0.33	1	4.02	0.59	0.61	4.66	0.40	0.94	2.17	0.0016106 2	5.01E-13	0.0001822 11
Other/unknown			Q9ZQ78	AT2G03420	1.09	1	1.49	1.21	0.74	2.18	1.24	0.49	1.49	0.0040203 5	7.74E-10	0.0069094 6
Other/unknown		Rhodanese-like domain-containing protein 14	Q94A65	AT4G27700	0.90	1	1.09	0.60	1.01	1.07	0.69	1.04	0.98	0.0311066	3.57E-08	0.0028677
Other/unknown		Thioredoxin-like 2-2	Q8LCT3	AT4G29670	0.43	1	1.17	0.86	0.42	1.15	0.47	0.52	0.56	3.42E-06	2.46E-06	7.04E-07
Pigment synthesis	At5g58250		Q9LVM3	AT5G58250	0.99	1	1.71	1.39	1.84	2.00	1.23	2.09	1.44	9.42E-06	1.89E-06	2.08E-05
Pigment synthesis	CAO	Chlorophyllide a oxygenase	Q9MBA1;A0A1P 8ARR2	AT1G44446	1.61	1	4.12	3.60	2.36	3.14	1.95	1.66	1.27	0.0004642 66	0.0061899 5	0.0019610 8
Pigment synthesis	CHLD	Magnesium-chelatase subunit ChID	Q9SJE1	AT1G08520	0.46	1	3.32	2.06	1.31	4.81	0.66	1.50	2.96	0.0001396 68	1.90E-09	0.0043500 9
Pigment synthesis	CHLG	Chlorophyll synthase	Q38833	AT3G51820	1.11	1	0.98	1.19	1.65	1.02	1.13	1.20	0.67	0.578517	0.0096651 3	0.650403
Pigment synthesis	CHL1	Magnesium-chelatase subunit Chl1-1	P16127	AT4G18480	0.27	1	0.62	1.65	0.23	1.25	0.96	0.62	0.28	9.13E-07	8.44E-05	4.51E-10
Pigment synthesis	CHLM	Magnesium protoporphyrin IX methyltransferase	A0A1P8B4G1;Q 9SW18	AT4G25080	1.21	1	1.37	1.27	1.26	1.39	1.20	1.35	1.46	0.0002137 18	1.17E-06	0.0028326 1
Pigment synthesis	CHLP	Geranylgeranyl diphosphate reductase	Q9CA67	AT1G74470	0.81	1	1.49	1.00	1.53	1.76	0.93	1.54	1.35	1.07E-07	2.62E-13	1.36E-06
Pigment synthesis	CRD1	Magnesium-protoporphyrin IX monomethyl ester [oxidative] cyclase	Q9M591;F4J0U9	AT3G56940	0.66	1	1.55	0.82	1.52	1.82	0.72	1.53	1.27	3.08E-07	1.32E-14	2.12E-07
Pigment synthesis	CYP97A3	Protein LUTEIN DEFICIENT 5	Q93VK5	AT1G31800	0.68	1	2.55	0.87	3.14	4.41	0.80	2.30	2.63	4.48E-05	2.63E-08	0.011154
Pigment synthesis	CYP97B3	Cytochrome P450 97B3	O23365	AT4G15110	1.53	1	2.65	2.06	2.69	2.99	1.31	2.37	2.64	0.0001264 35	3.73E-06	0.0032093 7
Pigment synthesis	CYP97C1	Carotene epsilon-monooxygenase	Q6TBX7	AT3G53130	1.13	1	2.07	1.14	1.95	2.85	0.95	1.78	2.29	5.62E-05	7.19E-10	0.0039119 6
Pigment synthesis	DVR	Divinyl chlorophyllide a 8-vinyl-reductase	Q1H537	AT5G18660	0.88	1	1.11	1.20	1.16	1.32	1.12	1.11	1.31	0.0026847 6	0.0230393	0.68891
Pigment synthesis	FC2	Ferrochelatase	F4IMT3;O04921	AT2G30390	0.73	1	2.30	0.95	1.84	2.62	0.83	1.80	1.79	0.0029001 8	1.69E-09	0.0027128 5
Pigment synthesis	GUN4	Tetrapyrrole-binding protein	Q9LX31	AT3G59400	1.24	1	2.08	1.79	1.44	3.99	1.13	1.80	2.34	0.0001162 86	1.55E-07	0.0005319 01
Pigment synthesis	GUN5	Magnesium-chelatase subunit ChIH	A8MR05;Q9FNB 0	AT5G13630	0.71	1	3.89	0.93	2.37	5.65	0.56	2.87	2.49	4.34E-11	1.70E-18	1.14E-12
Pigment synthesis	HCAR	7-hydroxymethyl chlorophyll a reductase	Q8GS60	AT1G04620	1.48	1	2.11	1.66	1.42	2.20	1.51	1.56	1.92	0.0098834 5	4.88E-09	0.0102375
Pigment synthesis	NOL	Chlorophyll(ide) b reductase NOL	Q8LEU3	AT5G04900	1.17	1	1.27	0.89	1.18	1.47	0.72	1.17	1.21	0.309263	9.76E-05	0.0871969
Pigment synthesis	PAO	Pheophorbide a oxygenase	Q9FYC2	AT3G44880	1.20	1	1.29	1.02	1.30	1.29	1.14	1.39	0.92	0.428084	0.182195	0.0092623 5
Pigment synthesis	PDS	15-cis-phytoene desaturase/chromoplastic	Q07356	AT4G14210	1.08	1	1.32	1.17	1.28	1.32	1.13	1.23	1.23	0.0038118 9	0.0024475 5	0.0056417 9
Pigment synthesis	POR C	Protochlorophyllide reductase C	F4I2F8;O48741	AT1G03630	0.83	1	1.48	0.90	1.72	1.69	0.69	1.62	1.38	7.60E-11	2.22E-17	5.92E-11

Pigment synthesis	PORB	Protochlorophyllide reductase B	P21218	AT4G27440;A5G54190	1.22	1	2.55	1.50	2.64	2.49	1.12	3.21	2.43	5.82E-10	2.07E-13	6.66E-11
Pigment synthesis	PPOX1	Protoporphyrinogen oxidase 1	P55826	AT4G01690	0.87	1	1.33	0.91	1.55	1.62	0.94	1.46	1.33	0.000461874	1.75E-08	0.0356063
Pigment synthesis	PPOX2	Protoporphyrinogen oxidase 2/mitochondrial	Q8S9J1;A0A1P8BE58;A0A1P8BE27	AT5G14220	1.74	1	4.60	1.49	0.90	3.90	1.04	1.50	3.46	0.00252118	1.85E-16	2.60E-05
Pigment synthesis	VTE3	2-methyl-6-phytyl-1,4-hydroquinone methyltransferase	Q9LY74	AT3G63410	0.67	1	2.63	0.93	0.90	3.00	0.67	0.87	2.09	1.91E-06	2.45E-19	5.39E-06
Pigment synthesis	VTE4	Tocopherol O-methyltransferase	Q9ZSK1	At1g64970	1.87	1	5.94	1.37	3.43	5.15	1.51	2.82	5.75	0.74656	2.41E-10	0.0614094
Pigment synthesis	ZDS1	Zeta-carotene desaturase/chromoplasic	Q38893	AT3G04870	5.32	1	1.07	5.92	1.01	2.27	4.38	0.82	1.29	0.000354973	4.65E-15	0.00431617
Pigment synthesis	Z-ISO	15-cis-zeta-carotene isomerase	Q9SAC0	At1g10830	2.36	1	2.10	2.51	2.01	2.70	2.13	1.81	2.30	0.0517968	0.00804294	0.282248
Plastoglobule	At3g07700		B9DGY1;F4JFM1	AT3G07700	1.32	1	7.24	1.49	1.40	8.55	1.60	0.84	8.32	0.028272	1.05E-17	0.072412
Plastoglobule	At3g24190		Q9LRN0	AT3G24190	1.07	1	4.55	1.00	1.67	6.54	1.14	1.90	4.76	0.00983454	3.29E-13	0.0155339
Plastoglobule	At4g39730		O65660	AT4G39730	0.92	1	2.38	0.82	0.77	2.23	0.78	1.09	1.81	0.0361657	8.16E-14	0.00336292
Plastoglobule	CCD4	Probable carotenoid cleavage dioxygenase 4	O49675	AT4G19170	0.67	1	0.70	0.75	1.16	1.03	0.59	1.13	0.96	5.74E-07	4.79E-13	9.17E-06
Plastoglobule	CSP41B	Chloroplast stem-loop binding protein of 41 kDa b	A0A1P8ATL2;Q9SA52	AT1G09340	0.65	1	1.81	0.99	2.25	2.37	0.44	1.26	1.82	3.67E-09	6.06E-13	0.00016043
Plastoglobule	CYP74A	Allene oxide synthase	Q96242	AT5G42650	0.98	1	1.36	0.92	0.93	1.22	0.81	0.69	1.23	5.71E-08	1.73E-12	0.0160622
Plastoglobule	PAP1	Probable plastid-lipid-associated protein 1	O81439	AT4G04020	0.49	1	2.67	0.61	1.14	2.44	0.48	0.99	2.30	0.141923	9.56E-16	0.227606
Plastoglobule	PAP10	Probable plastid-lipid-associated protein 10	Q8W4F1	AT2G46910	0.80	1	2.44	1.04	1.28	2.80	0.80	1.25	2.71	0.488236	3.99E-09	0.767761
Plastoglobule	PAP11	Probable plastid-lipid-associated protein 11	O81304	AT4G00030	1.65	1	43.99	1.40	0.85	2.99	1.40	1.11	40.17	0.599151	0.000611808	0.731785
Plastoglobule	PAP12	Probable plastid-lipid-associated protein 12	Q8LAP6	AT1G51110	0.50	1	0.96	0.60	1.12	1.28	0.54	0.99	0.94	7.40E-07	9.84E-15	0.00728743
Plastoglobule	PAP13	Probable plastid-lipid-associated protein 13	Q8S9M1;F4IM05;A8MRU9	AT2G42130	0.89	1	1.98	1.28	1.10	2.29	0.82	1.04	2.00	0.00192758	6.95E-12	0.409725
Plastoglobule	PAP2	Probable plastid-lipid-associated protein 2	O49629	AT4G22240	1.28	1	7.22	1.35	2.07	5.70	1.17	1.87	5.28	0.102846	1.55E-18	1.31E-06
Plastoglobule	PAP3	Probable plastid-lipid-associated protein 3	O82291	AT2G35490	0.83	1	2.07	0.95	1.45	2.13	0.79	1.24	1.94	4.10E-05	1.96E-15	0.028219
Plastoglobule	PAP4	Probable plastid-lipid-associated protein 4	Q9LU85	AT3G26070	0.78	1	1.33	0.74	0.78	1.42	0.72	0.77	1.34	0.0300552	5.40E-12	0.00968657
Plastoglobule	PAP5	Probable plastid-lipid-associated protein 5	A0A119LP70;Q6DBN2	AT3G26080	1.11	1	2.23	0.72	1.29	1.92	0.76	1.00	1.79	0.146906	1.87E-08	0.018819
Plastoglobule	PAP6	Probable plastid-lipid-associated protein 6	Q9LW57;A0A1I9LQU5;A0A1I9LQU3	AT3G23400	1.16	1	1.51	1.15	1.33	1.98	1.05	1.27	1.56	0.000892681	1.09E-08	0.00341678
Plastoglobule	PAP8	Probable plastid-lipid-associated protein 8	Q941D3;F4K2P2	AT5G19940	1.17	1	1.01	1.11	0.93	1.44	1.15	1.31	0.79	0.112989	0.149835	2.27E-07
Plastoglobule	PAP9	Probable plastid-lipid-associated protein 9	Q9M2P7	AT3G58010	1.39	1	1.52	1.34	1.14	1.60	1.36	1.10	1.26	0.130816	1.63E-06	0.055797
Plastoglobule	PSY	Phytoene synthase	F4KGX7;P37271	AT5G17230	1.21	1	4.74	1.28	1.63	5.38	1.27	1.62	3.49	0.00115616	3.08E-15	4.10E-05

Plastoglobule	T18D12_110		Q9M236;F4IZ56	AT3G43540	1.65	1	2.97	1.86	0.99	4.14	1.48	1.59	3.77	0.187972	9.27E-08	0.195898
Plastoglobule	VTE1	Tocopherol cyclase	Q94FY7	AT4G32770	0.56	1	1.83	0.89	1.53	2.11	0.71	1.06	1.64	4.16E-05	2.11E-11	0.358249
Plastoglobule		Uncharacterized oxidoreductase At1g06690	Q94A68	AT1G06690	0.19	1	3.02	0.33	1.08	3.36	0.26	0.96	2.23	2.55E-05	1.78E-17	1.17E-05
Plastoglobule		Uncharacterized protein At1g32220	Q9FVR6	AT1G32220	0.72	1	1.85	0.92	1.13	2.07	0.77	1.04	2.11	6.63E-05	3.27E-17	0.0401971
Plastoglobule		Acyltransferase-like protein At1g54570	Q9ZVN2	AT1G54570	0.60	1	5.71	1.41	2.07	4.61	1.54	1.84	3.59	0.0041676	1.43E-13	9.04E-06
Plastoglobule		Uncharacterized aarF domain-containing protein kinase At1g71810	Q94BU1	AT1G71810	0.76	1	6.34	0.69	1.86	7.68	1.18	2.81	5.22	0.173111	1.39E-10	0.0066467 6
Plastoglobule		Uncharacterized methyltransferase At1g78140	Q8LBV4	AT1G78140	0.62	1	1.76	0.50	1.57	2.80	0.44	1.25	2.08	0.0003703 06	1.13E-10	0.0028554 5
Plastoglobule		Uncharacterized aarF domain-containing protein kinase At1g79600	Q9MA15	AT1G79600	0.74	1	3.71	0.88	1.41	3.75	0.96	1.23	3.33	0.32132	3.70E-12	0.108198
Plastoglobule		Uncharacterized protein At2g34460	Q8H124	AT2G34460	0.86	1	1.40	0.94	1.18	1.60	0.89	1.11	1.44	1.79E-05	2.25E-14	0.180071
Plastoglobule		Uncharacterized methyltransferase At2g41040	Q0WPT7	AT2G41040	0.76	1	3.68	0.66	1.12	4.08	0.45	0.66	3.29	0.0064485 3	4.45E-14	0.150831
Plastoglobule		Heme-binding-like protein At3g10130	Q9SR77	AT3G10130	1.97	1	6.09	1.83	2.31	4.04	1.17	1.67	4.79	0.763648	4.56E-07	0.152891
Plastoglobule		Uncharacterized protein At4g13200	Q8LDV3	AT4G13200	1.13	1	2.59	1.01	0.71	2.31	1.06	0.98	2.12	0.0042606 6	7.36E-14	0.0672904
Plastoglobule		Uncharacterized aarF domain-containing protein kinase At5g05200	Q9ASX5	AT5G05200	0.88	1	6.65	0.46	1.81	5.52	0.63	2.11	5.99	0.0237313	5.78E-17	0.0012420 6
Protease	ARASP2	Probable membrane metalloprotease ARASP2	O23053	AT1G05140	1.00	1	1.99	1.11	2.09	2.37	1.23	1.72	1.68	0.0016985 9	1.15E-06	0.0039558 6
Protease	At2g21960		Q9SJ03	AT2G21960	0.54	1	1.02	0.64	0.89	1.19	0.66	0.76	0.95	0.0005962 95	1.20E-11	8.88E-05
Protease	CLPP4	ATP-dependent Clp protease proteolytic subunit 4	Q94B60	AT5G45390	0.88	1	3.48	0.97	1.55	4.45	0.66	1.65	2.71	7.69E-09	2.66E-19	3.29E-09
Protease	CLPP5	ATP-dependent Clp protease proteolytic subunit 5	Q9S834	AT1G02560	0.92	1	2.19	1.07	1.54	2.80	0.49	1.82	1.65	7.06E-05	1.00E-10	1.81E-05
Protease	EGY2	Probable zinc metalloprotease EGY2	F4K0T6;F4K0T7; Q9FFK3	AT5G05740	0.81	1	1.26	0.79	1.16	1.22	0.76	1.26	1.00	0.507076	6.73E-08	0.0118932
Protease	FTSH11	ATP-dependent zinc metalloprotease FTSH 11/mitochondrial	Q9FGM0	AT5G53170	1.19	1	8.49	1.26	2.87	9.08	0.85	2.84	5.23	2.78E-06	2.39E-17	3.26E-08
Protease	FTSH12	ATP-dependent zinc metalloprotease FTSH 12	A0A1P8ARE4;A0 A1P8ARD2;Q9S AJ3	AT1G79560	0.62	1	6.56	1.18	1.83	8.75	0.47	1.94	3.96	4.15E-08	3.75E-18	1.04E-09
Protease	SPPA	Serine protease SPPA	Q9C9C0;A0A1P 8AUG2	AT1G73990	0.78	1	3.00	0.90	1.73	3.25	0.72	1.32	2.24	0.0003042 03	4.96E-14	0.0029812 9
Protein folding	At1g80030		A0A1P8ART2;Q 0WN54	AT1G80030	1.17	1	2.20	1.17	1.74	3.55	0.77	1.47	2.37	0.048154	3.35E-06	0.233119
Protein folding	At3g12345		Q9LHH3	AT3G12345	0.85	1	0.31	1.11	1.11	0.88	0.79	0.95	0.44	0.0078165 3	0.0005789 13	0.938356
Protein folding	At4g39960		Q940V1	AT4G39960	1.64	1	3.48	1.55	1.51	5.94	1.05	1.88	3.57	0.0091689 7	5.68E-11	0.0030818 3
Protein folding	CLPB3	Chaperone protein ClpB3	Q9LF37	AT5G15450	0.36	1	4.32	0.79	0.58	3.76	0.40	0.46	2.50	1.47E-08	2.18E-20	4.54E-08
Protein folding	CPN21	20 kDa chaperonin	O65282	AT5G20720	1.82	1	2.91	1.49	0.98	4.30	1.31	0.65	3.57	1.41E-06	4.00E-20	2.27E-09
Protein folding	CPN60A1	Chaperonin 60 subunit alpha 1	P21238	AT2G28000	0.67	1	3.49	0.76	3.40	5.13	0.63	2.07	3.54	1.63E-06	1.24E-12	0.0012154 8

Protein folding	CYP26-2	Peptidyl-prolyl cis-trans isomerase CYP26-2	F4HTT6;A0A1P8APN5	AT1G74070	0.55	1	1.37	0.67	1.22	1.91	0.67	0.98	1.58	0.00548927	1.99E-11	0.475341
Protein folding	CYP28	Peptidyl-prolyl cis-trans isomerase CYP28	A0A1P8B9P2;O65220	AT5G35100	1.00	1	5.98	2.18	6.43	7.09	1.39	3.10	4.96	9.85E-11	1.16E-14	4.85E-08
Protein folding	CYP37	Peptidyl-prolyl cis-trans isomerase CYP37	P82869;A0A1I9LQ22;A0A1I9LQ23	AT3G15520	0.95	1	1.05	1.11	1.63	1.76	1.16	1.32	1.86	6.01E-10	1.33E-09	4.17E-06
Protein folding	FKBP16-3	Peptidyl-prolyl cis-trans isomerase FKBP16-3	A0A1P8B252;O22870	AT2G43560	1.89	1	2.29	1.59	4.15	2.84	1.36	1.66	2.24	6.73E-09	1.19E-05	9.30E-08
Protein folding	FKBP16-4	Peptidyl-prolyl cis-trans isomerase FKBP16-4	Q9SR70	AT3G10060	0.77	1	1.19	0.88	1.30	1.36	1.06	0.93	1.31	2.40E-05	1.50E-09	2.88E-05
Protein folding	FKBP17-2	Peptidyl-prolyl cis-trans isomerase FKBP17-2	Q9LDY5	AT1G18170	1.29	1	1.39	1.38	1.06	1.33	1.11	0.81	1.11	0.000830815	0.000110708	0.69728
Protein folding	FKBP18	Peptidyl-prolyl cis-trans isomerase FKBP18	A0A1P8APZ5;Q9LM71	AT1G20810	1.59	1	1.45	1.74	1.64	1.68	1.91	1.08	1.60	0.00876267	1.18E-05	0.0283767
Protein folding	FKBP19	Peptidyl-prolyl cis-trans isomerase FKBP19	Q9LYR5;A0A1R7T3F4;A0A1R7T3F3	AT5G13410	7.34	1	5.67	7.32	4.01	5.71	4.50	3.00	6.60	0.577542	0.00381478	0.119508
Protein folding	HSP70-6	Heat shock 70 kDa protein 6	Q9STW6	AT4G24280	0.93	1	2.73	1.07	2.58	3.47	0.84	1.71	2.80	1.68E-14	1.39E-21	7.85E-11
Protein folding	TIG	Trigger factor-like protein TIG	Q8S9L5	AT5G55220	0.39	1	1.94	0.75	0.96	2.82	0.42	1.15	1.68	1.23E-08	1.09E-17	5.35E-09
Protein translocation	CLPC1	Chaperone protein ClpC1	Q9FI56	AT5G50920	0.59	1	2.32	0.91	0.89	2.95	0.60	1.18	1.79	1.24E-10	1.53E-21	1.64E-12
Protein translocation	CLPC2	Chaperone protein ClpC2	Q9SXJ7;F4JF64	AT3G48870	1.65	1	4.72	3.64	5.36	8.22	3.04	6.57	5.76	0.000694892	3.11E-05	0.116238
Protein translocation	SCY1	Preprotein translocase subunit SCY1	Q38885	AT2G18710	0.78	1	0.60	0.86	0.69	0.79	0.89	0.66	0.87	0.814035	0.436607	0.157335
Protein translocation	SECA1	Protein translocase subunit SECA1	Q9SYI0;A0A1P8B485;F4JG57	AT4G01800	0.58	1	2.87	0.94	1.22	3.39	0.57	1.44	2.16	3.12E-07	6.38E-18	2.23E-07
Protein translocation	SECE1	Preprotein translocase subunit SECE1	O23342	At4g14870	0.53	1	0.91	0.69	1.29	1.14	0.58	1.10	0.72	0.00290252	3.62E-09	0.202419
Protein translocation	TATA	Sec-independent protein translocase protein TATA	Q9LKU2	AT5G28750	1.44	1	1.14	1.58	0.62	1.54	1.14	0.83	1.17	0.555771	0.000367777	0.208983
Protein translocation	TATB	Sec-independent protein translocase protein TATB	Q9XH75	AT5G52440	0.95	1	1.15	1.03	1.44	1.07	0.96	1.24	0.95	0.110903	0.00251303	0.0403187
Protein translocation	TATC	Sec-independent protein translocase protein TATC	Q9SJV5	AT2G01110	0.79	1	1.43	1.06	1.21	1.59	0.84	1.37	1.06	0.0290312	0.000267943	0.0164034
PSI	psaA	Photosystem I P700 chlorophyll a apoprotein A1	P56766	ATCG00350	1.41	1	1.03	1.33	1.14	0.98	1.14	1.23	0.81	0.000152881	1.31E-12	3.70E-08
PSI	psaB	Photosystem I P700 chlorophyll a apoprotein A2	P56767	ATCG00340	1.28	1	1.11	1.27	1.25	1.01	1.05	1.47	0.89	0.219257	2.28E-06	7.98E-07
PSI	psaC	Photosystem I iron-sulfur center	P62090	ATCG01060	1.49	1	1.09	1.39	1.95	0.89	1.25	1.78	0.88	0.000672615	2.03E-10	1.77E-08
PSI	psaD1	Photosystem I reaction center subunit II-1	Q9S7H1;Q9SA56	AT1G03130;AT4G02770	0.98	1	0.80	0.93	1.11	0.74	0.91	1.11	0.68	0.841764	1.54E-14	1.03E-05
PSI	PSAE1	Photosystem I reaction center subunit IV A	Q9S831	AT4G28750	1.51	1	0.93	1.43	1.13	0.84	1.38	1.08	0.86	0.0678846	6.11E-11	0.072354
PSI	PSAE2	Photosystem I reaction center subunit IV B	Q9S714	AT2G20260	1.78	1	1.43	1.61	1.25	1.43	1.71	1.35	1.27	0.991358	6.23E-09	0.00029578

PSI	PSAF	Photosystem I reaction center subunit III	Q9SHE8	AT1G31330	1.12	1	0.90	1.13	0.82	0.99	1.14	0.85	0.92	0.217997	7.13E-11	0.00149167
PSI	PSAG	Photosystem I reaction center subunit V	Q9S7N7	AT1G55670	1.23	1	0.81	1.17	1.44	0.74	1.18	1.17	0.74	0.0769836	2.41E-10	0.000568536
PSI	PSAH1	Photosystem I reaction center subunit VI-1	Q9SUI7;Q9SUI6	AT1G52230;AT3G16140	1.31	1	0.76	1.60	1.02	0.68	1.30	1.00	0.85	0.413697	1.22E-06	0.494878
PSI	PSAK	Photosystem I reaction center subunit psaK	Q9SUI5	AT1G30380	1.12	1	0.53	1.08	1.31	0.65	0.96	0.92	0.68	0.131304	2.73E-06	0.0504646
PSI	PSAL	Photosystem I reaction center subunit XI	A0A1P8B6D0;Q9SUI4	AT4G12800	1.23	1	0.71	1.30	0.93	0.70	1.23	1.00	0.73	0.71953	7.41E-09	0.944604
PSI	PSAN	Photosystem I reaction center subunit N	P49107	AT5G64040	1.16	1	0.66	1.11	0.36	0.88	1.07	0.44	0.80	5.37E-10	3.73E-17	3.76E-14
PSI	PSAO	Photosystem I subunit O	Q949Q5	AT1G08380	0.42	1	0.43	2.12	0.90	0.39	1.65	0.73	0.48	0.666453	0.00261171	0.532098
PSII	PSB28	Photosystem II reaction center Psb28 protein	F4JM05;Q8W0Y8	AT4G28660	0.61	1	0.99	0.82	0.84	1.40	1.04	1.07	1.03	0.0538572	0.00255195	0.0167688
PSII	PSB33		Q9C9I7	AT1G71500	0.97	1	1.20	1.08	1.17	1.32	1.02	1.10	1.11	7.32E-05	4.52E-06	0.103395
PSII	psbA	Photosystem II protein D1	P83755	ATCG00020	0.87	1	1.00	0.96	1.10	0.97	0.93	1.16	0.87	0.26518	3.35E-06	0.00158804
PSII	psbB	Photosystem II CP47 reaction center protein	P56777	ATCG00680	0.88	1	1.08	0.88	0.93	0.94	0.95	0.99	1.01	0.0029146	5.14E-05	0.0141694
PSII	psbC	Photosystem II CP43 reaction center protein	P56778	ATCG00280	0.93	1	0.88	0.92	1.06	0.88	0.87	1.19	0.81	0.634915	1.64E-10	9.76E-05
PSII	psbD	Photosystem II D2 protein	P56761	ATCG00270	0.91	1	1.05	0.91	1.05	0.94	0.98	0.97	0.98	0.702317	0.0143269	0.0174586
PSII	psbE	Cytochrome b559 subunit alpha	P56779	ATCG00580	0.85	1	1.04	0.80	0.95	1.01	0.95	0.98	1.06	0.0039558	8.67E-06	0.291038
PSII	psbF	Cytochrome b559 subunit beta	P62095	ATCG00570	1.26	1	1.04	1.10	0.49	0.86	1.54	0.61	1.10	4.97E-05	1.14E-08	0.000413444
PSII	psbH	Photosystem II reaction center protein H	P56780	ATCG00710	1.25	1	1.10	1.17	0.87	1.03	1.18	0.94	1.11	0.37312	2.75E-05	0.737786
PSII	PSBO1	Oxygen-evolving enhancer protein 1-1	P23321	AT5G66570	1.07	1	1.03	1.05	0.91	1.03	1.08	0.80	1.02	0.0157424	1.80E-07	0.00435844
PSII	PSBO2	Oxygen-evolving enhancer protein 1-2	Q9S841	AT3G50820	0.95	1	0.90	1.01	0.85	0.94	0.90	0.71	0.99	0.00214658	0.0110002	0.00740371
PSII	PSBP1	Oxygen-evolving enhancer protein 2-1	Q42029	AT1G06680	1.88	1	1.36	1.93	1.51	1.43	1.96	1.34	1.79	1.69E-05	1.13E-10	0.000133627
PSII	PSBQ1	Oxygen-evolving enhancer protein 3-1	Q9XFT3	AT4G21280	0.90	1	0.61	1.03	0.25	0.97	0.94	0.56	1.18	1.23E-05	7.97E-12	1.91E-13
PSII	PSBQ2	Oxygen-evolving enhancer protein 3-2	Q41932	AT4G05180	1.88	1	0.83	2.01	0.49	0.99	2.03	0.72	1.14	0.000640037	2.65E-18	3.39E-07
PSII	PSBR	Photosystem II 10 kDa polypeptide	P27202	AT1G79040	1.28	1	0.93	1.45	0.94	1.00	1.53	0.90	0.94	0.9626	0.000112506	0.536456
PSII	PSBT	Photosystem II 5 kDa protein	A0A1I9LS90;Q39195	AT3G21055	0.77	1	1.72	0.61	1.41	2.15	0.63	1.34	2.25	0.31164	4.41E-10	0.221113
PSII repair	ALB3	Inner membrane protein ALBINO3	Q8LBP4;F4IJM1	AT2G28800	0.30	1	0.57	0.25	1.46	0.96	0.31	1.90	0.55	0.00668217	1.19E-11	0.000637329
PSII repair	At5g07020		Q9FL44	AT5G07020	0.64	1	0.98	0.93	1.21	1.07	0.74	1.11	0.89	0.000962791	4.95E-06	0.378294
PSII repair	CPFTSY	Cell division protein FtsY homolog	O80842	AT2G45770	0.56	1	2.95	1.28	0.47	2.91	0.64	1.23	2.30	0.188661	1.81E-10	0.00356439
PSII repair	CTPA1	Carboxyl-terminal-processing peptidase 1	F4KHG6	AT5G46390	0.98	1	2.04	1.12	2.08	2.91	1.15	1.64	1.97	0.00064941	1.29E-07	0.193539

PSII repair	CYP38	Peptidyl-prolyl cis-trans isomerase CYP38	Q9SSA5	AT3G01480	1.33	1	1.11	1.30	1.86	1.55	1.16	1.13	1.22	4.11E-11	0.0657539	1.18E-07
PSII repair	DEG8	Protease Do-like 8	F4KfV6;Q9LU10	AT5G39830	0.83	1	2.08	1.14	2.54	2.29	0.84	1.47	1.68	6.92E-08	9.71E-10	6.93E-06
PSII repair	DEGP1	Protease Do-like 1	O22609	AT3G27925	1.49	1	1.91	1.35	2.02	2.46	1.19	1.71	2.03	4.25E-07	1.43E-10	7.05E-07
PSII repair	DEGP5	Protease Do-like 5	Q9SEL7;A0A1P8B643;A0A1P8B644	AT4G18370	2.84	1	8.57	2.89	10.03	5.57	1.87	7.21	5.73	0.0175227	4.63E-05	0.0001021 21
PSII repair	FKBP20-2	Peptidyl-prolyl cis-trans isomerase FKBP20-2	A0A1I9LRJ6;Q0WRJ7	AT3G60370	3.82	1	1.97	4.38	2.48	4.01	3.35	0.52	2.32	8.01E-08	2.65E-11	0.103187
PSII repair	FTSH1	ATP-dependent zinc metalloprotease FTSH 1	Q39102	AT1G50250	0.96	1	0.94	1.25	1.11	1.01	1.08	1.04	0.73	0.0115749	0.0031582 2	0.620582
PSII repair	FTSH2	ATP-dependent zinc metalloprotease FTSH 2	A0A1P8AXC1;O80860	AT2G30950	0.68	1	1.08	0.88	1.33	1.22	0.72	1.03	1.05	2.28E-05	7.49E-09	0.214495
PSII repair	FTSH5	ATP-dependent zinc metalloprotease FTSH 5	Q9FH02	AT5G42270	0.75	1	1.44	0.84	1.17	1.71	0.76	1.08	1.19	6.15E-06	5.55E-12	0.0006571 14
PSII repair	FTSH8	ATP-dependent zinc metalloprotease FTSH 8	Q8W585	AT1G06430	0.40	1	1.16	0.42	1.10	1.14	0.36	0.76	0.90	4.60E-05	9.03E-13	0.0353453
PSII repair	HHL1	Protein HHL1	Q8LDL0	AT1G67700	0.45	1	1.10	0.67	0.77	1.41	0.32	0.66	1.05	0.0001373 09	6.15E-10	0.0095781 9
PSII repair	HSP70-7	Heat shock 70 kDa protein 7	Q9LTX9	AT5G49910	0.73	1	3.08	1.01	1.81	3.37	0.96	1.39	2.86	0.0003343 12	2.80E-13	0.0072860 4
PSII repair	LPA1	Protein LOW PSII ACCUMULATION 1	Q9SRY4;A0A1P8ANG6	AT1G02910	1.03	1	1.53	1.05	1.13	1.81	1.07	1.20	1.62	0.0416679	1.69E-07	0.343433
PSII repair	LQY1	Protein disulfide-isomerase LQY1	Q8GSJ6	AT1G75690	0.93	1	1.52	0.98	1.55	1.62	0.85	1.71	1.57	0.0076242 4	2.02E-06	0.0055897 5
PSII repair	LTO1	Thiol-disulfide oxidoreductase LTO1	A0A1P8B950;Q8L540	AT4G35760	1.08	1	1.41	1.18	1.01	1.34	1.18	1.10	1.37	0.828622	0.0001565 6	0.914207
PSII repair	PBF1	Proteasome subunit beta type	F4JD01;P42742	AT3G60820	0.98	1	5.60	0.79	0.78	6.12	0.75	2.48	3.85	0.45106	6.20E-16	8.79E-08
PSII repair	PDIL1-2	Protein disulfide isomerase-like 1-2	Q9SRG3	AT1G77510	5.92	1	9.31	1.92	1.13	6.65	2.96	2.54	6.99	0.0001449 04	3.60E-12	7.02E-05
PSII repair	PPL1	PsbP-like protein 1	P82538	AT3G55330	1.14	1	1.17	1.47	1.29	1.32	1.25	1.09	1.34	8.04E-06	0.0006095 23	0.0060913 3
PSII repair	PSB27-1	Photosystem II repair protein PSB27-H1	Q9LR64	AT1G03600	0.77	1	0.80	0.74	0.57	0.87	0.77	0.45	1.00	0.0073099 4	3.25E-06	2.23E-06
PSII repair	PSB27-2	Photosystem II D1 precursor processing protein PSB27-H2	A0A1P8ASY3;Q9ZVZ9	AT1G05385	4.10	1	2.64	4.56	2.23	5.80	2.54	1.83	2.76	0.0134876	0.0003808 75	0.204629
PSII repair	VIPP1	Membrane-associated protein VIPP1	A0A178W0D3;O80796	AT1G65260	0.76	1	1.69	0.67	1.41	2.06	0.49	1.17	1.48	4.40E-07	8.20E-16	1.48E-05
PSII repair	ZKT		Q94BS2	AT1G55480	0.93	1	1.97	1.24	1.62	2.31	0.67	1.45	2.00	1.40E-07	2.04E-15	5.40E-05
PSII repair		UPF0603 protein At1g54780	Q9ZVL6	AT1G54780	1.13	1	0.88	1.23	0.91	1.00	1.16	0.83	0.92	0.00106	8.25E-11	0.0012527 5
Redox regulation	At1g14345		Q949S6	AT1G14345	0.58	1	1.06	0.83	1.20	1.40	0.62	0.82	1.12	8.32E-05	2.56E-08	0.379895
Redox regulation	At1g50450		Q94BZ0	AT1G50450	0.98	1	1.31	0.89	1.09	1.37	1.07	1.26	1.31	0.171315	8.01E-07	0.132865
Redox regulation	At5g58330	Malate dehydrogenase	Q8H1E2;F4KEX3	AT5G58330	0.44	1	0.66	1.20	0.40	0.82	0.60	0.48	0.41	2.94E-10	0.0029416 5	9.87E-13
Redox regulation	ATHM2	Thioredoxin M2	Q9SEU8;F4JG94	AT4G03520	0.77	1	0.97	1.12	1.06	1.19	0.79	0.89	1.06	5.84E-08	5.49E-06	0.0024805 4

Redox regulation	ATPRX Q	Peroxiredoxin Q	A0A1I9LR27;F4JBC9;Q9LU86	AT3G26060	2.72	1	1.70	2.82	1.84	2.59	1.60	2.29	2.04	3.66E-09	2.16E-09	2.07E-11
Redox regulation	BAS1	2-Cys peroxiredoxin BAS1	Q96291	AT3G11630	2.08	1	2.76	1.63	3.93	3.20	1.02	2.60	3.24	2.59E-08	1.48E-11	3.28E-10
Redox regulation	CITRX	Thioredoxin-like protein CITRX	Q9M7X9	AT3G06730	0.92	1	1.78	1.10	1.40	2.25	0.85	1.59	1.75	1.56E-05	3.93E-13	3.40E-05
Redox regulation	ENH1		Q9FFJ2;A8MSF2	AT5G17170	1.20	1	1.51	1.28	1.36	1.63	1.11	1.11	1.53	2.73E-05	1.54E-10	0.0517906
Redox regulation	F20D21.31		Q9SLI4	AT1G54500	1.21	1	1.35	1.23	1.58	1.42	1.14	1.46	1.28	0.00865973	0.0315632	0.00815537
Redox regulation	FSD3	Superoxide dismutase [Fe] 3	Q9FMX0	AT5G23310	1.04	1	1.65	1.20	1.60	1.59	1.16	1.64	1.56	0.259267	0.0472032	0.463294
Redox regulation	MED24.18		Q940I2	AT5G03880	0.56	1	1.06	0.58	0.97	1.03	0.54	0.88	0.79	1.90E-05	4.01E-13	0.00293465
Redox regulation	NTRC	NADPH-dependent thioredoxin reductase 3	O22229	AT2G41680	1.27	1	4.47	2.80	3.19	5.89	1.07	1.67	2.96	1.26E-09	3.02E-12	0.00568174
Redox regulation		Thioredoxin M1	O48737	AT1G03680	0.81	1	0.60	1.34	0.95	0.68	0.83	0.61	0.46	2.72E-11	2.89E-12	7.34E-08
Redox regulation		Thioredoxin F1	Q9XFH8	AT3G02730	0.32	1	0.61	0.76	0.64	0.91	0.33	0.56	0.54	0.000157638	0.000834693	0.00012489
Redox regulation		Thioredoxin M4	Q9SEU6	AT3G15360	0.56	1	0.80	0.84	0.95	0.89	0.67	0.84	0.94	0.000106911	2.23E-09	1.52E-06
Redox regulation		Malate dehydrogenase	Q9SN86	AT3G47520	1.05	1	3.48	0.94	1.92	3.94	0.74	1.56	3.27	0.128797	9.76E-12	0.0391197
Redox regulation		2-Cys peroxiredoxin BAS1-like	Q9C5R8;A0A1P8BD74	AT5G06290	1.87	1	2.15	1.27	3.43	2.92	0.86	2.35	2.69	6.55E-08	1.13E-10	2.25E-09
Ribosome	At1g68590	30S ribosomal protein 3-1	A8MQL0;Q9SX22	AT1G68590	0.50	1	0.75	0.51	1.14	2.18	0.25	1.32	1.44	0.0502466	0.000161483	0.137371
Ribosome	At3g52150		Q8VYM4	AT3G52150	0.53	1	1.34	0.62	1.78	2.09	0.50	1.43	1.57	8.51E-09	2.63E-14	0.000103318
Ribosome	PSRP5	50S ribosomal protein 5	Q9LER7	AT3G56910	0.76	1	1.89	0.77	1.48	2.67	0.49	1.48	1.62	2.49E-05	2.70E-11	2.88E-05
Ribosome	PSRP6	50S ribosomal protein 6	A0A1P8BCP6;Q9FKP0	AT5G17870	0.55	1	1.36	0.81	1.13	2.53	0.48	1.44	2.11	0.000957716	1.90E-09	0.00708473
Ribosome	RPL1	50S ribosomal protein L1	Q9LY66;F4J296	AT3G63490	0.68	1	1.76	0.92	1.60	2.26	0.60	1.39	1.66	1.10E-12	1.83E-19	6.37E-08
Ribosome	RPL10	50S ribosomal protein L10	Q9FY50	AT5G13510	0.73	1	2.36	1.08	1.71	3.04	0.76	1.47	2.06	6.68E-08	5.12E-15	0.000251975
Ribosome	RPL11	50S ribosomal protein L11	Q9MAP3	AT1G32990	0.80	1	1.78	1.02	1.73	3.66	0.70	1.94	2.30	3.24E-07	2.55E-11	1.32E-05
Ribosome	RPL12C	50S ribosomal protein L12-3	P36212;P36210	AT3G27830;AT3G27850	0.45	1	1.38	0.48	0.67	3.56	0.33	1.21	2.06	0.00892156	1.47E-07	0.000212789
Ribosome	RPL13	50S ribosomal protein L13	Q9SYL9	AT1G78630	4.21	1	3.02	1.81	1.65	3.81	1.33	1.31	2.51	0.0194609	0.000534452	0.0196048
Ribosome	rpl14	50S ribosomal protein L14	P56792	AtCg00780	0.79	1	1.63	1.02	1.97	2.74	0.70	1.84	1.69	4.52E-10	1.20E-13	5.27E-07
Ribosome	RPL15	50S ribosomal protein L15	P25873	AT3G25920	0.70	1	2.37	0.79	1.98	2.80	0.57	1.79	2.29	1.85E-08	1.19E-17	8.32E-07
Ribosome	rpl16	50S ribosomal protein L16	P56793	AT2G28830	0.82	1	2.36	1.01	2.00	3.07	0.66	1.95	2.08	2.28E-06	6.54E-13	2.84E-05
Ribosome	RPL17	50S ribosomal protein L17	Q9M385	AT3G54210	0.53	1	1.88	0.66	1.79	2.68	0.48	1.58	1.89	4.73E-10	2.49E-17	1.18E-06
Ribosome	RPL18	50S ribosomal protein L18	Q9SX68	AT1G48350	1.08	1	2.04	1.12	2.31	3.02	0.79	1.96	2.16	7.10E-08	1.21E-11	1.71E-05
Ribosome	rpl20	50S ribosomal protein L20	P56794	AtCg00660	0.66	1	2.24	0.87	2.38	3.54	0.51	1.30	2.86	0.00223968	1.34E-07	0.21718
Ribosome	RPL21	50S ribosomal protein L21	P51412	AT1G35680	0.96	1	2.66	1.15	1.67	3.45	0.85	1.82	2.74	7.02E-05	1.01E-12	0.00259445

Ribosome	rpl22	50S ribosomal protein L22	P56795	AtCg00810	0.65	1	1.60	0.66	2.17	2.04	0.48	1.87	1.55	0.0004412 6	2.87E-09	0.0012129 4
Ribosome	rpl23-A	50S ribosomal protein L23	P61845	AtCg00840	0.46	1	1.02	0.59	1.86	1.49	0.52	1.30	1.04	3.94E-07	4.29E-12	0.0018549
Ribosome	RPL24	50S ribosomal protein L24	P92959;F4K1S8	AT5G54600	0.43	1	1.39	0.51	1.71	1.87	0.25	1.52	1.25	3.72E-07	1.04E-13	3.73E-06
Ribosome	RPL27	50S ribosomal protein L27	Q9FLN4	AT5G40950	0.78	1	3.52	0.94	1.43	4.47	0.63	1.64	2.63	0.138836	1.70E-09	0.185726
Ribosome	RPL29	50S ribosomal protein L29	Q9FJP3	AT5G65220	0.71	1	2.09	0.79	1.83	3.11	0.55	1.54	1.85	2.33E-06	6.53E-13	0.0003672
Ribosome	rpl2-A	50S ribosomal protein L2	P56791	AtCg00830	0.68	1	2.54	0.78	2.26	4.28	0.53	2.52	2.74	2.75E-05	1.03E-11	2.26E-05
Ribosome	RPL31	50S ribosomal protein L31	Q9FWS4	AT1G75350	0.56	1	1.24	0.60	1.34	2.31	0.37	1.46	1.46	1.07E-07	2.04E-14	3.95E-07
Ribosome	rpl32	50S ribosomal protein L32	P61847	AtCg01020	0.37	1	0.92	0.37	1.70	1.97	0.41	1.73	1.68	0.0013167 5	1.05E-07	0.135996
Ribosome	rpl33	50S ribosomal protein L33	P56796	AtCg00640	0.88	1	2.37	1.11	1.39	2.31	0.75	1.99	2.84	0.0312664	7.97E-10	0.022061
Ribosome	RPL3A	50S ribosomal protein L3-1	Q9SKX4	AT2G43030	1.23	1	2.84	1.42	2.20	3.45	0.96	2.19	2.52	1.44E-06	3.34E-13	1.69E-06
Ribosome	RPL4	50S ribosomal protein L4	O50061;Q2V4Q4 ;Q3EDH2	AT1G07320	0.80	1	1.61	0.88	0.89	2.52	0.58	1.21	1.94	2.63E-06	1.90E-17	3.51E-09
Ribosome	RPL5	50S ribosomal protein L5	O04603	AT4G01310	0.72	1	1.84	0.86	1.59	2.69	0.62	1.48	1.80	8.89E-11	1.76E-17	1.23E-07
Ribosome	RPL6	50S ribosomal protein L6	O23049	AT1G05190	0.63	1	1.37	0.73	1.75	2.33	0.53	1.41	1.58	6.35E-09	6.55E-14	1.21E-05
Ribosome	RPL9	50S ribosomal protein L9	P25864	AT3G44890	0.96	1	2.15	1.15	1.99	2.77	0.87	1.86	2.17	1.31E-09	2.41E-15	1.12E-06
Ribosome	RPS10	30S ribosomal protein S10	Q9LK61	AT3G13120	1.27	1	4.29	0.87	2.80	6.06	0.80	2.25	4.28	0.0032865 6	2.92E-09	0.0800561
Ribosome	rps11	30S ribosomal protein S11	P56802	AtCg00750	1.08	1	2.74	1.28	2.13	3.77	0.89	2.25	2.75	9.18E-08	1.13E-14	5.20E-06
Ribosome	rps12-A	30S ribosomal protein S12	P62126	AtCg01230;At Cg00065;AtC g00905	0.38	1	1.46	0.46	2.58	2.43	0.33	2.28	1.88	1.86E-05	1.76E-10	0.0023335 3
Ribosome	RPS13	30S ribosomal protein S13	P42732;B3H631	AT5G14320	0.59	1	1.60	0.81	2.23	2.13	0.40	2.28	1.49	6.73E-09	2.72E-14	1.30E-07
Ribosome	rps15	30S ribosomal protein S15	P56805	AtCg01120	0.68	1	2.11	0.91	2.16	3.24	0.66	1.38	2.51	3.56E-11	4.22E-17	5.49E-06
Ribosome	RPS17	30S ribosomal protein S17	P16180	AT1G79850	0.59	1	1.96	0.73	2.36	2.36	0.53	1.79	1.99	5.09E-09	7.95E-15	2.71E-06
Ribosome	rps18	30S ribosomal protein S18	P56807	AtCg00650	0.44	1	1.92	0.47	1.77	3.09	0.42	1.07	1.97	0.0008150 34	1.00E-09	0.0755039
Ribosome	rps19	30S ribosomal protein S19	P56808	AtCg00820	1.03	1	2.08	1.21	1.44	2.85	0.89	1.23	2.00	2.07E-05	9.15E-12	0.0861068
Ribosome	rps2	30S ribosomal protein S2	P56797	AtCg00160	0.58	1	1.76	0.81	1.65	2.33	0.61	1.22	1.85	2.87E-06	1.19E-12	0.120559
Ribosome	RPS20	30S ribosomal protein S20	Q9ASV6	AT3G15190	0.82	1	1.86	0.96	1.77	2.44	0.66	1.54	1.98	7.16E-09	4.48E-15	4.30E-05
Ribosome	rps3	30S ribosomal protein S3	P56798	AtCg00800	0.58	1	1.83	0.75	2.15	2.33	0.54	1.76	2.04	2.70E-08	1.76E-14	2.61E-05
Ribosome	RPS31	30S ribosomal protein S31	O80439	At2g38140	1.93	1	7.30	1.05	1.63	7.58	0.67	7.59	7.89	0.511262	0.0007992 9	0.141184
Ribosome	rps4	30S ribosomal protein S4	P56799	AtCg00380	0.67	1	2.76	0.79	2.73	3.37	0.58	2.40	2.93	3.72E-07	1.19E-14	6.92E-06
Ribosome	rps5	30S ribosomal protein S5	P93014	AT2G33800	0.44	1	1.31	0.54	2.10	1.80	0.31	1.65	1.25	2.83E-10	2.33E-15	5.88E-08
Ribosome	RPS6	30S ribosomal protein S6 alpha	A0A1P8AV66;Q8 VY91	AT1G64510	0.49	1	1.90	0.79	1.20	3.45	0.54	1.73	2.15	0.0001906 31	9.55E-10	0.0005263 49
Ribosome	rps7-A	30S ribosomal protein S7	P61841	AtCg00900;At Cg01240	0.64	1	2.02	0.87	1.97	2.30	0.47	1.61	2.08	3.45E-06	6.85E-14	0.0008907 49
Ribosome	rps8	30S ribosomal protein S8	P56801	AtCg00770	0.58	1	2.23	0.69	2.70	3.23	0.47	2.15	3.58	0.0018405	2.82E-08	0.0945155
Ribosome	RPS9	30S ribosomal protein S9	Q9XJ27	AT1G74970	0.69	1	1.13	0.84	1.99	1.56	0.52	1.69	1.31	7.13E-06	1.26E-09	0.0030106 9

Ribosome		50S ribosomal protein L19-1	Q8W463	AT4G17560	0.15	1	1.60	0.16	1.49	2.39	0.14	1.47	1.74	3.25E-05	2.97E-14	0.0006639 39
Starch	BAM3	Beta-amylase 3	O23553	AT4G17090	0.38	1	1.43	1.05	0.12	1.51	0.60	0.37	0.77	7.39E-06	9.09E-10	5.43E-09
Starch	SS1	Starch synthase 1/amyloplastic	Q9FNF2	AT5G24300	0.30	1	2.41	0.81	0.25	2.59	0.44	0.73	1.49	1.24E-07	2.34E-19	1.13E-11
Stress responsive	APE1		Q2HIR7;A0A219 HZL6	AT5G38660	0.95	1	1.47	1.07	1.12	1.55	0.97	1.14	1.28	2.06E-06	5.42E-15	3.20E-05
Stress responsive	CCL		Q96500	AT3G26740	0.89	1	1.03	0.85	1.34	1.14	0.89	1.40	0.81	0.064187	3.02E-05	0.0146854
Stress responsive	CLH1	Chlorophyllase-1	O22527	AT1G19670	0.81	1	1.06	0.75	0.47	1.51	0.47	0.72	0.91	6.60E-05	1.00E-09	3.76E-07
Stress responsive	FLU	Protein FLUORESCENT IN BLUE LIGHT	F4JFR2;F4JFR1; Q940U6	AT3G14110	1.33	1	1.63	1.35	1.12	1.57	1.48	1.15	1.37	0.487876	1.34E-08	0.0070793 1
Stress responsive	PPD3	PsbP domain-containing protein 3	Q9S720	AT1G76450	0.74	1	2.85	1.04	3.47	4.72	0.89	2.29	3.00	5.60E-13	2.75E-17	2.65E-09
Stress responsive	PPD4	PsbP domain-containing protein 4	O49292	AT1G77090	1.48	1	2.53	1.61	3.05	3.21	1.32	1.83	2.40	5.66E-09	1.42E-10	2.75E-07
Stress responsive	PPD6	PsbP domain-containing protein 6	Q9LXX5	AT3G56650	2.08	1	2.01	2.51	1.18	2.54	1.63	1.12	1.64	2.48E-06	9.12E-11	0.0012481 2
Stress responsive	TL29	Thylakoid lumenal 29 kDa protein	A0A1P8B8W6;A 0A1P8B8Y3;P82 281	AT4G09010	0.82	1	1.18	0.87	1.07	1.29	0.76	1.08	1.00	0.012784	5.63E-09	0.0282379
Stress responsive			Q9FPH2	AT5G02160	2.24	1	0.66	2.12	0.89	0.64	2.03	1.10	0.65	0.930864	2.79E-16	0.10433
Thylakoid architecture	CURT1A	Protein CURVATURE THYLAKOID 1A	O04616	AT4G01150	0.74	1	0.98	0.99	0.95	0.97	0.87	0.96	0.74	0.202179	0.38184	0.0441454
Thylakoid architecture	CURT1B	Protein CURVATURE THYLAKOID 1B	Q8LCA1	AT2G46820	0.93	1	0.97	0.88	0.95	1.05	0.92	1.00	0.74	0.0477221	0.0153097	0.0003393 99
Thylakoid architecture	CURT1C	Protein CURVATURE THYLAKOID 1C	Q9M812	AT1G52220	1.09	1	1.32	1.14	1.04	1.38	1.01	0.88	1.23	0.0008002 58	2.00E-09	0.591948
Thylakoid architecture	CURT1D	Protein CURVATURE THYLAKOID 1D	A0A1P8B4V5;Q8 LDD3	AT4G38100	2.31	1	5.50	2.05	1.20	4.15	2.21	1.65	3.52	0.089181	1.45E-10	0.018299
Thylakoid architecture	FZL		Q1KPV0;A0A1P 8AUL4;A0A1P8A UL2	AT1G03160	0.75	1	1.67	0.74	1.47	2.37	0.68	1.49	1.98	0.211696	1.78E-08	0.367444
Thylakoid architecture	PLSP1	Chloroplast processing peptidase	A0A1I9LMR3;Q8 HOW1	AT3G24590	1.13	1	0.75	0.84	1.11	1.44	1.00	1.21	0.84	0.428458	0.293661	0.0094398
Thylakoid architecture	RIQ1	Reduced induction of non-photochemical quenching2	Q9SD79	AT5G08050	0.76	1	0.98	0.97	0.78	1.46	0.78	1.01	1.12	0.030052	0.0092728 5	0.230179
Thylakoid architecture	RIQ2	Reduced induction of non-photochemical quenching1	Q94F10	AT1G74730	0.56	1	0.56	0.90	1.10	0.67	0.62	1.28	0.50	0.0291748	1.01E-05	0.566469
Thylakoid architecture	THF1	Protein THYLAKOID FORMATION 1	Q9SKT0	AT2G20890	0.57	1	1.65	0.69	1.08	1.96	0.49	1.06	1.32	0.0499389	4.03E-09	0.602945

Table 15: Relative abundance of thylakoid-associated proteins in pgr5. Details of the 447 MS-quantified thylakoid proteins from pgr5 thylakoids relative to gl-1, including functional category, protein/gene name, description, UniProtKB identifier, TAIR ID and abundance ratios relative to gl-1. Significant changes were identified by a modified Welch's t-test ( $q < 0.05$ ). Median protein iBAQ values were used for the calculation of ratios.

Category	Protein/ gene name	Description	UniProtKB accession	TAIR ID	Ratio pgr5 vs gl-1	Welch's t-test sig.	Welch's t- test q- value
Assembly	ALB4	ALBINO3-like protein 1	F4I9A9;Q9FYL3	AT1G24490	0.85		0.798683
Assembly	At4g28740	LOW PSII ACCUMULATION-like protein	F4JM22	AT4G28740	0.84	+	0.0139178
Assembly	At5g48790	LOW PSII ACCUMULATION protein	Q94F50;Q9FKB7	AT5G48790	1.86		0.20055
Assembly	CCB1	Protein COFACTOR ASSEMBLY OF COMPLEX C SUBUNIT B CCB1	Q9LSE4	AT3G26710	0.82		0.14523
Assembly	CCB2	Protein COFACTOR ASSEMBLY OF COMPLEX C SUBUNIT B CCB2	Q9FJ81	AT5G52110	0.77	+	0.0439641
Assembly	CCS1	Cytochrome c biogenesis protein CCS1	Q9XIA4	AT1G49380	0.55	+	0.037198
Assembly	DAC		Q94BY7	AT3G17930	0.42		0.421672
Assembly	HCF101	Fe-S cluster assembly factor HCF101	Q6STH5	AT3G24430	0.94		0.645855
Assembly	HCF136	Photosystem II stability/assembly factor HCF136	A0A1P8BG37;O82660	AT5G23120	0.85	+	0.0070303
Assembly	HCF164	Thioredoxin-like protein HCF164	O23166	AT4G37200	0.98		0.897908
Assembly	HCF244	NAD(P)-binding Rossmann-fold superfamily protein	O65502	AT4G35250	0.73	+	0.0165085
Assembly	LPA2	Protein LOW PSII ACCUMULATION 2	F4KDA6	AT5G51545	1.00		0.748162
Assembly	LPA3	Protein LOW PSII ACCUMULATION 3	Q8H0W0	AT1G73060	0.47	+	0.0133333
Assembly	MPH2	Thylakoid lumenal 16.5 kDa protein	A0A1P8B5H3;O22773;A0A1P8B5G9	AT4G02530	0.89		0.528952
Assembly	PPD1	PsbP domain-containing protein 1	O23403	AT4G15510	0.66	+	0.0135354
Assembly	Y3IP1	Ycf3-interacting protein 1	Q9LU01	AT5G44650	0.97		0.145101
Assembly	YCF4	Photosystem I assembly protein Ycf4	P56788	AtCg00520	1.16		0.0998491
ATP synthase	ATPA	ATP synthase subunit alpha	P56757	ATCG00120	1.20	+	0.0434444
ATP synthase	ATPB	ATP synthase subunit beta	P19366	ATCG00480	0.93		0.0526076
ATP synthase	ATPC1	ATP synthase gamma chain 1	Q01908	AT4G04640	0.96		0.1841
ATP synthase	ATPD	ATP synthase subunit delta	Q9SSS9	AT4G09650	0.84	+	0.0309733
ATP synthase	ATPE	ATP synthase epsilon chain	P09468	ATCG00470	0.95		0.478177
ATP synthase	ATPF	ATP synthase subunit b	P56759	ATCG00130	0.94		0.118553
ATP synthase	ATPH	ATP synthase subunit c	P56760	ATCG00140	0.35	+	0.0138113
ATP synthase	ATPI	ATP synthase subunit a	P56758	ATCG00150	1.10		0.897256
ATP synthase	PDE334		Q42139	AT4G32260	1.22	+	0.0206494
Carbon fixation	BCA1	Beta carbonic anhydrase 1	A0A1I9LQB3;P27140	AT3G01500	0.77	+	0.0138182
Carbon fixation	RBCL	Ribulose biphosphate carboxylase large chain	O03042	AtCg00490	0.70	+	0.0102545
Carbon fixation	RBCS-1A	Ribulose biphosphate carboxylase small chain 1A	P10795	AT1G67090	0.69	+	0.0135467
Carbon fixation	RBCS-1B	Ribulose biphosphate carboxylase small chain 1B	P10796	AT5G38430	0.72	+	0.00989474
Carbon fixation	RBCS-2B	Ribulose biphosphate carboxylase small chain 3B	P10798;P10797;B3H5S2;F4KA76	AT5G38410;A5G38420	0.85	+	0.01128

Carbon fixation	RCA	Ribulose biphosphate carboxylase/oxygenase activase	P10896;F4IVZ7	AT2G39730	0.81	+	0.0136822
Chloroplast replication	FTSZ1	Cell division protein FtsZ homolog 1	Q42545	AT5G55280	0.32	+	0.033886
Chloroplast replication	FTSZ2-1	Cell division protein FtsZ homolog 2-1	A0A1P8AXD8;O82533	AT2G36250	0.81		0.152792
Chloroplast replication	FTSZ2-2	Cell division protein FtsZ homolog 2-2	Q9LXJ0;A0A1I9LSJ8	AT3G52750	0.46	+	0.0143099
Chlororespiration	PIFI	Post-illumination chlorophyll fluorescence increase	B3H4M0;F4J037;F4J034;Q9LVZ5;F4J036	AT3G15840	0.54	+	0.00459259
Cytochrome b6f	PETA	Cytochrome f	P56771	ATCG00540	0.91		0.116129
Cytochrome b6f	PETB	Cytochrome b6	P56773	ATCG00720	0.53	+	0.0138144
Cytochrome b6f	PETC	Cytochrome b6-f complex subunit 4	P56774	ATCG00730	0.97		0.925665
Cytochrome b6f	PETD	Cytochrome b6-f complex iron-sulfur subunit	Q9ZR03	AT4G03280	0.87	+	0.0309508
DNA/RNA	At2g21530		Q8GWP4	AT2G21530	0.33		0.0698167
DNA/RNA	At2g24060		O82234	AT2G24060	0.41		0.243821
DNA/RNA	At2g24420		Q9ZQ26	AT2G24420	0.88		0.381061
DNA/RNA	CP29A	29 kDa ribonucleoprotein	Q43349;F4JAF3	AT3G53460	0.90		0.0614815
DNA/RNA	CP29B	RNA-binding protein CP29B	Q9ZUU4	AT2G37220	0.87		0.153556
DNA/RNA	CP31A	31 kDa ribonucleoprotein	Q04836	AT4G24770	1.48	+	0
DNA/RNA	PTAC16	Protein PLASTID TRANSCRIPTIONALLY ACTIVE 16	Q9STF2	AT3G46780	0.70	+	0
DNA/RNA	rpoA		P56762	AtCg00740	1.21	+	0.0203846
DNA/RNA	TUFA	Elongation factor Tu	P17745	AT4G20360	1.07	+	0.0205161
Electron transfer	FD1	Ferredoxin-1	O04090	AT1G10960	0.16	+	0.0229701
Electron transfer	FD2	Ferredoxin-2	P16972	AT1G60950	0.14		0.996359
Electron transfer	FD3	Ferredoxin-3	Q9ZQG8	AT2G27510	0.78	+	0.0315106
Electron transfer	LFNR1	Ferredoxin--NADP reductase, leaf isozyme 2	Q8W493;C0Z2A8	AT1G20020	0.71	+	0
Electron transfer	LFNR2	Ferredoxin--NADP reductase, leaf isozyme 1	Q9FKW6;F4JZ46	AT5G66190	0.62	+	0.013679
Electron transfer	NDC1	Alternative NAD(P)H-ubiquinone oxidoreductase C1/mitochondrial	Q8GXR9	AT5G08740	0.89	+	0.0435733
Electron transfer	PC	Plastocyanin major isoform	P42699	AT1G20340	0.79	+	0.0183235
Electron transfer	PETE	Plastocyanin minor isoform	A0A1P8APR2;P11490	AT1G76100	0.94		0.851277
Electron transfer	PGR5	Protein PROTON GRADIENT REGULATION 5	Q9SL05	AT2G05620	0.04	+	0.0053913
Electron transfer	PGR6	Uncharacterized aarF domain-containing protein kinase At4g31390	Q8RWG1;A0A1P8B7P6	AT4G31390	1.06		0.170153
Electron transfer	PGRL1A	PGR5-like protein 1A	Q8H112;A0A2H1ZEN5	AT4G22890	0.52	+	0.008
Electron transfer	PGRL1B	PGR5-like protein 1B	Q8GYC7;F4JPU9	AT4G11960	0.58	+	0.018597
Electron transfer	TIC62	Protein TIC 62	Q8H0U5	AT3G18890	0.86	+	0.0193714
Electron transfer	TROL	Rhodanese-like domain-containing protein 4	A0A1P8B8J7;Q9M158	AT4G01050	0.89	+	0.0129362
Ion channel	DIT2-1	Dicarboxylate transporter 2.1	Q9FMF7	AT5G64290	1.04		0.868088
Ion channel	KEA3	K(+) efflux antiporter 3	Q9M0Z3	AT4G04850	1.07		0.336362
Ion channel	MNJ8.18	LOW protein: ammonium transporter 1-like protein	Q93Z11	AT5G37360	0.71	+	0.0268671
Kinase/phosphatase	At3g59780	Rhodanese/Cell cycle control phosphatase superfamily protein	F4J9G2	AT3G59780	1.00		0.930081

Kinase/phosphatase	At5g35170	Adenylate kinase 5	F4JYC0;Q8VYL1	AT5G35170	0.96		0.939308
Kinase/phosphatase	PGK1	Phosphoglycerate kinase 1	P50318;F4I3L1	AT1G56190;AT1G79550	0.59	+	0.0231084
Kinase/phosphatase	PGK1	Phosphoglycerate kinase 1	Q9LD57	AT3G12780	0.79		0.066976
LHCI	LHCA1	Chlorophyll a-b binding protein 6	A8MS75;Q01667;F4JE46;F4JE43	AT3G54890	0.89		0.478485
LHCI	LHCA2	Photosystem I chlorophyll a/b-binding protein 2	Q9SYW8	AT3G61470;AT5G28450	0.20		0.0635246
LHCI	LHCA3	Photosystem I chlorophyll a/b-binding protein 3-1	Q9SY97	AT1G61520	0.91		0.181572
LHCI	LHCA4	Chlorophyll a-b binding protein 4	P27521	AT3G47470	0.79	+	0.0433805
LHCI	LHCA6	Photosystem I chlorophyll a/b-binding protein 6	Q8LCQ4	AT1G19150	1.14		0.862739
LHCII	LHCB1.1;LHCB1.2	Chlorophyll a-b binding protein 2	Q8VZ87;P0CJ48	AT1G29910	1.69	+	0.0208662
LHCII	LHCB1.1	Chlorophyll a-b binding protein 1	P04778	AT1G29930	0.13	+	0.0340317
LHCII	LHCB1.4	Chlorophyll a-b binding protein	Q39142	AT2G34430	0.61		0.0639024
LHCII	LHCB1.5	Chlorophyll a-b binding protein	Q39141	AT2G34420	0.65	+	0.02656
LHCII	LHCB2	Chlorophyll a-b binding protein 2	Q9SHR7;Q9S7J7;Q9XF87;A0A1I9LMB4;A0A1P8AZ91	AT2G05070;AT2G05100;AT3G27690	0.50	+	0.0205867
LHCII	LHCB3	Chlorophyll a-b binding protein 3	Q9S7M0	AT5G54270	0.55	+	0.0379806
LHCII	LHCB4.1 (CP29.1)	Chlorophyll a-b binding protein CP29.1	Q07473	AT5G01530	1.08	+	0.0131373
LHCII	LHCB4.2 (CP29.2)	Chlorophyll a-b binding protein CP29.2	Q9XF88	AT3G08940	0.99		0.717814
LHCII	LHCB4.3 (CP29.3)	Chlorophyll a-b binding protein CP29.3	Q9S7W1;F4IGY6	AT2G40100	0.15	+	0.0106415
LHCII	LHCB5 (CP26)	Chlorophyll a-b binding protein CP26	Q9XF89	AT4G10340	0.83		0.265841
LHCII	LHCB6 (CP24)	Chlorophyll a-b binding protein	Q9LMQ2	AT1G15820	0.89	+	0.0139583
LHC-like	Lii3.1	Light-harvesting complex-like protein 3 isotype 1	Q9SYX1	AT4G17600	0.65	+	0.0311398
LHC-like	Lii3.2	Light-harvesting complex-like protein 3 isotype 2	Q6NKS4	AT5G47110	0.62	+	0.021546
LHC-like	OHP1	High-light-induced protein	O81208	AT5G02120	0.78	+	0.0179365
LHC-like	OHP2	Light-harvesting complex-like protein OHP2	Q9FEC1	AT1G34000	0.71	+	0.0136629
Light harvesting regulation	LCNP		Q9STS7	AT3G47860	0.76	+	0.0130753
Light harvesting regulation	PSBS	Photosystem II 22 kDa protein	Q9XF91;F4IEG8	AT1G44575	1.03		0.647354
Light harvesting regulation	ROQH1		Q8GYZ0;F4JSP1	AT4G31530	0.78		0.218736
Light harvesting regulation	SOQ1	Protein SUPPRESSOR OF QUENCHING 1	Q8VZ10	AT1G56500	1.08		0.47893
Light harvesting regulation	STN7	Serine/threonine-protein kinase STN7	Q9S713	AT1G68830	1.08	+	0.0374472

Light harvesting regulation	STN8	Serine/threonine-protein kinase STN8	Q9LZV4	AT5G01920	0.83	+	0.0447671
Light harvesting regulation	TAP38	Protein phosphatase 2C 57	P49599	AT4G27800	0.62	+	0.00516667
Light harvesting regulation	TSP9	Thylakoid soluble phosphoprotein	Q9SD66	AT3G47070	0.77	+	0.0133091
Light harvesting regulation	VDE1	Violaxanthin de-epoxidase	Q39249	AT1G08550	0.87		0.106007
Light harvesting regulation	ZEP	Zeaxanthin epoxidase	Q9FGC7	AT5G67030	0.82	+	0.0131892
NDH	NDHC	NAD(P)H-quinone oxidoreductase subunit 3	P56751	ATCG00440	NaN		1
NDH	NDHE	NAD(P)H-quinone oxidoreductase subunit 4L	P26289	ATCG01070	0.97		0.265701
NDH	NDHF	NAD(P)H-quinone oxidoreductase subunit 5	P56752	ATCG01010	0.23	+	0.0110588
NDH	NDHH	NAD(P)H-quinone oxidoreductase subunit H	P56753	ATCG01110	0.62		0.10645
NDH	NDHI	NAD(P)H-quinone oxidoreductase subunit I	P56755	ATCG01090	0.81	+	0.0194688
NDH	NDHJ	NAD(P)H-quinone oxidoreductase subunit J	P56754	ATCG00420	0.48		0.0509153
NDH	NDHK	NAD(P)H-quinone oxidoreductase subunit K	P56756	ATCG00430	0.68	+	0.0184593
NDH	ndhL		Q9CAC5	AT1G70760	0.78		0.170696
NDH	NDHM	NAD(P)H-quinone oxidoreductase subunit M	Q2V2S7	AT4G37925	0.88	+	0.021679
NDH	NDHN	NAD(P)H-quinone oxidoreductase subunit N	Q9LVM2	AT5G58260	0.68	+	0.0201633
NDH	NDHO	NAD(P)H-quinone oxidoreductase subunit O	Q9S829	AT1G74880	0.33		0.0923089
NDH	NDHS	NAD(P)H-quinone oxidoreductase subunit S	Q9T0A4	AT4G23890	0.88	+	0.0204414
NDH	NDHT	NAD(P)H-quinone oxidoreductase subunit T	Q9SMS0	AT4G09350	1.07		0.721985
NDH	NDHU	NAD(P)H-quinone oxidoreductase subunit U	Q84VQ4	AT5G21430	0.70	+	0
NDH	PNSB1	Photosynthetic NDH subunit of subcomplex B 1	Q9S9N6	AT1G15980	0.73	+	0.0146506
NDH	PNSB2	Photosynthetic NDH subunit of subcomplex B 2	Q94AQ8;F4I891;F4I890	AT1G64770	0.67	+	0.0211429
NDH	PNSB3	Photosynthetic NDH subunit of subcomplex B 3	Q9LU21	AT3G16250	0.60		0.0927231
NDH	PNSB4	Photosynthetic NDH subunit of subcomplex B 4	A0A1P8AS98;F4ICC6;Q8RXS1	AT1G18730	0.76		0.0855969
NDH	PNSB5	Photosynthetic NDH subunit of subcomplex B 5	Q9FG89	AT5G43750	0.61	+	0.0381659
NDH	PNSL1	Photosynthetic NDH subunit of luminal location 1	O80634	AT2G39470	0.83	+	0.0298242
NDH	PNSL2	Photosynthetic NDH subunit of luminal location 2	Q9XI73	AT1G14150	0.90	+	0.0349072
NDH	PNSL3	Photosynthetic NDH subunit of luminal location 3	Q9SGH4	AT3G01440	0.78		0.0560335
NDH	PNSL4	Photosynthetic NDH subunit of luminal location 4	F4JW56;Q9SCY3	AT4G39710	0.68	+	0.00955932
NDH	PNSL5	Photosynthetic NDH subunit of luminal location 5	Q9ASS6	AT5G13120	0.65	+	0.0108462
Other/unknown	AAC1		P31167	AT3G08580	0.95		0.551821
Other/unknown	AAC2		P40941	AT5G13490	0.89		0.198785
Other/unknown	AOC2		Q9LS02	AT3G25770	0.64	+	0
Other/unknown	APG3	Peptide chain release factor APG3	Q8RX79	AT3G62910	0.74		0.165974
Other/unknown	APXT	L-ascorbate peroxidase T	A0A1P8APU0;Q42593	AT1G77490;A2G18140;AT2G18150	0.83		0.139592

Other/unknown	At1g07660		P59259;A8MRV1	AT2G28740	1.25	+	0.00773333
Other/unknown	At1g18060		Q9LM40	AT1G18060	0.70	+	0.0257076
Other/unknown	At1g24360		P33207	AT1G24360	0.45	+	0.0131429
Other/unknown	At1g33810	Zinc finger/BTB domain protein	Q8L9M8	AT1G33810	1.02		0.469643
Other/unknown	At1g52510		Q8VZ57;F4ICZ4	AT1G52510	0.83	+	0.00442857
Other/unknown	At1g73110		Q9AST9;A0A1P8ATD8	AT1G73110	2.97		0.0504103
Other/unknown	At1g78915		Q8GWV1;F4IBX4;F4IBX5	AT1G78915	0.52	+	0.0207342
Other/unknown	At2g27290	FAM210B-like protein, putative (DUF1279)	Q9XIN6	AT2G27290	0.63		0.173873
Other/unknown	At2g27680		Q9ZUX0	AT2G27680	0.31	+	0.013977
Other/unknown	At3g14420		Q9LRR9;A8MS37;B3H4B8;Q2V3V9	AT3G14420	1.75	+	0.0105846
Other/unknown	At3g61870	Plant/protein	F4IX01;Q9M277	AT3G61870	0.83		0.094023
Other/unknown	At4g02725		Q6DBF6	AT4G02725	0.82	+	0.0340625
Other/unknown	At5g14910	Heavy metal transport/detoxification superfamily protein	Q93VK7	AT5G14910	1.13		0.175508
Other/unknown	At5g16660		A8MS48;Q8H0X5	AT5G16660	0.76	+	0.0166496
Other/unknown	At5g42070		Q8RWR9	AT5G42070	0.56	+	0.044362
Other/unknown	At5g51010		Q9FI47	AT5G51010	0.86		0.269959
Other/unknown	BASS2		Q1EBV7	AT2G26900	1.33	+	0.0115102
Other/unknown	CAC3		Q9LD43	AT2G38040	1.02		0.40389
Other/unknown	CAS	Calcium sensing receptor	Q9FN48;A0A1P8BCX7	AT5G23060	0.63	+	0
Other/unknown	CCR1		F4JVC0;F4JVC1;Q03251;F4JVB9	AT4G39260	1.80	+	0
Other/unknown	CCR2		F4IHK9;Q03250	AT2G21660	1.34	+	0.0128182
Other/unknown	CPP1		Q9FN50	AT5G23040	0.74		0.195938
Other/unknown	EGY2		F4K0T6;F4K0T7;Q9FFK3	AT5G05740	0.89		0.132382
Other/unknown	F11M15.26		Q9SYE2	AT1G51400	1.02		0.722554
Other/unknown	F13A11.2		Q9C7S3	AT1G42960	0.77	+	0.0290056
Other/unknown	F16M2_10		Q9M1X3	AT3G63160	1.33	+	0.0370101
Other/unknown	F17F16.7		A0A1P8AWY1;Q8W4D6;A0A1P8AWU9	AT1G16720	0.99		0.859842
Other/unknown	F24J8.11		Q9LPK9	AT1G21500	1.11	+	0.0188788
Other/unknown	FAB2	Acyl-[acyl-carrier-protein] desaturase	F4IS32;O22832;Q9LF04;Q9M879	AT2G43710;AT3G02630;AT5G16240	0.72		0.120937
Other/unknown	FBA1	Fructose-bisphosphate aldolase	Q9ZU52	AT2G01140	0.81		0.160647
Other/unknown	FBA1	Fructose-bisphosphate aldolase	Q9SJU4;F4IGL5;F4IGL7	AT2G21330	0.74	+	0.00590476
Other/unknown	FBA2	Probable fructose-bisphosphate aldolase 2	Q944G9;F4JUJ5	AT4G38970	0.54	+	0.0198926
Other/unknown	FFC		P37107	AT5G03940	0.96		0.95383
Other/unknown	FLAP1	Fluctuating light acclimation protein 1	Q8RWI0	AT1G54520	0.98		0.715969
Other/unknown	GAPA2		Q9LPW0;A0A1P8APR6;F4HNZ6	AT1G12900	0.56	+	0

Other/unknown	GC1		A0A1P8B167;Q9SJU9	AT2G21280	0.54	+	0.00972414
Other/unknown	GDCST		A0A2H1ZEA9;O65396	AT1G11860	1.25	+	0.0280226
Other/unknown	GLDP1		Q94B78;B3H5Y8	AT4G33010	1.25	+	0.0207843
Other/unknown	GLN2	Glutamine synthetase/mitochondrial	Q43127	AT5G35630	0.47	+	0.0100714
Other/unknown	GYRA		Q9CAF6	AT3G10690	1.13		0.45418
Other/unknown	H2AV		Q9C944;Q9SII0;O23628;F4JT33;Q9T0H7	AT1G52740	0.98		0.784715
Other/unknown	HSP70-3		O65719	AT3G09440	0.92	+	0.0441622
Other/unknown	LGUC		Q8W593	AT1G67280	0.54		0.0936641
Other/unknown	LOX2		P38418;A0A1I9LPH1	AT3G45140	0.84	+	0.0140769
Other/unknown	LTA2	Dihydrolipoyllysine-residue acetyltransferase component 4 of pyruvate dehydrogenase complex	Q9SQI8	AT3G25860	0.87		0.125417
Other/unknown	LTA3	Dihydrolipoyllysine-residue acetyltransferase component 1 of pyruvate dehydrogenase complex	F4J5T2;Q0WQF7	AT3G52200	1.00		0.274023
Other/unknown	MFP1		Q9LW85	AT3G16000	1.05		0.164271
Other/unknown	MNC6.3	Thylakoid lumenal 17.4 kDa protein	A0A1P8BAQ0;F4JX83;P81760	AT5G53490	0.72	+	0.0139429
Other/unknown	MRO11.7	GPI-anchored adhesin-like protein	A0A1P8BAU8;Q9FF91	AT5G23890	1.13		0.47671
Other/unknown	MXK3.17		Q93Y08	AT5G64940	0.93		0.867304
Other/unknown	NAGK		Q9SCL7	AT3G57560	0.79	+	0.0167931
Other/unknown	OEP161		Q9ZV24	AT2G28900	1.19	+	0.0133684
Other/unknown	PLGG1		Q9FVQ4	AT1G32080	0.94		0.188137
Other/unknown	PMDH2		F4KDZ4;Q9ZP05;A0A1P8BBQ0;A8MRP1;B3H560	AT5G09660	0.71	+	0.01
Other/unknown	PPD5	PsbP domain-containing protein 5	A0A178U9N5;P82715	AT5G11450	0.83	+	0.0169917
Other/unknown	PRXIIE		Q949U7	AT3G52960	1.14		0.0809255
Other/unknown	PRXIIE		Q949U7	AT3G52960	2.21177	+	0
Other/unknown	PTAC5	Protein disulfide isomerase pTAC5	A0A1P8B4I3;A1A6M1	AT4G13670	0.74	+	0.0133626
Other/unknown	RAT5		Q9LD28;O81826;Q9C681	AT5G54640	0.87		0.119237
Other/unknown	RAT5		Q9LD28;O81826;Q9C681	AT5G54640	2.02448	+	0.0465067
Other/unknown	RPI3		Q9S726	AT3G04790	1.12		0.916278
Other/unknown	RPI3		Q9S726	AT3G04790	2.3028		0.978054
Other/unknown	SHM1		Q9SZJ5	AT4G37930	1.30	+	0.0336754
Other/unknown	STR10	Rhodanese-like domain-containing protein 10	Q9SR92	AT3G08920	0.78	+	0.0386351
Other/unknown	STR11	Rhodanese-like domain-containing protein 11	Q0WWT7	AT4G24750	0.63		0.0660645
Other/unknown	STR14	Rhodanese-like domain-containing protein 14	Q94A65	AT4G27700	1.09		0.328374
Other/unknown	STR9	Rhodanese-like domain-containing protein 9	O48529	AT2G42220	0.77	+	0.0104444
Other/unknown	T6G15.50		Q9T0H1	AT4G13500	0.76		0.181743
Other/unknown	TL15A	Thylakoid lumenal 15 kDa protein 1	O22160	AT2G44920	1.17		0.129699
Other/unknown	TL17.9	Thylakoid lumenal 17.9 kDa protein	Q9SW33	AT4G24930	0.93		0.645323
Other/unknown	TL19	Thylakoid lumenal 19 kDa protein	P82658	AT3G63540	0.44	+	0.0195108
Other/unknown	TL20.3	Thylakoid lumenal protein TL20.3	Q8H1Q1;B6EUA5;A0A178W1Q3	AT1G12250	1.40	+	0.0163697

Other/unknown	TPT		A0A219HYB6;A0A219HZH3;A0A219I0W9;Q9ZSR7	AT5G46110	1.34	+	0.0140531
Other/unknown	YCF37	Homolog of Synechocystis YCF37	O64835	AT2G23670	1.11	+	0.0204503
Pigment synthesis	CAO	Chlorophyllide a oxygenase	Q9MBA1;A0A1P8ARR2	AT1G44446	0.59	+	0.0150526
Pigment synthesis	CHLD	Magnesium-chelatase subunit ChID	Q9SJE1	AT1G08520	0.91		0.280046
Pigment synthesis	CHLG	Chlorophyll synthase	Q38833	AT3G51820	0.59	+	0.0450526
Pigment synthesis	CHLH	Magnesium-chelatase subunit ChIH	A8MR05;Q9FNB0	AT5G13630	0.73	+	0
Pigment synthesis	CHL1	Magnesium-chelatase subunit ChI1-1	P16127	AT4G18480	1.24		0.127614
Pigment synthesis	CHL1	Magnesium-chelatase subunit ChI1-1	Q5XF33	AT5G45930	1.10		0.25116
Pigment synthesis	CHLM	Magnesium protoporphyrin IX methyltransferase	A0A1P8B4G1;Q9SW18	AT4G25080	0.79	+	0.0162333
Pigment synthesis	CHLP	Geranylgeranyl diphosphate reductase	Q9CA67	AT1G74470	0.87	+	0.0131163
Pigment synthesis	CRD1	Magnesium-protoporphyrin IX monomethyl ester [oxidative] cyclase	Q9M591;F4J0U9	AT3G56940	0.67	+	0.0142051
Pigment synthesis	CYP97B3	Cytochrome P450 97B3	O23365	AT4G15110	1.00		0.612597
Pigment synthesis	CYP97C1	Carotene epsilon-monooxygenase	Q6TBX7	AT3G53130	0.97		0.521825
Pigment synthesis	DVR	Divinyl chlorophyllide a 8-vinyl-reductase	Q1H537	AT5G18660	0.81		0.120589
Pigment synthesis	FC2		F4IMT3;O04921	AT2G30390	0.66		0.154528
Pigment synthesis	GUN4	Tetrapyrrole-binding protein	Q9LX31	AT3G59400	0.32		0.0636571
Pigment synthesis	HCAR	7-hydroxymethyl chlorophyll a reductase	Q8GS60	AT1G04620	0.66	+	0.0267126
Pigment synthesis	LUT5	Protein LUTEIN DEFICIENT 5	Q93VK5	AT1G31800	0.82		0.23658
Pigment synthesis	NOL	Chlorophyll(ide) b reductase NOL	Q8LEU3	AT5G04900	0.60	+	0.0136735
Pigment synthesis	PAO	Pheophorbide a oxygenase	Q9FYC2	AT3G44880	0.93		0.15339
Pigment synthesis	PDS	15-cis-phytoene desaturase/chromoplastic	Q07356	AT4G14210	0.58	+	0.0232485
Pigment synthesis	PORB	Protochlorophyllide reductase B	P21218	AT4G27440;AT5G54190	0.73	+	0.0135556
Pigment synthesis	PORC	Protochlorophyllide reductase C	F4I2F8;O48741	AT1G03630	0.76	+	0.011175
Pigment synthesis	PPOX1	Protoporphyrinogen oxidase 1	P55826	AT4G01690	0.72	+	0.0134286
Pigment synthesis	PPOX2	Protoporphyrinogen oxidase 2/mitochondrial	Q8S9J1;A0A1P8BE58;A0A1P8BE27	AT5G14220	1.18		0.896922
Pigment synthesis	VTE3		Q9LY74	AT3G63410	0.79	+	0.017312
Pigment synthesis	YCF54		Q9LVM3	AT5G58250	0.55	+	0.00652632
Pigment synthesis	ZDS1		Q38893	AT3G04870	0.98		1
Plastoglobule	ABC1K3	Uncharacterized aarF domain-containing protein kinase At1g79600	Q9MA15	AT1G79600	1.50	+	0.00748387
Plastoglobule	At1g06690		Q94A68	AT1G06690	0.53	+	0.0137313
Plastoglobule	At1g26090		Q6DYE4	AT1G26090	0.71	+	0.00682353
Plastoglobule	At1g32220	Uncharacterized protein At1g32220	Q9FVR6	AT1G32220	0.69	+	0.038819
Plastoglobule	At1g54570	Acyltransferase-like protein At1g54570	Q9ZVN2	AT1G54570	0.93		0.235867
Plastoglobule	At1g71810	Uncharacterized aarF domain-containing protein kinase At1g71810	Q94BU1	AT1G71810	0.97		0.295885
Plastoglobule	At1g78140		Q8LBV4	AT1G78140	0.56		0.113165
Plastoglobule	At2g34460	Uncharacterized protein At2g34460	Q8H124	AT2G34460	1.02		0.489202
Plastoglobule	At2g41040		Q0WPT7	AT2G41040	0.72	+	0.03788

Plastoglobule	At3g24190		Q9LRN0	AT3G24190	1.38	+	0.0244941
Plastoglobule	At4g13200	Uncharacterized protein At4g13200	Q8LDV3	AT4G13200	0.96		0.732355
Plastoglobule	At5g05200	Uncharacterized aarF domain-containing protein kinase At5g05200	Q9ASX5	AT5G05200	0.92		0.865887
Plastoglobule	CCD4	Probable carotenoid cleavage dioxygenase 4	O49675	AT4G19170	0.81		0.144741
Plastoglobule	CSP41B	Chloroplast stem-loop binding protein of 41 kDa b	A0A1P8ATL2;Q9SA52	AT1G09340	0.51	+	0
Plastoglobule	CYP74A	Allene oxide synthase	Q96242	AT5G42650	0.79	+	0
Plastoglobule	PAP1	Probable plastid-lipid-associated protein 1	O81439	AT4G04020	0.80	+	0.012303
Plastoglobule	PAP10	Probable plastid-lipid-associated protein 10	Q8W4F1	AT2G46910	0.37		0.0827969
Plastoglobule	PAP11	Probable plastid-lipid-associated protein 11	O81304	AT4G00030	0.70		0.10594
Plastoglobule	PAP12	Probable plastid-lipid-associated protein 12	Q8LAP6	AT1G51110	1.19	+	0.00688889
Plastoglobule	PAP13	Probable plastid-lipid-associated protein 13	F4IM05;Q8S9M1;A8MRU9	AT2G42130	0.51	+	0.0134312
Plastoglobule	PAP2	Probable plastid-lipid-associated protein 2	O49629	AT4G22240	1.10	+	0.0417488
Plastoglobule	PAP3	Probable plastid-lipid-associated protein 3	O82291	AT2G35490	0.72	+	0.00947368
Plastoglobule	PAP4	Probable plastid-lipid-associated protein 4	Q9LU85	AT3G26070	0.86	+	0.038488
Plastoglobule	PAP5	Probable plastid-lipid-associated protein 5	A0A1I9LP70;Q6DBN2	AT3G26080	0.81		0.0563333
Plastoglobule	PAP6	Probable plastid-lipid-associated protein 6	Q9LW57;A0A1I9LQU5;A0A1I9LQU3	AT3G23400	0.92		0.27007
Plastoglobule	PAP8	Probable plastid-lipid-associated protein 8	Q941D3;F4K2P2	AT5G19940	0.81	+	0.0187368
Plastoglobule	PAP9	Probable plastid-lipid-associated protein 9	Q9M2P7	AT3G58010	0.66	+	0.0125333
Plastoglobule	PLAT1	PLAT domain-containing protein 1	O65660	AT4G39730	1.15		0.142644
Plastoglobule	PSY	PHYTOENE SYNTHASE	F4KGX7;P37271	AT5G17230	1.05		1
Plastoglobule	VTE1	Tocopherol cyclase	Q94FY7	AT4G32770	0.54	+	0.00923077
Plastoglobule			B9DGY1;F4JFM1	AT3G07700	1.50		0.402259
Plastoglobule			Q9SR77	AT3G10130	0.76		0.994908
Plastoglobule			Q9LW26	AT3G26840	0.80		0.103521
Plastoglobule			Q9LSC4	AT3G27110	0.79		0.358734
Plastoglobule			F4IZ56;Q9M236	AT3G43540	0.46	+	0.0381188
Protease	ARASP2		O23053	AT1G05140	0.86	+	0.0501126
Protease	At2g21960		Q9SJ03	AT2G21960	0.94		0.130144
Protease	CLPP4		Q94B60	AT5G45390	0.46	+	0.0228333
Protease	CLPP5		Q9S834	AT1G02560	0.53	+	0.0135111
Protease	FTSH11	ATP-dependent zinc metalloprotease FTSH 11/mitochondrial	Q9FGM0	AT5G53170	0.91		0.924914
Protease	FTSH12	ATP-dependent zinc metalloprotease FTSH 12	A0A1P8ARE4;A0A1P8ARD2;Q9SAJ3	AT1G79560	0.80		0.29976
Protease	FTSH9	ATP-dependent zinc metalloprotease FTSH 9	Q9FIM2;Q9SD67	AT5G58870	0.76	+	0.037931
Protease	SPPA	Serine protease SPPA	Q9C9C0;A0A1P8AUG2	AT1G73990	0.88		0.118817
Protein folding	At3g12345	FKBP-type peptidyl-prolyl cis-trans isomerase	Q9LHH3	AT3G12345	0.78		0.125301
Protein folding	CLPB3	Chaperone protein ClpB3	Q9LF37	AT5G15450	1.05		0.961496
Protein folding	CPN21	20 kDa chaperonin	O65282	AT5G20720	1.09		0.41909

Protein folding	CPN60A1	Chaperonin 60 subunit alpha 1	P21238	AT2G28000	0.85		0.100227
Protein folding	CYP26-2	Peptidyl-prolyl cis-trans isomerase CYP26-2	F4HTT6;A0A1P8APN5	AT1G74070	0.50	+	0.0132174
Protein folding	CYP28	Peptidyl-prolyl cis-trans isomerase CYP28	A0A1P8B9P2;O65220	AT5G35100	0.60	+	0.009
Protein folding	CYP37	Peptidyl-prolyl cis-trans isomerase CYP37	P82869;A0A1I9LQ22;A0A1I9LQ23	AT3G15520	0.60		0.0506266
Protein folding	DJA5		Q940V1	AT4G39960	0.90		0.113986
Protein folding	DJA7		A0A1P8ART2;Q0WN54	AT1G80030	0.86	+	0.0469043
Protein folding	FKBP16-4	Peptidyl-prolyl cis-trans isomerase FKBP16-4	Q9SR70	AT3G10060	0.72	+	0.0062
Protein folding	FKBP17-2	Peptidyl-prolyl cis-trans isomerase FKBP17-2	Q9LDY5	AT1G18170	0.79	+	0.0168525
Protein folding	FKBP18	Peptidyl-prolyl cis-trans isomerase FKBP18	A0A1P8APZ5;Q9LM71	AT1G20810	0.29	+	0.0122609
Protein folding	FKBP19	Peptidyl-prolyl cis-trans isomerase FKBP19	Q9LYR5;A0A1R7T3F4;A0A1R7T3F3	AT5G13410	0.99		0.725306
Protein folding	HSP70-6	Heat shock 70 kDa protein 6	Q9STW6	AT4G24280	0.84		0.199397
Protein folding	TIG	Trigger factor-like protein TIG	Q8S9L5	AT5G55220	0.79	+	0.0206038
Protein translocation	CLPC1		Q9FI56	AT5G50920	0.91	+	0.0208732
Protein translocation	SCY1	Preprotein translocase subunit SCY1	Q38885	AT2G18710	1.17		0.0837977
Protein translocation	SECA1	Protein translocase subunit SecA	Q9SYI0;A0A1P8B485;F4JG57	AT4G01800	1.09		0.0782205
Protein translocation	TATA	Sec-independent protein translocase protein TATA	Q9LKU2	AT5G28750	0.90		0.819005
Protein translocation	TATB	Sec-independent protein translocase protein TATB	Q9XH75	AT5G52440	1.08		0.944842
Protein translocation	TATC	Sec-independent protein translocase protein TATC	Q9SJV5	AT2G01110	1.09		0.352552
Protein translocation	TIC110		Q8LPR9	AT1G06950	0.89		0.0968213
Protein translocation	TIC55		Q9SK50	AT2G24820	0.93		0.238982
PSI	PSAA	Photosystem I P700 chlorophyll a apoprotein A1	P56766	ATCG00350	0.94	+	0.0130714
PSI	PSAB	Photosystem I P700 chlorophyll a apoprotein A2	P56767	ATCG00340	0.82	+	0.0110968
PSI	PSAC	Photosystem I iron-sulfur center	P62090	ATCG01060	0.65	+	0.0307826
PSI	PSAD	Photosystem I reaction center subunit II-2	Q9SA56;Q9S7H1	AT1G03130;AT4G02770	0.97	+	0.0190229
PSI	PSAE1	Photosystem I reaction center subunit IV A	Q9S831	AT4G28750	1.03		0.152289
PSI	PSAE2	Photosystem I reaction center subunit IV B	Q9S714	AT2G20260	0.95		0.380676
PSI	PSAF	Photosystem I reaction center subunit III	Q9SHE8	AT1G31330	0.89	+	0.0440367
PSI	PSAG	Photosystem I reaction center subunit V	Q9S7N7	AT1G55670	1.11		0.265424
PSI	PSAH	Photosystem I reaction center subunit VI-1	Q9SUI7;Q9SUI6	AT1G52230;AT3G16140	0.35	+	0.0275682
PSI	PSAK	Photosystem I reaction center subunit psaK	Q9SUI5	AT1G30380	1.12		0.898867
PSI	PSAL	Photosystem I reaction center subunit XI	A0A1P8B6D0;Q9SUI4	AT4G12800	1.06	+	0.0471092

PSI	PSAN	Photosystem I reaction center subunit N	P49107	AT5G64040	0.91	+	0.0368367
PSI	PSAO	Photosystem I subunit O	Q949Q5	AT1G08380	0.17		0.105615
PSII	PSB28	Photosystem II reaction center PSB28 protein	F4JM05;Q8W0Y8	AT4G28660	1.15		0.381089
PSII	PSB33	Rieske (2Fe-2S) domain-containing protein	Q9C9I7	AT1G71500	0.96		0.108759
PSII	PSBA (D1)	Photosystem II protein D1	P83755	ATCG00020	0.62	+	0.0400566
PSII	PSBB (CP47)	Photosystem II CP47 reaction center protein	P56777	ATCG00680	0.82		0.0737302
PSII	PSBC (CP43)	Photosystem II CP43 reaction center protein	P56778	ATCG00280	0.95		0.1104
PSII	PSBD (D2)	Photosystem II D2 protein	P56761	ATCG00270	1.15	+	0.0210213
PSII	PSBE	Cytochrome b559 subunit alpha	P56779	ATCG00580	1.11	+	0.020475
PSII	PSBF	Cytochrome b559 subunit beta	P62095	ATCG00570	1.32	+	0.0498966
PSII	PSBH	Photosystem II reaction center protein H	P56780	ATCG00710	1.20	+	0.0291685
PSII	PSBO1	Oxygen-evolving enhancer protein 1-1	P23321	AT5G66570	1.09	+	0.00563636
PSII	PSBO2	Oxygen-evolving enhancer protein 1-2	Q9S841	AT3G50820	0.39	+	0.00496
PSII	PSBP1	Oxygen-evolving enhancer protein 2-1	Q42029	AT1G06680	0.76	+	0.0144762
PSII	PSBQ1	Oxygen-evolving enhancer protein 3-1	Q9XFT3	AT4G21280	0.75	+	0.0112787
PSII	PSBQ2	Oxygen-evolving enhancer protein 3-2	Q41932	AT4G05180	0.62	+	0.012
PSII	PSBR	Photosystem II 10 kDa polypeptide	P27202	AT1G79040	1.11	+	0.0207273
PSII	PSBT	Photosystem II 5 kDa protein	A0A1I9LS90;Q39195	AT3G21055	0.66		0.066332
PSII repair	ALB3	Inner membrane protein ALBINO3	Q8LBP4;F4IJM1	AT2G28800	1.25		0.300809
PSII repair	CTPA1		F4KHG6	AT5G46390	0.37	+	0.0338526
PSII repair	CYP38	Peptidyl-prolyl cis-trans isomerase CYP38	Q9SSA5	AT3G01480	0.71	+	0.00725
PSII repair	DEG5		A0A1P8B644;A0A1P8B643;Q9SEL7	AT4G18370	0.41	+	0.0203158
PSII repair	DEG8		F4KRV6;Q9LU10	AT5G39830	0.57	+	0.0141111
PSII repair	DEGP1	Protease Do-like 1	O22609	AT3G27925	0.59	+	0.0134
PSII repair	DEGP2	Protease Do-like 2	B3H581;O82261	AT2G47940	0.24	+	0.0191692
PSII repair	FKBP20-2	Peptidyl-prolyl cis-trans isomerase FKBP20-2	A0A1I9LRJ6;Q0WRJ7	AT3G60370	0.74		0.99859
PSII repair	FTSH1	ATP-dependent zinc metalloprotease FTSH 1	Q39102	AT1G50250	0.92		0.297777
PSII repair	FTSH2	ATP-dependent zinc metalloprotease FTSH 2	A0A1P8AXC1;O80860	AT2G30950	0.73	+	0.0352821
PSII repair	FTSH5	ATP-dependent zinc metalloprotease FTSH 5	Q9FH02	AT5G42270	0.92	+	0.0131948
PSII repair	FTSH8	ATP-dependent zinc metalloprotease FTSH 8	Q8W585	AT1G06430	0.98		0.151243
PSII repair	FTSY		O80842	AT2G45770	0.65	+	0.0193178
PSII repair	HHL1	Protein HHL1	Q8LDL0	AT1G67700	0.68	+	0.0255581
PSII repair	HSP70-7		Q9LTX9	AT5G49910	0.96		0.967427
PSII repair	LPA1	Protein LOW PSII ACCUMULATION 1	Q9SRY4;A0A1P8ANG6	AT1G02910	0.91		0.155896
PSII repair	LQY1	Protein disulfide-isomerase LQY1	Q8GSJ6	AT1G75690	0.51		0.0564979
PSII repair	LTO1	Thiol-disulfide oxidoreductase LTO1	A0A1P8B950;Q8L540	AT4G35760	0.91		0.172737
PSII repair	MET1	Protein MET1	Q94BS2	AT1G55480	0.77	+	0.0228293
PSII repair	MPH1	Protein MAINTENANCE OF PSII UNDER HIGH LIGHT 1	Q9FL44	AT5G07020	0.75	+	0.020027
PSII repair	PAM68	Protein PAM68	A0A1P8B8D1;O49668	AT4G19100	1.19	+	0.0226982

PSII repair	PBF1		F4JD01;P42742	AT3G60820	0.67		0.0547731
PSII repair	PDI6	Protein disulfide isomerase-like 1-2	Q9SRG3	AT1G77510	0.96		0.151747
PSII repair	PPL1	PsbP-like protein 1	P82538	AT3G55330	0.77	+	0
PSII repair	PSB27-1	Photosystem II repair protein PSB27-H1	Q9LR64	AT1G03600	0.94		0.97971
PSII repair	ROC4		F4IX28;F4IX26;P34791	AT3G62030	0.96		0.646816
PSII repair	RubA	Rubredoxin-like superfamily protein	Q9SLI4	AT1G54500	0.88		0.187553
PSII repair	TL18.3	UPF0603 protein At1g54780	Q9ZVL6	AT1G54780	0.82	+	0.01385
PSII repair	VIPP1	Membrane-associated protein VIPP1	A0A178W0D3;O80796	AT1G65260	1.06		0.730501
Redox regulation	At1g14345	NAD(P)-linked oxidoreductase superfamily protein	Q949S6	AT1G14345	1.03		1
Redox regulation	At1g50450	Saccharopine dehydrogenase	Q94BZ0	AT1G50450	0.61	+	0
Redox regulation	ATHM2	Thioredoxin M2	Q9SEU8;F4JG94	AT4G03520	0.61	+	0.0137561
Redox regulation	BAS1	2-Cys peroxiredoxin BAS1	Q96291	AT3G11630	0.60	+	0.0148293
Redox regulation	BAS1B		Q9C5R8;A0A1P8BD74	AT5G06290	0.79		0.0511319
Redox regulation	CITRX	Thioredoxin-like protein CITRX	Q9M7X9	AT3G06730	1.46	+	0.0306162
Redox regulation	ENH1	Rubredoxin family protein	Q9FFJ2;A8MSF2	AT5G17170	0.92		0.244119
Redox regulation	FSD3	Superoxide dismutase [Fe] 3	Q9FMX0	AT5G23310	0.92		0.352472
Redox regulation	MCK7.20	Malate dehydrogenase	F4KEX3;Q8H1E2	AT5G58330	0.67	+	0
Redox regulation	MDH	Malate dehydrogenase	Q9SN86	AT3G47520	0.95		0.375598
Redox regulation	MED24.18	Thioredoxin family protein	Q940I2	AT5G03880	0.88		0.0600826
Redox regulation	NTRC	NADPH-dependent thioredoxin reductase 3	O22229	AT2G41680	0.39	+	0.0109206
Redox regulation	PRXQ	Peroxiredoxin Q	A0A1I9LR27;F4JBC9;Q9L U86	AT3G26060	0.70	+	0.0141395
Redox regulation	TRXF1		Q9XFH8	AT3G02730	0.53	+	0.01075
Redox regulation	TRXM1	Thioredoxin M1	O48737	AT1G03680	0.54	+	0.00729412
Redox regulation	TRXM4	Thioredoxin M4	Q9SEU6	AT3G15360	0.91	+	0.0386731
Ribosome	PSRP2	30S ribosomal protein 2	Q8VYM4	AT3G52150	1.09		0.103143
Ribosome	PSRP5	50S ribosomal protein 5	Q9LER7	AT3G56910	1.09		0.237297
Ribosome	PSRP6		A0A1P8BCP6;Q9FKP0	AT5G17870	0.23		0.066747
Ribosome	RPL1	50S ribosomal protein L1	Q9LY66;F4J296	AT3G63490	1.06	+	0.0301556
Ribosome	RPL10	50S ribosomal protein L10	Q9FY50	AT5G13510	1.17	+	0.00476923
Ribosome	RPL11	50S ribosomal protein L11	Q9MAP3	AT1G32990	0.92		0.458547
Ribosome	RPL12A	50S ribosomal protein L12-3	P36212;P36210	AT3G27830;A T3G27850	0.67	+	0.0177953
Ribosome	RPL13		Q9SYL9	AT1G78630	0.75		0.471321
Ribosome	RPL14	50S ribosomal protein L14	P56792	AtCg00780	1.19	+	0.00972973
Ribosome	RPL15	50S ribosomal protein L15	P25873	AT3G25920	0.91		0.237453
Ribosome	RPL16	50S ribosomal protein L16	P56793	AT2G28830	0.96		0.804549
Ribosome	RPL17	50S ribosomal protein L17	Q9M385	AT3G54210	1.09		0.106059
Ribosome	RPL18	50S ribosomal protein L18	Q9SX68	AT1G48350	1.01		0.543251
Ribosome	RPL19-1		Q8W463	AT4G17560	0.52		0.113574

Ribosome	RPL21	50S ribosomal protein L21	P51412	AT1G35680	1.22	+	0.0442396
Ribosome	rpl22		P56795	AtCg00810	1.58	+	0
Ribosome	RPL23-A	50S ribosomal protein L23	P61845	AtCg00840	1.16		0.313148
Ribosome	RPL24	50S ribosomal protein L24	P92959	AT5G54600	0.93		0.381192
Ribosome	RPL27	50S ribosomal protein L27	Q9FLN4	AT5G40950	1.16	+	0.0205833
Ribosome	RPL29	50S ribosomal protein L29	Q9FJP3	AT5G65220	1.17	+	0.0140253
Ribosome	RPL2-A	50S ribosomal protein L2	P56791	AtCg00830	1.11	+	0.0377971
Ribosome	RPL31	50S ribosomal protein L31	Q9FWS4	AT1G75350	0.80		0.80213
Ribosome	rpl33	50S ribosomal protein L33	P56796	AtCg00640	0.72	+	0.0137297
Ribosome	RPL3A	50S ribosomal protein L3-1	Q9SKX4	AT2G43030	1.11		0.107458
Ribosome	RPL4	50S ribosomal protein L4	O50061;Q2V4Q4;Q3EDH2	AT1G07320	0.87	+	0.0437679
Ribosome	RPL5	50S ribosomal protein L5	O04603	AT4G01310	1.02		0.88071
Ribosome	RPL6	50S ribosomal protein L6	O23049	AT1G05190	0.98		0.458
Ribosome	RPL9	50S ribosomal protein L9	P25864	AT3G44890	1.08		0.610997
Ribosome	RPS10	30S ribosomal protein S10	Q9LK61	AT3G13120	0.88		0.852308
Ribosome	RPS11	30S ribosomal protein S11	P56802	AtCg00750	1.23	+	0.0187536
Ribosome	rps12-A	30S ribosomal protein S12	P62126	AtCg01230;AtCg00065;AtCg00905	1.31	+	0.0181898
Ribosome	RPS13	30S ribosomal protein S13	P42732;B3H631	AT5G14320	1.17		0.114681
Ribosome	rps14	30S ribosomal protein S14	P56804	AtCg00330	1.19	+	0.0398685
Ribosome	RPS15	30S ribosomal protein S15	P56805	AtCg01120	1.07		0.873854
Ribosome	RPS17	30S ribosomal protein S17	P16180	AT1G79850	1.19	+	0.029989
Ribosome	RPS18	30S ribosomal protein S18	P56807	AtCg00650	1.13		0.246255
Ribosome	RPS19	30S ribosomal protein S19	P56808	AtCg00820	0.88		0.194415
Ribosome	RPS2	30S ribosomal protein S2	P56797	AtCg00160	1.02		0.281353
Ribosome	RPS20	30S ribosomal protein S20	Q9ASV6	AT3G15190	1.19	+	0.0114667
Ribosome	RPS3	30S ribosomal protein S3	P56798	AtCg00800	1.08		0.151478
Ribosome	RPS4	30S ribosomal protein S4	P56799	AtCg00380	1.38	+	0
Ribosome	RPS5	30S ribosomal protein S5	P93014	AT2G33800	1.28	+	0.0203014
Ribosome	RPS6	30S ribosomal protein S6 alpha	A0A1P8AV66;Q8VY91	AT1G64510	0.92		0.901712
Ribosome	RPS7	Ribosomal protein S7	A0A2P2CLF5;P92557	AT2G07696	1.25		0.123512
Ribosome	rps7-A	30S ribosomal protein S7	P61841	AtCg00900	1.23	+	0.0102857
Ribosome	RPS8	30S ribosomal protein S8	P56801	AtCg00770	0.88		0.604115
Ribosome	RPS9	30S ribosomal protein S9	Q9XJ27	AT1G74970	1.11		0.923456
Ribosome	RRP31	30S ribosomal protein 3-1	A8MQL0;Q9SX22	AT1G68590	0.47		0.297644
Starch	BAM3	Beta-amylase 3	O23553	AT4G17090	0.91		0.727288
Starch	SS1	Starch synthase 1/amyloplastic	Q9FNF2	AT5G24300	1.14		0.152331
Starch	SS3	Starch synthase 3/amyloplastic	F4IAG1;F4IAG2	AT1G11720	NaN		1

Starch	SS4	Probable starch synthase 4/amyloplastic	Q0WVX5	AT4G18240	2.16		1
Stress responsive	APE1	Acclimation of photosynthesis to environment	Q2HIR7;A0A219HZL6	AT5G38660	0.97		0.116171
Stress responsive	AT5g02160		Q9FPH2	AT5G02160	0.66	+	0.0141053
Stress responsive	CLH1	Chlorophyllase-1	O22527	AT1G19670	0.82		0.202939
Stress responsive	FLU	Protein FLUORESCENT IN BLUE LIGHT	F4JFR2;F4JFR1;Q940U6	AT3G14110	1.00		0.797003
Stress responsive	LIR1	Light-regulated protein 1	Q96500	AT3G26740	0.46	+	0.0169391
Stress responsive	PPD3	PsbP domain-containing protein 3	Q9S720	AT1G76450	0.21	+	0.0445636
Stress responsive	PPD4	PsbP domain-containing protein 4	O49292	AT1G77090	0.62	+	0.0165806
Stress responsive	PPD6	PsbP domain-containing protein 6	Q9LXX5	AT3G56650	0.60		0.0743557
Stress responsive	TL29	Thylakoid lumenal 29 kDa protein	A0A1P8B8W6;A0A1P8B8Y3;P82281	AT4G09010	0.70	+	0.0135294
Thylakoid architecture	CURT1A	Protein CURVATURE THYLAKOID 1A	O04616	AT4G01150	0.95		0.166508
Thylakoid architecture	CURT1B	Protein CURVATURE THYLAKOID 1B	Q8LCA1	AT2G46820	0.84	+	0.0383085
Thylakoid architecture	CURT1C	Protein CURVATURE THYLAKOID 1C	Q9M812	AT1G52220	1.09	+	0.0413645
Thylakoid architecture	CURT1D	Protein CURVATURE THYLAKOID 1D	A0A1P8B4V5;Q8LDD3	AT4G38100	0.66	+	0.0142136
Thylakoid architecture	FZL	Probable transmembrane GTPase FZO-like	Q1KPV0;A0A1P8AUL4;A0A1P8AUL2	AT1G03160	0.77	+	0.0431894
Thylakoid architecture	PLSP1	Chloroplast processing peptidase	A0A1I9LMR3;Q8H0W1	AT3G24590	0.55	+	0.0143059
Thylakoid architecture	RIQ1	Reduced induction of non-photochemical quenching1	Q9SD79	AT5G08050	0.68	+	0.0167154
Thylakoid architecture	RIQ2	Reduced induction of non-photochemical quenching2	Q94F10	AT1G74730	0.58	+	0.0377451
Thylakoid architecture	THF1	Protein THYLAKOID FORMATION 1	Q9SKT0	AT2G20890	0.80	+	0.0132673